THE UNIVERSITY
of LIVERPOOL

AN INVESTIGATION INTO THE EFFECTS OF FOULING ON THE HEAT TRANSFER IN TUBULAR HEAT EXCHANGERS

by

ERTAN BUYRUK

Thesis submitted in accordance with the requirements
of the University of Liverpool
for the Degree of Doctor of Philosophy

Department of Mechanical Engineering
University of Liverpool

September 1996

STATEMENT OF ORIGINALITY

This thesis is submitted for the Degree of Philosophy in the Faculty of Engineering at the Liverpool University.

The research reported herein was carried out, unless otherwise stated, by the author in the Thermo-Fluid division of the Mechanical Engineering Department at the University of Liverpool, between September 1992 and 1996.

No part of this thesis has been submitted for a degree to any other University or educational establishment.

Ertan BUYRUK

September 1996

I would like to dedicate this piece of work to my mum and dad, Mr İhsan Buyruk and Mrs Elmas Buyruk, and my wife Mrs Gülçin Buyruk for all their help and support

ACKNOWLEDGEMENTS

The author wishes to thank Dr I. Owen and Dr J.W. Cleaver for their valuable advice encouragement, great patience and friendship.

The author is also extremely grateful to Dr H. Barrow for his help, great advice and infinite patience.

Thanks are expressed to Dr. M.W. Johnson for his help and guiding me to understand the application of his existing flow and temperature predictions and grid programs.

Many thanks to Mr. G. Williams and Mr. S. Bode for their help and friendship during the my study. And also the author would like to thank Mr. A. Abdel-Hameed for his help in tube bank experiments.

The author would like to express gratitude to the University of Cumhuriyet for their financial support and to the Mechanical Engineering Department at Liverpool University for the use of their facilities. And many thanks to Prof. Dr. A. Öztürk and Dr A. Pınarbaşı for their valuable advise.

SUMMARY

This thesis describes the results of an investigation into the heat transfer within tubular heat exchangers with particular reference to the effects of fouling. There have been many studies on tubular heat exchangers and these are widely reported in the literature. Despite this, however, there is still a lot of detail that is not understood, particularly in relation to fouling.

The effects on heat transfer of fouling thickness, its disposition and its thermal conductivity have been investigated theoretically by modelling the fouled tube as an eccentric annulus. A finite difference procedure in bipolar coordinates has been developed which has given detail of how the various parameters affect the heat transfer. A second technique was developed using a point matching method which essentially applies mixed Newton and Dirilicht boundary conditions and then at discrete points on the Newtononian boundary matches the convective heat transfer to the normal gradient of temperature in the solid. The two methods are seen to produce comparable results for the heat transfer and the internal temperature distribution with the point matching method being computationally more efficient.

The result of fouling is often that the effective diameter of the tubes can increase. The increased blockage to the flow presented by the fouled tubes will alter the flow pattern and the distribution of heat transfer coefficient around the tube surface. To investigate this, an experimental study has been carried out into the effect of different tube spacing on the heat transfer and pressure distribution. A heated tube instrumented with a heat flux sensor and a static pressure tapping was used to determine the heat transfer distribution around a single tube, around a tube in a single row transverse to the flow and around a tube in a bank. Results showed good agreement with the available data and provided much new data, particularly at low Reynolds number. An analytical model was developed to compare with the experimental data. A numerical calculation of the heat transfer and fluid flow around a single tube, around a single row of tubes and through a tube bank has been developed by solving the Navier-Stokes, Continuity and Energy equations for laminar flow using a stream function-vorticity formulation with second order accuracy centre differencing with a Gauss-Seidal over-relaxation procedure. The numerical solution of the equations was accomplished on orthogonal curvilinear grids. The results compared extremely well with the experimental data up to the separation point but less well in the wake region. This is believed to be due to the actual flow being unsteady because of vortex shedding thereby making the separation point difficult to locate.

In an attempt to gain an understanding of the distribution of foulant within a tubular heat exchanger an experimental rig was built where fly ash was injected into the gas flow and allowed to foul the water-cooled tubes; the tube surface temperatures were held above and below the dew point. Due to time restrictions this aspect of the research was limited but was successful in showing where fouling begins in relation to the known fluid flow patterns.

There are many aspects to fouling and its effects on heat transfer and only a few of these could be addressed within the research. However the investigations that were carried out were successful in providing new detailed information.

NOMENCLATURE

a	Eccentricity
A	Area
B	Blockage ratio
c	Semi-distance between poles
c	Specific heat at constant pressure
C_p	Pressure Coefficient
d	Fouled tube diameter
d_c	Clean tube diameter
d_1	Inside diameter of tube
d_o	Outside diameter of tube
D	Tube diameter
D	Dirichlet boundary condition
e	Dimensionless eccentricity
E	Electrical output voltage
g	Acceleration due to gravity
h($\bar{h}$)	Heat transfer coefficient, (Average heat transfer coefficient)
h_c	Clean tube heat transfer coefficient
h_1	Inside local heat transfer coefficient
h_2	Outside local heat transfer coefficient
h_θ	Local heat transfer coefficient around the tube
I	Current
k	Thermal conductivity
L	Length of the copper strip
m	An exponent see eq.3.3
m_w	Water Flow Rate

n	Separation Constant
n	Normal (to boundary) direction
N	Newton boundary condition
P	Static pressure
P_∞	Total Pressure
q	Heat flux
Q	Heat transfer rate
Q_g	Gas Side Heat Transfer
Q_w	Water Side Heat Transfer
r_o	Outside radius of the tube
r_i	Inside radius of the tube
R	Dimensionless Radius
R	Temperature dependent resistance
R_o	Resistance of the material at a reference temperature
R_2	Dimensionless outside radius of the tube
s_l	Longitudinal distance of tube bank
s_t	Transverse distance of tube bank
S_l	Longitudinal pitch of tube bank
S_t	Transverse pitch of tube bank
t	Dimensionless temperature
t_1, t_2	Dimensionless temperature of inside and outside of the tube
T_1	Inside tube temperature
T_2	Local outside temperature of the tube
T_G	Gas Temperature
T_o	Reference temperature
T_{fluid}	Fluid temperature
T_s	Surface temperature
T_∞	Ambient temperature

u, v Velocity components in x and y direction respectively

U_∞ Potential flow velocity around the confined single tube

$U_{\infty,s}$ Potential flow velocity around the unconfined single tube

V Voltage(Calculation of the copper strip technique)

V, V_∞ Upstream velocity

V_e Effective velocity

V_{max} Maximum velocity

V' Fluctuating velocity

$\bar{V}$ Average velocity

w Width of the copper strip

W Height of the duct

x Distance from the first stagnation point of the tube

X_1 Distance from origine of the clean tube

X_n Distance from origine of the fouled tube

z Rectangular coordinate plane

Coordinates

x, y Cartesian coordinates

r, θ Polar coordinates

ξ, η Bipolar coordinates

Greek Letters

α Fouled tube circumferential angle(For the point-matching method modelling)

α Thermal diffusivity (For the energy equation in numerical calculations)

α Temperature coefficient of resistance for material (Copper strip technique)

β Wedge angle

Δ Thermal boundary layer thickness

Δ_c Conduction thickness of thermal boundary layer

Δx Increment in x direction

Δy Increment in y direction

θ Clean tube circumferential angle

κ Constant (see eq. 4.15)

ℓ Metric coefficient

ℓ_m Mixing length

μ Dynamic viscosity

ν Kinematic viscosity

ν_e Effective viscosity

ν_ℓ Laminar viscosity

ν_t Turbulent viscosity

ρ Density

Φ Bipolar coordinate plane

ψ Stream function

Ω Vorticty

R,Θ Separation variables

Non-dimensional Numbers

Gr Grashof number

Re Reynolds number

Nu Nusselt number

Nu_b Local Nusselt number for confined tube

Nu_s Local Nusselt number for unconfined single tube

Pr Prandtl number

CONTENTS

CHAPTER 1

INTRODUCTION

CHAPTER 2

THEORETICAL ANALYSIS OF NON-UNIFORM FOULING ON A SINGLE TUBE IN CROSS-FLOW

CHAPTER 3

EXPERIMENTAL INVESTIGATION OF HEAT TRANSFER AND AIR FLOW CHARACTERISTICS OVER TUBES IN CROSS-FLOW

CHAPTER 4

NUMERICAL PREDICTION OF FLOW AND HEAT TRANSFER CHARACTERISTICS IN A TUBE AND TUBE BANK

CHAPTER 5

EXPERIMENTAL INVESTIGATION OF PARTICULATE FOULING ON THE GAS SIDE OF A HEAT EXCHANGER TUBE SURFACE

CHAPTER 6

CONCLUSIONS AND FUTURE WORK

CHAPTER 1

INTRODUCTION

This thesis describes a series of studies carried out in the Mechanical Engineering Department at Liverpool University over the years 1992 to 1996 into the heat transfer and flow characteristics of a multi tube cross-flow heat exchanger and to relate this to the effect of fouling as far as possible. Also, experimental and theoretical investigations were carried out to predict the effect of fouling on the heat exchanger tubes. At the outset of a research programme a researcher will have a series of aims and an intended path to follow. Whether or not the path can be kept to depends upon many things such as resources, outcomes and, unfortunately, luck. So it was with this research. The aim initially was to carry out a detailed study into a heat exchanger that was being fouled. Due to a number of factors, the rig only became available at the end of the research and therefore the study became more concerned with the detail of the heat transfer from the tubes, rather than the fouling of a complete exchanger.

1.1 Background

Energy conservation has always been of concern to engineers in industry mainly because it has a direct bearing on costs. Since the early 1970s there has been a greater appreciation of the need to conserve energy, not just because of rapidly increasing fuel prices but also on account of the general realisation of the value and the finite resource of energy. Heat exchangers with tube banks in cross-flow are of great practical interest in many thermal

and chemical engineering process. Heat exchanger designers often carry out investigations to find the tube arrangement that gives the best balance of thermal output against the power needed to send the gases through it. In order to find the optimum configuration, designers require detailed information on local and average gas side heat transfer coefficients. To investigate the process of flow and heat transfer in tube banks and their response to changes in different parameters, it is possible to make experiments or to build a model or chosen simple geometrical models where is possible to measure or to predict local values and consider the effect of only one parameter at a time.

Energy transfer often takes places in heat exchangers where energy in the form of heat is transferred from one fluid to another across a solid, separating boundary. If this surface becomes fouled, there is a direct effect on the heat transfer. Fouling is the formation of a layer of material, by mechanical or chemical means, onto the heat exchanger surfaces. The nature of the foulant is such that it is usually a poorer conductor of heat than the material of the heat exchanger and this leads to a reduction of heat transfer. Deposition on the tubes reduces the heat transfer rate and changes the gas flow patterns around the tubes and often adversely affects the rate of heat transfer. Figure 1.1 illustrates some deposit patterns on heat exchanger tubes. Figure 1.1(a) shows the effect of a high particle loading in the air flow through a finned tube cooler (Bott, 1990). Figure 1.1(b) illustrates fine graphite particle formation on tube surfaces with different conditions (Ots et al., 1986) and Figure 1.1 (c) shows the cross-flow heat exchanger particulate fouling pattern with a kaolin-water suspension around the tubes (Melo et al., 1984). Fouling is a serious problem in the operation of industrial boilers where the increased energy costs can lead to expensive manufacturing

processes. Figure 1.2 shows that the fan power consumed increases as fouling proceeds (Bott, 1983). According to experience and results obtained from industrial operations, three variables can be identified which have greater significance than others. These variables are fluid velocity, temperature and concentration of the foulant precursor and in a particular system these represent the determining factors in the accumulation of deposits on heat exchanger surfaces. The effect of particle (aluminium oxide) concentration on the asymptotic fouling resistance can be seen in Figure 1.3(a) (Blochl and Muller-Steinhagen, 1990). Figure 1.3 (b)shows the effect of velocity on magnetite deposition where increasing velocity caused a decreasing asymptotic fouling (Bott, 1990) and Figures 1.3(c)-(d) show the effect of temperature and temperature distribution on the particulate fouling mechanism. Other important parameters are fluid characteristics, fluid shear stress, surface material, and surface geometry.

The effect of flow velocity on the fouling process is complex. As the velocity increases the wall side viscous sub-layer becomes thinner and this will reduce the resistance to diffusion and mass transfer from the bulk fluid to wall, ie: it will tend to increase fouling. However increased velocity also increases the shearing action of the fluid on the deposit interface and this will result in increased removal of the deposit. Fluid characteristics include the thermodynamic and transport properties of the fluid such as density, thermal conductivity, viscosity etc. In gas side fouling, if the fluid contains condensible components, dew point temperature becomes an important parameter. The surface temperature can have another effect on the foulant since once it has deposited it can become "baked".

There have been many investigations into the modelling of fouling mechanisms. These have often been highly simplified in the sense that they are based upon several assumptions, such as:

- Only one type of foulant and mechanism of fouling is present
- The fouling is homogeneous throughout its thickness
- Fouling roughness can be neglected
- Changes in physical properties of the streams are ignored
- The initial and changing condition of the surface is not considered.

Whilst there are no successful models which encompass all the variables that effect fouling, researchers have paid particular attentions to:

- Time
- Velocity
- Temperature
- Concentration

It can be seen, therefore, that many mechanisms are involved in the fouling process and how these affect the heat exchanger performance. The combinations of these make modelling of the process very difficult.

1.2 Objectives of The Present Work

The main objective of this research has been to improve the understanding of how the heat transfer is modified by fouling on the external surface of cross-flow heat exchanger tubes. It is generally accepted that fouling increases the thermal resistance and therefore reduces heat transfer; this accepted wisdom will be questioned. It is also known that fouling can increase the effective outside diameter of the tubes thereby increasing the blockage to flow and therefore effecting the flow velocity and the convective heat transfer coefficient. The research reported in the following chapters consists of experimental and theoretical studies of the effect of fouling on the heat exchanger tubes.

Chapter 2 contains a theoretical study of the thermal resistance of uniform and non-uniform fouling on cross-flow heat exchanger tubes. Modelling the fouling geometry as an eccentric and concentric annulus, a finite difference procedure in polar and bipolar coordinates has been developed to predict the effect of fouling on the thermal performance. Results are presented for a range of geometry, thermal conductivity and variable convection boundary conditions. Another theoretical investigation was developed to calculate the coupled convection and conduction heat transfer on a fouled tube. A point matching method was applied which refers to the problem of determining steady state energy transfer in two dimensions with mixed Dirichlet and Newtonian boundary conditions which may occur in a convectively cooled body. The Laplace equation was used in the conduction domain to give a general solution for temperature and the point-matching method was used at the boundary to find the temperature associated with low conductivity variable thickness fouling. The results of the point-matching prediction were compared with those obtained by the finite

difference analysis.

Chapter 3 describes an experimental study to measure local heat transfer coefficients around a heated cylinder with air in cross-flow. Experiments have been carried out to investigate the heat transfer and flow characteristics for a single tube, a single tube row and staggered tube bundle geometries for a range of subcritical Reynolds numbers. Also for a single tube row, a theoretical study was carried out to calculate the front stagnation region and laminar boundary layer region heat transfer with different blockage ratios. Local heat transfer coefficients were obtained by a micro-foil heat flow sensor and experiments were carried out using a low speed wind tunnel and up-stream velocity was recorded using a hot-wire anemometer.

Chapter 4 presents a numerical prediction of the flow and heat transfer structure around the single tube with variable blockage ratios and a tube in a bundle for low Reynolds numbers. Predictions are made using Computational Fluid Dynamics and the results are presented as two dimensional constant variables of streamline and isotherm contours. Local Nusselt number and local pressure values were plotted versus angle for different geometries. Results were obtained using second order accuracy centre differencing with a Gauss-Seidel over-relaxation procedure for laminar flow conditions. The results obtained have been compared with experimental work.

Chapter 5 describes an experimental study that was carried out to investigate the deposition of ash particles on the gas side of heat exchanger tubes. An experimental rig has

been built and using fixed process conditions such as ash loading, flow rate, heating power and water flow rate, results were examined for structure of deposit around the tubes.

Finally Chapter 6 presents the main conclusions of the work and discusses possible future research.

During the course of the research three papers have been published in the technical literature and these are included in Appendix B. It is anticipated that further publications will be produced.

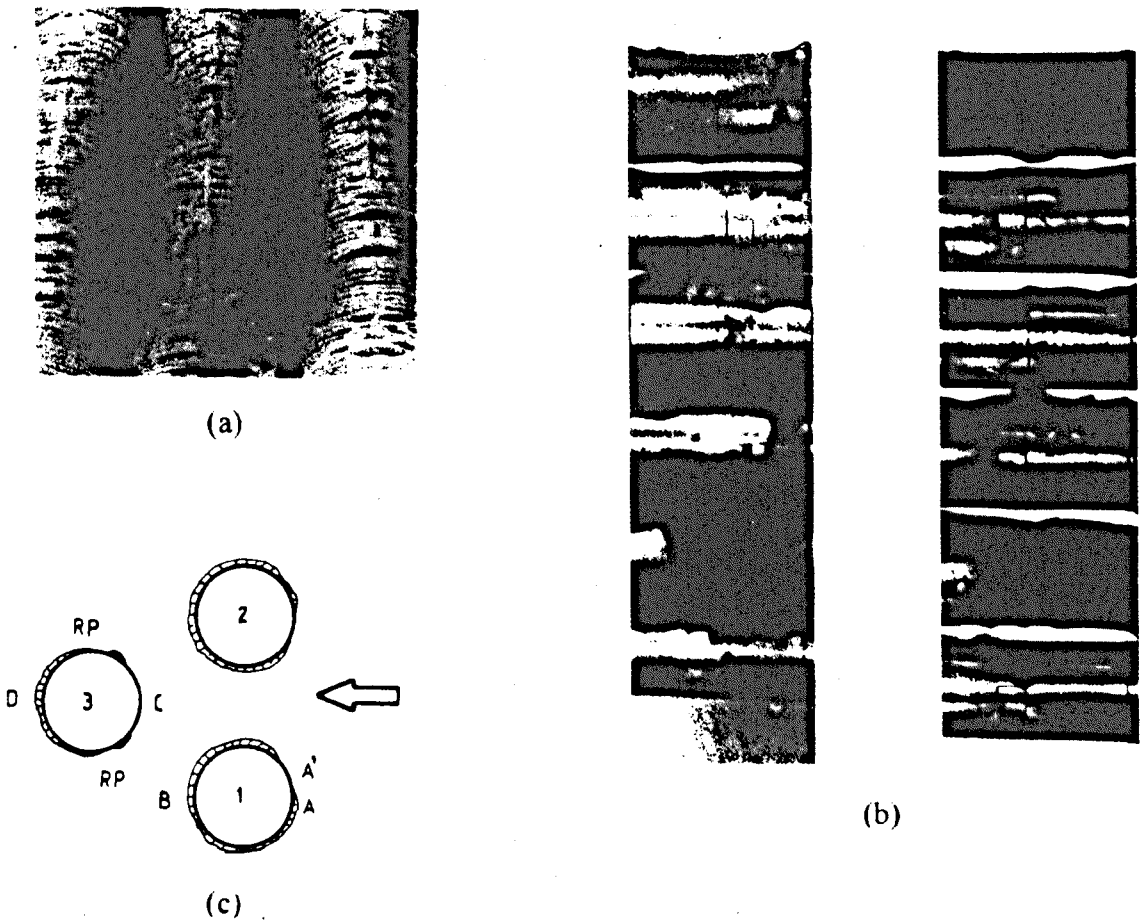

Figure 1.1 Deposition Patterns on the Heat Exchangers Tubes

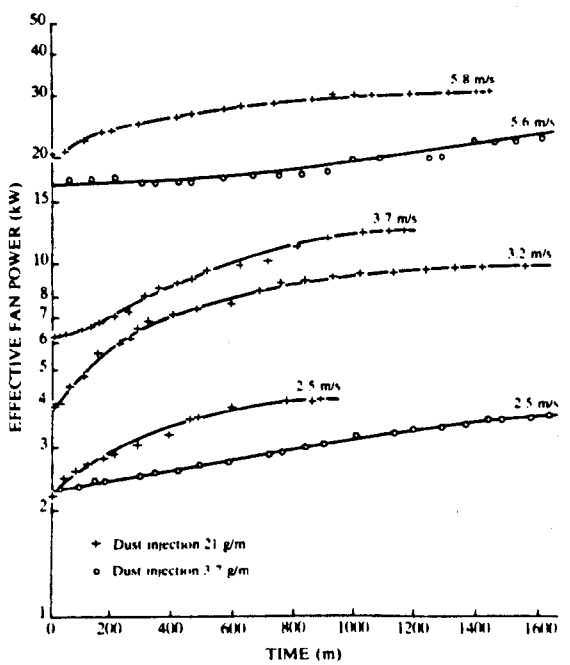

Figure 1.2 Effect of Fouling on the Fan Power Consumption

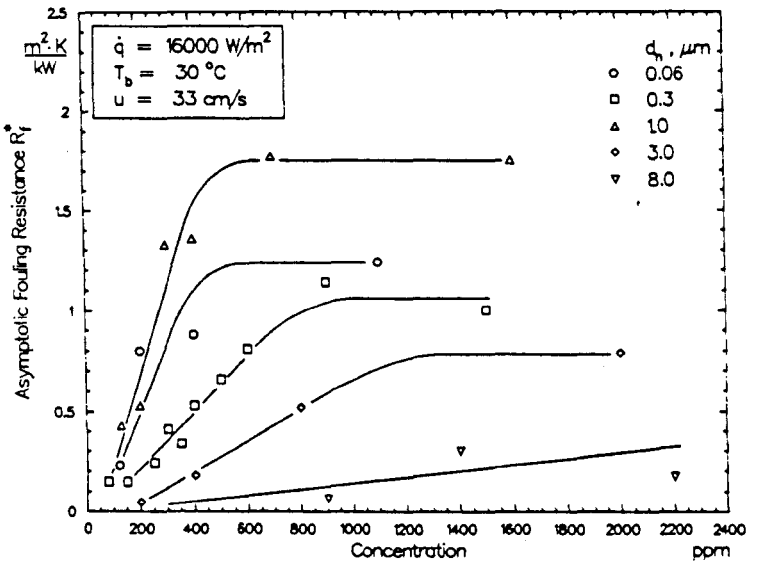

(a)

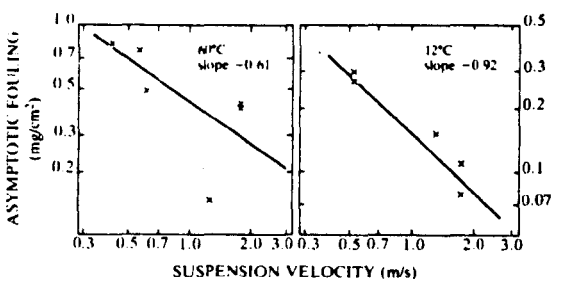

(b)

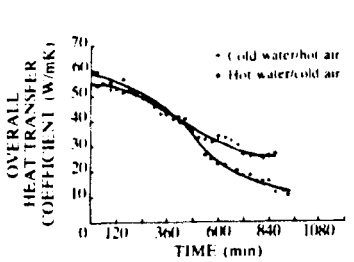

(c)

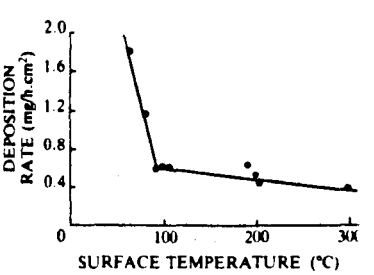

(d)

Figure 1.3 Effect of Particle Concentration, Velocity and Temperature

CHAPTER 2

THEORETICAL ANALYSIS OF NON-UNIFORM FOULING ON A SINGLE TUBE IN CROSS-FLOW

2.1 Introduction

The nature of fouling on heat exchanger surfaces and the procedure for predicting the effect on thermal performance have been widely investigated and are reported in detail in the literature, for example Bott (1983), Barrow and Sherwin (1994), Muller-Steinhagen et al. (1988). However fouling continues to be major problem and is of concern to engineers engaged in the design and operation of heat exchange equipment. Specific information is often not available, except perhaps in certain situations, on what allowance should be made at the design stage for increased resistance to heat transfer due to fouling.

While the principal effect of fouling is to increase the thermal resistance and hence to reduce the energy transfer, there are other interdependent effects which are less familiar. Changes in the nature of the surface arising out of the fouling affects the convective heat transfer rate as does the change in velocity caused by the blockage. The latter effect is considered by Barrow and Sherwin (1994). Essentially, as fouling takes place the pressure drop across the heat exchanger increases giving rise to a reduction in flow rate and hence

convective heat transfer coefficient. To quantify this, both the system and fan or pump characteristics must be known. Furthermore, visual observation of the fouling of surfaces such as in the frosting of the fins of a heat pump evaporator or the tubes of a cross-flow heat exchanger (Melo and Pinheiro (1984), Ots et al.(1986)) indicate that in most cases fouling is non-uniform in thickness. Mechanical and chemical deposition of fouling processes also result in non-homogeneity of the material which further adds to the complexity of assessing the effect of fouling on the heat transfer rate to the surface.

This chapter contains two theoretical studies. In the first study, a theoretical analysis of steady-state heat conduction through homogenous fouling on the external surface of tubes in cross-flow has been made. Modelling the fouling geometry as an eccentric annulus, a finite difference procedure in bipolar coordinates has been developed to predict the effect of fouling on the thermal performance. Theoretical prediction for a range of geometry, thermal conductivity and variable convection boundary conditions are presented. It is shown how, for a range of foulant thickness, eccentricity and thermal conductivity, the rate of heat transfer to a given size tube can be reduced or increased. The case of non-homogeneity of the fouling is explored with view to eventually extending the analysis towards varying thermal conductivity.

The second study is concerned with the calculation of coupled convection and conduction heat transfer. Specifically, it refers to the problem of determining steady-state energy transfer in two dimensions with mixed Dirichlet and Newtonian boundary conditions as may occur in a convectively cooled body. As in the first case described above, the

conduction domain has also been modelled as an eccentric annulus and the thermal performance determined for various annular geometries, the calculation being effected numerically using the bi-polar co-ordinate system. Clearly numerical analysis by conventional finite difference and finite element methods is most appropriate when the boundaries coincide with the chosen co-ordinate system. With irregular geometries an alternative method may be sought, and the point-matching method has been applied. This technique was described by Cheng et al (1981) in connection with ice-growth on a tube in cross-flow.

In the point-matching method for conjugated heat transfer the Laplace equation is used in the conduction domain to give the general solution for the temperature. Where Newtonian boundary conditions pertain, a number of points are then selected and the Newton equation applied to each in turn. This procedure together with the use of any temperature boundary conditions results in a system of linear equations for the unknown constants. Solution of these equations by formal methods then yields the temperature solution for the particular problem and hence the heat transfer.

In the present work, the point matching method has been employed for the mixed boundary condition situation and a number of problems associated with low conductivity variable thickness fouling are examined. The results of the point-matching prediction are then compared with those obtained by the more familiar finite-difference analysis (where it can be applied) and other possible uses of the method are suggested.

2.2 Theoretical Analysis of the Thermal Resistance of Non-Uniform Fouling on Cross-flow Heat Exchangers Tubes

In this investigation, attention is focused first on non-uniform thickness geometry, with special reference to fouling on a plain tube in cross-flow. In order to effect a quantitative and systematic investigation of non-uniformity, a geometry which is amenable to theoretical analysis must be chosen if meaningful results are to be obtained. Since the complete heat transfer problem involves conjugated convection and conduction, the geometry of the fouling must also provide for a convective boundary condition which can be specified with confidence.

With these considerations in mind, it was decided that the eccentric annulus met the requirements. The external surface is circular and will be unchanged even when the eccentricity and hence thickness geometry is altered. Figure 2.1 shows the geometry which has been used. The shaded area represents the fouling deposit on the enclosed circular tube. Because the external flow is always over a cylinder in cross-flow, the distribution of the external heat transfer, in terms of the Nusselt number, is prescribed for a given Reynolds number [see, for example, Chapman (1987)]. It should be noted, and this will be referred to again later, that the heat transfer coefficient will vary with the outside diameter. Figure 2.1 shows the deposit having built up on the leading edge; it may also build up in such a way that it is thicker at the rear stagnation point than at the forward. These cases, and indeed the general case can be explored by rotating the distribution of the external heat transfer coefficient in the θ direction. In practice, of course, the deposit will not be perfectly circular but this geometry enables the situation to be explored theoretically and the general trends

observed will hold regardless of the actual cross-sectional profile of the deposit. The tube is assumed to be thin and to have a constant inside surface temperature. Furthermore, the temperature drop across the tube wall is assumed to be very much less than that in the external thermal boundary layer. If the temperature drop across the wall is to be less than 1 percent of the external temperature drop, then the Biot number (Bi=th/k) must be less than 0.01. This criterion for accuracy is met in normal heat exchanger practice involving gas cross-flow. As will be seen later, the domain of integration may be discretized using a well-defined curvilinear coordinate system. Finally, the extreme case of uniform thickness (zero eccentricity) must conform to the conventional polar coordinate system which may be used as a yardstick for comparison.

The second feature of this study is spatially varying conductivity within the non-uniform fouling and how this might be accommodated in the analysis. Accordingly, a fictitious distribution of conductivity needs to be chosen to assess trends in heat transfer performance of the tube. This may be achieved by dividing the whole fouling cross-section into sub-domains with different thermal conductivities matching the conditions at their interfaces during the calculation.

2.2.1 Numerical Solution

To effect a numerical solution of the temperature distribution and heat transfer in the non-uniform fouling, advantage is taken of the geometry of the bipolar coordinate system. The origin and the properties of this system are written in the present case as described below (Jaeger,1951).

Laplace transformation is a method for solving equations of hyperbolic and parabolic types. By the use of the theory of functions of a complex variable, many two dimensional regions can be transformed into regions with rectangular boundaries and in this way Laplace's equation solved in them. Before explaining the specific problem, the two dimensional steady state temperature distribution in a body in cartesian coordinates can be written as:

$$\nabla^2 T = \left(\frac{\partial^2 T}{\partial x^2} + \frac{\partial^2 T}{\partial y^2} \right) = 0 \qquad (2.1)$$

Now we suppose that $\Phi = \xi + i\eta$ is a function of f(z) of a complex variable $z = x + iy$. Here presenting z by its rectangular coordinates (x,y) in the z plane and same way Φ by its coordinates (ξ,η) in the Φ plane, then:

$$\nabla^2 T = \left(\frac{\partial^2 T}{\partial \xi^2} + \frac{\partial^2 T}{\partial \eta^2} \right) = 0 \qquad (2.2)$$

The region is bounded by the curves $\xi=\xi_1$, $\xi=\xi_0$,$\eta=\eta_0$ and $\eta=\eta_\pi$ in the (x,y) plane which are determined by a transformation $\Phi = f(z)$.

A transformation of the type:

$$z = -c \, \mathrm{Coth}(2\Phi) \qquad (2.3)$$

generates orthogonal circles in the x,y plane . From equation (2.3), the following equations are obtained.

$$x=\frac{c\sinh(\xi)}{\cosh(\xi)-\cos(\eta)}\ ,\ y=\frac{c\sin(\eta)}{\cosh(\xi)-\cosh(\eta)}$$

These two systems form a right-handed orthogonal curvilinear or bipolar coordinate system. The following relationships are of concern to the present work. The centre of a circle and its radius are a function of ξ then:

$$X_1=c\ \mathrm{Coth}(\xi_1)\ ;\ r_1=\frac{c}{\mathrm{Sinh}(\xi_1)}$$

$$X_n=c\ \mathrm{Coth}(\xi_n)\ ;\ r_n=\frac{c}{\mathrm{Sinh}(\xi_n)}$$

then ξ_1 and ξ_n can be defined as:

$$\mathrm{Cosh}(\xi_n)=\left[\frac{a^2-r_1^2+r_n^2}{2ar_n}\right]\ ,\ \mathrm{Sinh}(\xi_1)=\left[\left(\frac{r_n}{r_1}\right)\sinh(\xi_n)\right] \qquad (2.4)$$

Here a is the eccentricity that is expressed as:

$$a=c[\coth(\xi_n)-\coth(\xi_1)]$$

In the orthogonal curvilinear system, the metric coefficients are needed to find different length, areas and volumes. As the definition of metric coefficient is the partial derivative of lengths with respect to coordinates, in the bipolar coordinate system the metric coefficients are given by:

$$\frac{ds}{d\xi}=\ell_\xi=\left[\frac{c}{\cosh(\xi)-\cos(\eta)}\right]$$
$$\frac{ds}{d\eta}=\ell_\eta=\left[\frac{c}{\cosh(\xi)-\cos(\eta)}\right] \qquad (2.5)$$

Substituting equation (2.5) into equation (2.2) gives:

$$\frac{\partial}{\partial\xi}\left[\left(\frac{\ell_\eta}{\ell_\xi}\right)\frac{\partial T}{\partial\xi}\right]+\frac{\partial}{\partial\eta}\left[\left(\frac{\ell_\xi}{\ell_\eta}\right)\frac{\partial T}{\partial\eta}\right]=0 \qquad (2.6)$$

The idealised eccentric annular geometry of the fouling is defined by the inner and outer diameters and their eccentricity. Accordingly, the domain may be discretized in terms of curvilinear orthogonal co-ordinates ξ and η of the system between known limits as indicated in Figure 2.1. In this figure, which refers to the case when the external cross-flow is along the x-axis, only half the fouling geometry needs to be considered. To determine the temperature field $T(\xi,\eta)$ and hence the heat transfer rate in the homogeneous conductor, equation (2.2) is solved. It is written above in equatiaon 2.5 that here the metric coefficients in the ξ and η co-ordinate system are equal.

Four boundary conditions are used in the present case. The boundary conditions are as follows:

(i) $\eta=0,\pi;\quad \xi_o\le\xi\le\xi_i;\quad \frac{1}{\ell}\frac{\partial T}{\partial\eta}=0$

(ii) $\xi = \xi_1;\ 0 \le \eta \le \pi;\ T = T_1$

(iii) $\xi = \xi_o;\ 0 \le \eta \le \pi;\ h(T_G - T) = \frac{k}{\ell}\frac{\partial T}{\partial \xi}$

With regard to (ii), should there be a convective boundary condition then one similar to (iii) would be used with the appropriate internal heat transfer coefficient which would be approximately constant around the boundary.

In the present investigations, a finite difference formulation of equation (2.2) is used with specified T_G and T_1 and peripheral distribution of heat transfer coefficient, h_o. Once the outside diameter (and hence ξ_o) is known, together the prescribed value of the cross-flow stream velocity, h_o may be evaluated "once and for all" from standard heat transfer correlations, relationship described in the following section.

2.2.2 The External Heat Transfer Coefficient and Critical Radius Analysis

For a given fluid and stream velocity, the local external heat transfer coefficient on a cylinder in cross-flow is dependent only upon the angular position θ and the external diameter d_o. If the external diameter is increasing due to fouling, then the values of the external heat transfer coefficients must be adjusted accordingly. Now for range of Reynolds number of interest here, (about 4,000 to 40,000), the average Nusselt number for air flow across the

cylinder as reported in Eckert and Drake (1959), is given by:

$$Nu = 0.174\ Re^{0.618}$$

Since the distribution of local heat transfer coefficient is well defined in this range, the heat transfer coefficient on the surface of the foulant, h_o, can be related to the heat transfer coefficient of the clean tube, h_c, as:

$$\frac{\frac{h_o d_o}{k} = 0.174\left(\frac{U_\infty d_o}{\nu}\right)^{0.618}}{\frac{h_c d_c}{k} = 0.174\left(\frac{U_\infty d_c}{\nu}\right)^{0.618}}$$

then h_o can be written as:

$$h_o = h_c\left(\frac{d_o}{d_c}\right)^{-0.382} \qquad (2.7)$$

This relationship then provides for a systematic change (i.e decrease) in the heat transfer coefficient on the external boundary as the diameter increases due to fouling. It is important to emphasise that the heat transfer coefficient on the external surface is dependent on the diameter, d_o, irrespective of the disposition of the foulant over the surface of the clean tube.

In the development of this relationship, the fluid velocity must of course be assumed constant, which is justified in the analysis of a single tube. However, in a tube bundle, where fouling increases the pressure drop in the system, correction to the velocity must be made as

explained earlier. Such an adjustment to the external heat transfer coefficient is essential to the analysis of the thermal performance of a tube which is progressively fouled. In this way, the energy transfer for the fouled tube may be normalised with respect to that for the clean condition, provided of course the external velocity and the temperature boundary conditions are fixed.

The derivation of the critical radius of an insulated round pipe or tube is familiar and is reported in detail in the standard heat transfer texts. With the assumption of constant external heat transfer coefficient, the critical radius equals $(k/\bar{h}_o)$. More accurately, the heat transfer coefficient changes with increase in external radius as explained above and this refinement may easily be incorporated into the critical radius analysis. For a fixed value of r_c (clean tube radius), the rate of heat flow is a function of r_o (fouled tube radius) and radial heat flow rate is maximum at the value of r_o when $dQ/dr_o=0$. Putting equation (2.7) into the standard axisymmetric heat conduction equation which is given as:

$$Q = \frac{T_i - T_o}{\frac{1}{h_i 2\pi r_i} + \frac{1}{h_o 2\pi r_o} + \frac{\ln(r_o/r_i)}{2\pi k}}$$

Then critical radius may be shown to be:

$$r_{crit.} = \left(\frac{0.618\, k^{1/0.618}}{\bar{h}_o\, r_c^{0.382}} \right) \qquad (2.8)$$

Of course, as in the simpler derivation, cognizance of the peripheral variation of h_o cannot be taken and the average value is used.

It is to be noted that the value of the critical radius predicted by equation (2.8) is smaller than that given by $(k/\bar{h}_o)$. It does show that where there is a marked variation in the thermal conductivity of the fouling deposit and its peripheral disposition, this gives rise to significant variations of thermal performance.

2.2.3 Calculation Procedure

To obtain results two computer programmes were applied based on an iteration programming as seen in Appendix A. In the case of concentric fouling, the two dimensional conduction equation in cylindrical co-ordinates has been applied as:

$$\nabla^2 T = \frac{\partial^2 T}{\partial r^2} + \frac{1}{r}\frac{\partial T}{\partial r} + \frac{1}{r^2}\frac{\partial^2 T}{\partial \theta^2} = 0$$

As part of the program development, and to test the calculation procedure and its accuracy, the external surface temperature was made constant and equal to the stream temperature T_G corresponding to infinite h_o. In this situation $(\partial^2 T/\partial \xi^2)=0$ (there being no dependency on η) and T is linear in ξ, as;

$$T = T_1+(T_G - T_1)\frac{\xi-\xi_1}{\xi_O-\xi_1} \tag{2.9}$$

If in the calculation $\Delta\xi$ is made constant, then the corresponding ΔT must also be constant. A further check on accuracy may be made by evaluating both the convective heat transfer and conduction heat transfer at the external interface. These should balance when:

$$\sum_i h_{oi}(T_G-T_{\xi_o})_i=k\sum_i(\frac{\Delta T}{\ell_i\Delta\xi}) \tag{2.10}$$

where ℓ_i is the local metric coefficient, the summation being made around the boundary. With regard to critically examining the calculation using bipolar coordinates for accuracy, progressive reduction of the eccentricity to zero should lead to a result consistent with that using polar coordinates r, θ. Furthermore, if a constant value of h_o is imposed on the external surface then the result should correspond with the familiar text book result for axisymmetric heat conduction through the insulation:

$$Q = \frac{(T_G - T_1)}{\frac{1}{\bar{h}_o \pi d_o}+\frac{\ln(d_o/d_1)}{2\pi k}} \tag{2.11}$$

When the flow is in the direction θ, (the most general case), then the calculation must be carried out over the whole domain (i.e. the symmetry about the x-axis will be lost). Now equation (2.2) is a second-order differential equation and the 4 boundary conditions (two in ξ and two in η) are furnished by (i) to (iii), advantage being taken of the symmetry at θ =

0 and $\theta = \pi$. In the whole domain the boundary conditions (ii) and (iii) still pertain and the boundary conditions in η are automatically incorporated by continuity at any η line. Accordingly, special provision for η in this respect need not be made.

In the following section, typical results are presented in graphical form.

2.2.4 Results and Discussion

To quantify the effects of fouling on the thermal performance of a single tube in cross-flow, calculations have been made for a wide range of fouling geometry and thermal conductivity following the procedure described in the previous section. The heat flow is measured relative to that of a clean tube of diameter 0.016 m in an air cross-flow of 5 m/s corresponding to a Reynolds number equal to 4,400 (based on the clean tube diameter). The gas temperature is 373 K and the inner wall temperature is 283 K. Thermal conductivity values for the foulant were varied between 0.2 and 2.0 W/m K. These reflect the typical values of k for loose deposits and slagging deposits respectively, Anderson et al.(1987). All the results were obtained using a 20 x 20 grid although other mesh sizes were explored. The peripheral distribution of heat transfer coefficient for the base-case, (i.e. the clean tube), can be seen in Figure 2.2. It was obtained from experimental data given in the literature (Giedt, 1949 and Eckert and Soehngen,1952) adjustment being made to the values as outlined in section 2.2.2

A selection of the results are presented in Figures 2.3 to 2.7. In Figure 2.3 the effect of variation of the thermal conductivity is shown for given outside diameter or eccentricity of fouling. Not surprisingly, increase in k leads to an increase in heat transfer for both

geometries shown. However, as indicated the heat transfer rate is increased when the fouling is concentrated downstream. This is accountable to the greater asymmetry of conjugated convective and conductive resistance, as the fouling is deposited in the region of smaller heat transfer coefficient. Another noteworthy point is the fact that for thermal conductivities greater than about 0.4 and 0.6 for the two cases, the heat transfer increases above that for a clean tube, even though the surface is fouled. This reflects the concept of the critical radius which was discussed earlier in section 2.2.2. Thus it is clearly demonstrated in Figure 2.3 that fouling can actually increase the rate of heat transfer under certain conditions, governed mainly by the thickness of the deposit and its thermal conductivity.

Figure 2.4 likewise refers to the case when r_o = 0.011 m, but here the effect of asymmetry of fouling is investigated with k chosen equal to 0.5 W/m K. The results presented in Figures 2.3 and 2.4 are consistent as a critical examination will indicate. In Figure 2.4, the eccentricity or asymmetry varies continuously and again greater heat transfer occurs with the fouling concentrated near the rear stagnation point. The result for the concentric case has been identified because this value may be determined using a separate program employing polar coordinates. It is clearly seen that the result is compatible with interpolated values for the eccentric geometry.

At this point, it is important to again mention the "critical radius" in connection with the results for changing outer diameter and thermal conductivity. This matter was particularly addressed in section 2.2.2 where a revised analysis was presented to incorporate the variation of external heat transfer coefficient which is normally assumed constant but which actually

changes with diameter. These considerations are relevant when the case of increasing fouling thickness is investigated as demonstrated in Figure 2.5.

Figure 2.5 shows the effect on heat transfer of varying the outside diameter (and hence h_o) with simultaneous change in the eccentricity. Again the results for the concentric cases feature in the plot; furthermore, the data match those in Figure 2.4 since the same value of k equal to 0.5 W/m K was chosen. The most interesting characteristic of the graph is shown by the constant external radius lines, which indicate that as r_o increases the heat transfer rate diminishes. Referring to the "critical radius" comments, it is evident that the radii considered here exceed the critical radius particularly when this is determined by the result of the extended analysis in section 2.2.2. Of course, the model does not cater for the asymmetric heat flow but it serves as a guide in this matter.

In practice, fouling density and hence thermal conductivity may vary. As a contribution to an understanding of the result of this effect, the domain of integration was subdivided into two regions as illustrated in Figures 2.6 and 2.7. In Figure 2.6, a region of large k (2 W/m K) was located adjacent the tube with a small k material (0.2 W/m K) outside. This represents the case, which is often found in practice, where the deposit closer to the surface is more dense. The geometry is fixed as indicated. The heat transfer is plotted versus the extent of the domain using the bipolar coordinate, ξ, for convenience. Once more, the behaviour concerning increase in thermal conductivity (Figure 2.3) and the effect of the disposition of the fouling are repeated. Extrapolation of the two curves A and B to values of $(\xi_n - \xi_o)/(\xi_1 - \xi_o)$ corresponding to 0 and 1 give results for the heat transfer rates

corresponding to the uniform thermal conductivity cases shown in Figure 2.3, again confirming the consistency in the calculations.

The effect of circumferential variation of thermal conductivity, particularly associated with cross-flow deposition of foulant, may be studied by dividing the foulant cross-sectional area using the η co-ordinate as shown in Figure 2.7. A selected number of geometries has been investigated. The data for $\eta = 0$ and $\eta = \pi$ match exactly the values shown in Figure 2.3 for k = 0.2 W/m K and k = 2 W/m K respectively, again showing the consistency of the results of the calculation procedure. The variation of heat transfer Q over the whole spectrum is of the order of approximately ± 25%, this being attributable primarily to the variation of the thermal conductivity as reflected in Figure 2.3.

More accurately, the thermal conductivity of the foulant varies continuously across the domain, and provided it is only dependent on the spatial co-ordinates, then it is a simple matter to extend the accuracy of the variable conductivity prediction. However, in the absence of detailed information on the distribution of k representing real situations, such an enquiry is not warranted at this stage

2.2.5 Conclusion

Finally, this theoretical investigation of fouling in cross-flow has indicated that there is a significant dependence (as far as heat flow is concerned), on the disposition of the deposit around the tube and the spatial variation of its thermal conductivity. However, a general conclusion concerning the absolute change of heat transfer rate with respect to the clean tube

performance cannot be made because of the large number of interdependent parameters involved. The results of the investigation show the trends brought about by the variation of the geometry and the thermal properties of the foulant on the tubes of a cross-flow heat exchanger.

2.3 Calculation of Coupled Convection and Conduction Heat Transfer Using The Point-Matching Method

2.3.1 Introduction

Steady conjugated convection and conduction heat transfer occurs in many engineering processes and underlying principles are well-known and fully documented. The essential feature of this coupling between the energy transfers at a fluid-solid interface is the balance between the convected energy in the fluid with the thermal conduction in the solid at all points along the interface. At the interface heat flows only by conduction, the rate of heat flow can be calculated and related to the heat transfer coefficient and the temperature gradient at the wall, then we can obtain:

$$q_{surface-fluid} = -k\frac{dT}{dx} = h(T_s - T_\infty)$$

This is the so called Newton Boundary condition and of course, may occur in conjunction with specified temperature (Dirichlet) and specified heat-flux conditions (Neuman) over other parts of the boundary of the conduction domain. The general two dimensional situation is depicted diagrammatically in Figure 2.8(a), while Figure 2.8(b) shows the more familiar one dimensional counterpart, viz. the plane wall, for which a simple

analytical solution is available. A typical two-dimensional engineering problem is also given in Figure 2.8(c) and refers to a hot gas in flow across a tube with variable thickness fouling. Now the general thermal problem is the determination of the temperature field and hence heat transfer for the prescribed boundary conditions, and while this may be effected analytically in many cases, it is frequently necessary to resort to standard finite difference or finite element methods. The problem displayed in Figure 2.9, for example, has been solved by a finite difference method in the previous section, using the bi-polar co-ordinate system for the discretization of the idealised eccentric-annular domain. Mixed Dirichlet and Newton boundary conditions were imposed in keeping with realistic conditions for this situation. On the inner boundary it was assumed that the temperature was known, (the Dirichlet condition), and that the peripheral variation of the heat transfer coefficient h was also known on the outer surface (the Newton condition). It is clear that the finite difference method suffices with simple geometries but that alternative methods may be required when more irregular shapes are encountered, as for example in very non-uniform ice deposition. In this connection the work of Cheng, et al.(1981) is particularly valuable, since they employed a point-matching method in their theoretical considerations of the energy transfers in a variable thickness ice-layer on a tube in cross flow. The essentials of the point-matching procedure are best understood by considering first the simple conjugated heat transfer problem of the plane wall shown in Figure 2.8(b), and the formulation of its exact mathematical solution.

2.3.2 Point-Matching Method

With the mixed Dirichlet and Newton boundary conditions as indicated, and in the notation shown in Figure 2.8(b), integration yields:

$$T=ax+b \text{ (where a,b constants)}$$

$$\text{with, (i) } T=T_1 \text{ at } x=0, \text{ the Dirichlet condition} \qquad (2.12)$$

$$\text{and , (ii) } -k(dT/dx)_l = h\,(T-T_\infty) \text{ at } x=l, \text{ the Newton condition}$$

Here the matching aspect of the problem is basically the fitting of the boundary conditions. In this very simple illustration this presents no difficulty and results in the familiar linear relationship for the temperature in the solid. In effect, the relative magnitudes of the internal and external resistances dictate the value of the uniform temperature on the Newton boundary. However, had h been a point function, then it would become necessary to effect this matching at a sufficient number of variable temperature points along the Newton boundary. Of course the relevant starting point is then:

$$\nabla^2 T=\left(\frac{\partial^2 T}{\partial x^2}+\frac{\partial^2 T}{\partial y^2}\right), \text{ since } T=T(x,y)$$

and the point matching involves the evaluation of the integration constants of the general solution of the Laplacian corresponding to that for the simple one-dimensional model given in equation (2.12). This will become more evident as particular problems are considered. The important point to make at this stage is that in the point-matching method, the general solution for the temperature is first obtained from a solution of a set of linear equations which result from the imposition of the boundary conditions at a number of points.

To investigate the method further the real problem described in the previous section will be considered since the finite-difference results from that enquiry may then serve as a

yardstick for comparison. Furthermore, as shown in Figure 2.8(b), realistic mixed boundary conditions have been employed and so the usefulness of the method in these circumstances may also be studied. It is to be noted that the work of Cheng et al.(1981), pertain to the Dirichlet problem consistent with known temperatures on the interface of the ice-layer, and the tube and that their objective was the determination of the local external heat transfer coefficient, h_o. In the present case the converse problem is first explored, the variation of h around the external interface being prescribed and then the boundary temperature determined. The main steps in the calculation procedure are now outlined.

2.3.3 Cross-flow with Non-Uniform Fouling

The properties of this system are written in the present case as described below (Hildebrand,1976). In the notation listed in Figure 2.9, using polar coordinates, the Laplace equation is written as:

$$\nabla^2 T = \frac{\partial^2 T}{\partial r^2} + \frac{1}{r}\frac{\partial T}{\partial r} + \frac{1}{r^2}\frac{\partial^2 T}{\partial \theta^2} = 0 \qquad (2.13)$$

By applying the method of separation of variables which consists of particular product solutions that are written as:

$$T(r,\theta) = R(r)\ \Theta(\theta) \qquad (2.14)$$

Here R is a function of r alone and Θ is a function of θ alone. Combining equation (2.14) with (2.13) then it follows:

$$\frac{d^2R}{dr^2}\Theta+\frac{1}{r}\frac{dR}{dr}\Theta+\frac{1}{r^2}R\frac{d^2\Theta}{d\theta^2}=0 \qquad (2.15)$$

To separate variables of equation (2.15), it is multiplied by r^2 and divided by Θ and it can be written as:

$$\frac{1}{R}\left(r^2\frac{d^2R}{dr^2}+r\frac{dR}{dr}\right) = -\frac{1}{\Theta}\frac{d^2\Theta}{d\theta^2} = n^2 \qquad (2.16)$$

The quantity n is called a separation constant. Equation (2.16) implies two ordinary equations:

$$r^2\frac{d^2R}{dr^2}+r\frac{dR}{dr}-n^2R=0$$
$$\frac{d^2\Theta}{d\theta^2}+n^2\Theta=0 \qquad (2.17)$$

General solution of equation (2.17) and the general solution of T is given by Hildebrand (1976), as:

$$R=a_n r^n+b_n r^{-n} \quad (n\neq 0)$$
$$R=a_o+b_o \mathrm{Log} r \quad (n=0) \qquad (2.18)$$

and

$$\Theta=c_n \mathrm{Cos}(n\theta)+d_n \mathrm{Sin}(n\theta) \qquad (n\neq 0)$$
$$\Theta=c_o+d_o\theta \qquad (n=0) \qquad (2.19)$$

and T is given as:

$$T = a_o + b_o \ln r + \sum_n [(a_n r^n + b_n r^{-n}) \cos(n\theta) + (c_n r^n + d_n r^{-n}) \sin(n\theta)] \quad (2.20)$$

If we restrict the problem to symmetrical condition about the horizontal ($c_n=d_n=0$) and when a Newton boundary condition is applied to the outside surface and a Dirichlet boundary conditions is applied at the inlet surface of tube ($a_o=0$, $a_n=-b_n$) then equation (2.20) can be written as:

$$t = b_o \ln R + \Sigma_{1,2,..} a_n (R^n - R^{-n}) \cos(n\theta)$$

$$\text{with;} \quad t = \frac{T_2 - T_1}{T_\infty - T_1}; \quad R = (r/r_1) \quad (2.21)$$

Applying the boundary conditions:

(i) at R=1, t=0

(ii) at $R=R_2$ then

$$-h_\theta (T_2 - T_\infty) = k(T_\infty - T_1)\left[\frac{dt}{dZ}\right]_{R_2}$$

This incorporates the Dirichlet boundary condition, viz. t=0. Now on the Newton boundary, where h is known,

$$t_2 = 1 - \frac{k}{h}\left[\frac{\partial t}{\partial n}\right]_N \quad (2.22)$$

(It is important to emphasise at this point that h is always defined in terms of the normal component of the flux at the interface).

Accordingly, equation (2.22) may be applied at selected points around the boundary N. Furthermore in the present case, the normal gradient ($\partial t/\partial n$) may be related analytically to the radial and peripheral temperature gradients through the eccentric annular geometry. Finally combining equation (2.21) and (2.22) results in:

$$1=b_0\left[\ln R_2+\frac{k}{hr_1}\frac{\cos(\theta-\alpha)}{R_2}\right]+\sum a_n\left[(R_2^{n}-R_2^{-n})\right.$$
$$\left.\left(\cos(n\theta)+\frac{\sin(\theta-\alpha)kn\sin(n\theta)}{hr_1R_2}\right)+\frac{k\cos(\theta-\alpha)}{hr_1}(nR_2^{n-1}+nR_2^{-n-1})\cos(n\theta)\right] \quad (2.23)$$

Equation (2.23) is now used at a number of peripheral locations and its solution for b_0 and the values for a_n effected numerically. The dimensionless temperature t is then determined from equation (2.21). Calculations were made for n=10, 20, 30 and it was decided that n=20 was adequate. To investigate the numerical effect on the values of a_n and b_0 of how many points, n, were used, a critical examination was carried out as described in the following section.

If required, the total heat transfer may be calculated by integrating the internal flux around the interface: This of course, should equal the conjugated convection heat transfer calculated using the local heat transfer coefficients and the corresponding external temperature differences.

2.3.4 An Examination of the Accuracy of Point-Matching Method

Here, the theoretical results for two dimensional conduction are compared with those

obtained using the point-matching method. If we consider two-dimensional heat conduction in a rectangular plate as shown Figure 2.10, the Laplace equation can be written as:

$$\nabla^2 T=\left(\frac{\partial^2 T}{\partial x^2}+\frac{\partial^2 T}{\partial y^2}\right)=0 \tag{2.24}$$

Obtaining boundary conditions from Figure 2.10, then the general solution of temperature is given as a series solution;

$$T=\sum a_n \frac{\mathrm{Sin}\left(\frac{n\pi x}{a}\right)\mathrm{Sinh}\left(\frac{n\pi (b-y)}{a}\right)}{\mathrm{Sinh}\left(\frac{n\pi b}{a}\right)} \tag{2.25}$$

$$a_n=\frac{2}{a}\int_0^a f(x)\,\mathrm{Sin}\left(\frac{n\pi x}{a}\right)dx$$

With equation (2.25) the values of a_n may be evaluated, if f(x) is known. In this section f(x) is chosen as f(x)=(x/a)100 for $0 < x < a$ then the values of a_n are calculated both analytically and by the point-matching method. As can be seen Figure 2.10 calculation has been carried out using the point matching method using a different number of point along the (0→a) direction i.e. 3, 9, and 19. Results show that increasing number of point along the (0→a) direction brings the numerical calculations closer to the analytically obtained results.

2.3.5 Newtonian Boundary Conditions

In the most general case, Newtonian boundary conditions with different convective

heat transfer coefficients over parts of the boundary occur. If the same geometry as employed in Figure 2.9 is considered but now with an internal fluid at temperature T_s and convective coefficient h, then the following relationships corresponding to these given in the section 2.3.3 dealing with cross-flow with non-uniform fouling pertain:

$$t=a_o+b_o\ln R+\sum_{0}^{\infty}(a_n R^n+b_n R^{-n})\cos(n\theta) \tag{2.26}$$

$$t=\left(\frac{T-T_s}{T_\infty-T_s}\right) \quad ; \quad R=(r/r_1) \tag{2.27}$$

$$t_2=1-\frac{k}{h_2}\left[\frac{\partial t}{\partial n}\right]_{R_2} \quad ; \quad t_1=\frac{k}{h_1 r_1}\left[\frac{\partial t}{\partial R}\right]_{R_1} \tag{2.28}$$

Again relating $\partial t/\partial n$ at the outer boundary to radial and peripheral temperature gradients there, then after some algebra, the following equations result. On the outer boundary :

$$\begin{aligned} 1=&a_o+b_o\left(\ln R_2+\frac{k\cos(\theta-\alpha)}{h_2 r_1 R_2}\right) \\ &\vdots \\ &+\sum a_n\left(\frac{k\cos(\theta-\alpha)\cos(n\theta)(nR_2^{n-1})}{h_2 r_1}+\frac{k\sin(\theta-\alpha)\sin(n\theta)(nR_2^{n})}{r_1 R_2 h_2}+R_2^{n}\cos(n\theta)\right) \\ &\vdots \\ &-\sum b_n\left(\frac{k\cos(\theta-\alpha)\cos(n\theta)(nR_2^{-n-1})}{h_2 r_1}-\frac{k\sin(\theta-\alpha)\sin(n\theta)(nR_2^{-n})}{h_2 r_1 R_2}-R_2^{-n}\cos(n\theta)\right) \end{aligned} \tag{2.29}$$

While for the inner boundary,

$$0=a_o-\frac{b_o k}{h_1 r_1 R_1}+\sum a_n\left(1-\frac{kn}{h_1 r_1}\right)\cos(n\theta)+\sum b_n\left(1+\frac{nk}{h_1 r_1}\right)\cos(n\theta) \qquad (2.30)$$

Of course if h_1, the internal coefficient, is very large, then $T_1 \rightarrow T_s$ and equation (2.30) reduces to:

$$0=a_o+\sum (a_n+b_n)\cos(n\theta) \qquad (2.31)$$

This is of course, exact correspondence with the result of the internal Dirichlet condition of the earlier analysis (equation 2.21). Furthermore, if h_2 is very large, then from (2.29)

$$1=b_o \ln R_2+\sum_0^{\infty} a_n\left(R_2^{\,n}-R_2^{\,-n}\right)\cos(n\theta) \qquad (2.32)$$

which (remembering that $T_2 \rightarrow T_\infty$) is in agreement with equation (2.21). In other words, the result for the most general analysis is in accord with that for mixed Dirichlet and Newton boundary conditions.

2.3.6 The Concentric Tube Geometry

It is easy to demonstrate that the results for the eccentric annular geometry with varying convective heat transfer coefficients concur with the simple axisymmetric case for the radial heat flow in the tube. Of special interest however is the case of the axisymmetric geometry in the situation of cross-flow with h varying peripherally. This problem is frequently encountered in the laboratory when the local heat transfer coefficient has to be determined from temperature measurements on the outer wall of the tube in cross-flow. The situation is shown diagrammatically in Figure 2.11(a). Now the local heat transfer coefficient distribution

may be determined in three different ways according to the accuracy required. Most simply,

$$h=\frac{Q}{2\pi r_2(T-T_\infty)} \tag{2.33}$$

where T is the local temperature. This assumes that the surface heat flux is uniform.

The second method recognises the peripheral heat conduction but assumes that T is a function of θ only, then an energy balance can be obtained in the working domain:

$$\frac{Qr_1 d\theta}{2\pi r_1} - \frac{k\delta dT}{r_2 d\theta} = hr_2 d\theta(T_s - T_\infty) - \frac{k\delta}{r_2}\frac{d}{d\theta}(T+\frac{dT}{d\theta}d\theta) \tag{2.34}$$

Rearranging equation (2.34) the heat transfer coefficient is written as;

$$h=\left(\frac{Q}{2\pi r_2(T-T_\infty)}\right)+(\frac{k\delta}{r_2^2})\frac{1}{(T-T_\infty)}\frac{d^2T}{d\theta^2} \tag{2.35}$$

h may then be determined numerically from the measured power input Q and the curvature of the peripheral temperature profile. The smaller the thickness, the closer does this value approach that given in equation (2.33). Finally the full calculation using the previously described point-matching method may be employed. This recognises the complete two dimensionality aspects of the heat conduction problem. Again, beginning with the Laplacian in polar coordinates, the temperature boundary conditions, (Dirichlet condition), need to be imposed on both surfaces. The external values were determined from experiment in the usual way for a given experimental power input and temperature measured with a thermocouple.

Initially the inner value of temperature is unknown and so an arbitrary figure is chosen to effect the calculation. Proceeding in the usual way, the values of h are determined and hence the heat transfer. This in turn may be adjusted until agreement with the experimental power is achieved.

To demonstrate this procedure, a realistic temperature profile has been chosen for a concentric geometry in cross-flow and h has been calculated following the three methods outlined above. These distributions of h are shown plotted in Figure 2.11(b). The averaged values according to the three different methods of calculation are 36.47 W/m^2K, 36.45 W/m^2K and 41.91 W/m^2K, respectively. The difference between the values according to equations (2.33) and (2.35) is negligible and is accounted for by the small variation of the chosen surface temperature distribution. In the experimental procedure, a mild steel tube was used to determine temperature distribution around the body. A copper constantan thermocouple had been soldered externally. However, to obtain better results (to read temperature differences in angular positions) a tube material could have been chosen with low conductivity; also the thermocouple could have located just below the surface. Therefore as can be seen in Figure 2.11(b) the value obtained using the point-matching method is significantly different indicating that caution needs to be exercised in determining average heat transfer rates in experiments.

2.3.7 Average Heat Transfer Coefficient, $\bar{h}$

A useful engineering parameter for measuring the overall thermal performance in conjugated convection and conduction heat transfer, is the average heat transfer coefficient $\bar{h}$ and it is of paramount importance that its meaning is fully appreciated. $\bar{h}$ may be defined as:

$$\frac{1}{\pi}\int_0^{\pi} h\,d\theta \quad \text{or as} \quad \frac{1}{\pi(\bar{T}-T_b)}\int_0^{\pi} h(T-T_b)\,d\theta$$

the former being the true mathematical average value. The latter value is based on overall heat transfer and average temperature difference. For the problem studied in the previous section, these have been evaluated as 41.33 W/m^2K and 43.12 W/m^2K respectively when the eccentricity is 0.002m. The interesting point here is that these values are different, the former being smaller than the latter, and this is in accord with the simple analysis of average heat transfer coefficient presented by Barrow (1986), where it is pointed out that when considering numerically predicted average coefficients and experimentally determined values the differences have to be taken into account since a direct comparison is not valid.

2.3.8 Discussion & Conclusions

Using turbulent forced-convection heat transfer in cross-flow over a circular tube as a model, the point-matching method in two dimensions has been used to determine the temperature in the conjugated heat conduction domain. For the special case of non-uniform fouling on the outer surface of the tube, the results have been compared with those obtained using a finite-difference bipolar coordinate procedure described in Section 2.2. In particular, two fouling geometries simulated by eccentric annuli have been examined with mixed boundary conditions appropriate to a real situation. In the point-matching method the polar co-ordinate system was used, while in the finite-difference analysis, bipolar coordinates were chosen to discretize the two-dimensional heat conduction domain.

Typical results for the temperature around the external surface of the fouled-tube in cross-flow are in good agreement as can be seen in Figures 2.12(a)-(d). As shown in Figure 2.9 hot air flows from left to right. Figure 2.12(a) shows the smallest eccentricity case (closest a concentric tube). The front stagnation point temperature is higher than the rear side. Increasing eccentricity causes a temperature drop on the front stagnation point, because the cold surface tube (283 K) becomes closer to the outside surface and the front stagnation point's temperature falls and the rear stagnation rises. When the thermal resistance of the conduction domain decreases, the temperature difference between the outside tube surface and inside tube surface decreases. It is clear in Figure 2.12(d) that at the front stagnation point region, the thickness of the wall is thinner than at the rear side. As expected, smaller temperature differences between the outer and inner surfaces occur at the front region. There are differences between the point-matching and bipolar coordinate methods that may be

considered to be a result of using different sizes of conduction domain. Of special interest is the axisymmetric geometry with peripherally varying heat transfer rate. Here the point-matching method has been used as a yard-stick to investigate the accuracy of various approximate methods for calculating the local heat transfer coefficients from experimentally measured surface temperatures. This part of the investigation showed that considerable error may be involved if the full two-dimensional nature of the heat conduction in the wall is not modelled correctly.

The average heat transfer coefficient in this situation has also been carefully examined. In this connection, distinction needs to be made between the true mathematical average of the local values of heat transfer coefficient along the interface, and an average value based on the quotient of the average surface heat flux and average surface to fluid temperature difference. The present numerical results confirm that, in general, there is a difference between these two values. The difference, in turn, depends on the gradients of both heat flux and temperature difference along the surface.

The point-matching method is not restricted to the solution of the temperature field in heat conduction. It has been used by Cheng et al.(1981), to solve fully-developed laminar forced convection in an eccentric annular channel with uniform heat sources and uniform heat fluxes at both boundaries. There is, of course, no reason why other cases should not be studied, and such an investigation might be a useful extension in the present area of study.

2.4 Concluding Remarks

Fouling represents a major and costly problem for the designers and operators of heat exchangers. The extent of the fouling experienced in particular situations is a complex function of one or any number of factors. Because of the different mechanism involved and the effects of process variables on those mechanisms, it is not possible to offer a general solution to the problem of fouling.

In the present chapter, firstly a theoretical analysis of non-uniform fouling geometry on external surfaces of the heat exchanger tubes in cross-flow has been described. Of course, the nature of fouling on the surfaces is not smooth and thickness of deposition does not have the same geometrical features as modelled in this study. However as useful indication for engineering use, a theoretical model has been developed using an eccentric annulus by using finite difference procedure in bipolar coordinates.

In particular, it has been demonstrated that:

(i) As for the axi-symmetric case, the heat transfer rate for the asymmetrically fouled tube may increase or decrease depending on the geometry and thermal conductivity of the fouling.

(ii) For a given mass of fouling, increasing the asymmetry progressively changes the heat transfer , and,

(iii) When the fouling is asymmetric, the heat transfer is greatest when high conductivity fouling is concentrated towards the rear of the tube.

In conclusion it is important to again highlight the fact that fouling does not necessarily lead to a reduction in heat transfer.

In the second stage of theoretical consideration, the point-matching method was employed for the conduction domain to give the general solution for the temperature. The point-matching method provides a simple and straightforward way to obtain numerically a closed form solution for the temperature field. Even with a small number of unknown coefficients, a_n and b_n, this method gives reasonable results. A solution was obtained for a low conductivity variable thickness fouling case and this was compared with that obtained in the first theoretical investigation. Comparisons have shown that in the case of small eccentricity, agreement in the temperature data is better. However increasing eccentricity caused small deviations.

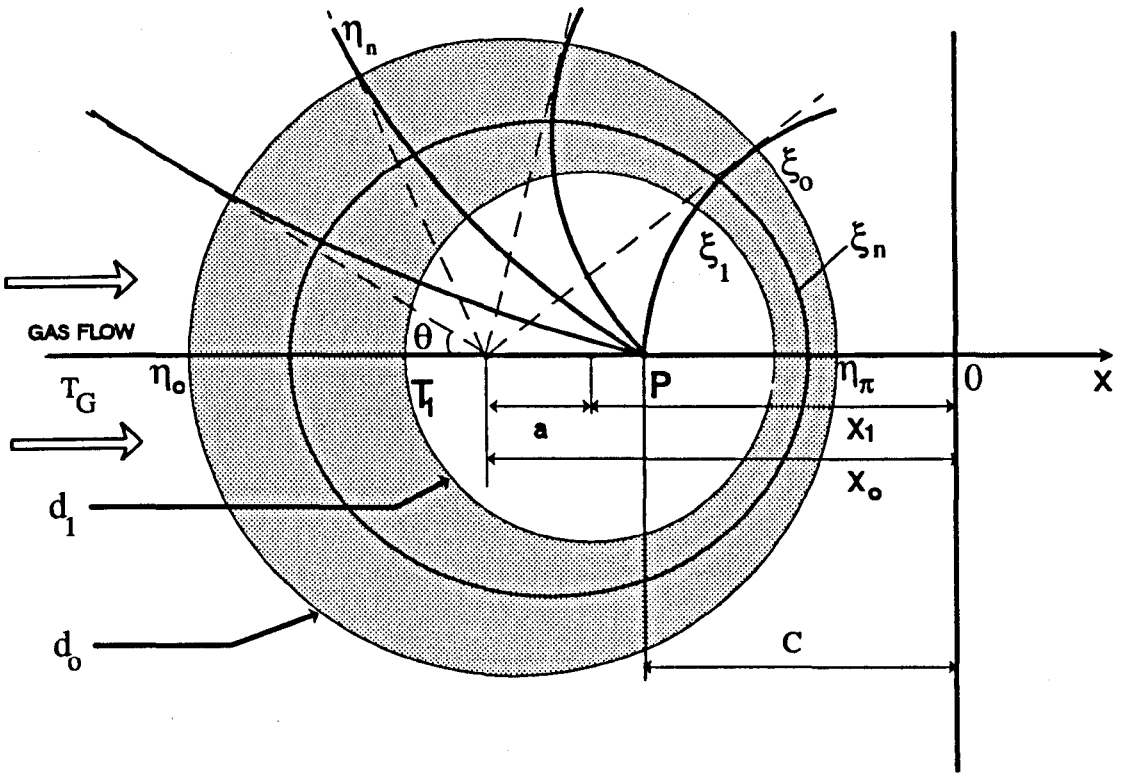

Figure 2.1 Theoretical Model of Bipolar Coordinate System

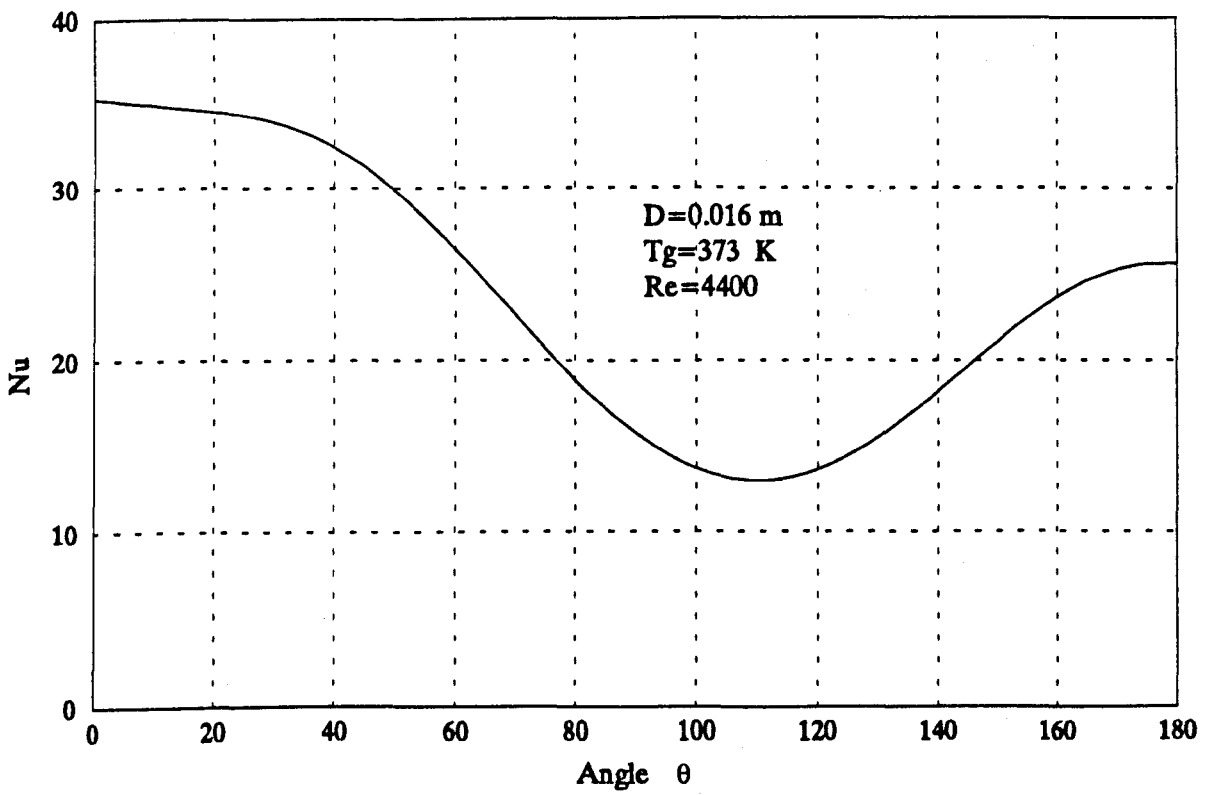

Figure 2.2 Calculated Local Nusselt Number Distribution

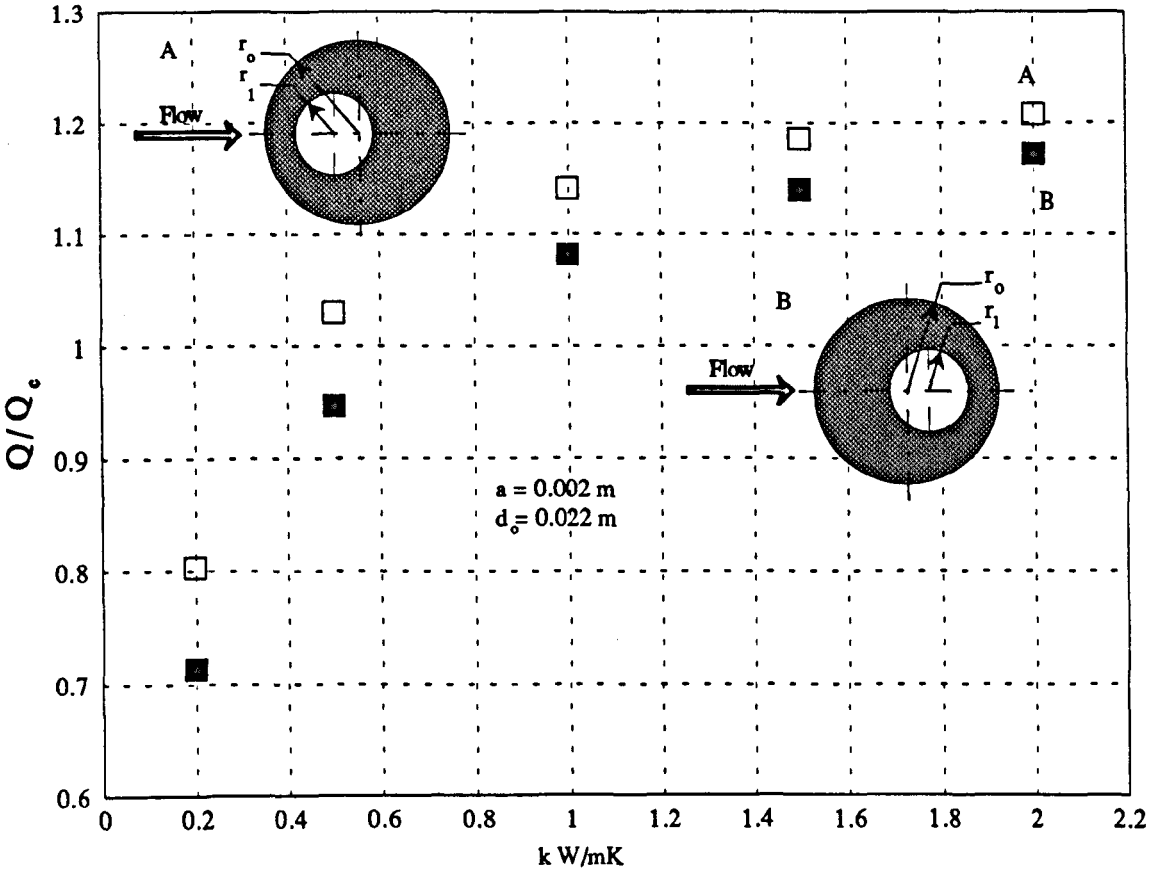

Figure 2.3 Effect of Variable Thermal Conductivity

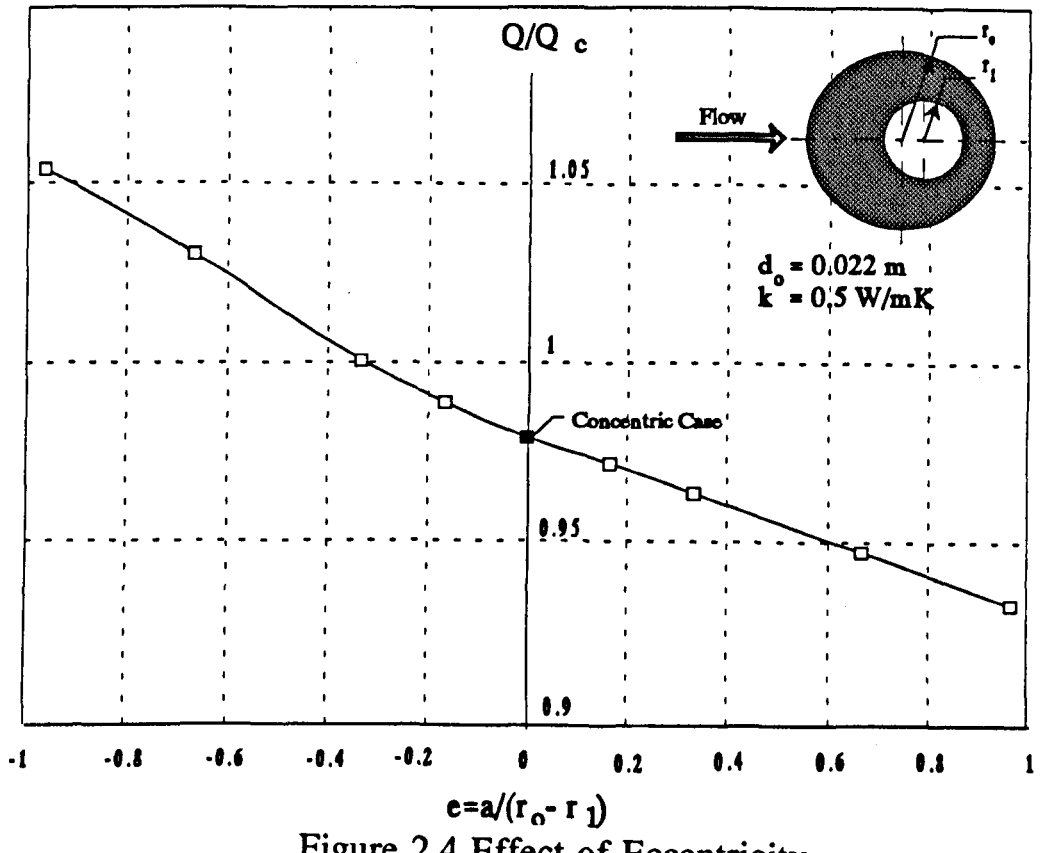

Figure 2.4 Effect of Eccentricity

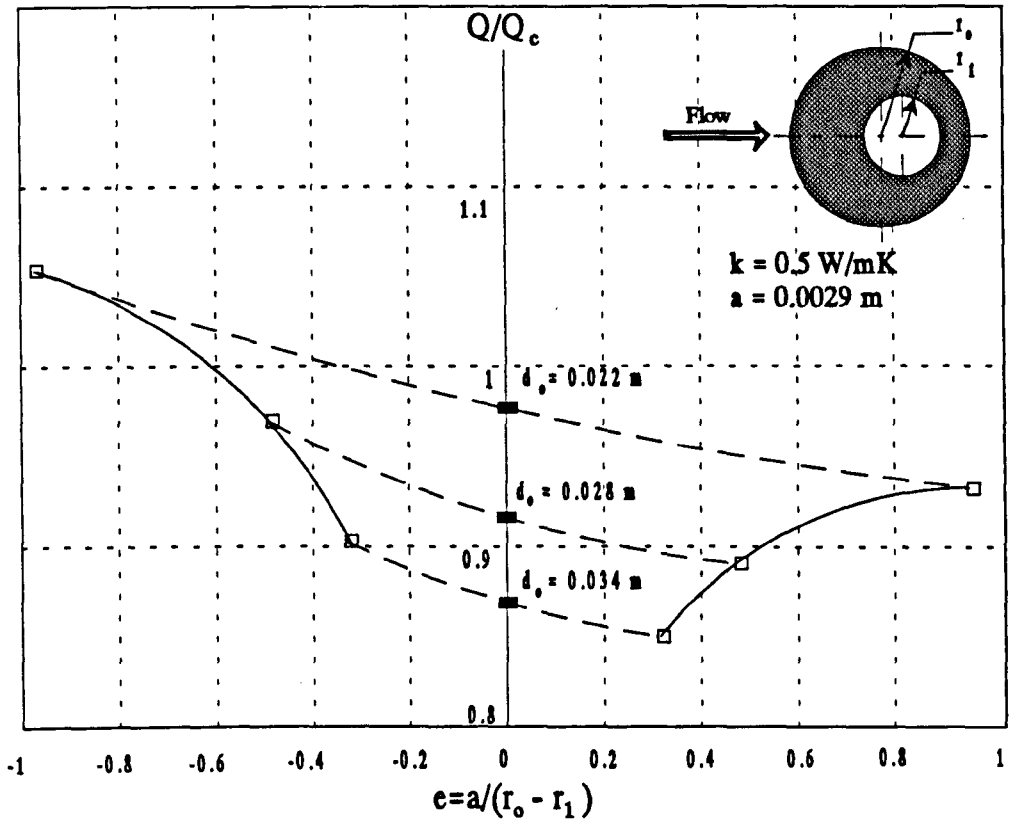

Figure 2.5 Effect of Eccentricity by Varying External Diameter

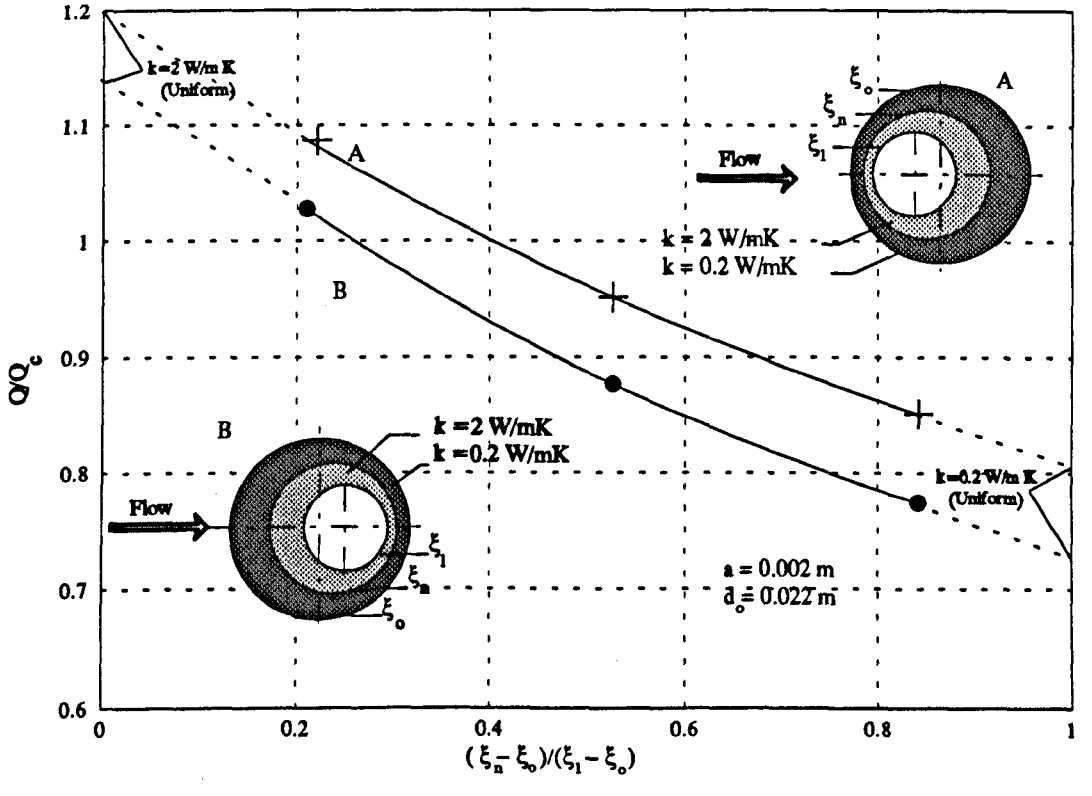

Figure 2.6 Composite Wall-ξ Varying

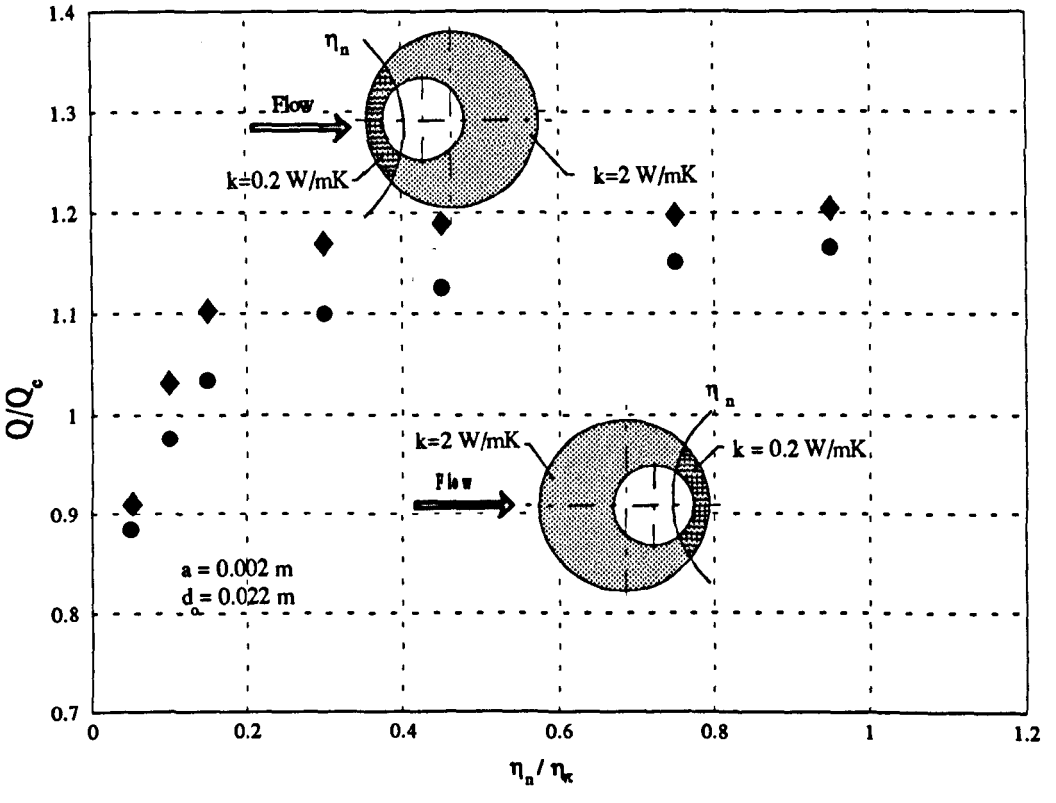

Figure 2.7 Composite Wall-η Varying

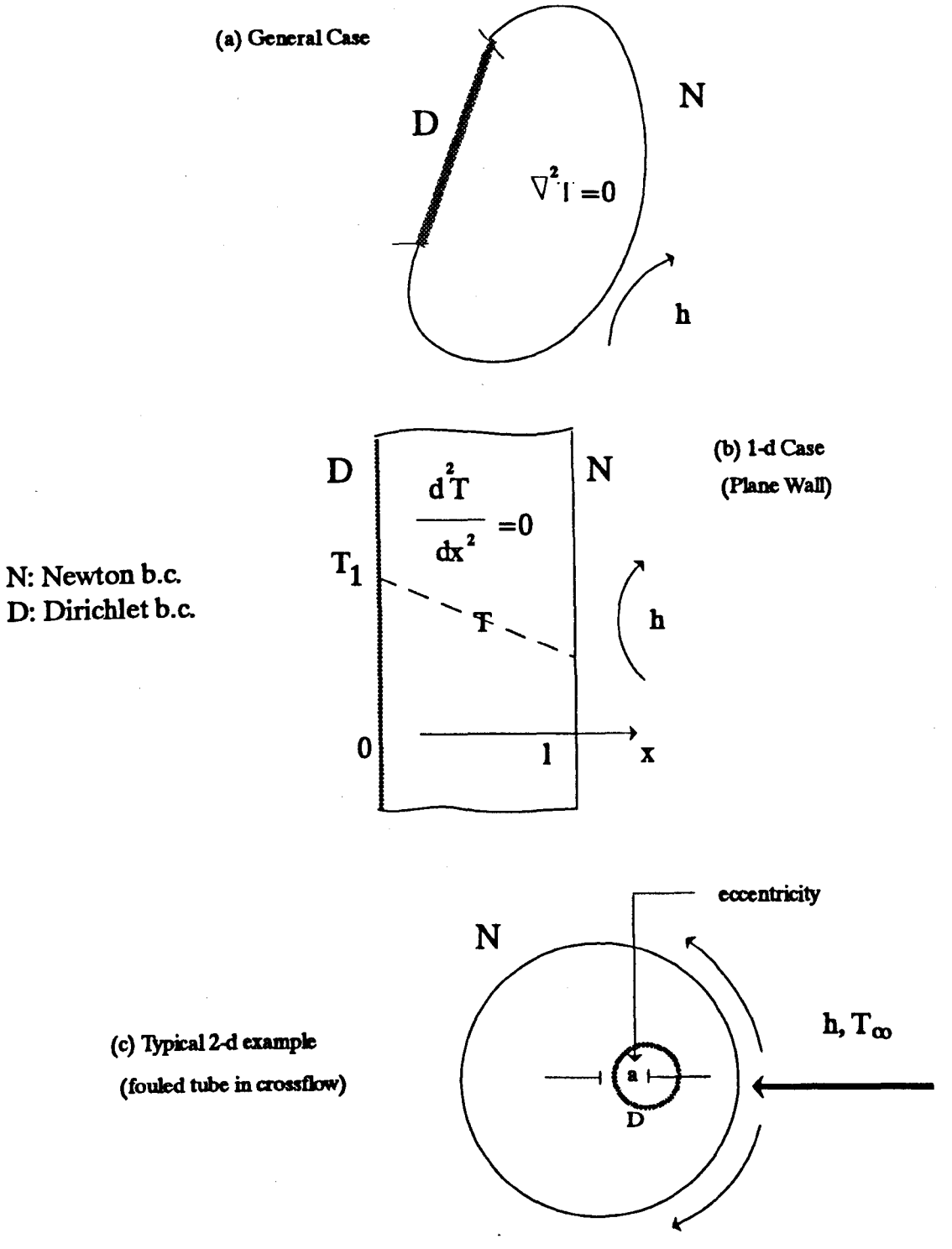

Figure 2.8 Example in Conjugated Conduction&Convection Heat Transfer with Mixed Boundary Conditions

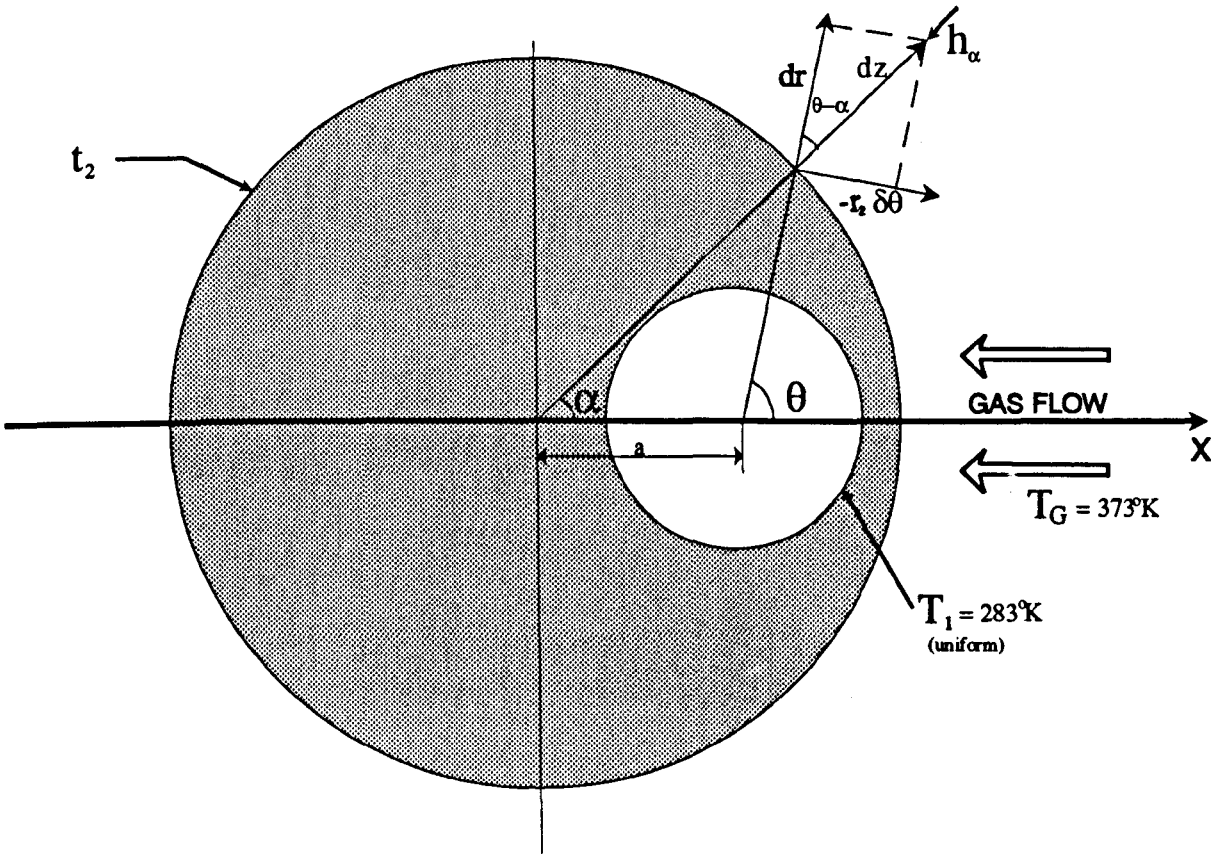

Figure 2.9 Theoretical Model of Point-Matching Method

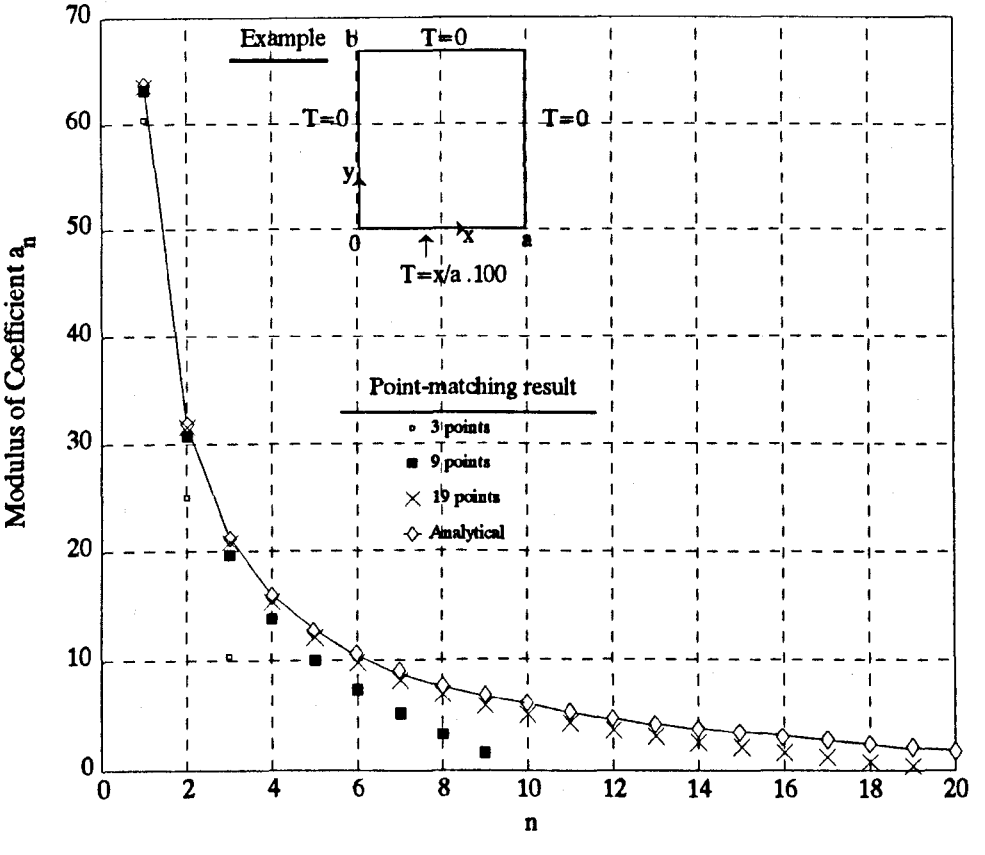

Figure 2.10 Examination of Accuracy of Point Matching Method

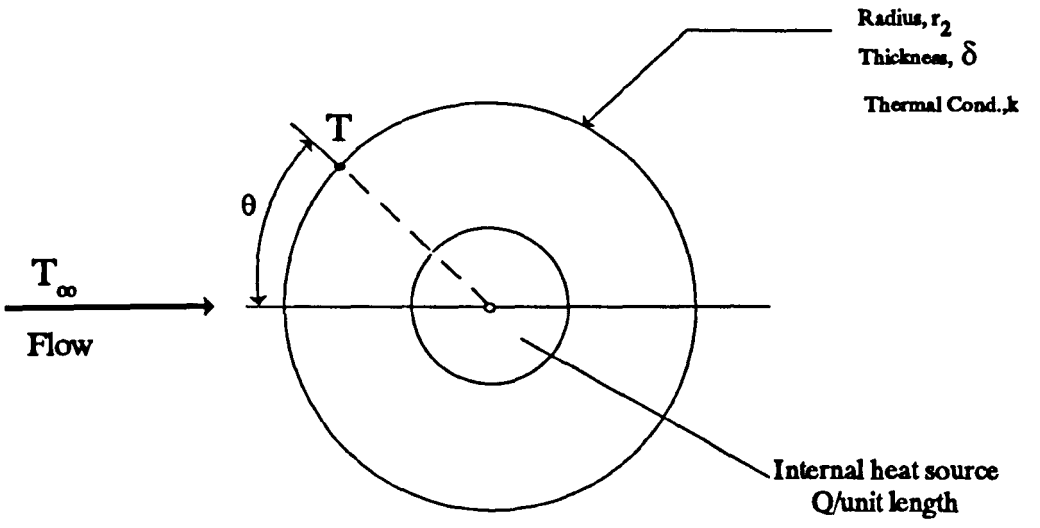

Figure 2.11(a) Cross-flow Over a Constant Thickness Tube

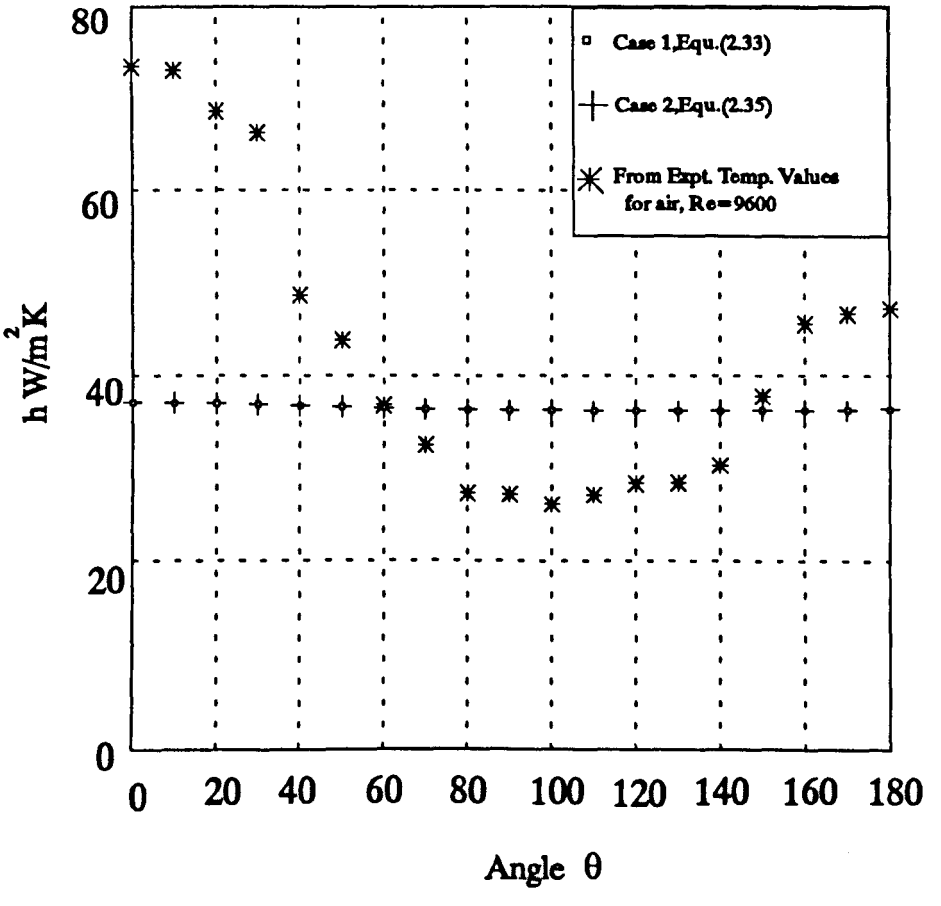

Figure 2.11(b) Heat Transfer Coefficient Distribution

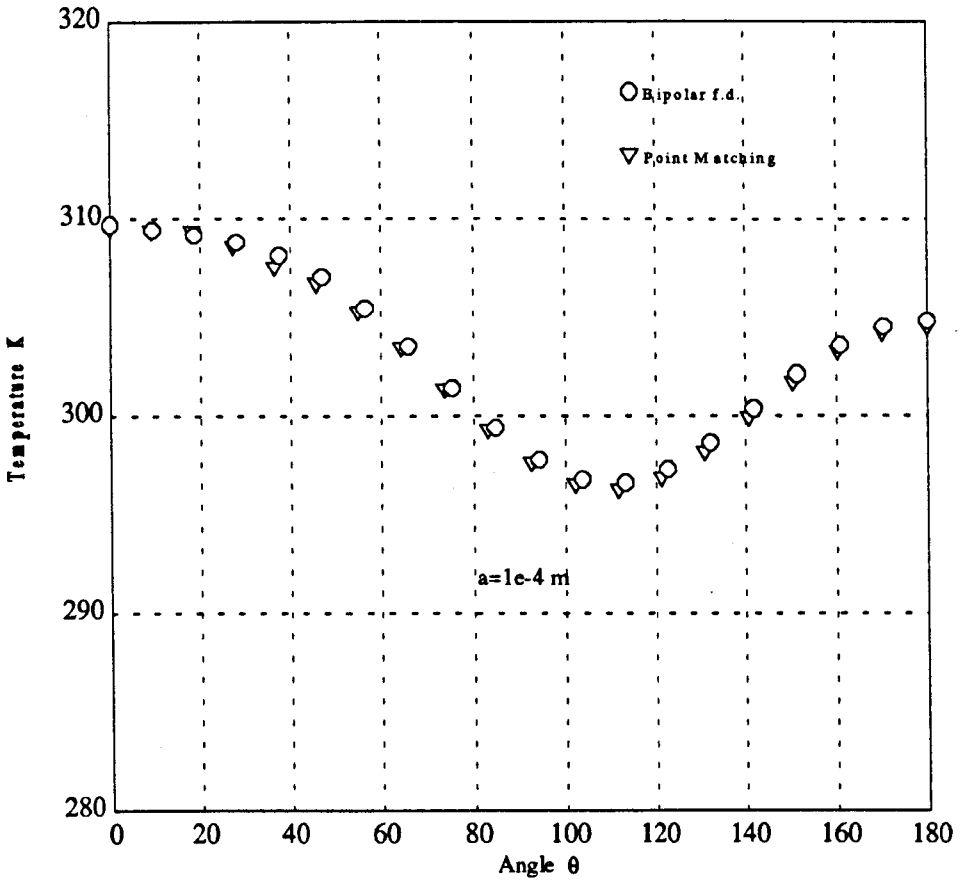

Figure 2.12(a) Temperature Distribution Around the Fouled Tube with a=1e-4

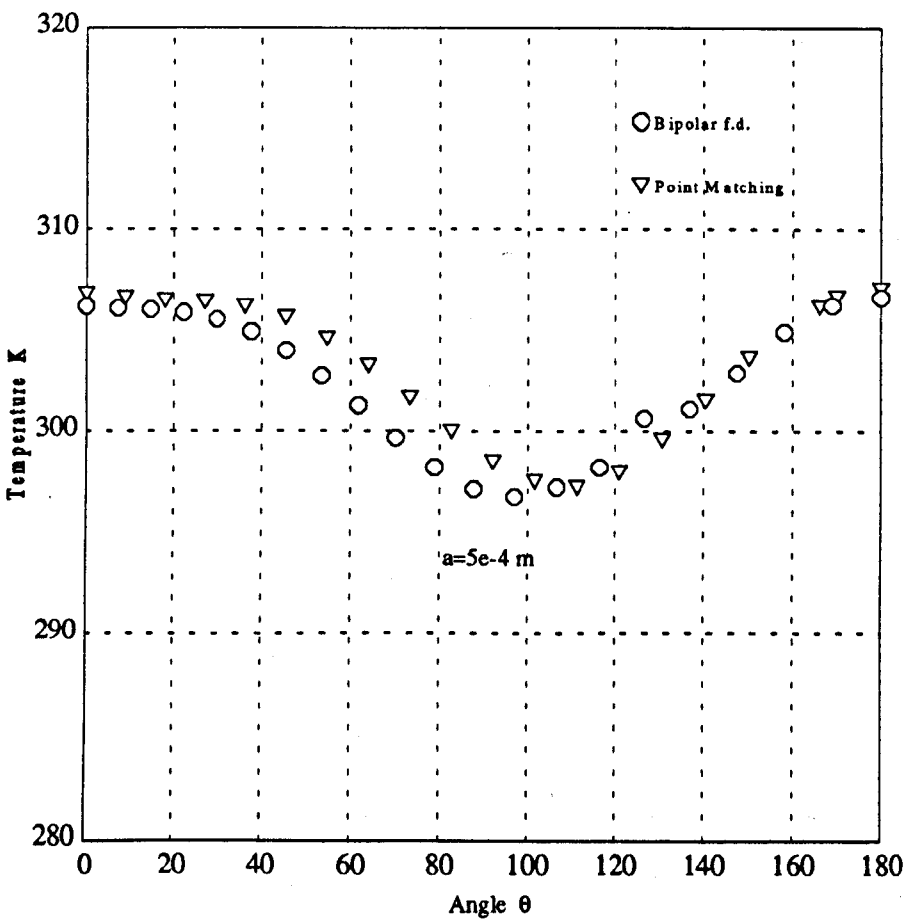

Figure 2.12(b) Temperature Distribution Around the Fouled Tube with a=5e-4

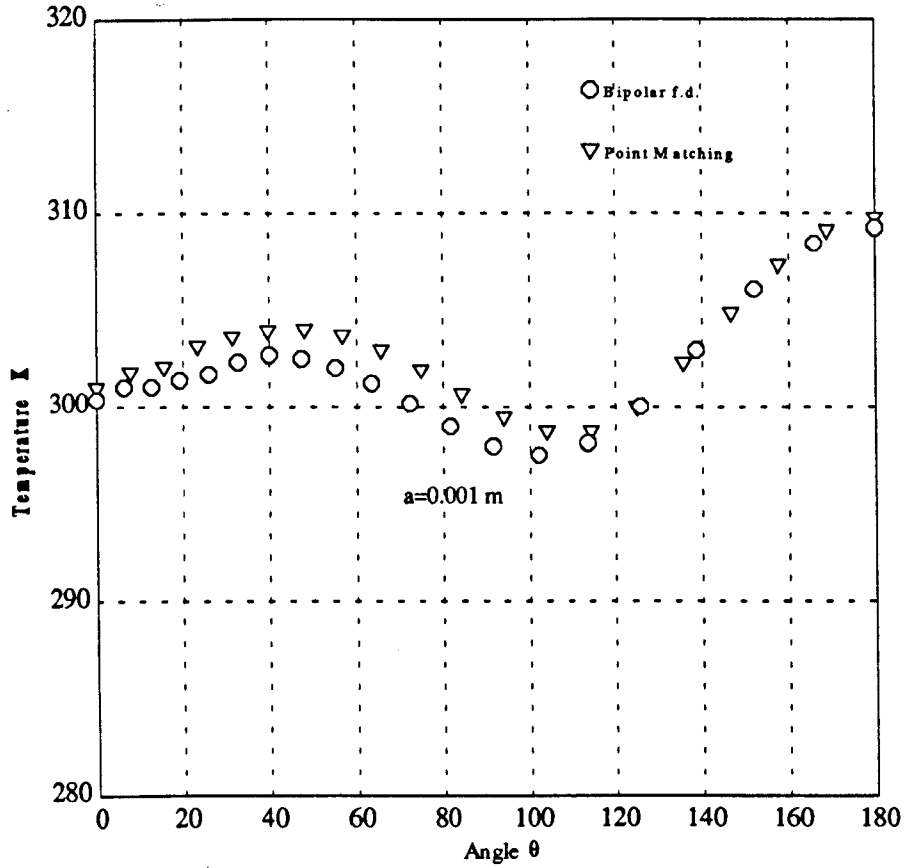

Figure 2.12(c) Temperature Distribution Around the Fouled Tube with a=1e-3

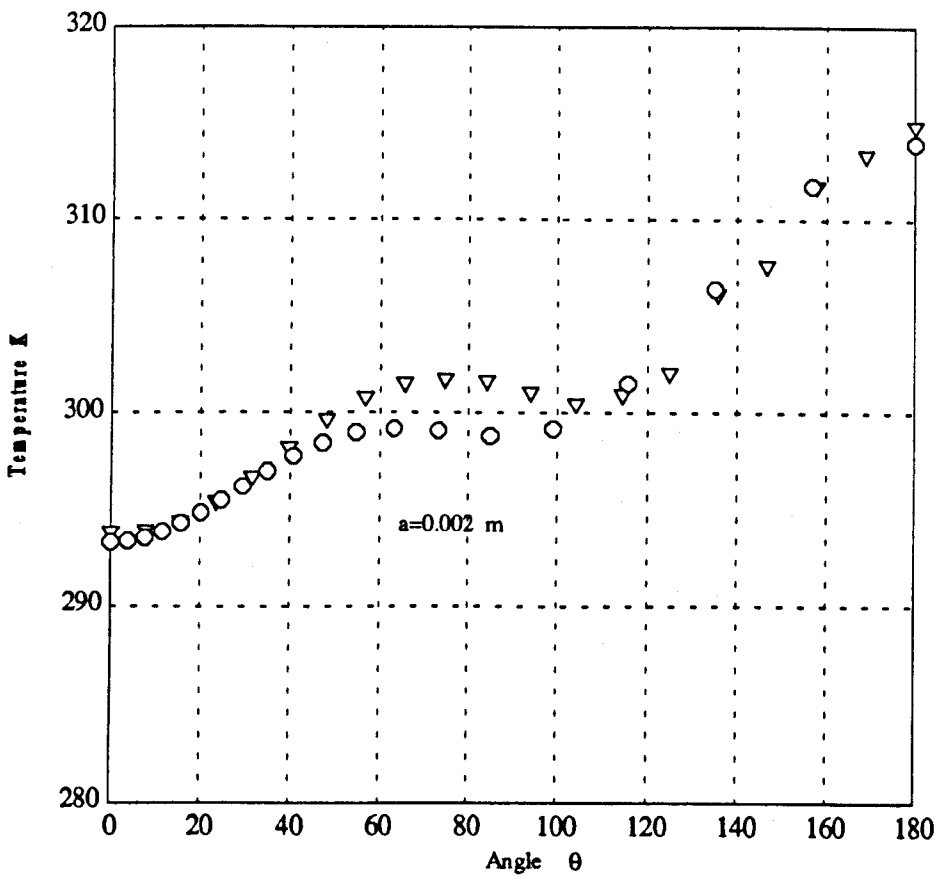

Figure 2.12(d) Temperature Distribution Around the Fouled Tube with a=2e-3

CHAPTER 3

EXPERIMENTAL INVESTIGATION OF HEAT TRANSFER AND AIR FLOW CHARACTERISTICS OVER TUBES IN CROSS-FLOW

3.1 Introduction

Heat exchangers with tube banks in cross-flow are of great practical interest in many thermal and chemical engineering processes. A large number of studies have been carried out concerning the features of heat transfer of tube banks. Despite all the experimental data, it is not yet possible to get a clear idea about the flow and heat transfer processes in the tube banks because of the very complicated geometry and the great number of parameters involved.

In order to examine the process of flow and heat transfer in tube banks and their response to the change of different parameters, it is possible to make experiments on chosen, simple geometrical models where it is possible to measure local values and to consider the effect of only one parameter at a time.

The accumulation of deposition on heat transfer surfaces can have a considerable

insulating effect that reduces the heat transfer performance; this deposit can be difficult to remove. The fouling process is a function of many parameters including the surface temperature, fluid velocity, and flow geometry. Fouling is a serious problem in the design and operation of heat exchangers. In the analysis of the heat transfer performance of tubular heat exchangers, it is usual to consider all the tubes as being of equal diameter and being located in a regular 'in line' or 'staggered' pattern. In reality the effective tube diameters can increase as the tube fouls and the matrix geometry can become distorted as a result of thermal stress and buckling. These may lead to significant changes in flow pattern and hence to both local and overall heat transfer rates. An aim of the investigation reported in this chapter was to examine the thermal performance of different tube geometries. Single tube, single tube row and staggered tube geometries were used for the measurement of the local heat transfer coefficient and local static pressure. Also, for a single tube row a theoretical study has been completed to calculate the front stagnation region and laminar boundary layer region heat transfer for different blockage ratios.

3.2 Theoretical Consideration

The underlying principles for the determination of heat transfer through a laminar boundary layer on an isothermal cylinder in cross-flow are reported in detail by, for example, Kays and Crawford (1993). To determine the heat transfer rate to multiple cylinders located transversely in a cross-flow, the procedures given in Kays and Crawford (1993) have been used with appropriate modification for the flow pattern outlined in the following section.

3.2.1 The Stagnation Region

For a single cylinder, the potential flow velocity outside the boundary layer is given as $U_\infty=2V\sin\theta$. The heat transfer coefficient at the front stagnation point is given in Kays and Crawford (1993)

$$Nu_s=1.14Re^{0.5}\ Pr^{0.4} \tag{3.1}$$

In order to make use of equation 3.1, it is necessary to know the variation of the free-stream velocity in the vicinity of the stagnation point. The essential feature is the use of the approximation to the potential flow around the stagnation point:

$$U_\infty=2V\sin\theta \approx 2V\theta \approx 2V\left(\frac{x}{R}\right) \tag{3.2}$$

for very small θ, this is illustrated as;

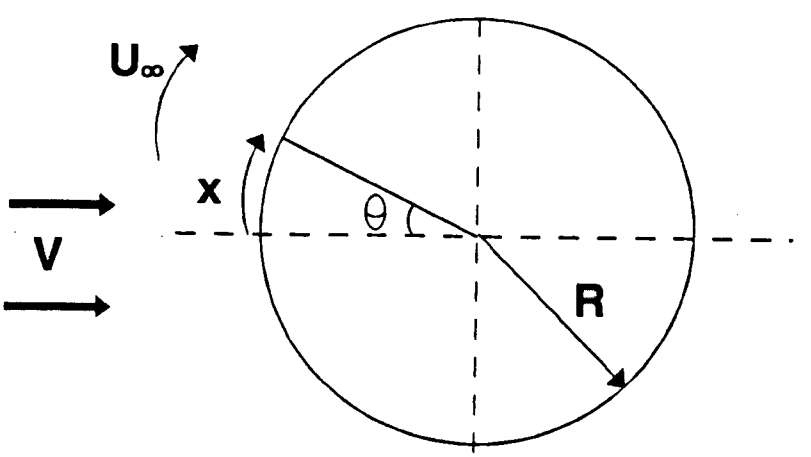

Boundary layer equations can be applied to heat transfer from wedge-shaped bodies, having a velocity variation outside the boundary layer that is expressed by the exponential relation as:

$$U_\infty = Cx^m \tag{3.3}$$

This method can be used only for some definite portion of a circular cylinder. Thus for the region near the stagnation point the value of m should be defined. m is expressed as:

$$m = \frac{\beta/\pi}{2-\beta/\pi} = \frac{x}{U_\infty}\frac{dU_\infty}{dx}$$

The boundary layer solution corresponding to potential flows are frequently called wedge flow solutions. Some wedge flow configurations are presented below.

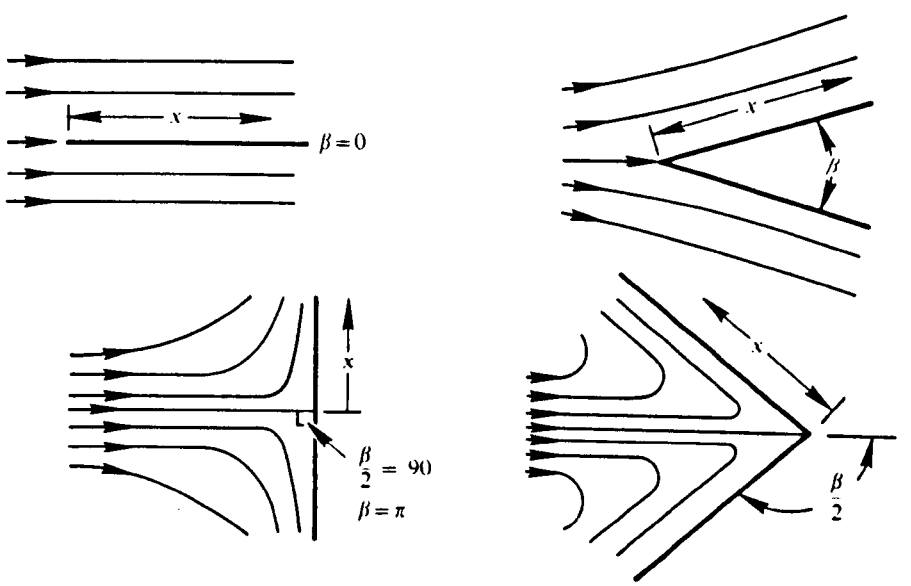

Therefore for the front stagnation point region of a single cylinder, m has the value of 1, then equation (3.3) becomes; U_∞=C.x. It is assumed that the potential flow velocity in the front stagnation region of a single cylinder can be described by

$$U_\infty = U_{\infty,s}\, f(G) \tag{3.4}$$

f(G) is a function of multi-tube or confined cylinder geometry. In the zero blockage case that

exists where the tube is in an infinite channel, f(G) is simply equal to 1. However in the confined cylinder geometry, f(G) should be defined to determine the correction for the effect of blockage on the heat transfer. Therefore, Reynolds number can be written for confined cylinder geometry as:

$$Re = \frac{D\,V}{\nu}\,\frac{U_\infty}{U_{\infty,s}}$$

f(G) may be determined from the theoretical potential flow velocity presented by Perkins and Leppert (1964) for equal spaced cylinder for any given tube diameter, D, and spacing, W. U_∞ is given by them as:

$$U_\infty = V\sin\theta - \left(\frac{wV}{\pi}\sinh^2\left(\frac{\pi D}{w}\right)\right) \cdot \cdot \cdot \left(\frac{\cos[(2\pi D/w)\sin\theta](2\pi/w)\sin\theta}{\cosh[(2\pi D/w)\cos\theta]-\cos[(2\pi D/w)\sin\theta]}\right) \cdot \cdot \cdot \left[\frac{\sin[(2\pi D/w)\sin\theta](\sinh[(2\pi D/w)\cos\theta](2\pi/w)\cos\theta+\sin[(2\pi D/w)\sin\theta](2\pi/w\sin\theta)}{(\cosh[(2\pi D/w)\cos\theta]-\cos[(2\pi D/w)\sin\theta])}\right] \quad (3.5)$$

However, according to Perkins and Leppert (1964) , equation (3.5) is only valid for blockage ratios D/W of less than 0.5.

Considering equation (3.4) and the relation in equation (3.1), Nusselt number may be written for confined or multi-cylinder geometry as:

$$Nu_b = Nu_s\, f(G)^{0.5} \quad (3.6)$$

In the present study, f(G) has been determined for a range of blockage ratios using equation (3.4), where U_∞ is given by equation (3.5) and $U_{\infty,s}$ by equation (3.2).

3.2.2 The Laminar Boundary Layer Region

Here, the results of the analysis given in Kays and Crawford (1993) for the heat transfer in the developing boundary layer around any body is employed. The rate of growth of the thermal boundary layer thickness Δ is a function of local parameters:

$$\frac{d\Delta}{d\theta} = g\left(\Delta, U_\infty, \frac{dU_\infty}{d\theta}, \nu, Pr\right)$$

The basis of the method lies in the assumption that the function 'g' for an arbitrary variation of free stream velocity is the same as in a wedge flow. For constant surface temperature and constant free stream temperature, employing the wedge flow condition as $U_\infty = Cx^m$, the conduction thickness of thermal boundary layer can be written as:

$$\Delta_c^2 = \frac{11.68\ \nu \int_0^\theta U_\infty^{1.87}\, d\theta}{U_\infty^{2.87}} \qquad (3.7)$$

Stanton number is a non-dimensional version of the heat transfer coefficient that is given as:

$$St = \frac{h}{c\rho U_\infty} \qquad (3.8)$$

Defining thermal conduction thickness (Δ_c) as $\Delta_c = k/h$, transposing to form the Stanton number, and for Pr=0.7 then the Stanton number can be obtained as:

$$St = 0.418 \frac{\nu^{0.5} \, RU_{\infty}^{0.435}}{\left(\int_0^x U_{\infty}^{1.87} R^2 dx\right)^{0.5}} \tag{3.9}$$

Arranging equations (3.8) and (3.9) any variation of U_{∞}, which is obtained by potential flow theory for confined tube geometry as developed by Perkins and Leppert (1964), local heat transfer coefficient can be calculated as:

$$Nu = \frac{0.414 \, D^{0.5} U_{\infty}^{1.435}}{\nu^{0.5} \int_0^{\theta} U_{\infty}^{1.87} d\theta} \tag{3.10}$$

The original formulation of equation 3.10 is completely general and it can also be used in other cases such as unequally spaced cylinders provided the corresponding velocity field can be determined. The calculation of Nusselt number at the front stagnation point and the laminar boundary layer region for a single row of tubes with varying blockage ratio will be compared with experimental data late in the chapter.

3.3 Measurement of The Local Heat Transfer Coefficient

3.3.1 Introduction

One of the most important applications of convective heat transfer theory is in the analysis and design of heat exchange devices to transfer heat from one fluid to another. These are found in a variety of thermal systems which are designed in an almost infinite variety of sizes, shapes and configurations

In a heat exchanger there is a hot fluid and a cold fluid. Energy is transferred from

the hot fluid to the dividing wall, and then into the cold fluid. The heat transfer between the fluid and dividing walls is by convection and in either case the local rate of heat transfer between the fluid and the wall, using the fundamental equation defining a heat transfer coefficient, is:

$$\frac{Q}{A} = q = h(T_{fluid} - T_{surface}) \tag{3.11}$$

Experimental studies are often conducted to find information on the local heat transfer coefficients over a surface where the convection is controlled by the boundary layer conditions on the surface. In the uniform wall flux case q is held at a constant value over the whole surface and then surface temperature is recorded. Giedt (1949), Aiba and Yamazaki (1976), Baughn (1986) have worked under constant heat flux condition.

The uniform wall temperature case depends on the surface temperature being kept at a constant value over the entire surface. There have been many studies that have been carried out with the constant wall temperature condition (Achenbach (1981), Biyikli et al.(1983)). In the present study because of the nature of the principal experimental equipment the thermal boundary condition was that of uniform wall temperature.

3.3.2 Measurement of Local Heat Flux

Local heat flux was measured by Achenbach (1981) using two thermocouples that recorded temperature difference between a heated plug embedded in a tube wall. Kraabel et al.(1982) measured temperature with a similar sensor to control boundary conditions. One

technique used for some applications employs a thin circular foil called a Gardon gauge, Gardon (1953). Another method for heat transfer measurement both to and from surfaces uses micro-foil type sensors that record the temperature gradient across a thin insulating layer stuck to the surface. Murray and Fitzpatrick (1988) measured the local heat transfer coefficient in heat exchanger tubes by using a micro-foil type sensor. Hollworth and Gero (1985) used the same technique to measure heat transfer in a heated air jet impinging on a flat surface, whilst Shallcross and Wood (1986) have used the micro-foil sensor to measure local heat transfer rate around axisymmetric bodies.

In the following two sections, two different techniques that have been used to measure heat transfer coefficient are described. The first technique, despite considerable effort, was found to be unsatisfactory. The second technique was much more successful.

3.4 Measurement of The Heat Transfer Coefficient Using Copper Strip

This measurement technique has been applied by Watt and Williams (1981). They measured heat transfer coefficient using a copper-clad plastic laminate as a flat plate, and they obtained fairly good results. This technique was applied as a part of the present research for measuring the heat transfer coefficient around a circular cylinder. The copper strip was flexible and had one adhesive surface and could therefore be located on both flat and curved surfaces

The principle of this technique is that if the measured current I is passed through a copper strip and the voltage drop between the edges of strip is obtained then the heating

power can be calculated as V x I. As long as the current and voltage drop of the strips are known, the resistance of each strip is calculated as V/I.

The basic equation for temperature dependent resistance is:

$$R = R_0(1+\alpha(T_s-T_0)) \tag{3.12}$$

R_0 is the resistance of the strip at a reference temperature T_0. With equation 3.12, surface temperature of the strip can be obtained as:

$$T_s-T_0=\frac{V-IR_0}{\alpha\ I\ R_0} \tag{3.13}$$

α is the temperature coefficient of resistance for copper which was taken to be $4x10^{-3}$. The heat transfer coefficient is calculated from Newton's cooling law:

$$h=\frac{I\ V}{A(T_s-T_0)} \tag{3.14}$$

Substituting equation (3.13) into equation (3.14) the heat transfer coefficient becomes:

$$h = \frac{I^2\ V\ \alpha\ R_0}{A(V-I\ R_0)} \tag{3.15}$$

i.e. the heat transfer coefficient can be measured without having to measure temperature.

3.4.1 Design and Construction of Experimental Model

Copper strip is commercially available with a thickness of 0.076 mm and width of 10 mm. In the present study 24 strips were cut, each 15 cm in length and 5 mm in width. A smooth wood tube was prepared to locate copper strips upon and each strip was attached with a small copper bridging piece onto the tube to produce a continuous circuit. Between the strips, unheated gaps were formed of 1 mm width. The apparatus and copper strips with connections are shown schematically in Figure 3.1. Voltage and power connections were soldered to the rear side of the strip and kept away from the central measuring section so that flow patterns were not disturbed. A low speed wind tunnel was used with an outlet section of 40 cm x 40 cm .The tunnel's outlet section velocity profile and turbulent intensity was obtained using a hot-wire anemometer. The instrumented tube was located at the centre of the outlet section. The voltage value for each strip was recorded with a digital multimeter via a voltage selector unit.

3.4.2 Experimental Procedure and Uncertainty Analysis

The instrumented tube was located at the centre of the outlet section of the wind tunnel. Air velocity and heating power were fixed and after allowing sufficient time for thermal equilibrium, readings were recorded. As explained in the previous section, the instrumented tube consisted of 24 copper strips and readings were monitored using a voltage selector unit. Measurement of resistance of each strip was performed separately by potentiometer and also the effective area of each strip was measured for more accurate reading and calculation. However during the reading of voltages, significant fluctuation was seen for each strip. Therefore reading were taken for minimum, maximum and average

voltage values. The heat transfer coefficient was calculated using equation (3.15). An uncertainty analysis was also carried out to assess the accuracy of the copper strip technique. Below, an example is given of the calculation of the heat transfer coefficient and this is followed by an uncertainty analysis.

R_o=0.016 Ω	L=0.15 m	V_{min}=87.83mV	T_{min}=30.1°C	h_{min}=60.78
I=5.275 A	W=0.005 m	V_{max}=89.65mV	T_{max}=25.5°C	h_{max}=40.5

The uncertainty in the heat transfer coefficient can be found by performing partial differentiation for the variables of equation (3.15)

$$\delta h = \left(\frac{\partial h}{\partial V}\right) \delta V + \left(\frac{\partial h}{\partial I}\right) \delta I$$

The fractional error in h can then be written as:

$$\frac{\delta h}{h} = \left(\frac{-R_o I}{V - R_o I}\right) \frac{\delta V}{V} + \left(\frac{2V - R_o I}{V - R_o I}\right) \frac{\delta I}{I} \qquad (3.16)$$

From the above analysis, it would seem that in the test carried out, the error in the heat transfer coefficient would be about 50 percent. It was assumed that the current was not fluctuating and that the only error was due to the voltage readings. It is evident therefore that a very small voltage difference gives very considerable error in the heat transfer coefficient.

Watts and Willams (1981) recommended the copper foil technique to calculate heat transfer coefficient without measuring surface temperature, however in the present work, results have been unsatisfactory. The copper foil technique could be improved for the present

case by more accurate instrumentation, however, this would be more costly and even then there could be an unacceptable uncertainty. Therefore in the present work the measurement of the heat transfer coefficient was carried out using the heat flow sensor technique.

3.5 Local Heat Flux Measurement Technique with Heat Flow Sensor

Following the aborted experiments using the resistance technique for heat flux measurement, the micro-foil heat flow sensor was found to be the most convenient and appropriate for the present work. Another advantage of this method is that the sensor can be located onto a curved surface to measure the local heat transfer coefficient for a single tube and for a bank of tubes in cross-flow.

Experiments were carried out using a low-speed wind tunnel. Velocity and turbulence measurement were recorded with a hot-wire anemometer. Tubes were located horizontally across the duct of dimensions 37x37x80 cm. For the single tube row case, the spacing of tubes was adjusted using slender wedges at the end of the row to ensure the correct gap was maintained. For the multi-tube case, half dummy tubes were used to maintain the correct gap.

3.5.1 Design and Construction of Model

A thick-walled copper cylinder heated internally by an electric cartridge heater was used as the heat transfer section. The heater was inserted into the centre of the instrumented tube as shown in Figure 3.2. The copper section was held in two PVC tubes to form a single tube assembly. The heat flux from the surface of the cylinder was measured using an RdF micro-foil heat flux sensor type 27034 attached to the surface with an epoxy resin adhesive.

The sensor consists of three thin layers of insulating material bonded together with a copper-constantan thermocouple on both sides of the central layer. The heat flux through the sensor causes a temperature difference across the central layer of insulating material, thus the temperature gradient is recorded by the thermocouples where output voltage is proportional to the heat flux. The output from the sensor was connected to a digital multimeter. Surface temperature was also measured by the heat flux sensor and was recorded by a digital thermometer; the surface temperature was also checked with a thermocouple placed close to the sensor. These temperature readings were seen to be slightly higher than that recorded by the thermocouple in the sensor. This difference was also noticed by Murray and Fitzpatrick (1988) who observed that after attaching the sensor onto the surface, it forms a small area of insulation due to the sensor material and the resistance of the adhesive layer.

Only one heat flux sensor was used on the tube surface and the angular position of the tube was varied from 0° to 360° in 10° steps. A protractor was fitted to one end of the tube to allow the angular location to be monitored. The heat transfer tube was heated to temperatures of 30-50° above the air temperature. Air temperature was recorded by a mercury thermometer placed into the upstream section. A single pressure tapping was used to measure static pressure at the tube surface with an inclined alcohol manometer.

The digital multimeter used for measuring the heat flux had a zero error of about 5 μV. This error was taken into account in the calculation. The experimental uncertainty of the sensor is given by manufacturers as ±5 per cent. Sensor accuracy has been confirmed by Hollworh and Gero (1985) for an impinging jet flow study.

3.5.2 Velocity Measurement and Hot-wire Calibration

A Disa 55M10 type hot-wire anemometer was used for the measurement of the flow velocities. All switch settings were selected from the Disa instruction manual. The probe output was connected to the A/D converter of a computer, and 2000 readings were taken in each measurement using a specially written computer program.

To find out the calibration curve, King's Law was followed where E is related to the effective cooling velocity V_e in the following relationship

$$E^2 = A+B\ V_e^C$$

where A represents the heat loss through natural convection and conduction along the prongs at zero velocity and B and C are constants.

Firstly a velocity-voltage relationship between the cooling velocity V_e (measured by a pitot static tube) and electrical output voltage E, of the anemometer was performed for each wire with the wire normal to the flow direction. To find the calibration constants A,B,C a least RMS error curve fitting technique was used. To calibrate the hot-wire sensor, the probe and pitot static tube were located at the outlet section of the wind tunnel. To obtain more accurate curve-fitting, 25 readings were taken over a velocity range of 3 m/s< V < 18 m/s.

The wind tunnel used has 1.1 kW power consumption at 1440 rpm. It consists of several mesh screens and honeycomb section to produce an uniform flow. The wind tunnel is controlled by using a variable gearbox between the fan and the motor. A photograph of the

wind tunnel can be seen in Figure 3.3. According to the velocity measurement, the turbulence level was 1-2 per cent,calculated by:

$$Tu=\frac{\sqrt{(\bar{V}')^2}}{\bar{V}}$$

$V'=V-\bar{V}$, (V' is fluctuating part of velocity)

3.6 Experimental Observation of Heat Transfer and Flow Characteristics of Single Tube and Tube Bundle

3.6.1 Introduction

As is well known from the literature, the laminar boundary layer over the front stagnation point of a tube in cross-flow is thinnest and its thickness increases with displacement downstream. Separation of the laminar boundary layer takes place when low velocity fluid close to tube wall can not overcome the adverse pressure gradient over the rear portion of the tube and eventually the flow stops and begins to move in the opposite direction. Fluid movement starts to curl and gives rise to vortices that shed from the tube. Zukauskas (1972) has given some useful information to show how separation of the laminar boundary layer varies with Reynolds number. When Reynolds number is smaller than 1, inertial forces are negligible relative to the viscous forces and laminar boundary separation takes places at the rear stagnation point. When Reynolds number is greater than 5, the laminar boundary layer separates from the tube before the rear stagnation point, and also symmetrical stable vortices are formed behind the tube. In the case of Reynolds number greater than 40 the

stability of the flow disappears and vortices are shed from the rear of the tube. Reynolds number of the flow determines both the thickness of the laminar boundary layer and the point at which it separates from the tube. For example, when Reynolds number is around $5x10^3$ the boundary separates at about 90°, and further increasing Reynolds number to $7x10^4$ causes the separation point to move to the front face at nearly 80°. With a further increase in Reynolds number, the boundary layer becomes turbulent and receives additional energy from the main flow through turbulent fluctuations. This results in the turbulent boundary layer continuing through to the downstream side. According to Achenbach (1968) the separation point is moved to 115° at a Reynolds number of $2x10^6$.

Flow around circular cylinders and boundary layer separation have been investigated by Kraabel et al. (1982), Zukauskas (1972), Schimith and Wenner (1951), Boulos and Pei (1974). Variation in local Nusselt number around the cylinder is affected by boundary layer development in the front of the tube and by separation and vortex shedding over the side and the wake region. The maximum Nusselt number occurs at the front stagnation point where the boundary layer and resistance to heat transfer is minimum. The minimum Nusselt number is found to correspond to the point before the boundary layer separates. The minimum Nusselt number location is dependent on the Reynolds number of the flow.

The variations in the hydrodynamic conditions in the flow around the tube are described by the distribution of local pressure and local velocity. The boundary layer separation is due to internal friction within the boundary layer and is also related to the pressure and velocity distribution around the cylinder. A certain amount of energy is

consumed in overcoming the internal friction in the boundary layer, at the rear of tube the flow velocity decreases and pressure increases (dP/dx>0) the energy in the flow is insufficient to overcome the increasing pressure and the flow separates from the surface. Local pressure and also velocity distribution around the tube up to 50° (from the front stagnation point) does not depend on the Reynolds number. It has been observed (Zukauskas (1972), Fage and Falkner (1931), Achenbach(1968)) that the effect of Reynolds number begins when $\theta > 50°$.

Variation of heat transfer and flow around a tube in a bank is determined by the flow pattern which depends greatly on the arrangements of the tubes in the bank. In both the inline and staggered tube arrangement, flow around a tube in the first row is similar to the single tube case but with delayed separation due to the increased blockage. A tube in one of the inner rows is affected by the highly turbulent flow. Considering the staggered tube bank case, the front of the tubes in the second row is influenced by the fluid acceleration and the blockage from the first row. The rear side of an internal tube is affected by high turbulence from the other inner tubes. A tube in the third row of a staggered array is influenced by very high turbulence, therefore for a tube in the third row a higher level heat transfer is monitored. This has been observed by Murray and Fitzpatrick (1988), Baughn (1986) and Zukauskas (1972). Downstream from the third row, the heat transfer becomes stable and equal to the value for the third row. Heat transfer from a tube in a bank is influenced by the same parameters that are observed for a single tube. Increasing Reynolds number produces a higher Nusselt number. Changing both longitudinal and transverse spacing causes great changes in the velocity distributions around the inner tubes in the bank. The effect of the longitudinal spacing on the flow pattern for second and subsequent tubes in a column has been

investigated by, for example, Aiba et al. (1980) and Igarashi (1986). Furthermore mean Nusselt number has been investigated for a complete array of 10 or more rows, Grimison (1937), Bergelin et al. (1952) and Zukauskas (1972). The results obtained have shown that mean Nusselt number for a tube in a bank increases with an increase of Reynolds number and is enhanced by an increase in the transverse pitch ratio and a decrease in the longitudinal pitch ratio. Pressure drop across the tube bank has been investigated by Grimison (1937) and Zukauskas (1972). Results have shown that increasing Reynolds number and decreasing transverse tube spacing causes an increase in pressure drop. The longitudinal spacing is found to have less of an effect on the tube array pressure drop. The largest pressure drop is observed across a bank with closely spaced tubes.

3.6.2 Single Tube and Single Tube Row Measurement

The aim of this part of the investigation was to explore the influence of the blockage of a single tube in a duct and the transverse pitch for a single tube row. Experiments were completed in the subcritical region of flow in a tube bank, that is in a Reynolds number range from 10^3 to $2x10^5$ using a low-speed wind tunnel and a number of 0.0485 m diameter tubes arranged horizontally in a single row across the duct. The spacing of the tubes could be adjusted and slender wedges were used at the end of the row to ensure the correct gap was maintained. The central tube was instrumented and it was rotated about its axis. A schematic view of the single tube and a single tube row can be seen in Figure 3.4.

Experiments began with a single instrumented tube over a Reynolds number range 7960 to 47770. The heat transfer and pressure characteristics obtained were used as a bench-

mark against which the remaining data could be compared. In this initial test the blockage ratio, D/W, for the single tube in the duct gave value of 0.132. Tubes were then added and the gaps adjusted to give different blockage ratios until the tubes were quite close with a blockage ratio of 0.843. Upstream free-stream turbulence was approximately 1-2 %.

3.6.3 Tube Bundle Measurement

The experimental apparatus for a tube bundle was essentially the same as used in the single -tube row experiments. In this section heat transfer and pressure measurements for a staggered tube bundle were considered. The geometrical configuration is illustrated in Figure 3.5. The geometry of the tube bundle is specified in terms of D, S_t and S_l. Thirty one tubes were located vertically into the same duct as has been used in previous measurements. Eight half tubes were used to ensure the correct gap at the wall. Seven tube rows were assembled and the instrumented tube was used in the various positions to measure local heat transfer and pressure readings. The configuration of the bundle was that the transverse pitch was kept constant for all measurements at S_t of 1.5. The longitudinal pitch, S_l was 1.25 and 1.5 where the dimensionless parameter S_t and S_l are defined as;

$$S_l=\frac{S_l}{D} \qquad S_t=\frac{S_t}{D}$$

Reynolds number was kept constant at 4.8×10^4 and has been calculated by:

$$Re_D=\frac{\rho V_{max} D}{\mu} \qquad \left[V_{max}=V\frac{S_t}{S_t-D}\right]$$

3.6.4 Experimental Procedures

For all measurements, constant up-stream velocity conditions were used and the instrumented tube was heated until thermal equilibrium was obtained while the wind tunnel was running. During the experiments up-stream air temperatures were recorded and turbulence levels were measured for different configurations. Symmetry of readings were monitored over the 360° of the tube. Local static pressure coefficients have been plotted against angle θ, for each configuration. For the single tube and the single tube row cases, heat transfer coefficient at the stagnation point and the laminar boundary layer regions have been calculated and plotted against the experimental results.

The results are presented in a dimensionless form. The following definitions are used for the static pressure and heat transfer for single tube and single tube row cases:

$$C_p=\frac{P-P_\infty}{\frac{\rho}{2}V_\infty^2} \quad \text{and} \quad Nu=h_\theta\frac{D}{k}$$

$P=P(\theta)$ is the static pressure at the peripherical angle of θ of the cylinder and P_∞ the static pressure of the upstream flow. For a tube bundle, the definition of pressure coefficient is given by Zukauskas (1972), as:

$$C_p=1-\frac{P_{\theta=0}-P_\theta}{\frac{\rho}{2}V_{max}^2}$$

where V_{max} is the mean velocity in the minimum free cross-section.

3.7 Results and Observations

3.7.1 Single Tube

Figure 3.6 shows local Nusselt number and local pressure coefficient for a cylinder in Reynolds number range of 7960 to 47770. For the single cylinder, the blockage ratio was 0.132 (corresponding to D/W). The local static pressure drops with increasing distance from the stagnation point. As the flow accelerates around the cylinder the static pressure deviates more from the distribution given by potential theory. At about 70° the pressure becomes a minimum value of between -0.5 and -1 (for varying Reynolds number range) this is considerably higher than the potential flow value of -3.

For a smooth surfaced cylinder, four flow ranges can be obtained (Achenbach (1989)), the critical, the subcritical, the supercritical and the transcritical. Here, typical subcritical results have been presented where the laminar boundary layer separates at an angular position of 80°. As is known that the local heat transfer is largest at the front stagnation point and decreases with distance along the surface as boundary layer thickness increases. The heat transfer reaches a minimum on the sides of the cylinder near the separation point. After the separation point the local heat transfer increases because considerable turbulence exists over the rear side of the tube where the eddies of the wake sweep the surface. However, the heat transfer over the rear is not larger than the front, because the eddies recirculate part of the heated fluid. Increasing Reynolds number causes an increase in heat transfer due to the thinning of the laminar boundary layer. In the present study, the separation point was identified from the local Nusselt number graphs where it reaches the first minimum value. In Figure 3.6 with the lowest Reynolds number case, the laminar boundary layer separates at

nearly 90° and for the highest Reynolds number case the separation point is moved to 80°. This is also consistent with the previous work of Chen (1972) and Zukauskas (1972).

As pointed out by other authors, such as Murray and Fitzpatrick (1988), Boulos and Pei (1974), Baughn et al. (1986), the local Nusselt number in the wake region shows a second minimum. This second minimum point was explained by Kraabel et al.(1982) to be a consequence of the laminar nature of the reattaching shear layer at the rear of tube. Baughn et al (1986) explained further that the initially laminar shear layer that exists for low Reynolds numbers gives less mixing than the turbulent shear layer experienced at higher Reynolds number.

3.7.2 Single Row of Cylinders

In this study, the instrumented tube was placed at the centre of the duct in a single transverse row of tubes. Five different blockage ratios were used and results have been presented as local Nusselt number and local static pressure coefficient against angle for different Reynolds numbers.

As expected, increasing blockage markedly increased the velocity around the cylinders. It is seen from the results that the separation point is dependent on the blockage, as higher blockage causes separation to be delayed (for example compare Figure 3.7 and Figure 3.11). Figures 3.7-3.11 show the influence of blockage on the local heat transfer and local pressure coefficient. The blockage ratio is from 0.132 to 0.843 and the Reynolds number is from 7960 to 47770 (defined on upstream velocity and tube diameter). In the high blockage case high

velocities could not be reached due to the resistance to the flow. The 0.132 blockage represents the single tube case that was seen in Figure 3.6. As the blockage increases so too does the heat transfer due to higher flow velocities in the vicinity of the cylinder.

When the blockage ratio increases from 0.132 to 0.5 the average Nusselt number changes by about 10 %, and the separation point is seen to move, however the distribution of local heat transfer and local static pressure values are similar in character to that of the single tube. This can be seen in Figure 3.7 and Figure 3.8, blockage ratios of 0.395 and 0.5 respectively; compared with Figure 3.6. When the blockage is 0.395, on the front side of the cylinder the laminar boundary layer develops, and the separation point moves back with increasing Reynolds number. When the blockage ratio increases from 0.395 to 0.5, local static pressure distribution changes considerably. Both minimum local Nusselt number and minimum local static pressure are moved to downstream side of the tube by about 10°.

Figure 3.9 shows results at a blockage ratio of 0.668 and the effect of the changing flow can be seen on both the heat transfer in the wake region and in the pressure distribution where the value of local static pressure coefficient falls as the flow accelerates through the narrowest gap. Over the front face of cylinder the heat transfer coefficient is relatively constant due to the accelerating flow and the resulting thinner boundary layer.

Figure 3.10 and 3.11 show the results for blockage ratios of 0.75 and 0.843 respectively. When the gap gets smaller, the distribution of local Nusselt number and pressure coefficient show quite different character to that seen earlier. The flow through the row of

cylinders with such a small transverse gap is very similar to that through a venturi type of nozzle. Increasing blockage ratio from 0.132 to 0.843 shows the minimum pressure point to have moved from 70° to 90°, and the separation point moves downstream to about 105°. Especially when the blockage ratio is 0.843, the front portion of the tube's heat transfer distribution increases, and front and rear side values are no longer the maxima.

Figure 3.12 shows different blockage ratio for only one Reynolds number. It can be seen that blockage has a significant influence on the heat transfer due to its effect on the velocity distribution around the cylinder. Obviously high blockage increases the velocity around the cylinder. The separation point also depends on the blockage. According to the experimental work high blockage causes the separation point to be delayed to the downstream side. Furthermore the changes in average Nusselt number as a function of blockage ratio as can be seen in Figure 3.13. Changing of mean Nusselt number is based on single tube case.

In Figure 3.14 the stagnation point Nusselt number has been expressed as a ratio of the value obtained for the single cylinder and it can be seen to increase with blockage. The theoretical calculation for the stagnation point heat transfer using the expression developed in this work and shown in equation 3.5 shows good agreement with the data. The line is shown dotted for blockage ratio above 0.5 because Perkins and Leppert (1964) only recommended their potential flow velocity distribution, upon which f(G) is based, for blockage ratios up to 0.5, however agreement beyond this range is still good. Perkins and Leppert's own prediction also agrees closely with the present model although their experimental data does not agree so well. It has been noted however that the turbulence

intensities in the flow were measured by Perkins and Leppert to be about 3%, whilst in the present study they were about 1 %. Furthermore, geometrical configurations of the experiments were different. The theoretical prediction offered by Akilbayev et al (1966) diverges from the present model and again there is only moderate agreement between their experimental data and their model.

Figure 3.15 shows the heat transfer in the developing boundary layer, calculated using equation 3.10, along with experimental data for three different blockage ratios. The agreement is again seen to be satisfactory but only up to about 60°. It is at this angle, however, that the flow around a cylinder deviates from that predicted by potential flow theory, upon which the present model is based, and the divergence beyond this angle is only to be expected.

3.7.3 Tube Bundle

As mentioned in the previous section, the heat transfer in flow over the tube bank depends largely on the flow pattern and the intensity of turbulence that in turn are functions of the velocity of the fluid and size and arrangement of the tubes. As observed by many investigators flow structure around the first transverse rows is similar to the flow around a single tube. The turbulent wakes extend to tubes located in the second transverse row. As a result of the high turbulence in the wakes, the boundary layer around the tubes in the second and subsequent rows become thinner. Therefore it is expected that heat transfer coefficients of tubes in the first row are smaller than the tubes in subsequent rows.

In this section, results are reported for 1.5x1.5 and 1.5x1.25 (S_txS_l) staggered tube

bundle configurations for Reynolds number $4.8x10^4$ corresponding to maximum flow velocity at the minimum sectional area.

3.7.3.1 First Row

The distribution of local Nusselt number and local pressure coefficient around the tube in the first row for both configurations are shown in Figure 3.16. The results for the tube in the first row are very similar to the single row case when blockage ratio is the equivalent 0.668 with Re=15922. Two minimum Nusselt numbers occur at 100° and 140°, as observed in single tube and single tube row cases. It can be seen in other experimental work (Kraabel et al.(1982), Baughn et al.(1986)) that this may be thought to result from the laminar free shear layer. After this second minimum point, the local Nusselt number on the rear side of the tube is higher than the front half of the tube due to the influence of the subsequent inner tubes. The local static pressure coefficient is also very similar to single tube row results. In the both configurations the results are rather similar but there is a small effect due to the influence of different longitudinal spacing.

3.7.3.2 Second Row

As seen in Figure 3.17 from the local Nusselt number distribution around the second row in a bank, two local minimum points occur. Baughn et al. (1986) commented that this could be due to the turbulence being more effective on the inner rows although where these points are due to transition from the laminar to turbulent boundary layer and then separation or laminar separation followed by turbulent reattachment and separation may not be determined. In both configurations, the local Nusselt number at the front stagnation point

is 45% higher than the first row front stagnation point due to flow acceleration caused by the blockage. The decrease in Nusselt number as the laminar boundary layer develops from the front stagnation points is more noticeable than in the first row. The minimum Nusselt number occurs in both case at around 80° from the stagnation point. The distribution of local static pressure coefficients are similar up to nearly 50° and after this point, they deflect then become constant at about 140°.

3.7.3.3 Third Row

The distribution of local Nusselt number and pressure coefficient with angle over the tube in the third row are shown in Figure 3.18. The shape of the distributions are similar to the first and second row but at the front of the tube Nusselt number is higher than in the second row due to the high turbulence produced by the previous two rows. The decreasing nature of Nusselt number as the laminar boundary layer develops is more pronounced.

As mentioned for the second row, two minimum Nusselt number are seen at about 105° and 140°. After the second minimum point, it rises up to rear stagnation point. The first minimum point occurs at 105° and has moved to the downstream side of the tube compared with the second row. This is considered to be a result of the high turbulence existing from the second row. Local static pressure coefficient falls to about 100° then after 140° it becomes steady.

3.7.3.4 Fourth Row

The variations in local Nusselt number and pressure coefficient with angular position

in the fourth row are shown in Figure 3.19. Again the laminar boundary layer develops quickly. Nusselt number and pressure distributions are very similar to the third row but the first minimum Nusselt number moves to the upstream side at nearly 95° in both configurations. In the wake region slightly higher Nusselt values are seen compared with the third row. Local static pressure distributions becomes constant after 150°.

3.7.3.5 Fifth Row

The local Nusselt number and pressure coefficient in the fifth row is shown in Figure 3.20. As can be seen the distribution of Nusselt number over the front side of tube is slightly lower than in the fourth row but is essentially the same and is considered to be constant thereafter. Minimum Nusselt number occurs at the same point as in the fourth row and the wake region is the same as observed in the fourth row.

3.7.3.6 Sixth and Seventh Row

The local Nusselt number and pressure coefficient in the sixth and seventh rows are shown in Figure 3.21 and Figure 3.22. The local Nusselt numbers vary with a similar trend as the fifth row. The laminar boundary layer develops and the separation point occurs at nearly 95° for both rows. The local Nusselt numbers at the rear side of the tube are similar compared with the previous row. For the sixth row and seventh row, the front stagnation point Nusselt number values are slightly lower than the fifth row. Local pressure values become constant after nearly 145° for both cases. It is clear that the pressure curves are similar compared to each other and with fifth row.

Figure 3.23 shows the comparison of average Nusselt number for both geometries and different rows of tubes. It is clear that mean Nusselt number rises up to the fourth row, after this, a decrease is seen for both geometries. Also altering the longitudinal pitch ratio from 1.25 to 1.5 did not give any noticeable effect on the mean Nusselt Number.

3.8 Discussion of The Results

This chapter has presented results of the heat transfer and pressure distribution measured around a single tube and a bank of tubes. Of particular interest to this study is the effect of fouling by changing the tube spacing in a single tube row and in a tube bank.

In the present investigation the effect of blockage and different tube arrangement have been examined. To measure local heat transfer coefficient, two different measurement techniques were applied. These were the copper strip resistance technique where the results were found to be inaccurate due to sensitivity of the measurements. Reliable measurements of local heat transfer coefficient were obtained using a micro-foil heat flux sensor and local static pressure measurements were recorded using a single pressure tapping at the tube surface. As can be seen from the results, heat transfer and pressure measurements agree with previously published data where it is available. This gives confidence that measurements made with a single tube and a bank of tubes are reliable.

For the single row experiments, if the blockage ratio is less than 0.5, the general shape of local Nusselt number distribution around the cylinder varies only slightly with blockage. When the blockage ratio is greater than 0.395, increasing blockage caused the minimum

pressure and minimum Nusselt number to move to the downstream side of the cylinder. For the blockage ratio in the range of 0.668-0.843, there is a distinct change in the flow compared with the lower blockage cases. Local Nusselt number and static pressure are remarkably different. Due to the great acceleration of the flow minimum local static pressure values reached very low values.

For a single row of tubes, a theoretical calculation was carried out for the front stagnation point and the laminar boundary layer region. Results have shown that prediction and experiments agreed well.

Hydraulic resistance is one of the important characteristics of a heat exchanger and is characterized by the total pressure drop in the flow across the tube banks. It is well known that the total pressure drop across a bank is a function of flow velocity, bank arrangement and the physical properties of the fluid. As fouling progresses, there is an increase in pressure drop through the heat exchanger resulting in a reduction in volume flow rate and a change in the air side heat transfer performance. Deposit disposition is not uniform in shape through the heat exchanger, but changes in both longitudinal and transverse pitch have been observed to cause noticeable influence on the velocity distribution around the tubes in a bank. For example for the staggered tube bundle geometry, the mean Nusselt number of the inner tubes becomes higher by increasing the transverse pitch and decreasing longitudinal pitch ratios. In the present study, only the longitudinal ratio has been changed from 1.5 to 1.25 and results have shown that did not make any difference on the mean Nusselt number. The investigation needs to be extended for different geometries. The tube bundle results have shown that the

highest Nusselt number was observed in the fourth row in the bank. Zukauskas (1972), Murray and Fitzpatric (1988) have observed that the highest heat transfer takes place in the third row of a tube bank. Porkas and Survilo (1983) obtained that the effect of turbulence becomes steady from the fourth or fifth row onwards. Also as a result of high turbulence and blockage, it was found that the first transverse row heat transfer is lower than the subsequent rows.

3.9 Concluding Remarks

Mechanical and chemical deposition of a film, in the form of dirt,ash or frost on heat exchanger surfaces is generally referred to as fouling. Provided other parameters remain constant the effect of fouling is generally to increase the resistance to heat flow by thermal insulation. As the deposits builds up in the flow passages in a heat exchanger then the flow area is reduced. The reduction of the flow area causes an increase in velocity and hence an increased resistance to flow. This results in an influence on the heat transfer performance.

In this chapter, heat and flow characteristics of a single tube and bank of tubes in a cross-flow heat exchanger have been measured in the subcritical Reynolds number range. The results show the importance of blockage and tube arrangement on the cross-flow heat exchanger's performance. Fouling geometry and effect of fouling can not be catered for directly by the present study, however the investigation may give some ideas to researchers and designers on the effect of blockage due to fouling on the heat exchanger performance.

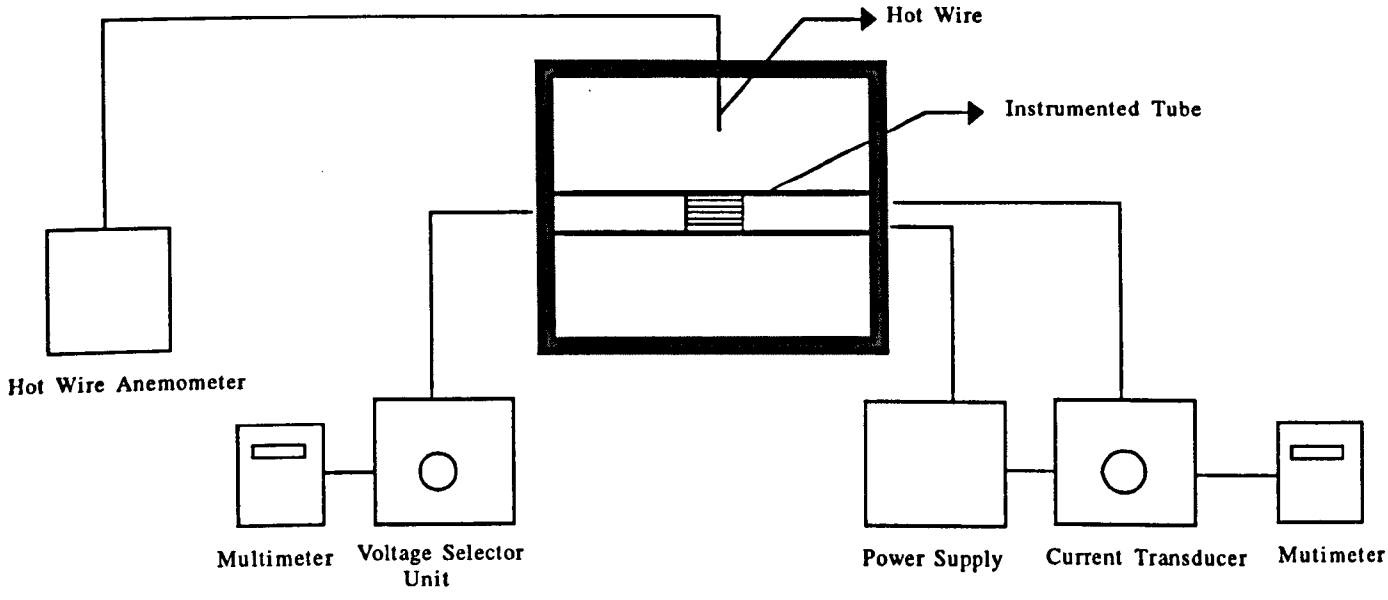

(a) Apparatus

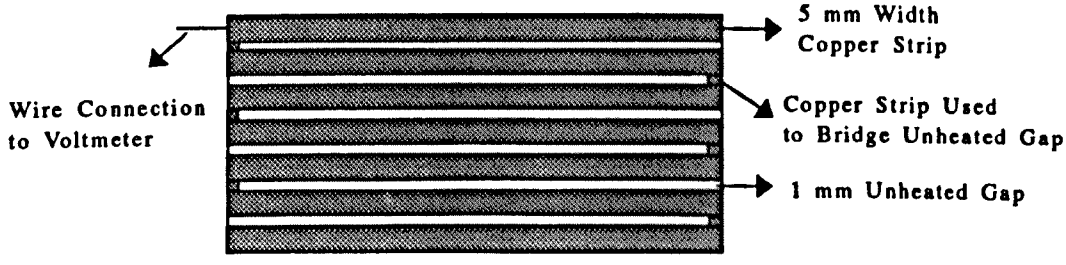

(b) Instrumented Tube

Figure 3.1 The Apparatus and Instrumented Tube for Copper Foil Technique

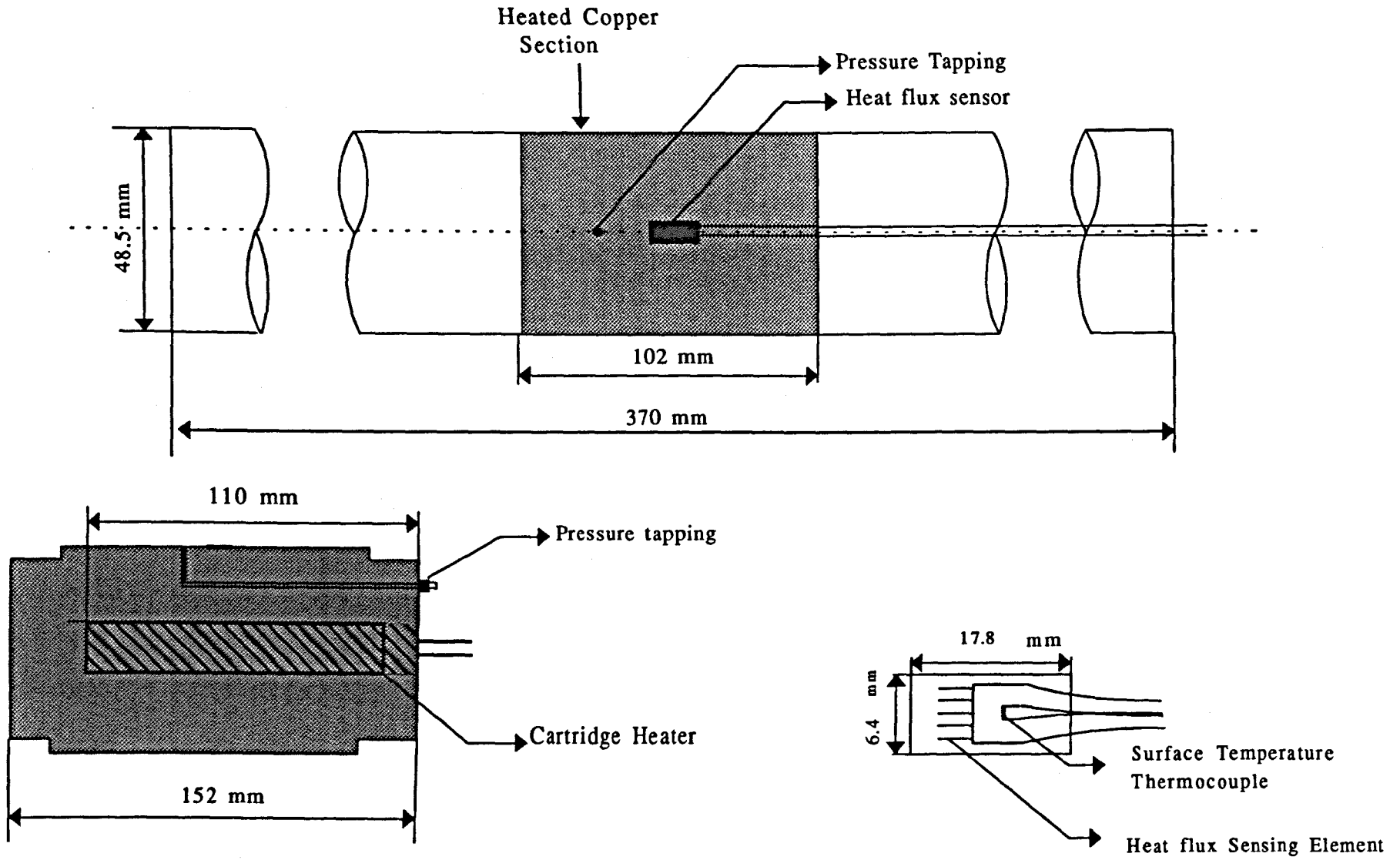

Figure 3.2 Instrumented Tube and Heat Flux Sensor

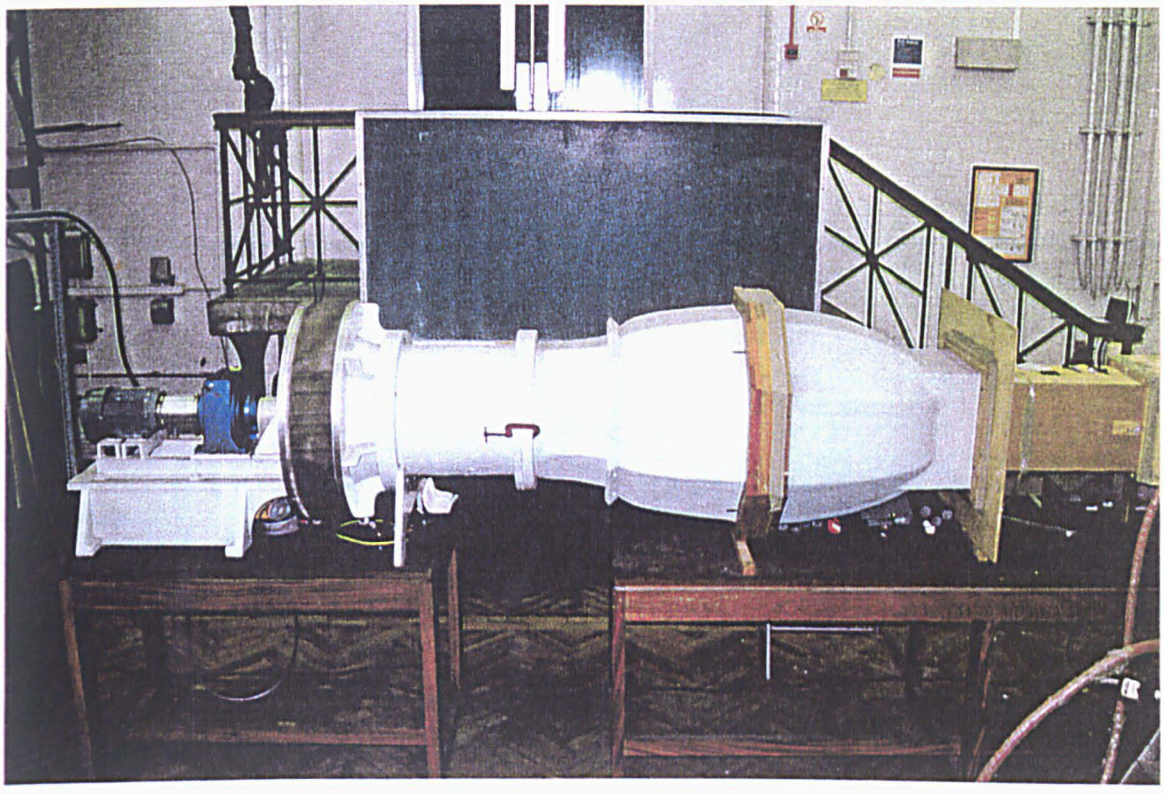

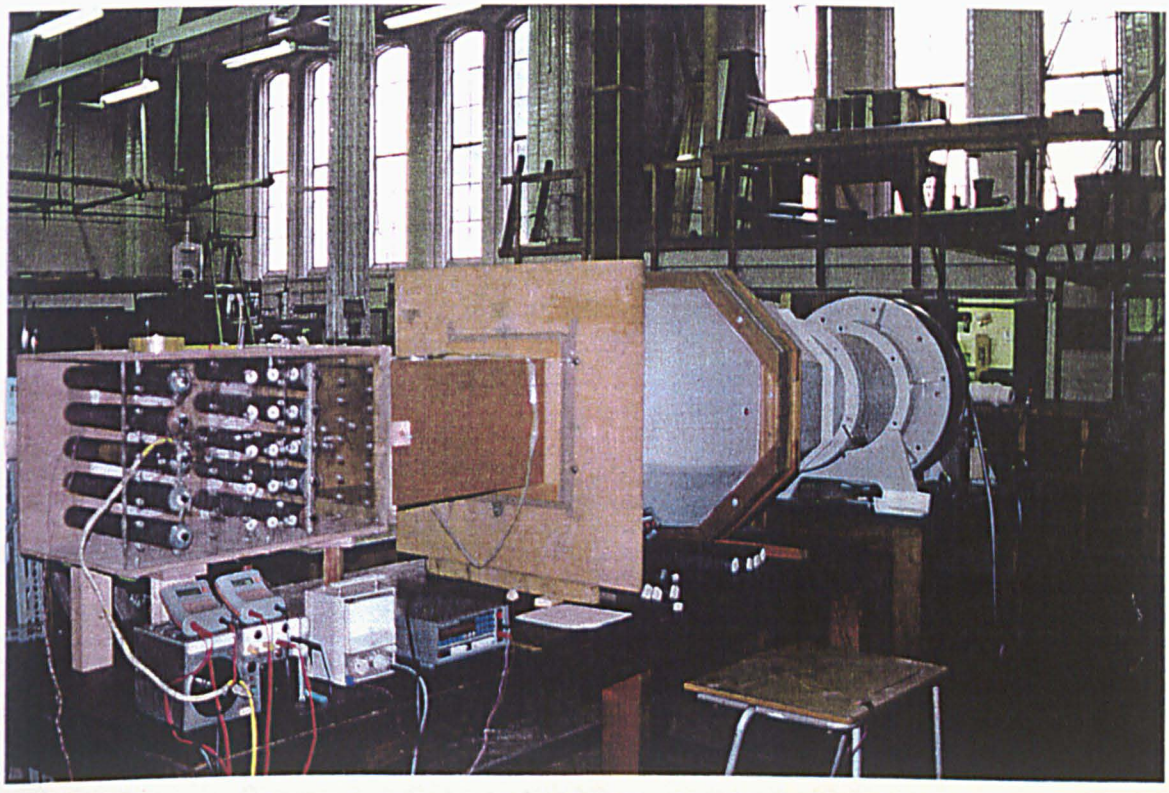

Figure 3.3 Photographs of Wind Tunnel

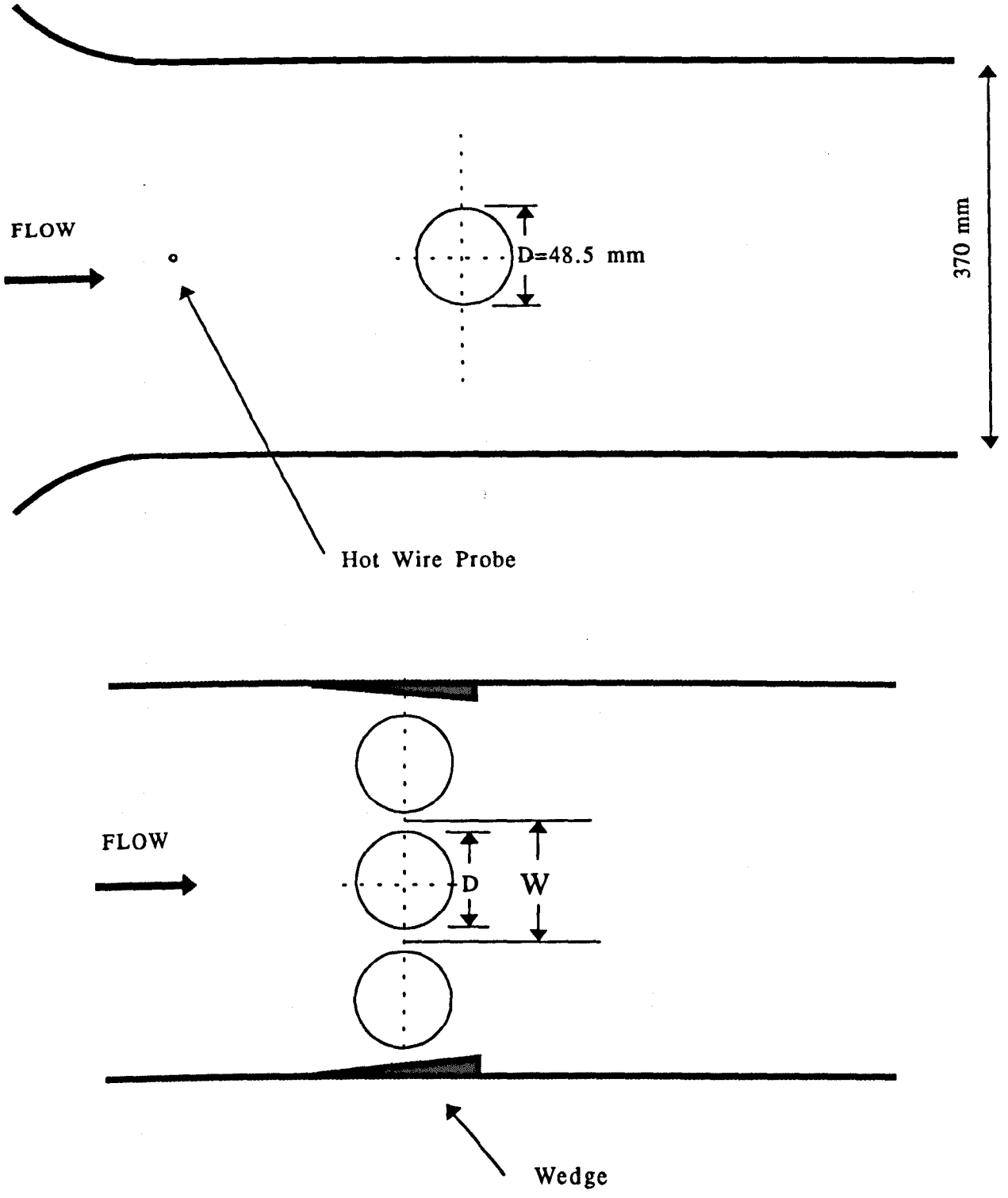

Figure 3.4 Schematic View of Single Tube
and Single Tube Row

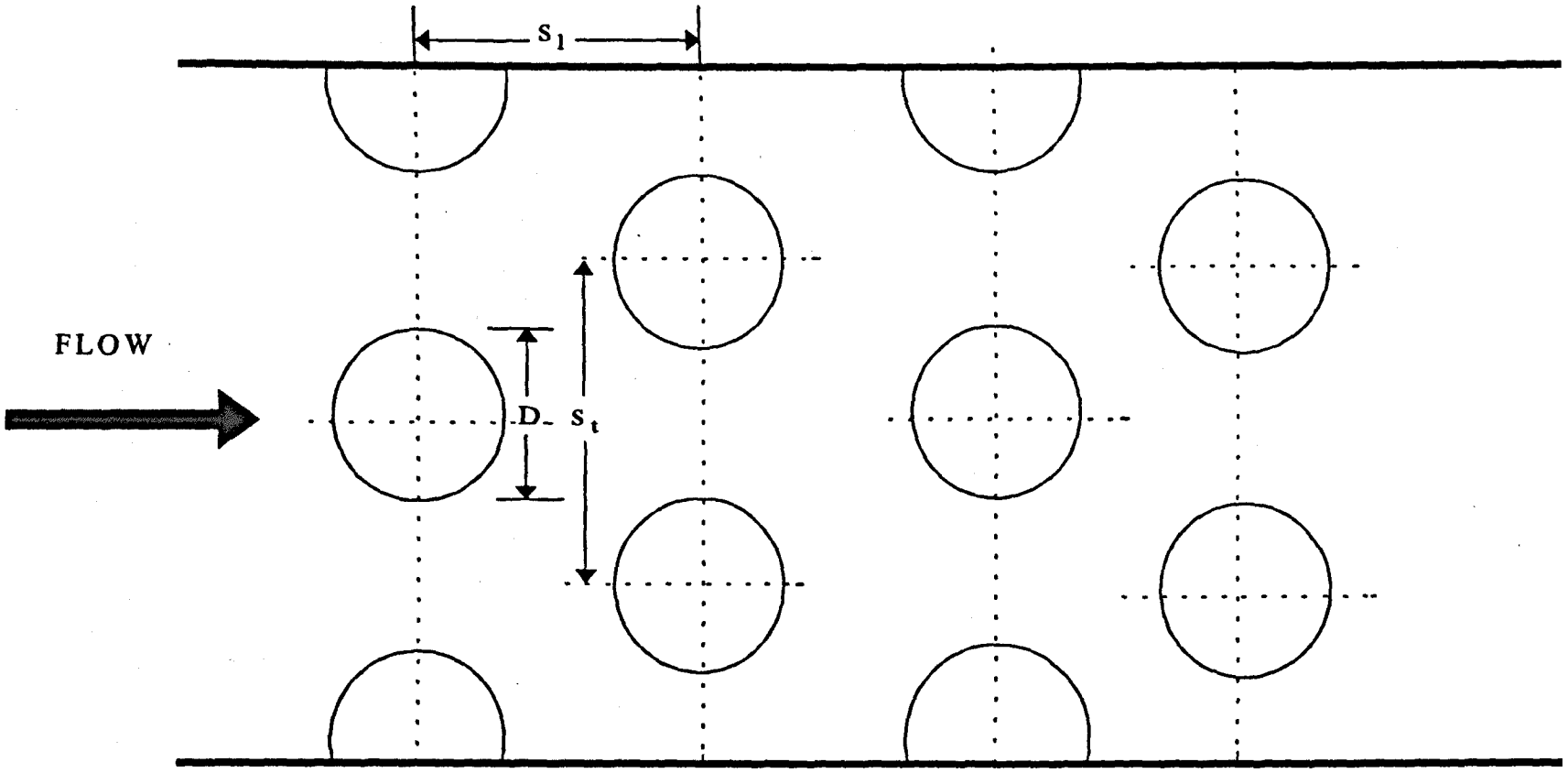

Figure 3.5 Bank of Cylinders in Cross-flow vs. Staggered Array

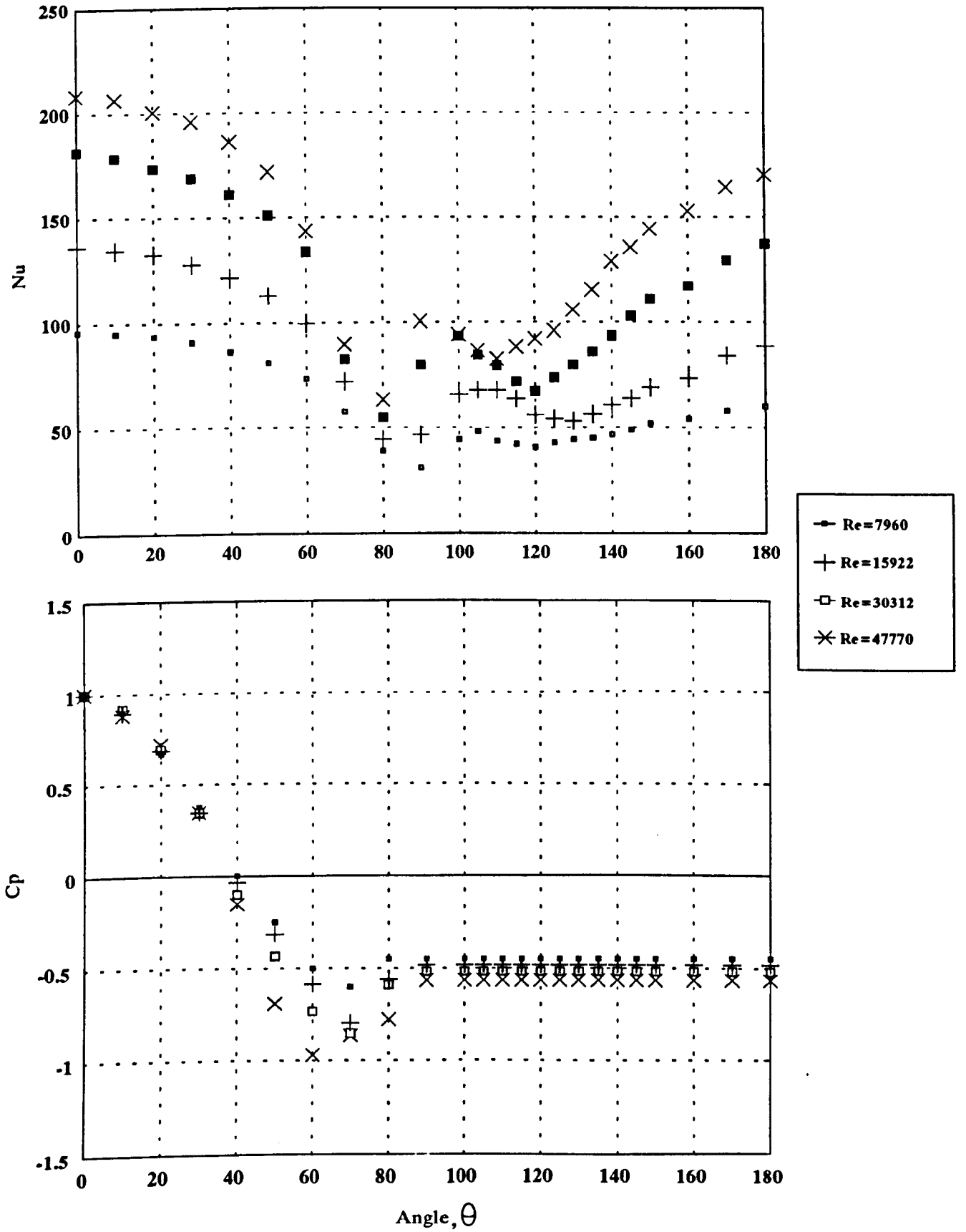

Figure 3.6 Distribution of Local Nuselt Number and Pressure Coefficient for Single Tube

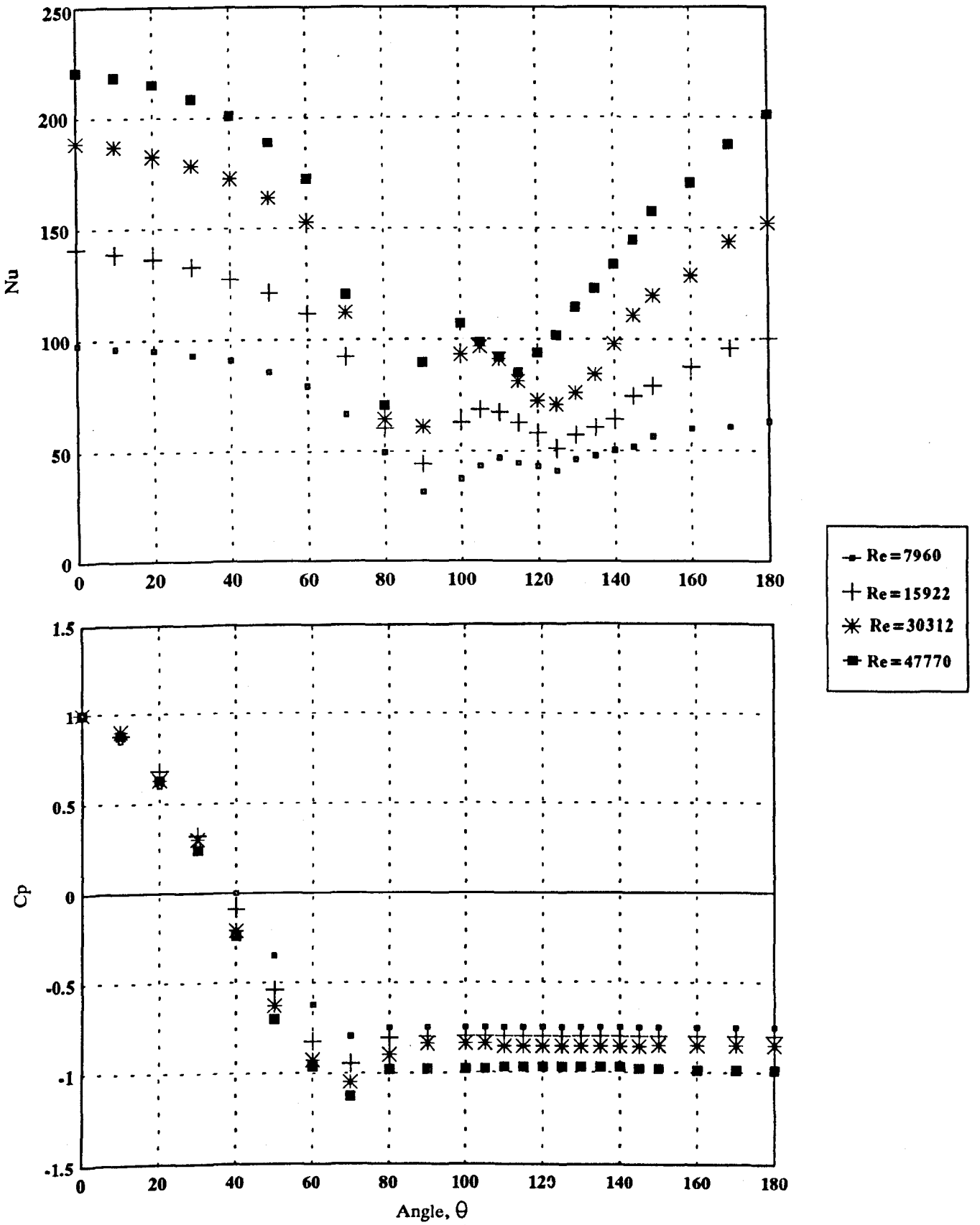

Figure 3.7 Distribution of Local Nusselt Number and Pressure Corfficient for B=0.395

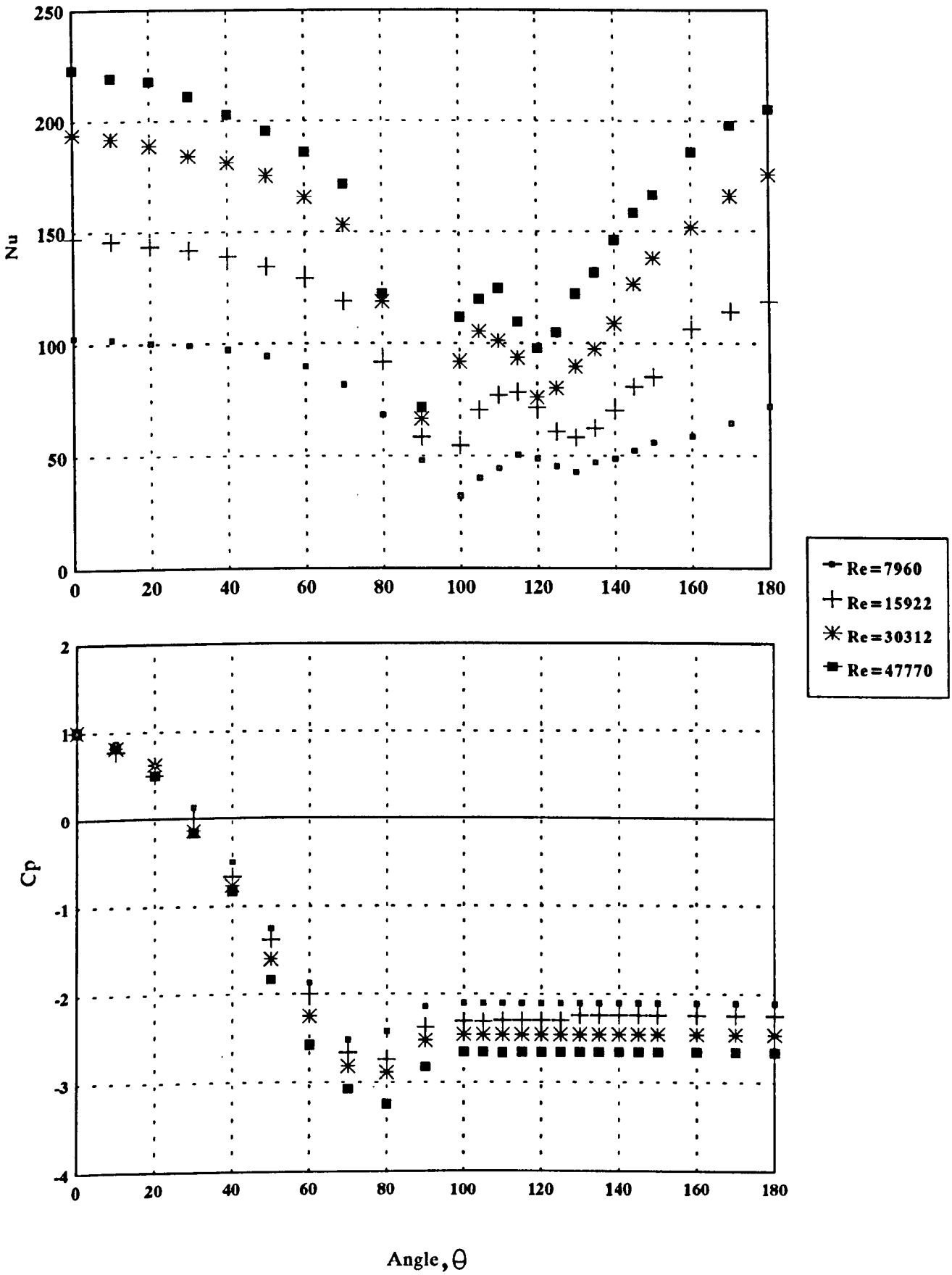

Figure 3.8 Distribution of Local Nusselt Number and Pressure Coefficient for B=0.5

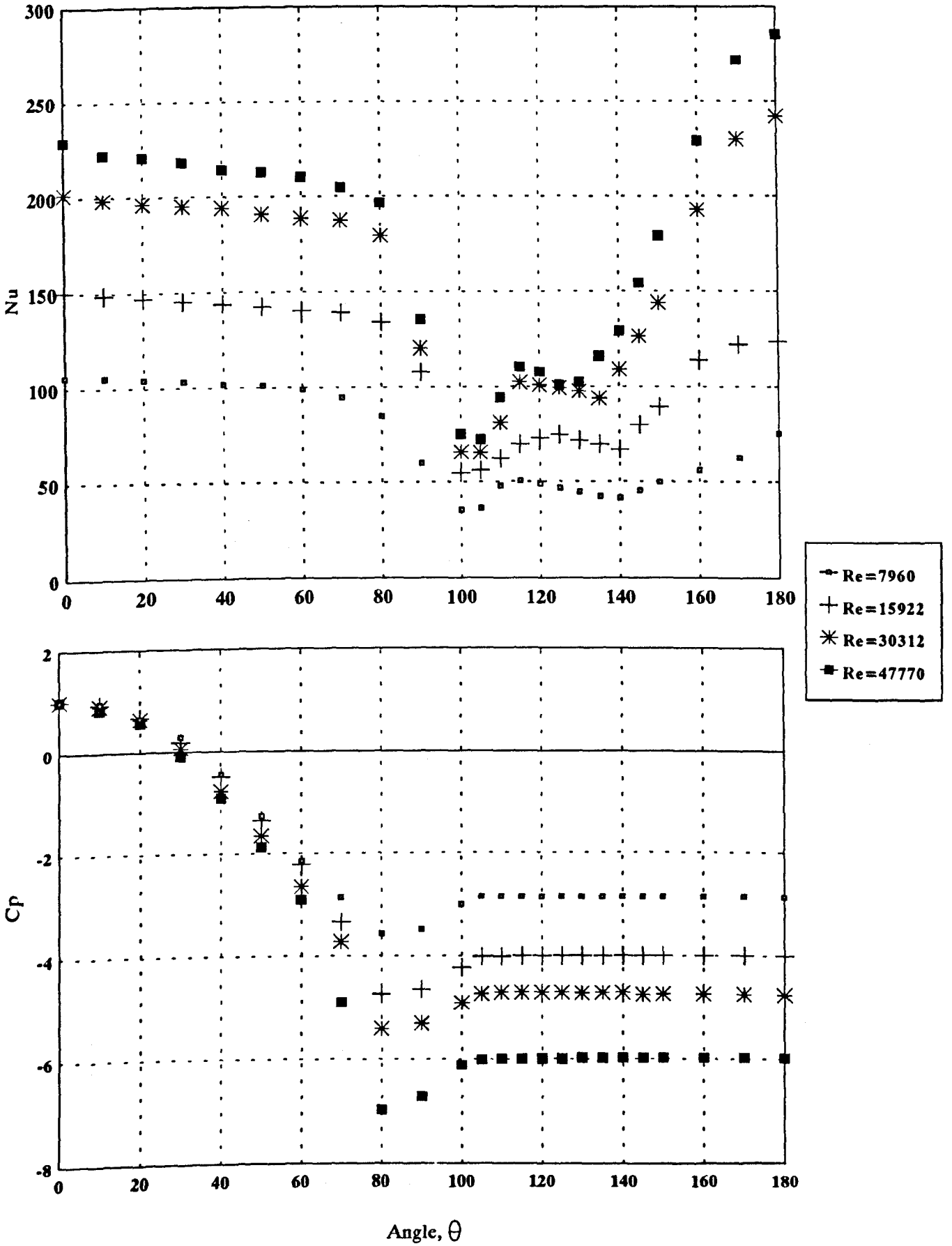

Figure 3.9 Distribution of Local Nusselt Number and Pressure Coefficient for B=0.668

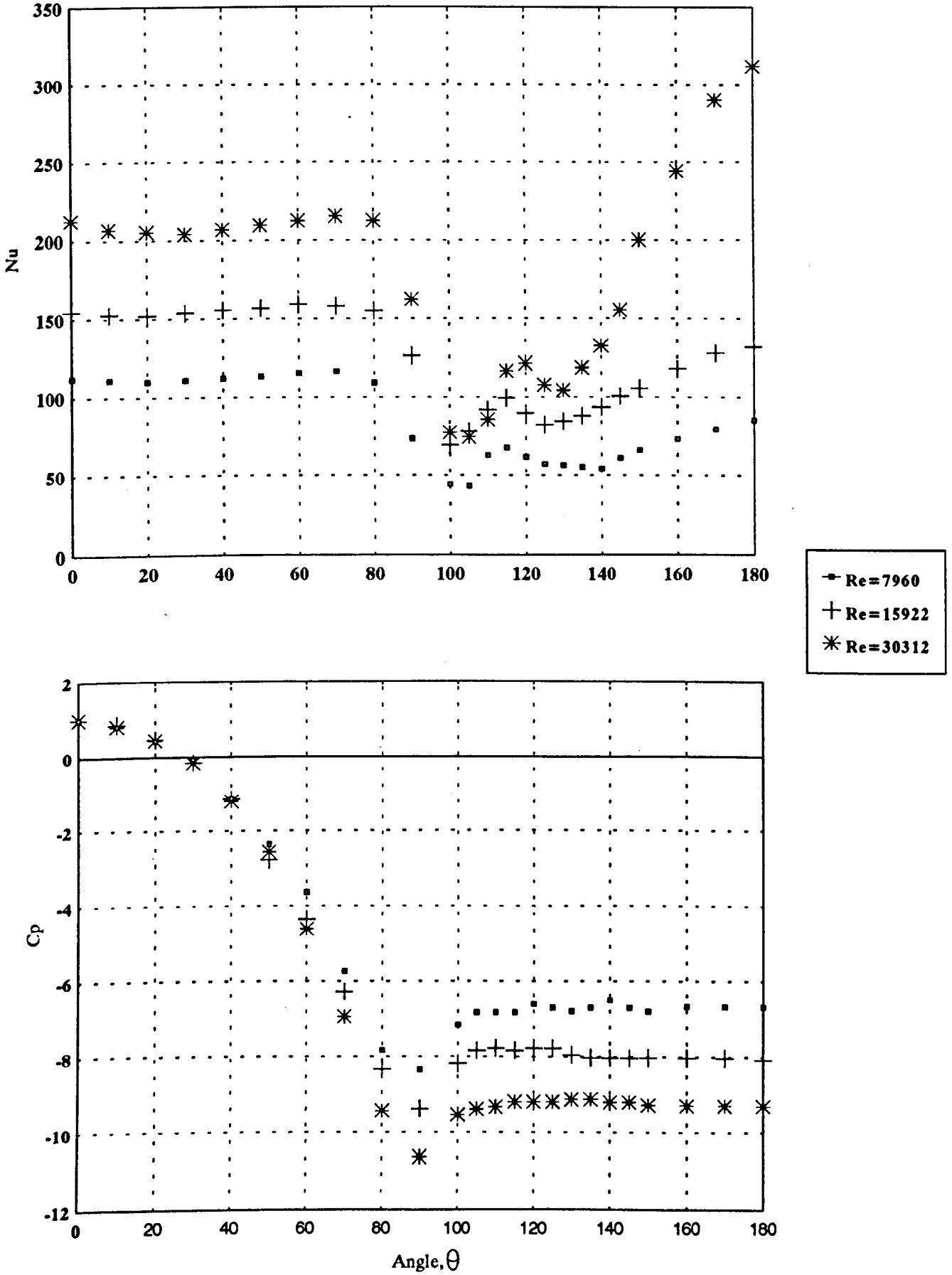

Figure 3.10 Distribution of Local Nusselt Number and Pressure Coefficient for B=0.75

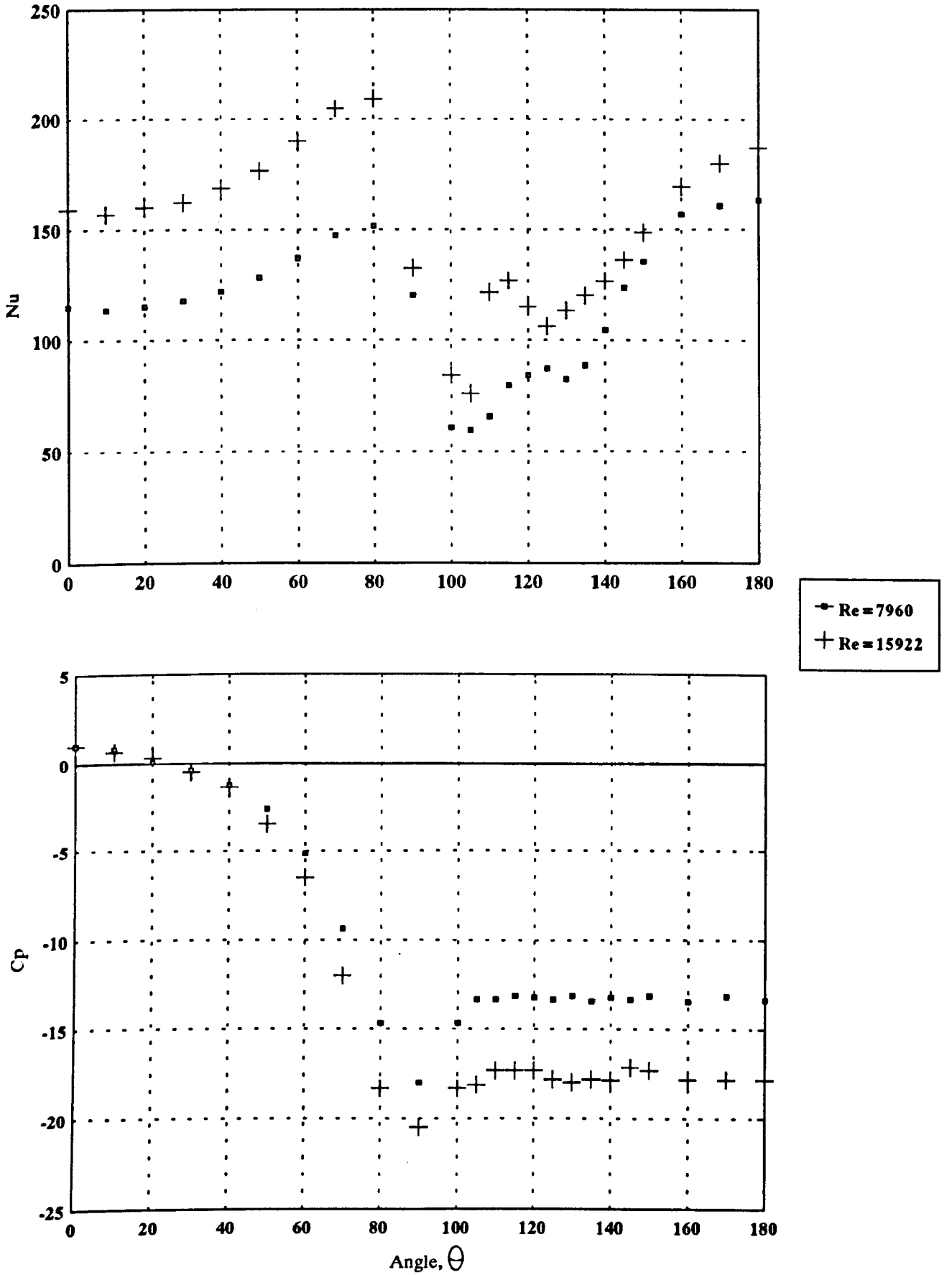

Figure 3.11 Distribution of Local Nusselt Number and Pressure Coeffient for B=0.843

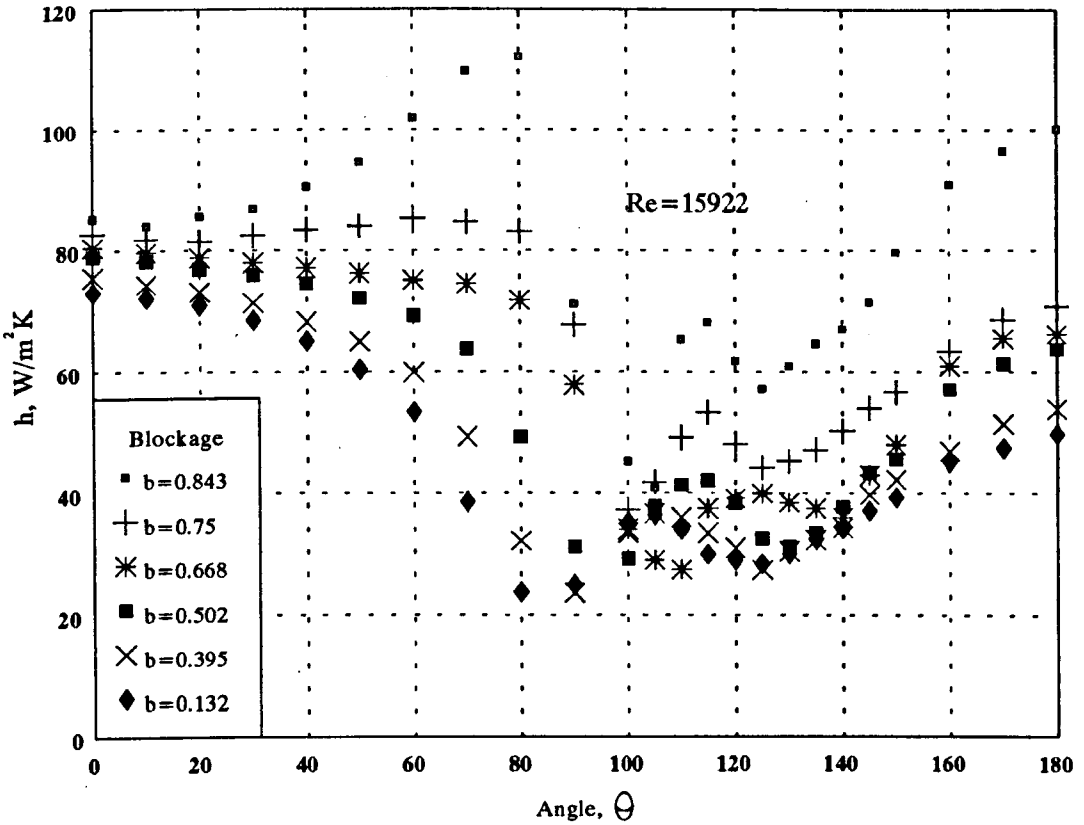

Figure 3.12 Typical Experimental Local Heat Transfer Coefficient Distribution for Multiple-Cylinders Geometry with Equal Spaces

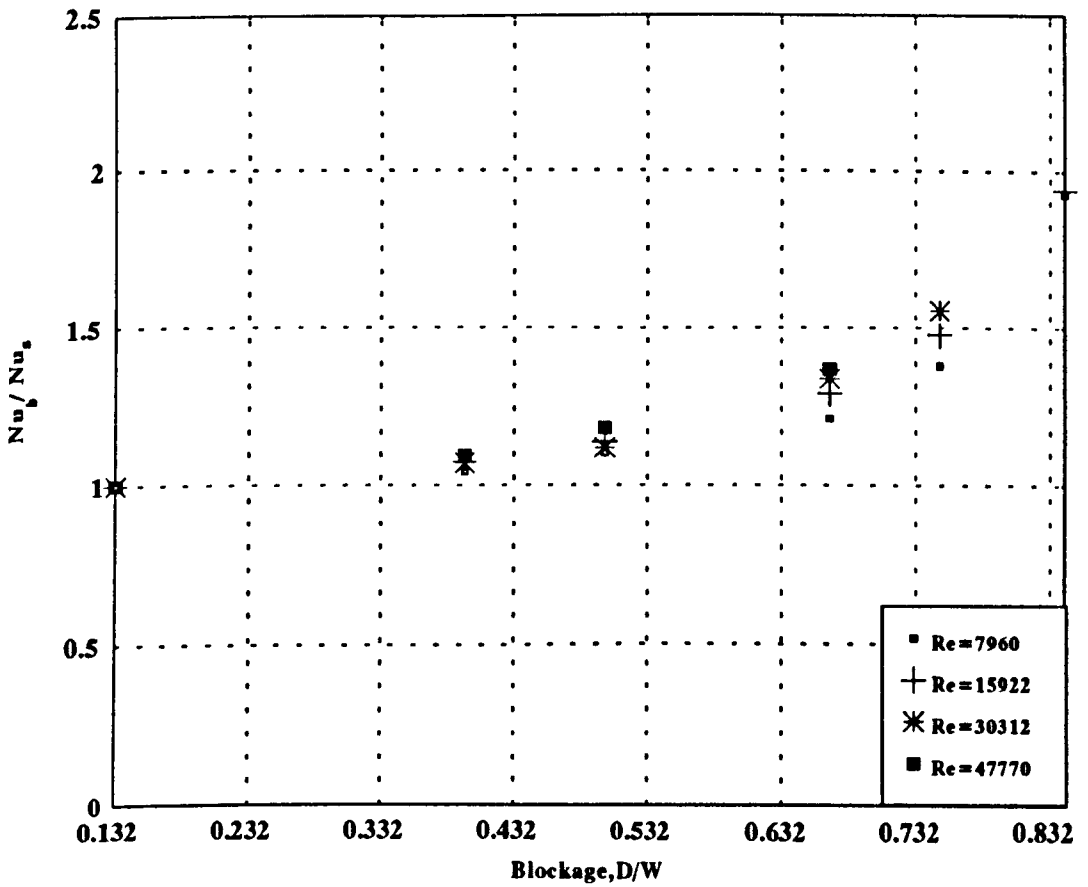

Figure 3.13 Effect of Blockage on the Mean Nusselt Number

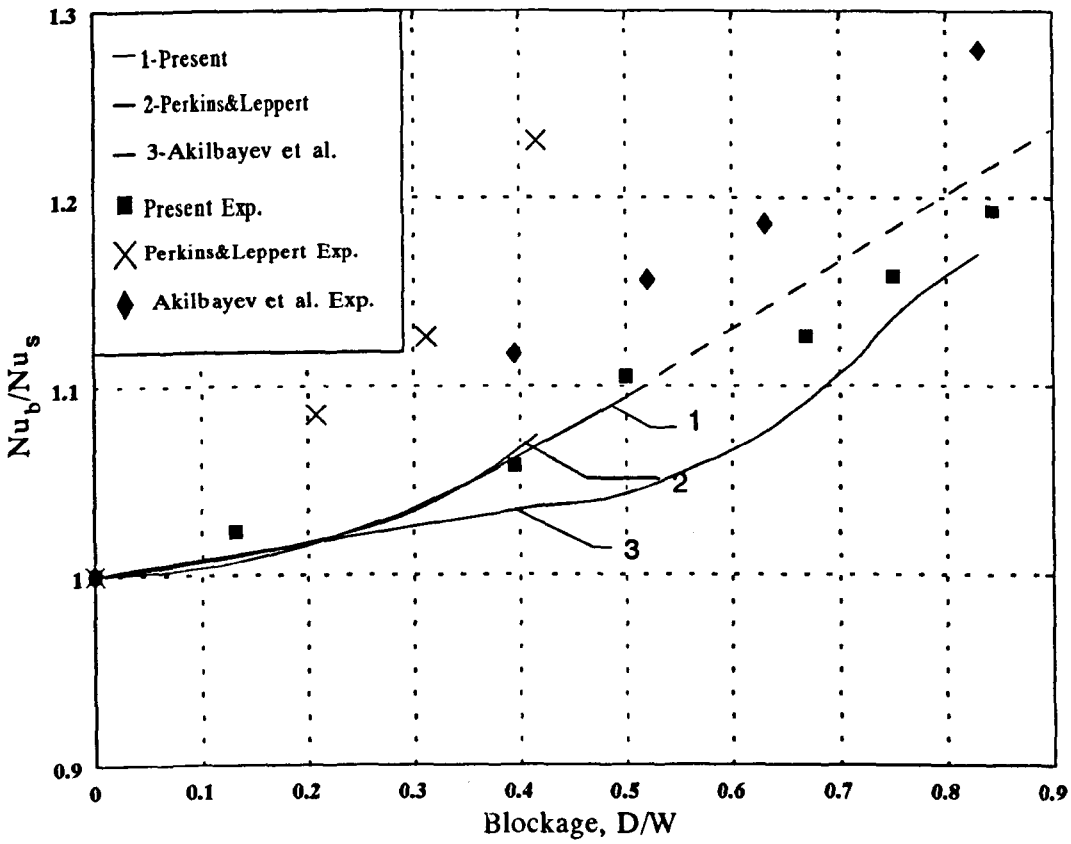

Figure 3.14 Comparison Between Theoretical and Experimental Stagnation Point Heat Transfer Coefficients

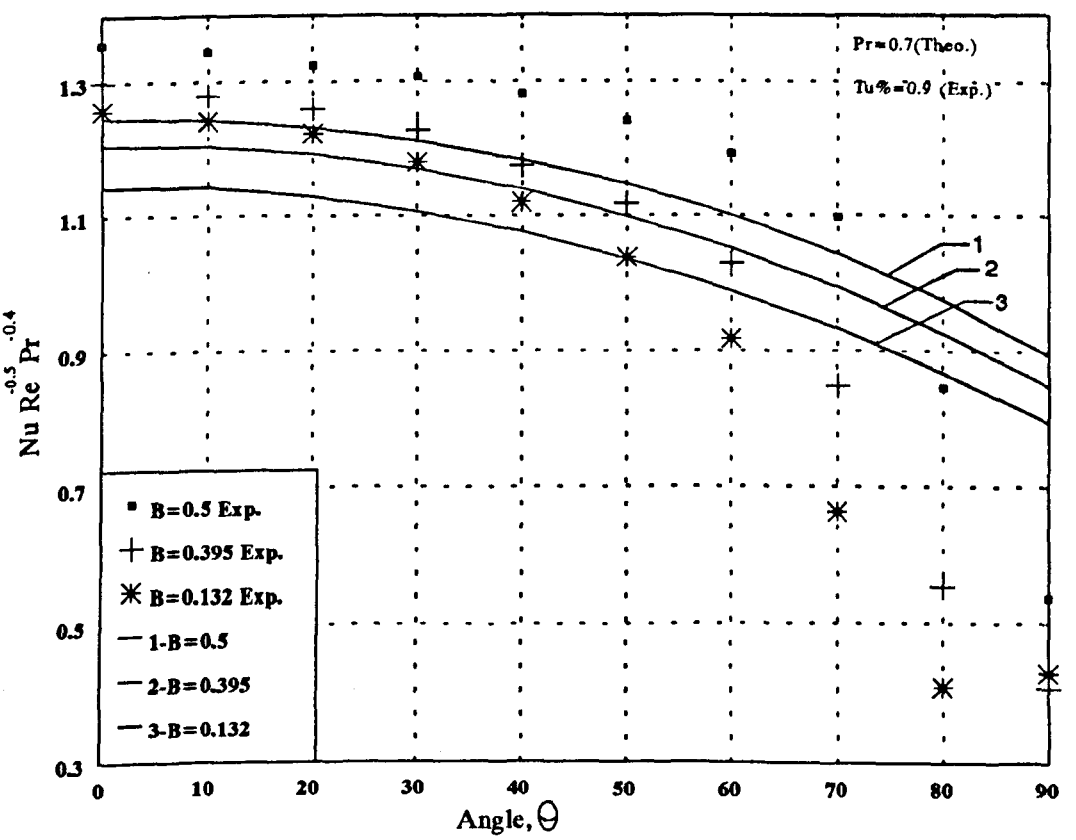

Figure 3.15 Theoretical Prediction and Experimental Results for Laminar Boundary Layer Region

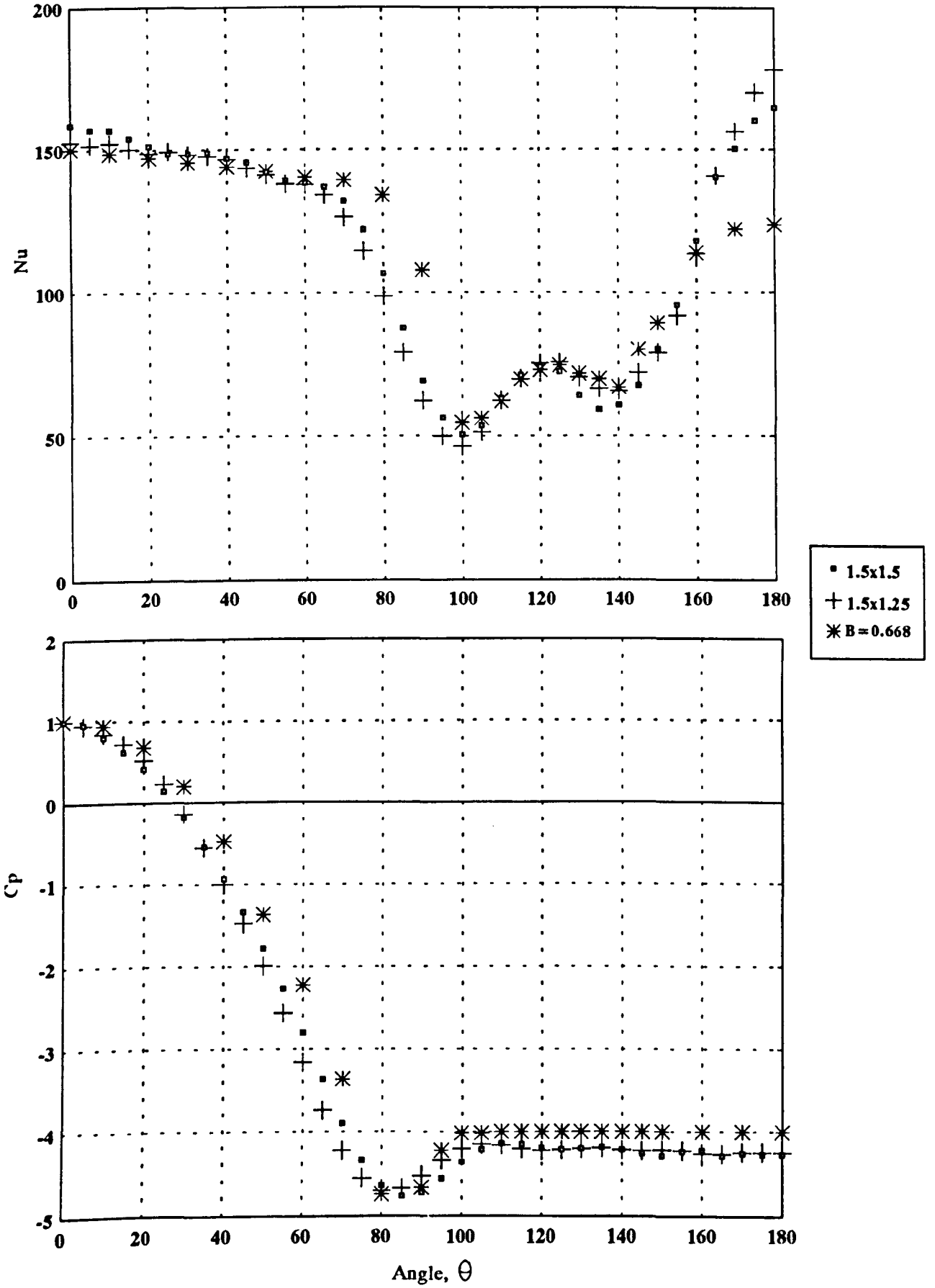

Figure 3.16 Distribution of Local Nusselt Number and Pressure Coefficient for First Row

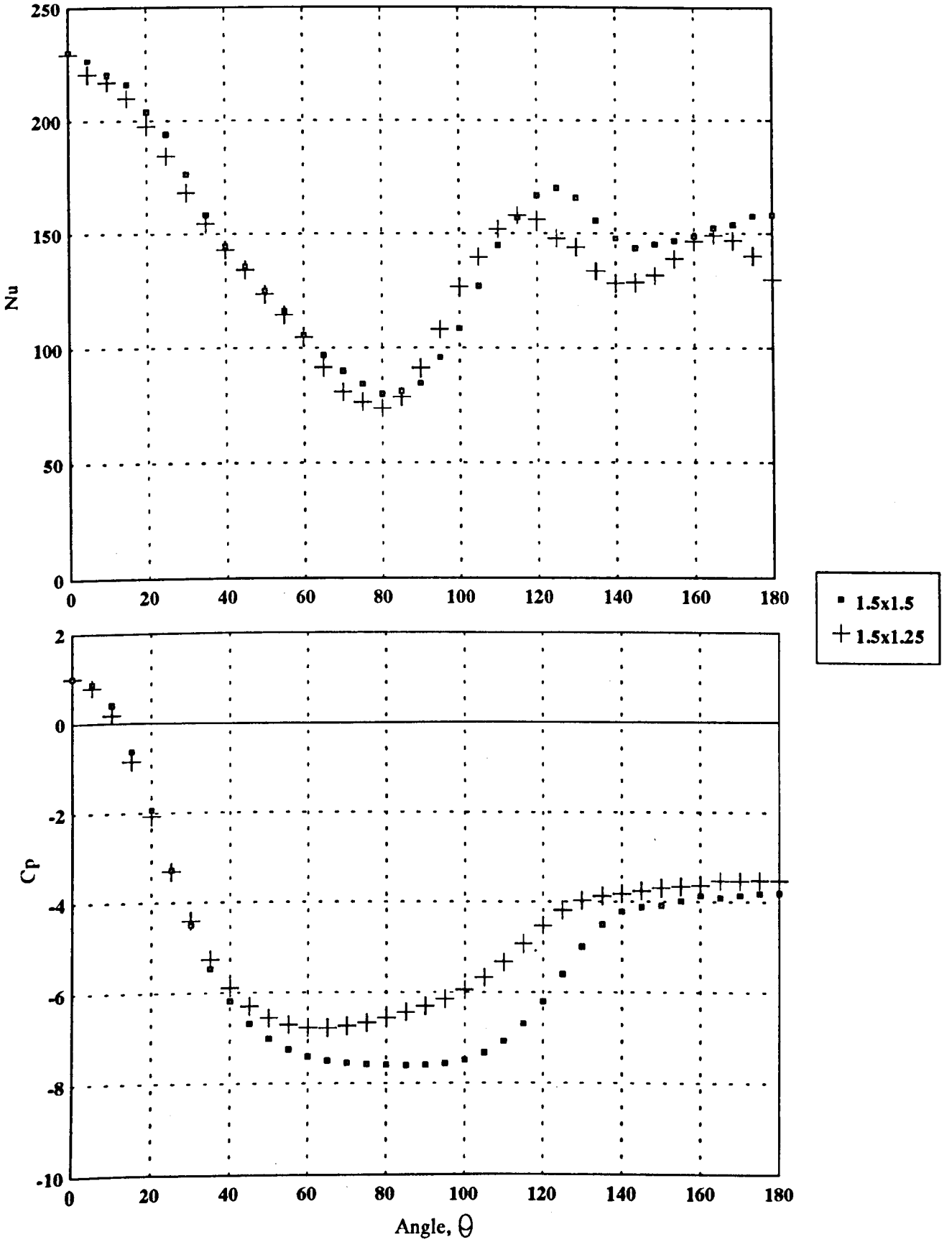

Figure 3.17 Distrubution of Local Nusselt Number and Pressure Coefficient for Second Row

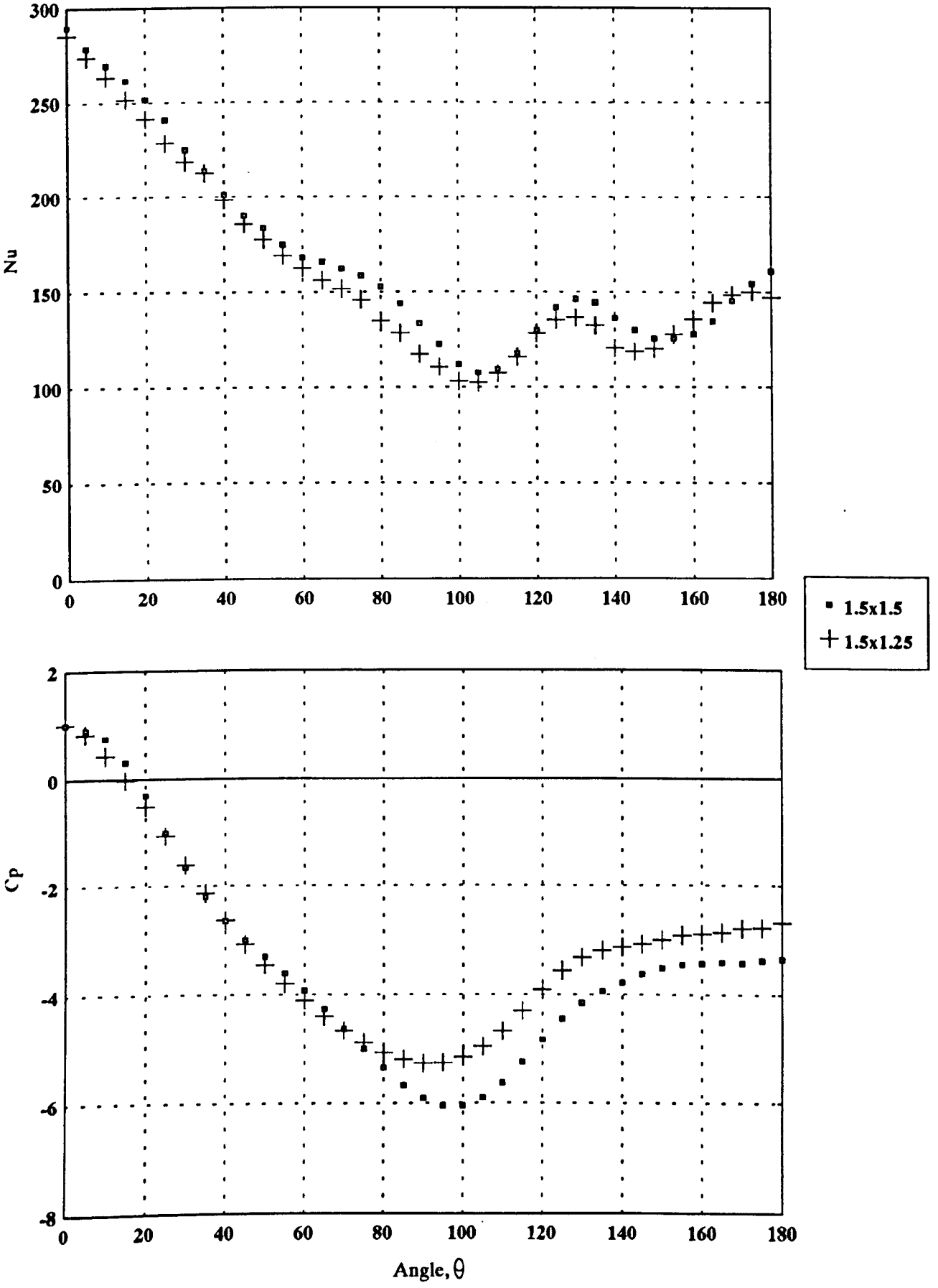

Figure 3.18 Distribution of Local Nusselt Number and Pressure Coefficient for third Row

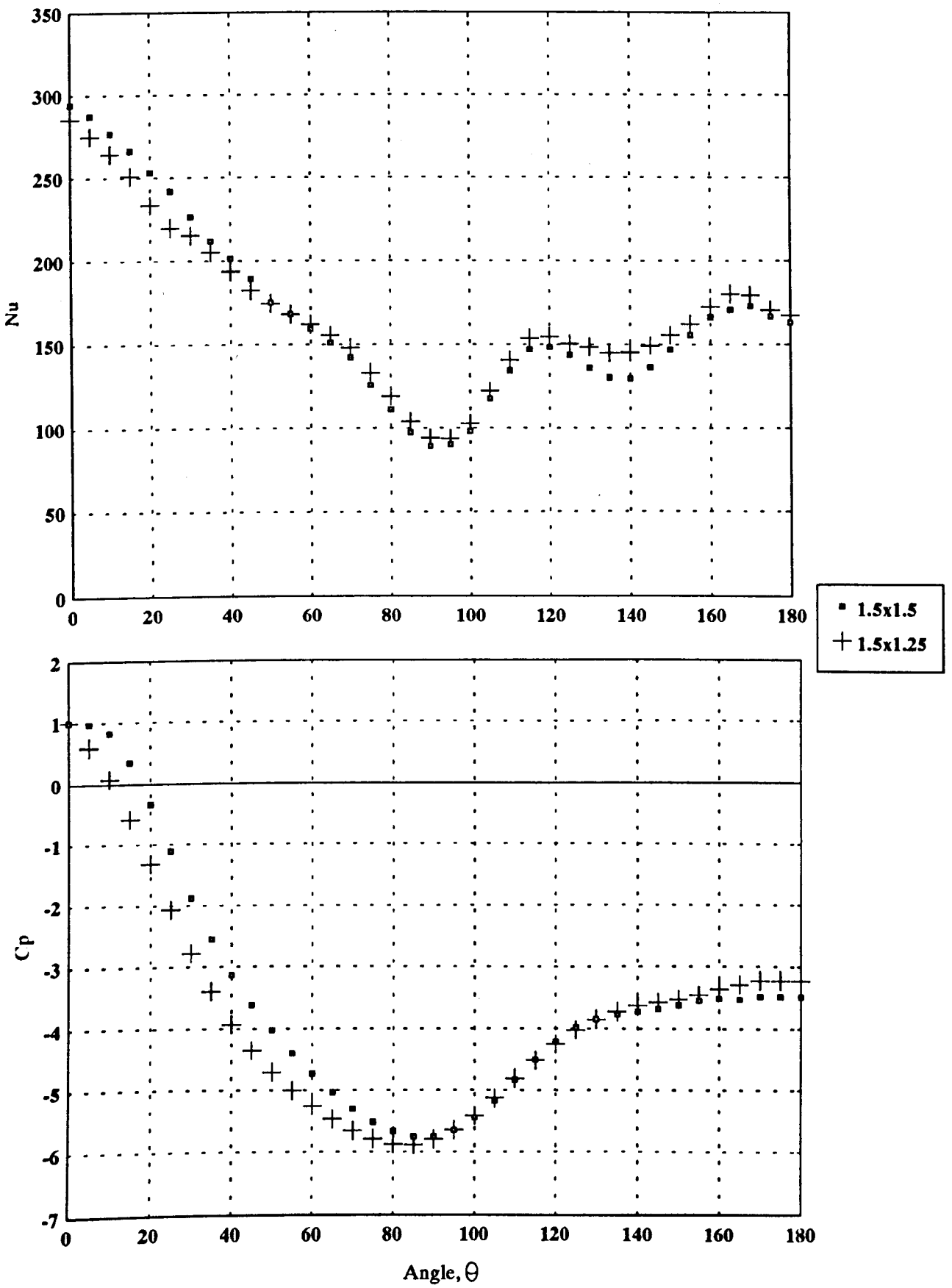

Figure 3.19 Distribution of Local Nusselt Number and Pressure Distribution for fourth Row

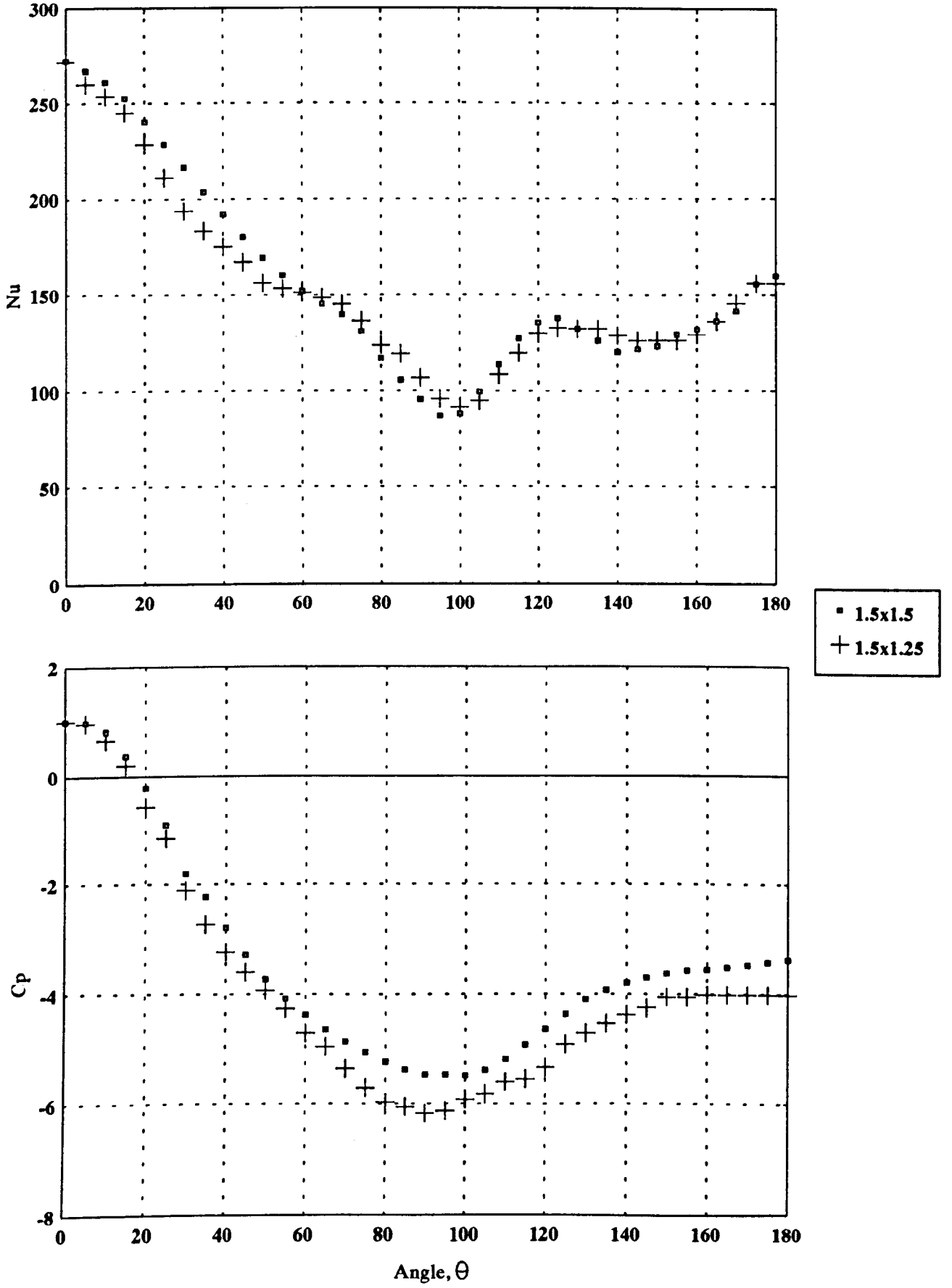

Figure 3.20 Distribution of Local Nusselt Number and Pressure Coefficient for Fifth Row

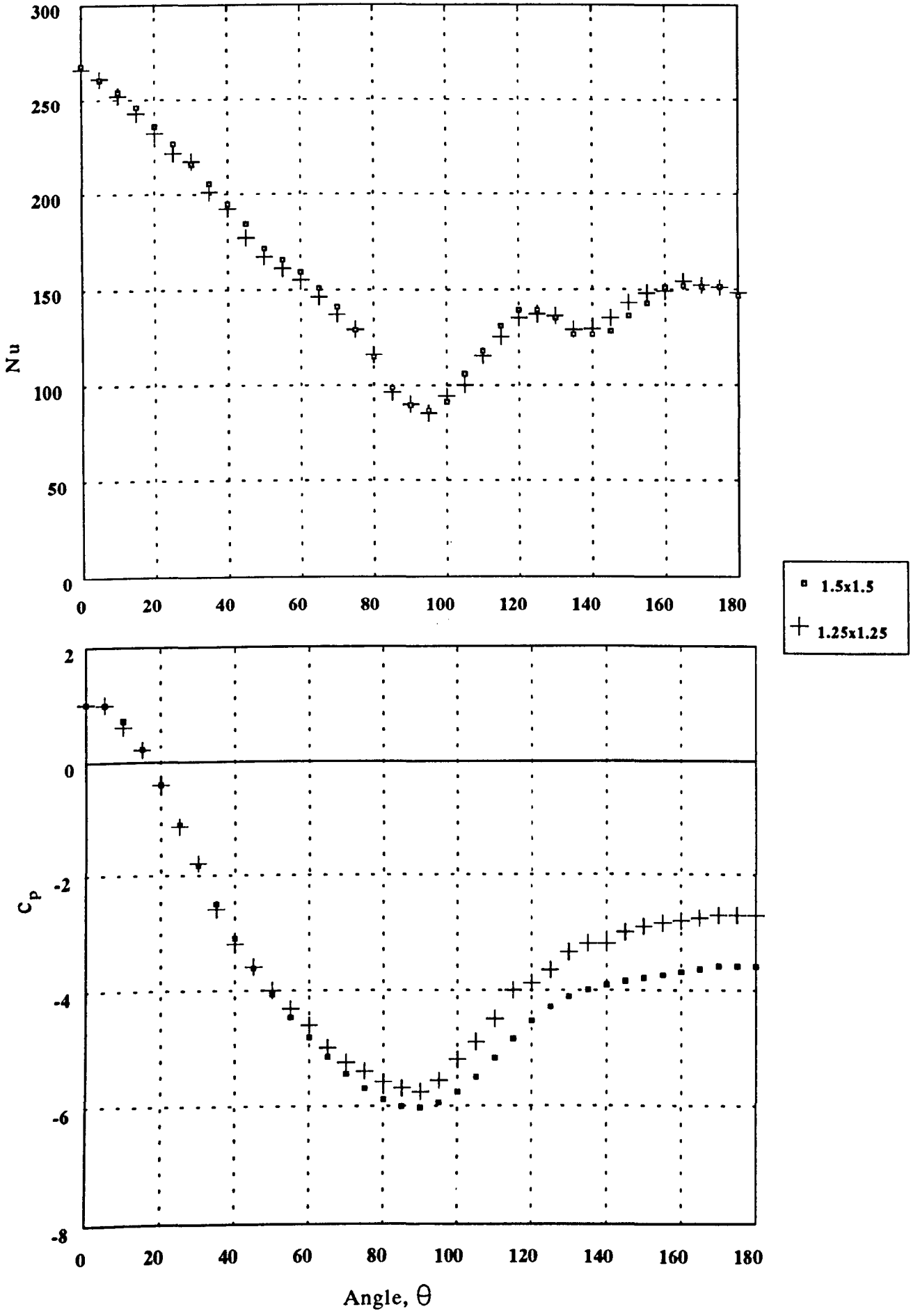

Figure 3.21 Distribution of Local Nusselt Number and Pressure Coefficient for Sixth Row

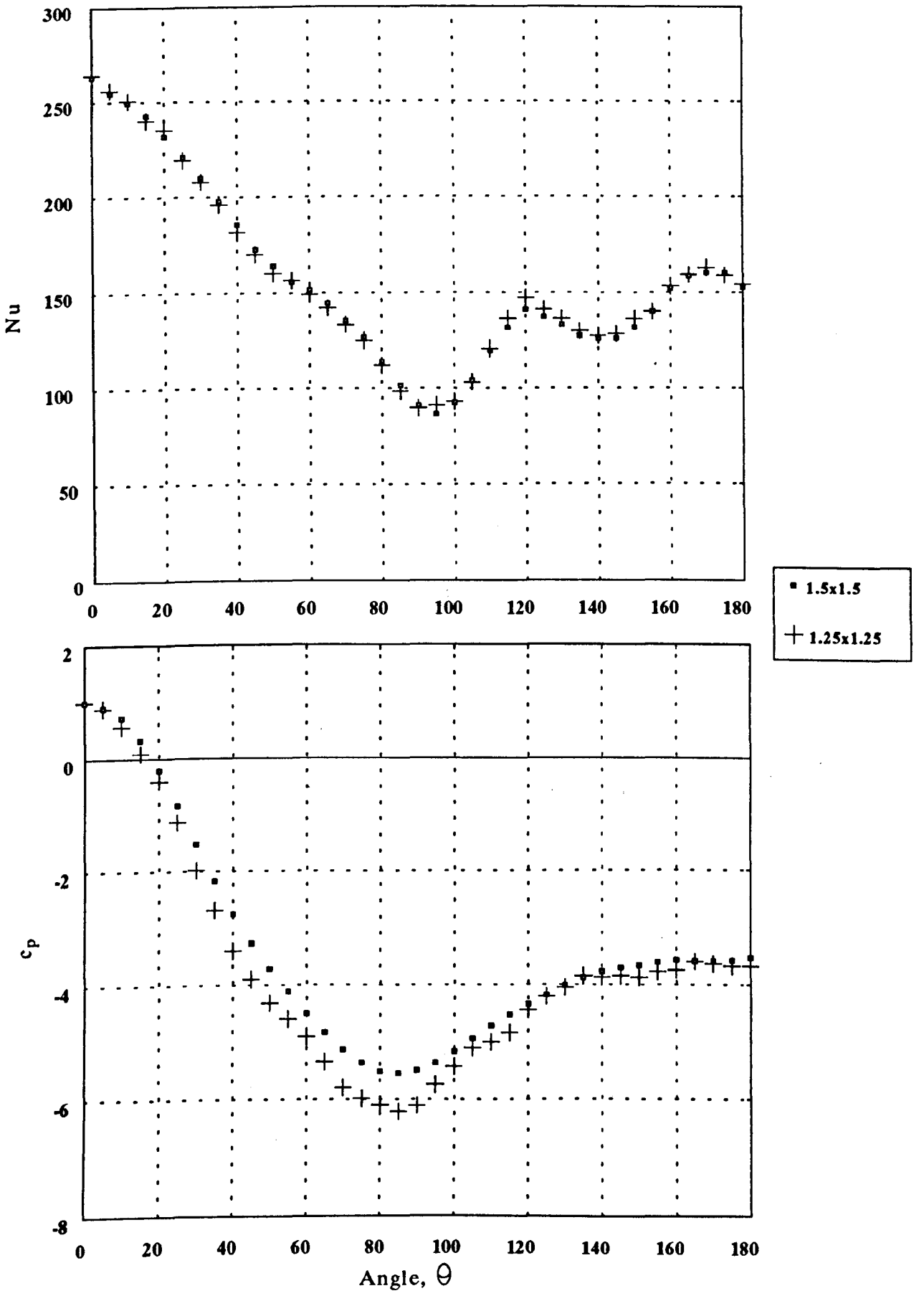

Figure 3.22 Distribution of Local Nusselt Number and Pressure Coefficient for Seventh Row

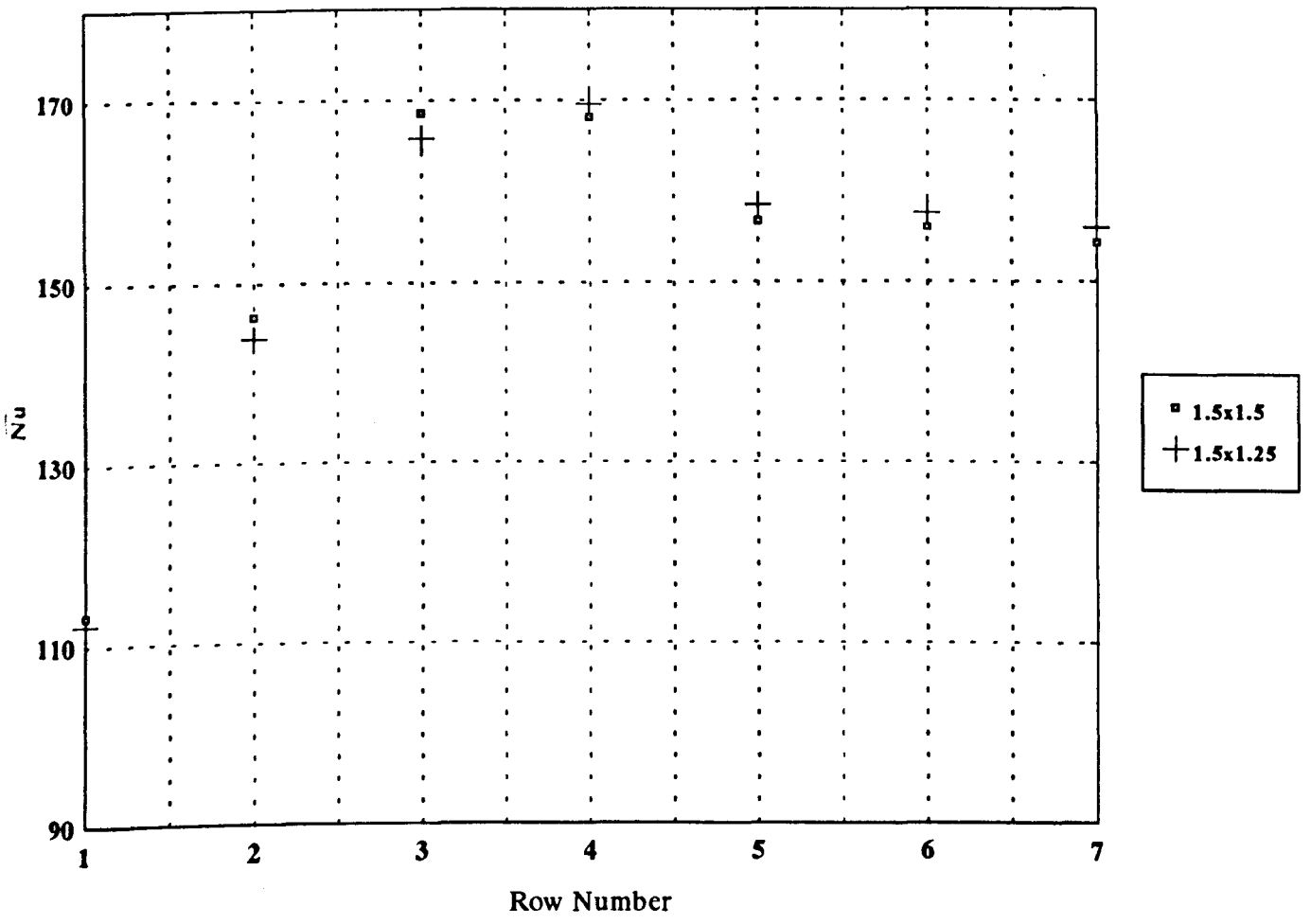

Figure 3.23 Comparison of Average Nusselt Number for(1.5x1.5) and (1.5x1.25) Staggered Tube Bundle Geometries

CHAPTER 4

NUMERICAL PREDICTION OF FLOW AND HEAT TRANSFER CHARACTERISTICS IN A TUBE AND TUBE BANK

4.1 Introduction

Heat exchangers containing tube banks in cross-flow are widely used in industrial and power engineering applications. As was shown in Chapter 3, flow and heat transfer characteristics around a tube in a tube bank are complex and depend on many conditions such as turbulence, surface roughness and the arrangement of the tube bank. As was also seen in previous chapters many experimental studies have been carried out for heat transfer and flow characteristics around tubes and tubes in a bank. Experimental work usually involves high costs and sometimes technical difficulties in obtaining direct full-scale measurements.

Heat exchanger designers often struggle to find the tube arrangement that gives the best balance of thermal output against the power needed to send the gases through it. In order to find an optimum configuration designers require detailed information on local and average gas side heat transfer coefficients. These are also of importance in predicting regions of high heat flux on the tubes which can lead to corrosion and possible tube failures. A practical approach to finding the heat transfer characteristics is to build a model of a tube bank under

consideration. Hot gases are then blown over the tubes and cooling fluid is circulated within them so that measurements can be made over the expected range of operating conditions. Correlations are considered of the variations of the heat transfer coefficients with Reynolds number and geometry. An alternative method of finding the heat transfer coefficient is to develop a theoretical model that provides data quickly and cheaply for all range of geometries and conditions. Therefore to achieve these tasks, equation of conservation of mass, momentum and energy for the whole domain will have to be solved.

Flow and heat transfer characteristics of fluid in cross-flow for a single tube and a tube bank have been described in the subcritical Reynolds numbers range in the previous chapter. Experiments were carried out for different blockage ratios for a tube within a single row with variable Reynolds number and also for different arrangements of a staggered tube bank with fixed Reynolds number. In the previous chapter, it was shown that blockage and Reynolds number had significant effects on the heat transfer from the heat exchanger tubes. An aim of this chapter is to develop a theoretical method for predicting the heat transfer and fluid flow characteristics of a single tube with different blockages and of a tube bank with different tube arrangements in the low Reynolds number range. The computational technique used is a stream function-vorticity formulation of the laminar flow steady state incompressible Navier-Stokes and energy equations developed by Johnson (1990) at Liverpool University. This application has been successful. Also, a Prandtl turbulent mixing length turbulence model developed by Johnson was applied to the case of a single cylinder. The results obtained were not consistent with the experimental data and due to the author's limited time, the necessary modification of the turbulence modelling was not possible. Results obtained with the turbulent

flow case will be explained later in the chapter.

The flow and heat transfer characteristics around a cylinder or a cylinder in a bank vary in character with changing Reynolds number. When Reynolds number is smaller than 5, the flows is laminar with closed vortices occurring behind the cylinder and remaining stable. The vortices grow up to about Reynolds number of 40. Above this value, vortex shedding occurs up to Reynolds number of about 10^3, In the tube bank, the flow is predominantly laminar in character, Zukauskas(1972). As the Reynolds number increases further, the flow becomes more turbulent but the boundary layer in the front portion of each cylinder up to the separation point remains laminar. Only a few experimental studies exist which have investigated the flow and heat transfer past a tube or tube bank in the low Reynolds number range. Eckert and Soehngen (1953) used a Mach-Zehnder Interferometer to obtain the temperature field in the wake of a heated cylinder with low Reynolds number. Krall and Eckert (1973) investigated the local heat transfer coefficient around a cylinder at low Reynolds number from 7.4 to 4640. For tube banks, the overall flow and heat transfer characteristics have been investigated by several investigators. Omohundro et al. (1949) obtained results on the overall pressure drop and heat transfer of laminar flow through a staggered tube bank. Bergelin et al. (1949) produced similar work on inline and staggered tube bank geometries.

The numerical solution of the Navier-Stokes equations and energy equation for flow and heat transfer problems may give reliable information when experimental measurements are difficult. The degree of approximation in numerical work depends on a large numbers of

factors including the solution method, mesh size, boundary conditions and stability and convergence criteria used to obtain the solution. Many related engineering applications of the numerical heat transfer and flow characteristics of a single tube and tube banks have been studied. The earliest numerical solution for steady flow of viscous incompressible fluid past a circular cylinder were reported by Thom (1933) for Reynolds numbers of 10 and 20. Dennis et al.(1968) studied steady laminar forced convection on a circular cylinder in a Reynolds number range from 0.01 to 40. Chen (1986) et al. developed a finite element solution of laminar flow and heat transfer in a tube bank. They obtained local Nusselt number, pressure distribution and the surface shear stress distribution for staggered and in line tube bank configurations with combined convection conditions. Jain and Goel (1976) obtained results for unsteady laminar forced convection from a circular cylinder. They used finite difference equations to solve the Navier Stokes and energy equations. Local Nusselt number distribution of their results is in good agreement with Eckert and Soehngen's (1953) experimental results. Another numerical analysis of unsteady flow and heat transfer to a cylinder in cross-flow was developed by Paolino et al.(1986). They used two dimensional flow with a viscous and incompressible fluid of constant properties and analyzed this by integrating the vorticity transport equation and the energy equation. They predicted local and average Nusselt numbers in unconfined cross-flow. Their comparison of local Nusselt number distribution with Giedt's (1949) experimental work is found to be good only in the front region of the tube. Launder and Massey (1978) carried out a numerical prediction of viscous flow and heat transfer in tube banks. Their numerical results for laminar flow have given close agreement with experimental data at Reynolds numbers of 10 and 10^3. Fujii et al.(1986) considered a theoretical prediction of heat transfer characteristics in a tube bank. They considered first the

case where only one tube was heated within the bank and then, second, when all the tubes in the bank were heated. Reynolds numbers were in the range of 120-300. They found that for the first row, the heat transfer coefficient was nearly the same as when only the single tube was heated and when all the tubes were heated. For the third row, the heat transfer rate of the single tube was higher than the corresponding case when all the tubes were heated due to the interference between the temperature fields. Zdrovistch et al.(1995) developed a numerical prediction of laminar and turbulent fluid flow and heat transfer in tube banks. They presented their results in two-dimensional form of velocity vectors, stream lines, pressure coefficients and temperature contours.Their results were found to be in good agreement with experimental results. Antonopoulas (1985) studied the heat transfer in the tube assemblies under conditions of laminar axial, transverse and inclined flow. Faghri and Rao (1987) carried out a numerical study to predict fluid flow and heat transfer characteristics in an inline tube bank for Reynolds numbers from 1 to 1000.

4.2 Numerical Modelling

4.2.1 Grid

The resolution obtained in a flow calculation is limited firstly by the number of grid points and secondly by their distribution. The distribution of a fixed number of grid points can be varied throughout the flow domain to obtain an optimum overall accuracy or optimum resolution of detail in the flow region of particular interest. Rapid changes in the spacing of the grid lines may cause poor accuracy, therefore such rapid changes should be avoided. It is therefore well advised to concentrate grid points in areas where strong velocity gradients occur.

Some flow problems can be solved using an orthogonal coordinate system (ξ,η) where ξ and η are known functions of x and y and the flow boundaries are lines of constant ξ or constant η. The grid is then simply made up of lines of constant ξ and lines of η. Common examples are cylindrical and spherical co-ordinate arrangements.

In the present study, the grid generation is based on that of Thompson et al.(1974) and developed by Johnson(1990). The method generates orthogonal curvilinear grids by solving the two Laplace equations for ξ and η which are solved using centre difference and Gauss-Seidel relaxation technique. Thompson et al. specify the x,y coordinates on all the constant ξ boundaries whilst the values on the η boundaries are allowed to float. The geometries considered by Thompson et al. are for external flows where a rectangular ξ and η grid is wrapped around the body with η boundaries coincident, this is called the 'O' grid. This means that points on the η boundaries can in fact be treated as internal points. Multiple bodies are also handled in a similar fashion.

4.2.2 Computational Technique of Solving Conservation Equations

Flow and heat transfer through the geometry is governed by partial differential equations derived from the laws of conservation of mass, momentum and energy. The governing equations for laminar flow and steady state are given (for simplicity, cartesian coordinates (x,y) equations are presented, but can be transformed to orthogonal (ξ,η) system) as:

Continuity Equation

$$\frac{\partial u}{\partial x}+\frac{\partial v}{\partial y}=0 \tag{4.1}$$

Momentum Equations

$$\frac{\partial P}{\partial x}+\rho u\frac{\partial u}{\partial x}+\rho v\frac{\partial u}{\partial y}=\mu\left[\frac{\partial^2 u}{\partial x^2}+\frac{\partial^2 u}{\partial y^2}\right] \tag{4.2}$$

$$\frac{\partial P}{\partial y}+\rho u\frac{\partial v}{\partial x}+\rho v\frac{\partial v}{\partial y}=\mu\left[\frac{\partial^2 v}{\partial x^2}+\frac{\partial^2 v}{\partial y^2}\right] \tag{4.3}$$

Energy Equation

$$u\frac{\partial T}{\partial x}+v\frac{\partial T}{\partial y}=\alpha\left[\frac{\partial^2 T}{\partial x^2}+\frac{\partial^2 T}{\partial y^2}\right] \tag{4.4}$$

Two momentum and one continuity equations together with the appropriate boundary conditions contain enough information for solution of the velocity components u and v and pressure at any point. The temperatures can be found by application of the energy equation. In the present study, the computational technique used is a stream function-vorticity formulation of laminar, steady Navier-Stokes equations with assumed constant density developed by Johnson (1990). A stream function, ψ, which satisfies equation (4.1), is

introduced as:

$$\frac{\partial \psi}{\partial y} = u \quad , \quad -\frac{\partial \psi}{\partial x} = v \tag{4.5}$$

and the vorticity Ω is then written as:

$$\Omega = \frac{\partial u}{\partial y} - \frac{\partial v}{\partial x} = \frac{\partial^2 \psi}{\partial x^2} + \frac{\partial^2 \psi}{\partial y^2} \tag{4.6}$$

$$\Omega = \nabla^2 \psi$$

Replacing u and v in equations (4.2) and (4.3) using equation (4.5) and equation (4.6) then gives

$$\frac{1}{\rho}\frac{\partial P}{\partial x} + \frac{\partial \psi}{\partial y}\frac{\partial \psi}{\partial x \partial y} - \frac{\partial \psi}{\partial x}\frac{\partial^2 \psi}{\partial y^2} = \nu \frac{\partial \Omega}{\partial y} \tag{4.7}$$

$$\frac{1}{\rho}\frac{\partial P}{\partial y} - \frac{\partial \psi}{\partial y}\frac{\partial^2 \psi}{\partial x^2} + \frac{\partial \psi}{\partial x}\frac{\partial \psi}{\partial x \partial y} = -\nu \frac{\partial \Omega}{\partial x} \tag{4.8}$$

However the solution of the continuity and momentum equations is not easy since there is no equation when pressure (P) is the subject and it will need complex reorganization, therefore equations (4.7) and (4.8) are cross-differentiating with respect to x and y respectively and subtracting to eliminate the pressure terms. This then leads to

$$\nu\nabla^2\Omega = \frac{\partial\psi}{\partial y}\frac{\partial\Omega}{\partial x} - \frac{\partial\psi}{\partial x}\frac{\partial\Omega}{\partial y} \tag{4.9}$$

Equations (4.4), (4.6) and (4.9) are solved simultaneously to obtain temperature, stream function and vorticity values. Once stream function is known, the velocities can be determined from equation (4.5).

Now, to calculate pressure distribution on the boundaries, equations (4.7) and (4.8) are integrated around the perimeter of the calculation domain. When static pressure distribution is needed through the flow, it is necessary to derive a Poisson equation for the pressure by summing equations (4.7) and (4.8) after differentiating with respect to x and y respectively, hence

$$\frac{1}{\rho}\nabla^2 p = 2\left(\frac{\partial^2\psi}{\partial x^2}\frac{\partial^2\psi}{\partial y^2} - \left(\frac{\partial\psi}{\partial x\,\partial y}\right)^2\right) \tag{4.10}$$

Pressure values can be obtained using the values of ψ already obtained.

The conservation laws governing the flow and heat transfer have been reduced to partial equations of stream function, vorticity and temperature. Boundary conditions are used at the inlet, outlet, sidewalls and solid boundaries. The sidewalls are lines of symmetry between cylinder arranged in arow across the flow.

- In the inlet section, both velocity components are known therefore ψ, and $\partial\psi/\partial n$ can

and be specified along the inlet boundary, where n is the direction normal to the boundary.

- In the outlet section, assuming the outlet is sufficiently far downstream of the bluff body and the static pressure is constant across the outlet then $\partial\Omega/\partial n = 0$ and cross velocity will be zero also $\partial\psi/\partial n = 0$.

- On the side boundaries the cross velocity is zero and so ψ is constant. T is also assumed to be equal to inlet free stream temperature.

- On the cylinder, again both velocity components are zero and temperature is constant.

The present scheme utilises second order accuracy centre differencing. Equations (4.4), (4.6) and (4.9) can be then solved by finite difference formulation as:

$$\Omega_c = \frac{\psi_w + \psi_e - 2\psi_c}{(\Delta x)^2} + \frac{\psi_n + \psi_s - 2\psi_c}{(\Delta y)^2} \tag{4.11}$$

$$\nu\left[\frac{\Omega_w + \Omega_e - 2\Omega_c}{(\Delta x)^2} + \frac{\Omega_n + \Omega_s - 2\Omega_c}{(\Delta y)^2}\right] = \frac{(\psi_n - \psi_s)(\Omega_e - \Omega_w) - (\psi_e - \psi_w)(\Omega_n - \Omega_s)}{4\Delta x \Delta y} \tag{4.12}$$

Equation (4.11) can be rearranged as:

$$\text{New } \psi_c = \frac{\dfrac{\psi_w + \psi_e}{(\Delta x)^2} + \dfrac{\psi_n + \psi_s}{(\Delta y)^2} - \Omega_c}{\dfrac{2}{(\Delta x)^2} + \dfrac{2}{(\Delta y)^2}} \tag{4.13}$$

and also equation (4.12) as:

$$\text{New } \Omega_c = \frac{\dfrac{\Omega_w + \Omega_e}{(\Delta x)^2} + \dfrac{\Omega_n + \Omega_s}{(\Delta y)^2} - \dfrac{Re_{\Delta x}(\Omega_w - \Omega_e)}{2(\Delta x)^2} - \dfrac{Re_{\Delta y}(\Omega_n - \Omega_s)}{2(\Delta y)^2}}{\dfrac{2}{(\Delta x)^2} + \dfrac{2}{(\Delta y)^2}}$$

and the energy equation can be written in finite difference form as:

$$\text{New } T_c = \frac{\dfrac{T_w + T_e}{(\Delta x)^2} + \dfrac{T_n + T_s}{(\Delta y)^2} - \dfrac{Re_{\Delta x} v (T_w - T_e)}{2\alpha(\Delta x)^2} - \dfrac{Re_{\Delta y} v (T_n - T_s)}{2\alpha(\Delta y)^2}}{\dfrac{2}{(\Delta x)^2} + \dfrac{2}{(\Delta y)^2}}$$

Where $Re_{\Delta x}$ and $Re_{\Delta y}$ are the cell Reynolds number that are given as:

$$Re_{\Delta x} = \frac{\psi_n - \psi_s}{\Delta y} \frac{\Delta x}{\nu} = \frac{u \Delta x}{\nu}$$

$$Re_{\Delta y} = -\frac{\psi_e - \psi_w}{\Delta x} \frac{\Delta y}{\nu} = \frac{v \Delta y}{\nu}$$

The subscripts represent the centre, north, south, east and west mesh positions. To maintain stability an upwinding therm was added to Ω_c and T_c equations $|Re_{\Delta x}|$ or $|Re_{\Delta y}| > 2$.

Nusselt number is obtained since the conductive heat transfer rate of the fluid over the solid boundary equals its convective heat transfer rate as:

$$-k\left(\frac{dT}{dn}\right)_{surface} = h_\theta (T_{surface} - T_\infty) \qquad (4.14)$$

and the local Nusselt number is obtained:

$$Nu = \frac{h_\theta D}{k}$$

Flow and temperature solutions are obtained using a Gauss-Seidel over-relaxation procedure. The numerical solution of the equations was accomplished on orthogonal curvilinear grids. The computer code is given in more detail by Johnson(1990).

4.2.3 Eddy-Viscosity Turbulence Model

The fundamental difference between the laminar and turbulent flow lies in the unstable random behaviour of the various fluid parameters. Such variations occur in the components of the velocity, the shear stress, the temperature and the pressure. The concept of turbulent viscosity was first proposed by Boussinesq in 1877. It is based on the fact that the turbulent shear stresses in the momentum equations can be replaced by the product of the mean velocity gradient and the turbulent viscosity ν_t. It is reported in the literature that Prandtl in 1925 proposed the first turbulence model which has become known as the mixing length theorem, according to which turbulent viscosity is to be calculated as: (Cebeci and Smith, 1974)

$$\nu_t = \ell_m^2 \left|\frac{\partial u}{\partial y}\right| \tag{4.15}$$

With equation (4.15) Prandtl proposed that the turbulent process could be viewed as the random transport of bundles of fluid particles over a certain distance, ℓ_m, the mixing length, from a region of one velocity to another region of different velocity. Close to the solid boundary Prandtl suggested that $\ell_m = \kappa.y$. κ is a constant and generally treated as a value of 0.4. The variable y is the closest and perpendicular distance between a mesh point and the nearest wall.

The main laminar flow program was developed by El-Wahed et al. (1993) to cater for turbulent effects by replacing the viscosity term in the vorticity and energy equations with the effective viscosity which can be written as:

$$\nu_e = \nu_l + \nu_t$$

where ν_e is the effective viscosity. In the calculation, laminar viscosity, ν_l, was taken as a constant value while the turbulent viscosity was computed using the Prandtl mixing length turbulence model.

4.3 Computational Procedure

The flow domain under consideration, taking into account symmetry, for a single tube and a tube bank can be seen in Figures 4.1(a) and 4.1(b). For the single tube geometry which is confined by the walls parallel to the flow direction, blockage ratio is defined as D/W where W is the height between the side walls and D is the diameter of tube. Blockage ratio was varied between of 0.18 and 0.47. This range was chosen to enable a comparison with experimental data which was obtained for low Reynolds numbers as described later in section 4.4. For the staggered tube bank the transverse pitch ratio and the longitudinal pitch ratio ($S_t=s_t/D$ and $S_l=s_l/D$) were arranged such that the transverse pitch was fixed $S_t=1.5$ and the longitudinal pitch was altered from 1.25 to 1.5. An experimental comparison was also examined for the case of 1.5x1.25 with Re=1180.

The computations of the flow and heat transfer characteristics for the confined tube and the tube bank were performed using the computation grids shown in Figures 4.2(a) and 4.2(b). In the confined case, as mentioned in section 4.2.1 an 'O' type grid was used to avoid rapid changes in the spacing of the grid cell near the solid body. This type of grid could only be used for the single body. In both the tube bank and the single tube cases, the grid is

generated in two stages. Firstly the desired point distribution is chosen on the physical domain boundary and secondly the interior coordinate lines are generated according to the point distribution in the previous step.

Large variations in the stream function, vorticity and temperature occur near the surface of the body. Therefore, smaller mesh sizes were created in the physical domain. For the single tube, refined meshes were used near the surface of the cylinder and coarser ones away from the body. In the tube bank case, a high grid density was used in the whole physical domain.

To vary Reynolds number (Re=V.D/ν), the upstream velocity, V, was altered with the other variables fixed at the following values:

Diameter of tube, D=0.05656 m

Kinematic viscosity of air, ν_ℓ=1.58e-5 m^2/s

The stream-function on the boundaries was calculated assuming that the value on the bottom boundary is zero and then the value on the top boundary is ψ=V.W, where W is the width of the channel.

Predictions were made for the confined tube geometry for range of Reynolds number between 120 and 390. For the staggered tube bank Reynolds numbers were chosen to be 390, 500 and 1180. Reynolds number was evaluated for the tube bank using the maximum velocity

at the minimum transverse distance:

$$V_{max} = \frac{S_t - D}{S_t} V_{upstream} \tag{4.16}$$

Local Nusselt numbers were calculated using equation (4.14) and plotted against the angular position on the tube. The local pressure coefficient was defined as:

$$C_p = \frac{P_\theta}{\frac{1}{2}V^2\rho}$$

Here, for single tube V is taken as the upstream velocity, for tube bundle case V is taken as maximum velocity that is calculated with equation (4.16), P_θ is surface static pressure obtained from equation (4.10)

The Reynolds number used in the calculation is within the range for which buoyancy effects may be safely neglected because the Reynolds number yields a forced convection velocity that is very much higher than the characteristic free convection velocity. Therefore the following relationship was satisfied (Kreith, 1965):

$$\frac{Gr}{Re^2} < 1 \tag{4.17}$$

Where Gr is Grashof number defined by the following equation:

$$Gr = \frac{g\ \beta\ V\ \Delta T\ D^3}{\nu^2}$$

where g is the acceleration due to gravity, ν is the kinematic viscosity, D is the diameter of tube and ΔT is the temperature difference between the wall and free stream. In the present study equation (4.17) was limited between $0.036 < Gr / Re^2 < 0.558$.

4.4 Experimental Procedure

An experimental investigation was carried out to obtain data to compare with the numerical results obtained in the low Reynolds number range. The experimental apparatus for the single row and the tube bundle was the same as described in Chapter 3. For the single tube row, heat transfer measurements were completed for three different blockage ratios; these were 0.18, 0.4 and 0.47. Reynolds number was fixed at a value of 390.

The tube bundle heat transfer measurement was carried out for a configuration of 1.5x1.25 (S_t x S_l) with a Reynolds number of 1180. The tube bundle was set up with four rows of tubes and measurements were obtained for the first three row of tubes. Measurement procedures were the same as carried out in Chapter 3.

The wind tunnel's inlet section was covered by a piece of thick curtain to reduce the flow rate. Velocity measurement was obtained using a pitot static tube and a Baratron pressure transducer. The pitot static tube was connected directly to the Baratron sensor head and pressure results were monitored and upstream velocity was obtained.

4.5 Results and Discussion

4.5.1 Single Tube and Single Tube Row

In practice, circular tubes are usually in a flow channel restricted by walls and with considerable blockage of the flow section. The blockage has a great influence on the heat transfer. As blockage increases, the velocity around the boundary layer increases and the pressure and velocity distribution change accordingly. In the previous chapter, the effect of blockage on the heat transfer characteristics of a single tube row was examined. Experimental results were compared with a theoretical study for the stagnation point and laminar boundary layer regions. Other investigators have carried out studies into the effect of blockage on heat transfer and flow structure. Akilbayev et al(1966), Perkins and Leppert (1964), West and Apelt(1982) and Hiwada and Mabuch (1980) have investigated the effect of blockage by either changing duct width or by altering tube diameter.

Figures 4.3-4.7 show laminar heat transfer and flow characteristics of confined single cylinder corresponding to a Reynolds number of 120 and blockage ratios from 0.18 to 0.47. As mentioned in Chapter 3, the local heat transfer coefficient becomes minimum at the separation point. Streamline contours are shown in Figure 4.3 for different blockage ratios and it is seen that the angle of the separation point increases as a result of increasing blockage. It is seen from the isotherm contours in Figure 4.4 that the thermal boundary layer develops around the cylinder and the thickness of the thermal boundary layer is very similar for the three different blockage cases. The isotherm contours diverge from the tube surface at a position which coincides with the streamline separation point.

In order to evaluate the accuracy of the heat transfer calculation procedure developed in this study, local Nusselt number distribution for the low blockage case (b=0.18) for a Reynolds number of 120 was compared with the Eckert and Soehngen's (1953) data (experimental and calculation) that are shown in Figure 4.5. There is very good agreement between the measurement and calculations for most of the range. However in their calculation results minimum Nusselt number takes places at about 155° and also their experimental data are slightly lower than the presently predicted values. This can be due to different blockage and free convection effects which were not specified by Eckert and Soehngen. Local distribution of Nusselt number and local surface pressure are shown in Figures 4.5, 4.6 and 4.7 when the blockage increases from 0.18 to 0.47, minimum Nusselt number and minimum pressure values move back to the downstream side of the tube. Also local values of Nusselt number and pressure increase with increasing blockage.

Figures 4.8-4.12 show the laminar heat transfer and flow characteristics of a confined single cylinder corresponding to a Reynolds number of 390 with the same blockage ratios as used in the previous case. The streamline contours can be seen in Figure 4.8 and show the separation point is about 115° at a blockage ratio of 0.18 and it moves further along the downstream side of the tube with increasing blockage. When the blockage is altered from 0.18 to 0.47 separation takes place nearly 10° further downstream. The effect of higher Reynolds number is seen to be that the separation point moves backwards to the upstream side. Isotherm contours are shown in Figure 4.9 where the thermal boundary layer forms around the cylinder and its thickness is less than for the previous Reynolds number of 120 as a result of higher flow velocity.

Local Nusselt number distribution has been plotted with the experimental results in Figures 4.10, 4.11 and 4.12. The results show that when the blockage is 0.18, agreement is excellent up to 110°, after this point numerically predicted values become less than the experimental values. Numerical prediction shows that the minimum Nusselt number occurs at nearly 120°, after this minimum point it increases through to the rear stagnation point. However experiment shows the minimum value takes place at about 115°. When the blockage is altered to 0.4 and 0.47 agreement is still very good up to nearly 110°. After this point the numerical predictions behave the same as on the previous blockage case. For the three cases, it is seen that experiments and calculations are slightly different in the region at the rear of the cylinder. However, the streamline contour agrees well with experimental work for the separation point location.

The differences in the heat transfer predictions may due to the nature of the experiments where there is a single heated tube and vortices can carry cooling air into the wake region hence increasing the effective temperature differences which increase the heat transfer from the surface. These unsteady shed vorticies are modelled in the numerical calculations which is for steady flow.

4.5.2 Tube Bundle

The flow pattern around a tube in a bank is affected by the surrounding tubes. In the staggered tube bank heat transfer and pressure distributions around the tubes in different rows have a similar character. The flow in the boundary layer is laminar, such a flow pattern existing at Reynolds number smaller than 10^3 may be described as predominantly laminar

(Zukauskas 1972). According to Zukauskas, three flow regimes are observed in a tube bank: predominantly laminar regime at Re< 10^3, mixed or subcritical flow regime $5x10^2$< Re < $2x10^5$ and predominantly turbulent or critical flow regime at Re>$2x10^5$.

In the present study, heat transfer and flow characteristics of a cylinder in a bank were examined. Firstly the geometry was fixed as 1.5x1.25 (S_t x S_l) and Reynolds number was altered. Secondly longitudinal pitch was increased from 1.25 to 1.5 with fixed Reynolds number and the results were compared with each other. Thirdly an experiment was carried out to obtain data to compare with the numerical prediction of heat transfer coefficient for the 1.5x1.25 case for a Reynolds number value of 1180. Calculations were carried out for the first three rows of tubes. Local Nusselt number and local surface pressure distribution were plotted against the angular position on the tube.

4.5.2.1 Tube Bundle (1.5x1.25) with Re=360

Figures 4.13-4.15 show the numerical prediction for the isotherms, streamlines. Local Nusselt number and local pressure distribution for Re=360 and Pr=0.7 in the 1.5x1.25 staggered tube bank. Constant temperature boundary conditions were imposed on only one tube in a bank for all cases. Isotherm contours are shown in Figure 4.13 where it is seen that the first row thermal boundary layer is relatively thick compared with that on the tube in the second and third rows. As a result of the thinner boundary layer there is a higher temperature gradient and heat transfer rate. Streamlines are shown in Figure 4.14 and it is seen that the separation points are nearly at the same angular position for all three cases, i.e. about 130°. It can be seen in Figure 4.15 that the front stagnation point Nusselt number for first tube is

nearly 60 percent less than for the second and third tube. The minimum Nusselt number occurs at nearly 145° corresponding to the boundary layer separation point. After separation local Nusselt number increases gradually up to the rear stagnation point.

The local Nusselt number distributions on the second and third tubes follow the same trend as the first row but the heat transfer is seen to fall quickly from the high stagnation value. The high velocity flow from the first row increases the heat transfer of the second tube. The effect is less pronounced for the third row where the local Nusselt Number is only slightly higher than the second row. Both curves decrease to nearly 145° and then increase gradually through to the rear stagnation point. Local surface pressure distributions show that the minimum pressure point locations are the same for the three cases.

In an effort to improve the accuracy of the present calculations, the mesh density was refined in the whole physical domain to give 360x48 grid squares. However it can be seen from the isotherms, local Nusselt number and surface pressure that a distortion takes place at 45°. This point represents the junction of the grid lines. It is well known that numerical truncation errors can increase with sudden changing of the grid cells where in this region the velocity gradient is very strong.

4.5.2.2 Tube Bundle(1.5x1.5) with Re=360

Figures 4.16-4.18 show the numerical prediction for the isotherms, streamlines, local Nusselt number and surface pressure distribution corresponding to a Reynolds number value of 360 in the 1.5x1.5 staggered tube bank.

The isotherms contours are shown in Figure 4.16 where it can be seen that the temperature field is less constrained than the previous case of 1.5x1.25; the thermal boundary layer thicknesses are nearly the same as the previous case. The streamline contours can be seen in Figure 4.17 where separation takes place at about 130°, after this point the wake length becomes wider than in the 1.5x1.25 case as a result of expanding the longitudinal pitch of the tubes. Other than this, generally, flow and temperature patterns are about the same as in the previous case. Figure 4.18 shows that the local Nusselt number distributions are slightly lower compared with the smaller longitudinal pitch case due to less blocking of the duct. Again the first tube front stagnation point Nusselt number value is nearly 60 percent less than the second tube front stagnation value.

4.5.2.3 Tube Bundle (1.5x1.25) with Re=500

Figures 4.19-4.21 show streamlines and isotherms with local Nusselt number and local surface pressure distribution corresponding to a Reynolds number of 500. Streamlines and isotherms are about the same as the case of 1.5x1.25 with Re=360. However resulting from the higher Reynolds number, the separation point is shifted up by about 5°. It is seen from the isotherm contours in Figure 4.19, that increasing velocity causes the thermal boundary layer to be slightly thinner. The local Nusselt number distributions shown in Figure 4.21 behaves much the same as in the previous case. Due to the higher Reynolds number local values are increased compared with the lower Reynolds case; for example it can be seen that for first tube the front stagnation value is 20 percent higher. This effect is also seen in the second and third row values. This is due to the increased flow rate making the boundary layer thinner and hence increasing the heat transfer rate from the wall. Minimum Nusselt number

and minimum surface pressure values move about 5° towards the upstream side compared with the lower Reynolds number case and after the minimum value the Nusselt number increases gradually up to the rear stagnation point

4.5.2.4 Tube Bundle (1.5x1.25) with Re=1180

Flow and heat transfer structures were examined for laminar flow through the 1.5x1.25 tube bank both experimentally and numerically for a Reynolds number of 1180. Zukauskas (1972) mentioned that when the Reynolds number is smaller than 10^3 flow can be thought of as being predominantly laminar. Massey and Launder(1978) obtained good agreement for the numerical prediction of heat transfer and flow characteristics in a tube bank for a Reynolds number range of 10 to 10^3. Also Faghri and Rao (1987) found good agreement for tube bank heat transfer prediction with Reynolds numbers up to 10^3. In the present experimental work, the Reynolds number of 1180 was the minimum capacity of the wind tunnel. This Reynolds number is in the range of transition from laminar to turbulent flow.

Figures 4.22-4.26 show isotherms, streamlines and experimental and numerical local Nusselt number distribution. It is clear from the isotherm contour in Figure 4.22, that the thermal boundary layer around the cylinder is thinner compared with the low Reynolds number cases for three tubes. Streamlines show that separation takes place nearly 5° earlier compared with the Reynolds number of 500.

Experimental local Nusselt number distribution was plotted against angular position in Figure 4.24. The first row is comparable with the single tube at a blockage ratio of 0.47

(Figure 4.12). The results are similar; however the local Nusselt number values for the front row in a bank are slightly higher than for a single tube due to the blockage effect of the subsequent tubes.

Numerical and experimental heat transfer predictions are considered to be very good up to 80° for the three tube cases. However at the front grid lines junction, a distortion takes place, it is more noticeable in the second and third rows (see 4.26). After 80° the numerical prediction falls below the measured values and they continue to fall to about 130° then increase through to the rear stagnation point value of nearly 7. Beyond 80° the experimental curves do not fall as quickly as predicted and they reach a minimum at about 115° corresponding to the separation point, they then increase slightly towards the rear stagnation point. Differences between the measurement and the predictions are significant after 80°. This may be due to the reason mentioned earlier where in the experimental work the vortices are more effective in the wake region. In a tube bank, flow and heat transfer characteristics are complex and delayed separation and other differences can be due to unaccounted transition phenomena which affect the nature of the boundary layer and its point of separation.

4.5.3 Single Tube for Turbulent Flow Case with Re=7900

Figures 4.27 and 4.28 show turbulent flow numerical prediction of a confined single cylinder corresponding to a Reynolds number of 7900 with a blockage ratio of 0.18. Streamline and isotherm contours can be seen in Figure 4.27 where because of the high flow rate, the separation point is shifted towards the upstream side of the tube relative to that in laminar flow case. Streamlines show that separation occurs at nearly 100° from the stagnation point. Isotherm contours show that the thermal boundary layer develops around the cylinder

and due to the high flow rate the thermal boundary layer is noticeably thinner compared with low flow rate cases.

The local Nusselt number distribution around the cylinder is shown in Figure 4.28. The minimum value of the Nusselt number takes places at nearly 108° and corresponds to the separation point which is further downstream compared with the experimental results. A comparison of the numerical and experimental values at the stagnation point value show the Nusselt numbers are significantly different. These differences are due to a number of factors. As is known for high flow rates the thermal boundary layer is thinner than in the laminar flow case, for the calculation of local heat transfer coefficient, especially for the turbulent flow case very high density of grid is needed to obtain more accurate results. In the present calculation the grid density used was the same as in the laminar flow calculation. It was the maximum grid density that could be reached with the grid program. An insufficient number of grid points near the body causes significant error in the local calculations because the thermal boundary layer is so thin that it is between the first grid point and the surface. In the wake region local Nusselt number values are considerably lower than the experimental data. This may possibly be due to a time-dependent calculation being needed to include the effects of periodic vortex shedding. In the prediction of laminar flow, boundary conditions were fixed on the wall and calculations were made for the constant fluid viscosity. However, for the turbulent flow case, the gradient of dependent variables near the wall changes rapidly. Therefore turbulent flow requires a different wall boundary treatment to the laminar flow case (Gosman et al., 1969). In the present study, wall functions will be needed to adopt the turbulent flow program to model the resistance of the near wall region.

Unfortunately, in the present study, these factors could not pursued within the time available to the author. Therefore further investigations of the turbulent flow case will be considered as a future work.

4.6 Concluding Remarks

Numerical calculations have been carried out for laminar flow and heat transfer for flow past a confined single cylinder and a tube in a tube bank. The numerical investigation has considered the effect of blockage, of longitudinal pitch in a tube bank and of Reynolds number on the heat transfer and flow characteristics. Calculations for the single tube were carried out in the Reynolds number range of 120 to 390. Blockage ratio was varied from 0.18 to 0.47 and results were compared with experimental work. Calculations for the tube bank were obtained for Reynolds number values of 360, 500, and 1180. With these values transverse and longitudinal pitches were fixed as 1.5x1.25. Also for Re=360, the longitudinal pitch was altered from 1.25 to 1.5. The main conclusions are as follows:

Confined Single Tube:

- Increased blockage causes the angle of separation to increase. Experimental separation point locations agreed with the flow predictions.

- Increasing blockage influenced the overall heat transfer rate from the cylinder

- Increasing Reynolds number causes the angle of separation to decrease and the overall heat transfer to increase

- Experiment and numerical prediction of heat transfer in the rear recirculation did not agree. Therefore, time dependent calculations are needed to investigate this further to accommodate vortex shedding.

- Turbulent flow calculations did not agree with experimentally obtained results. It was thought that the number of grid points used for the calculations was insufficient and also wall functions would be needed in the turbulent flow program.

Tube Bank

- Changing longitudinal pitch did not affect too much the heat transfer and flow structures. Wider longitudinal pitch caused a bigger wake on the rear side of the tube and overall heat transfer was slightly less.

- Increasing the Reynolds number from 360 to 1180 caused the overall heat transfer to increase and the angle of separation to decrease.

- Comparison of experiment and numerical prediction of heat transfer agreed in the front region of the tubes up to 80°. After this point, differences were seen over the rear side of the tube. However the flow separation predictions agreed well with experiment.

- The local heat transfer and pressure distributions were influenced by the non-uniformity of the grid at 45° where there is a junction of the grid lines. At this point,

results were distorted as seen from the tube bank predictions. This aspect will have to be reconsidered to obtain a more uniform grid.

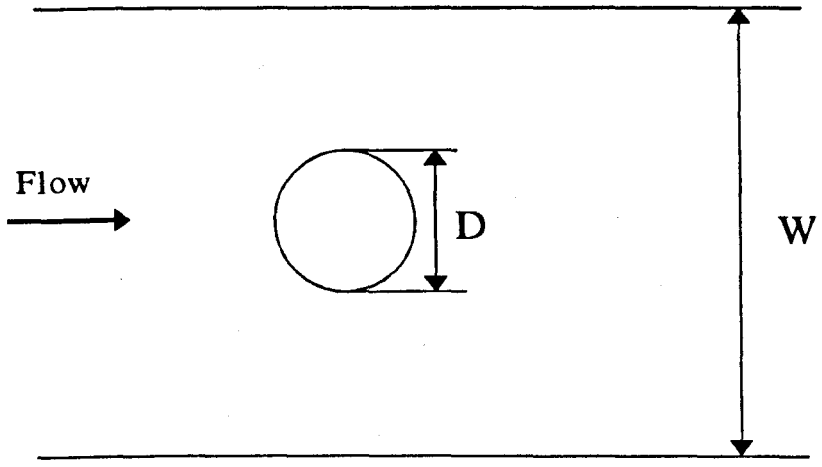

Figure 4.1(a) Confined Single Cylinder, B=D/W

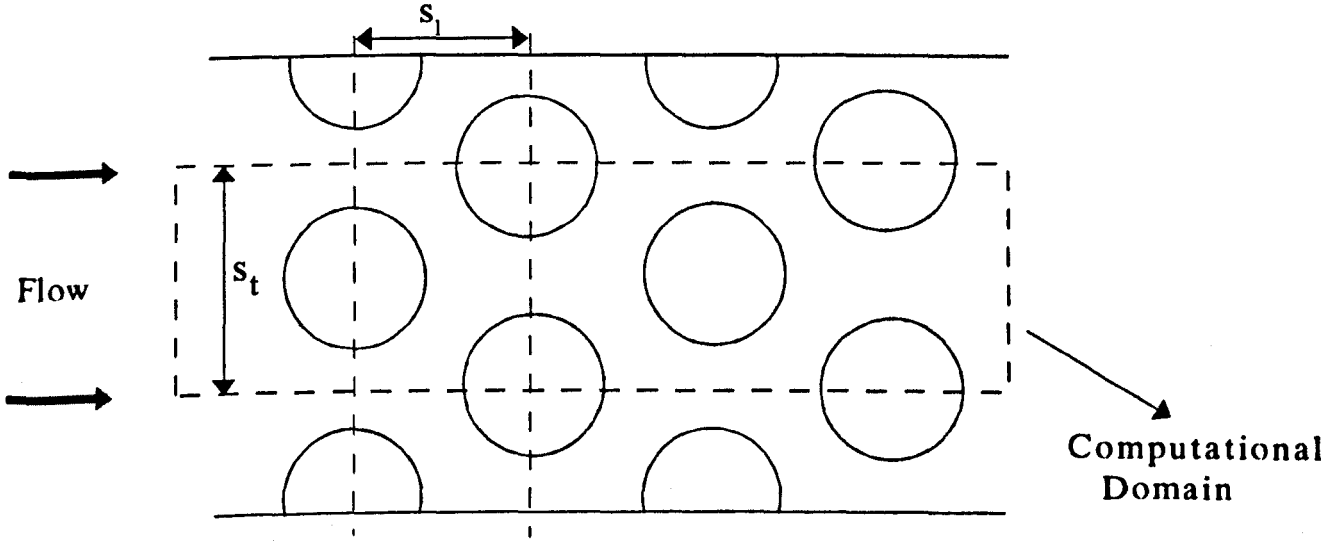

Figure 4.1(b) Staggered Tube Bank and Computational Domain

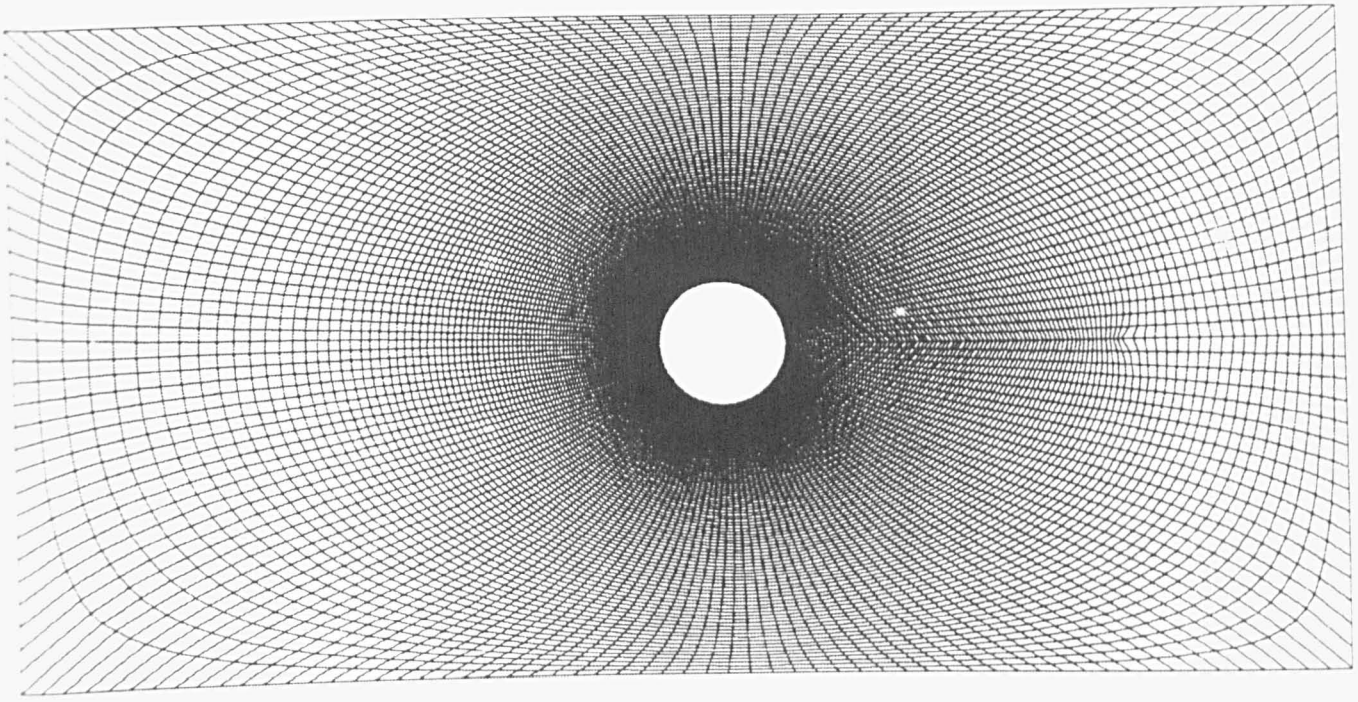

Figure 4.2 (a) Computational Grid For a Single Cylinder

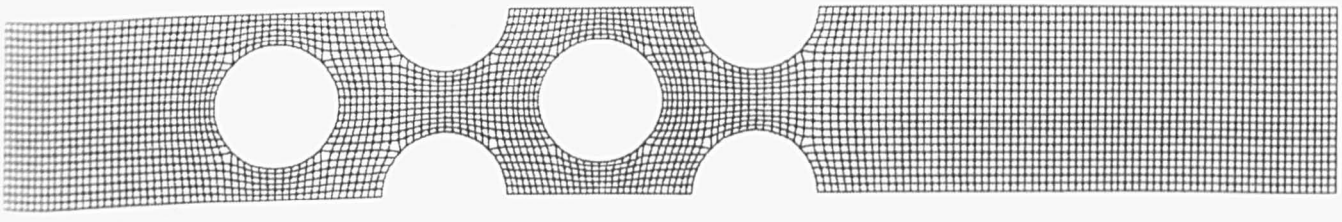

Figure 4.2 (b) Computational Grid For a Tube Bank
(180x24 shown, 360x48 actually used)

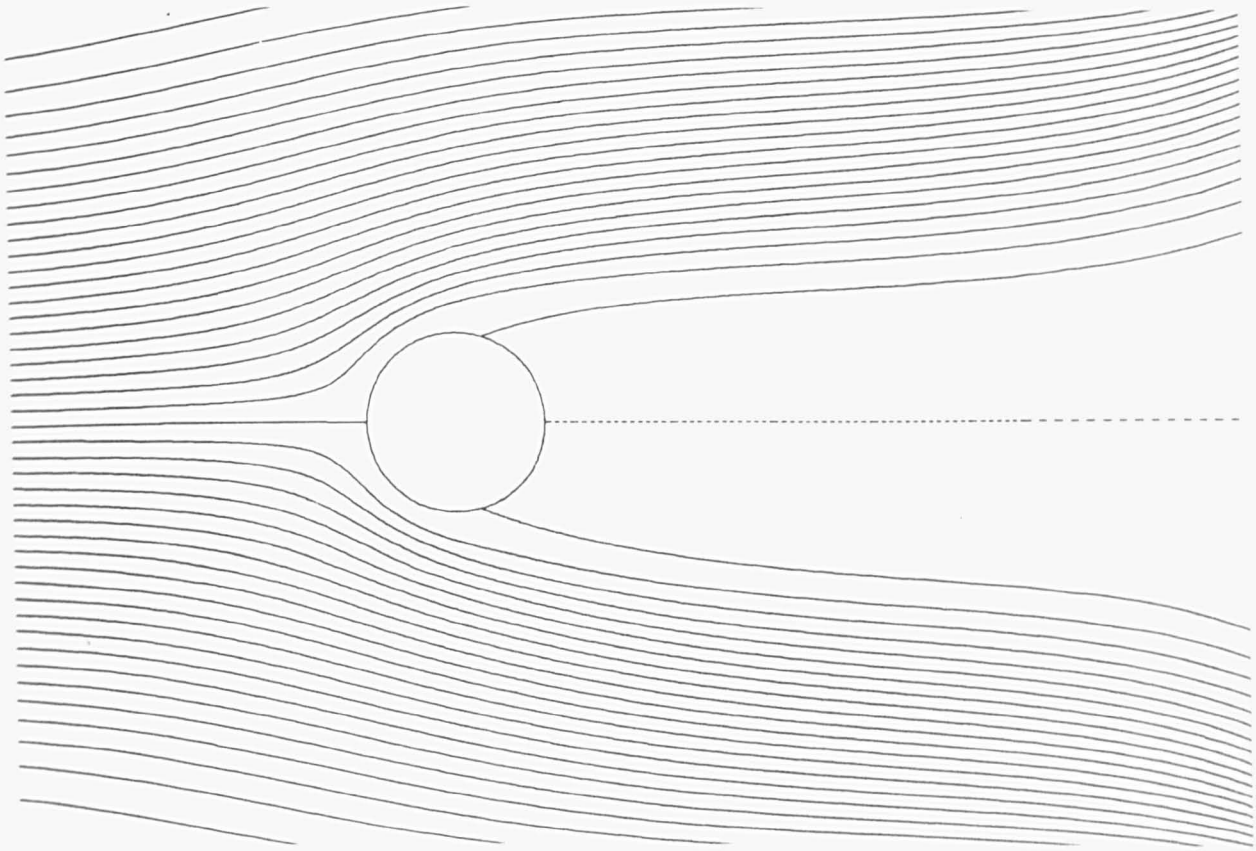

(a) B=0.18

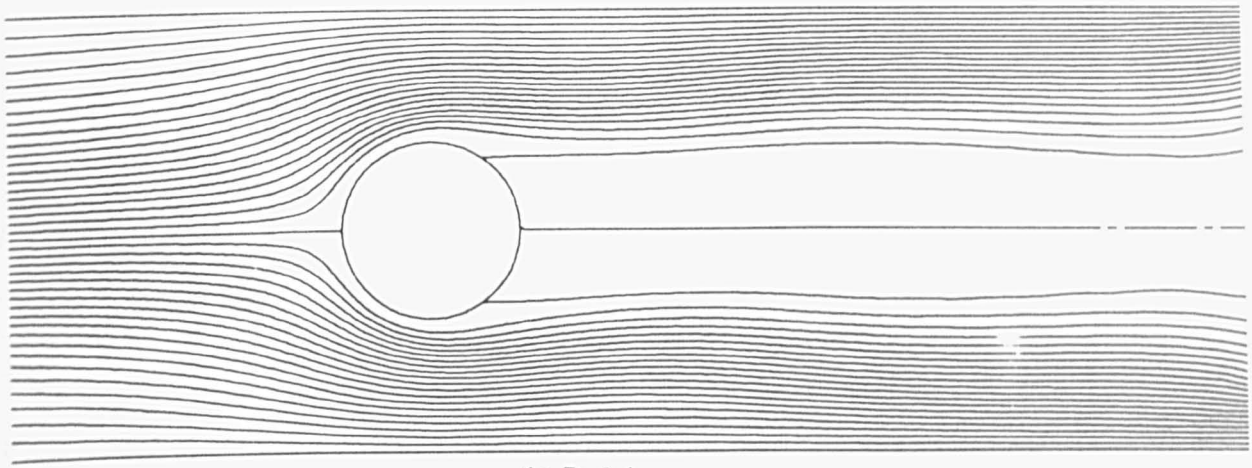

(b) B=0.4

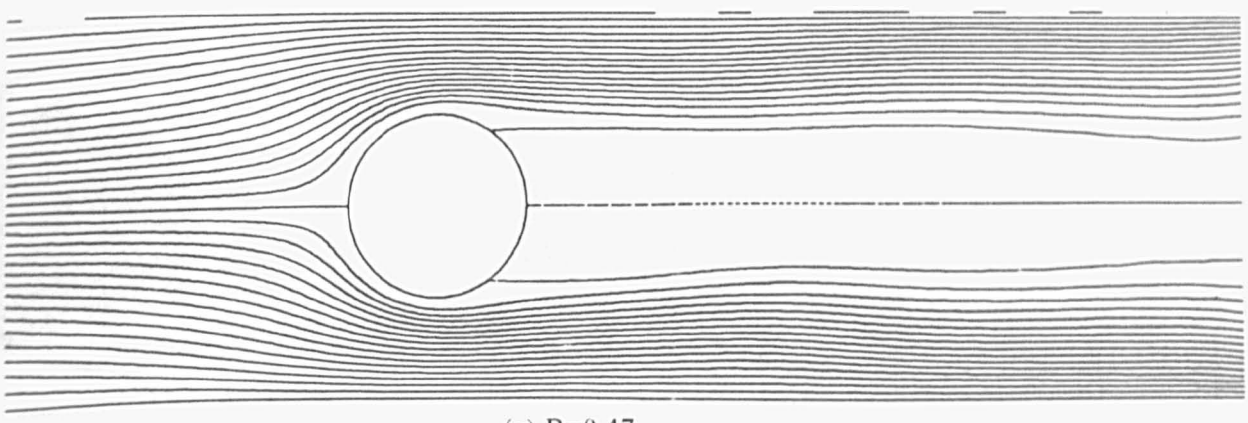

(c) B=0.47

Figure 4.3 Streamlines for Different Blockage Ratios with Re=120

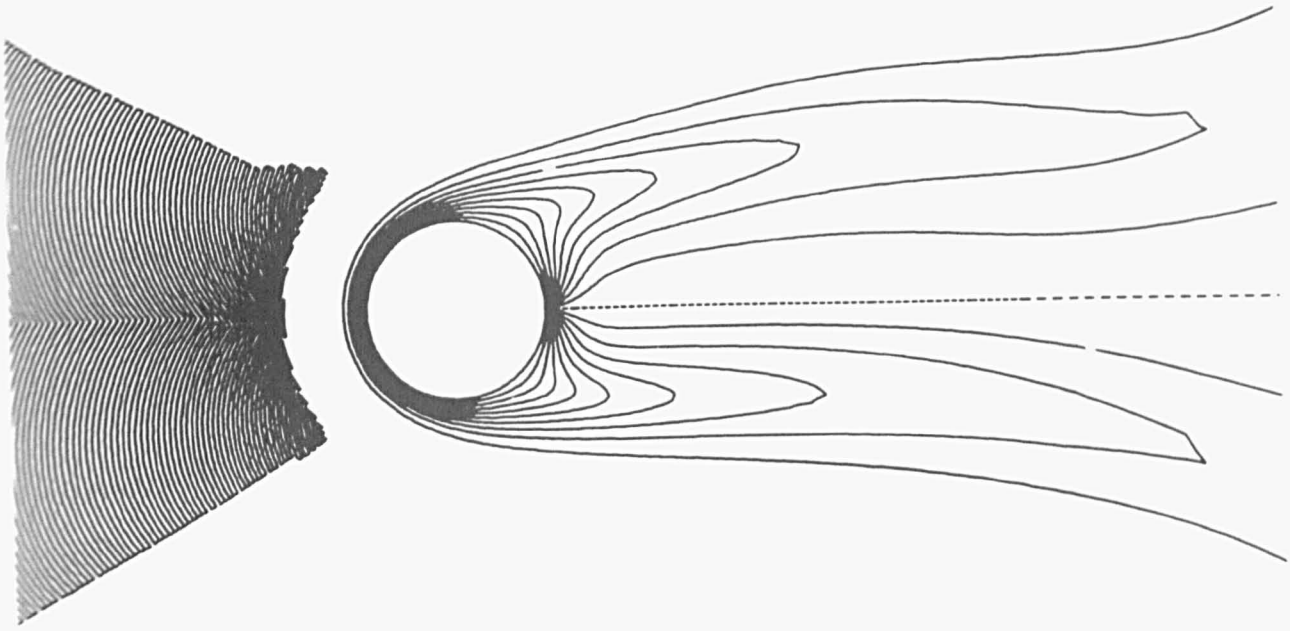

(a) B=0.18

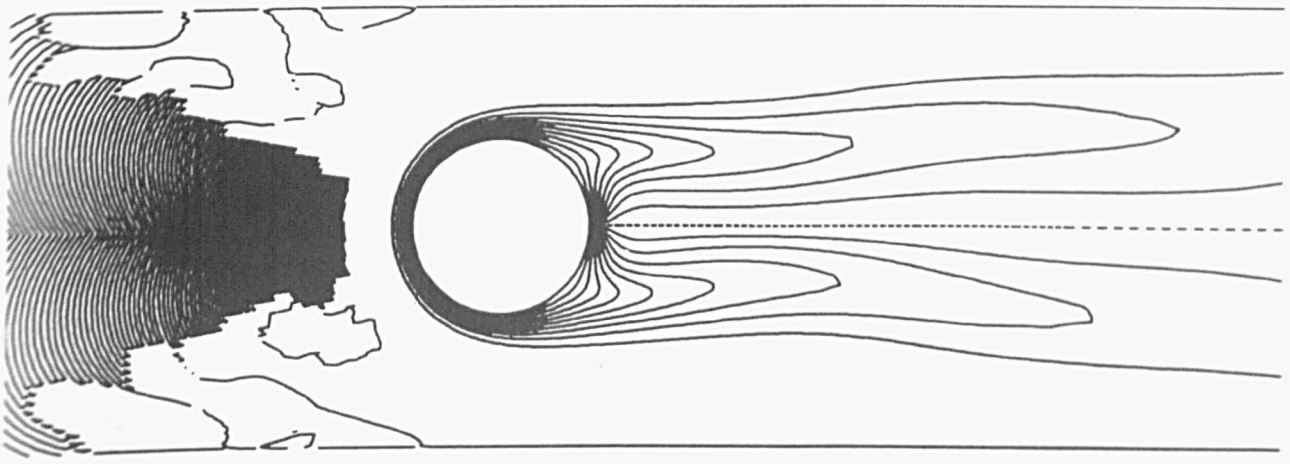

(b) B=0.4

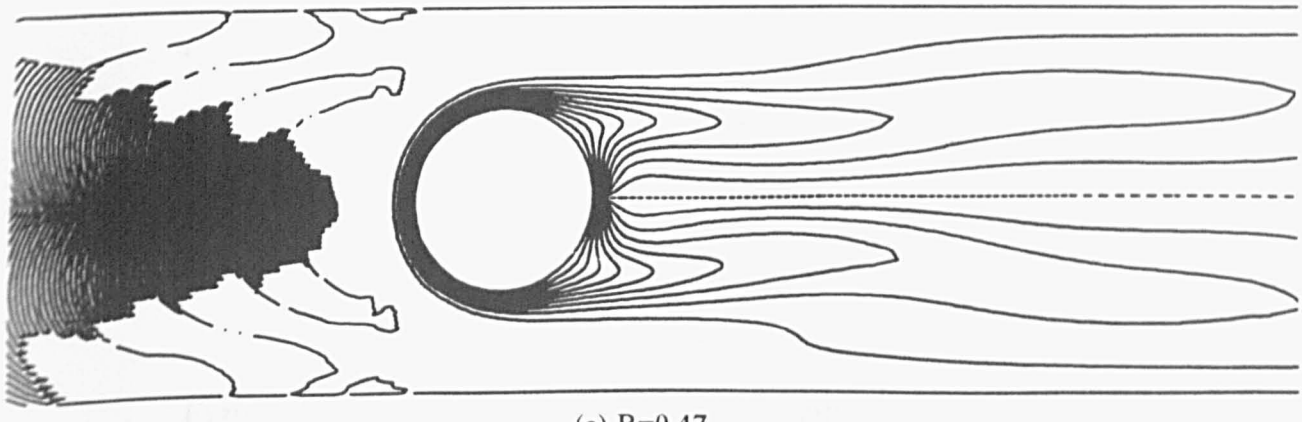

(c) B=0.47

Figure 4.4 Isotherms for Different Blockage Ratios with Re=120

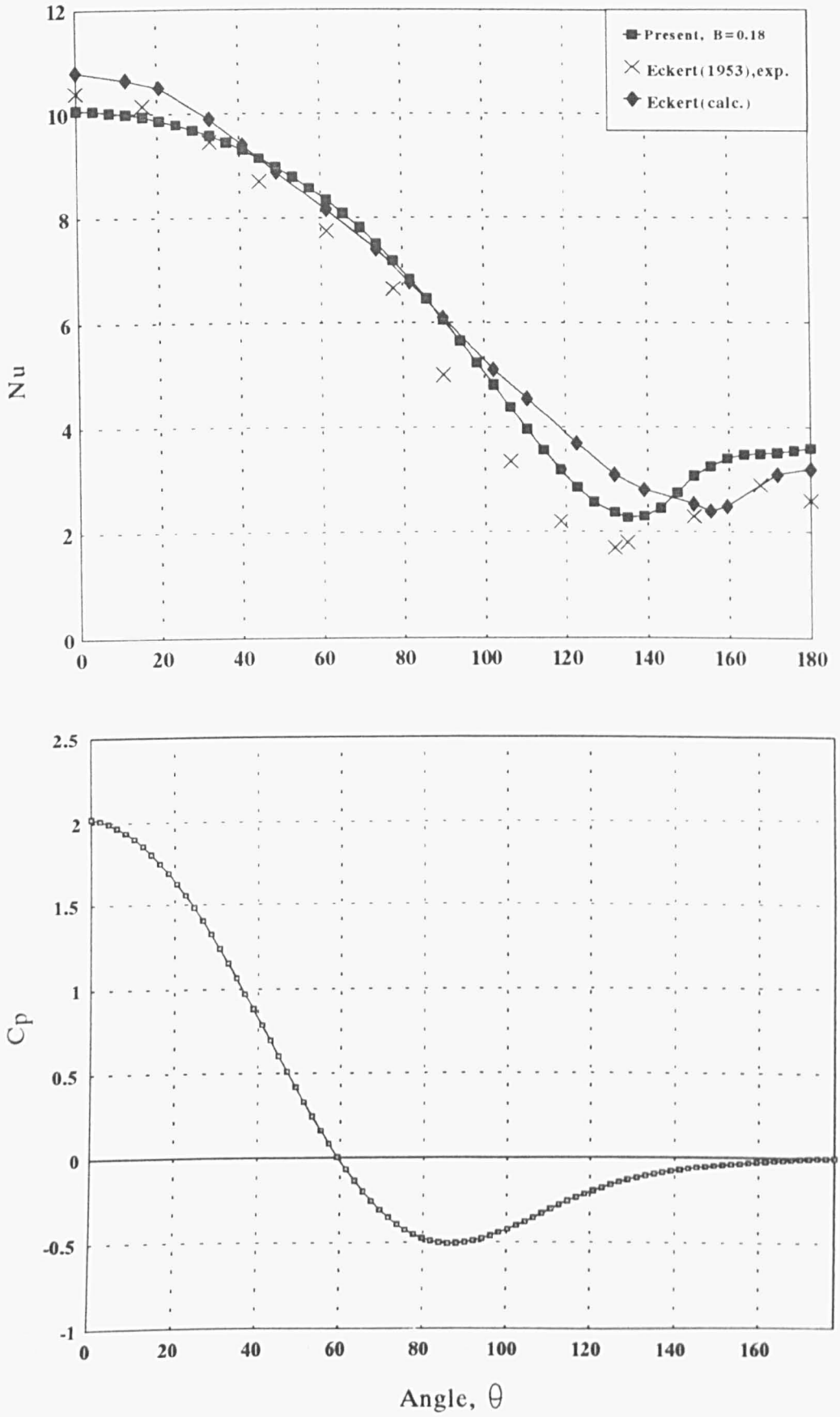

Figure 4.5 Calculated Local Nusselt Number and Pressure Coefficient for B=0.18 and Re=120

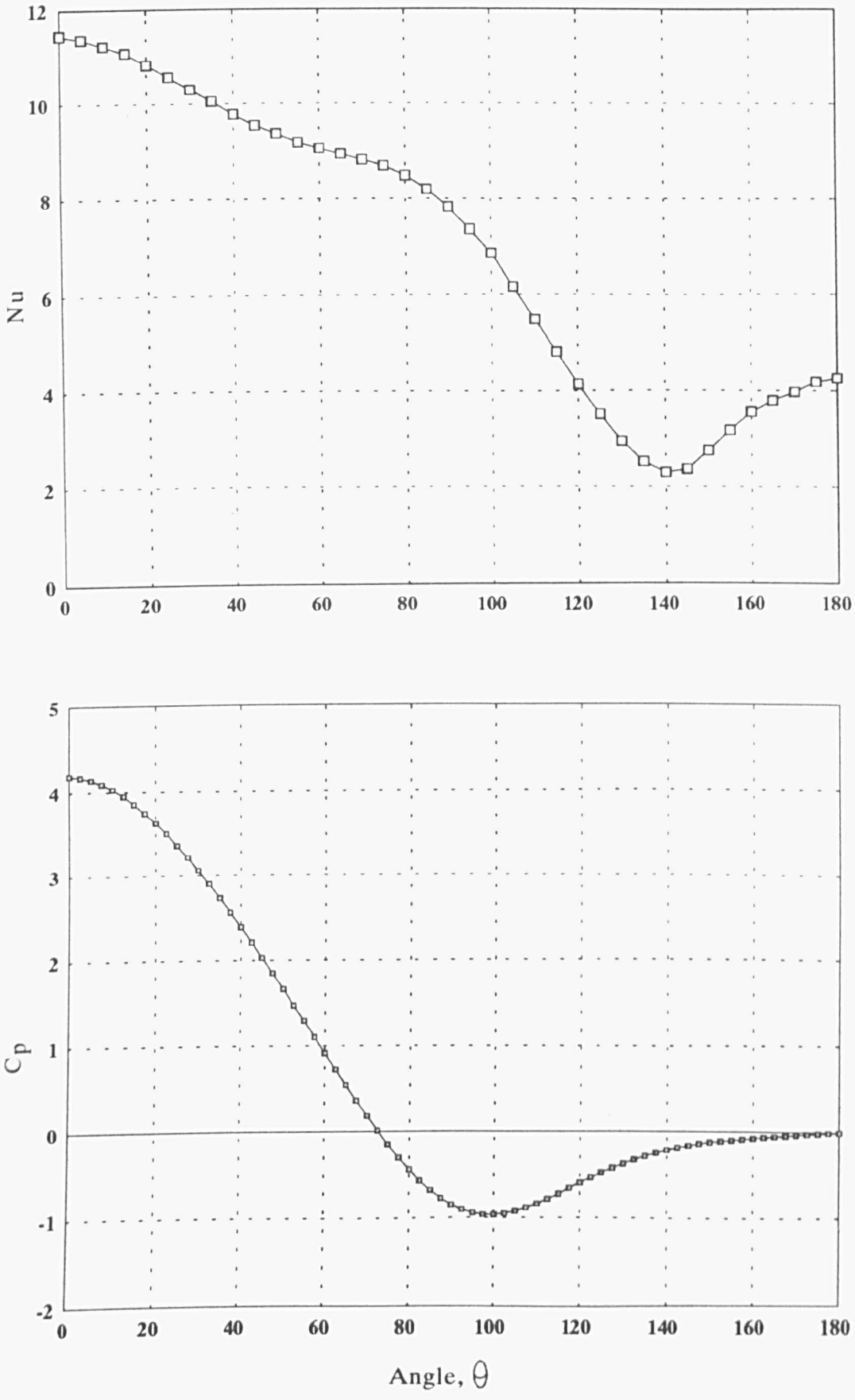

Figure 4.6 Calculated Local Nusselt Number and Pressure Coefficient for B=0.4 and Re=120

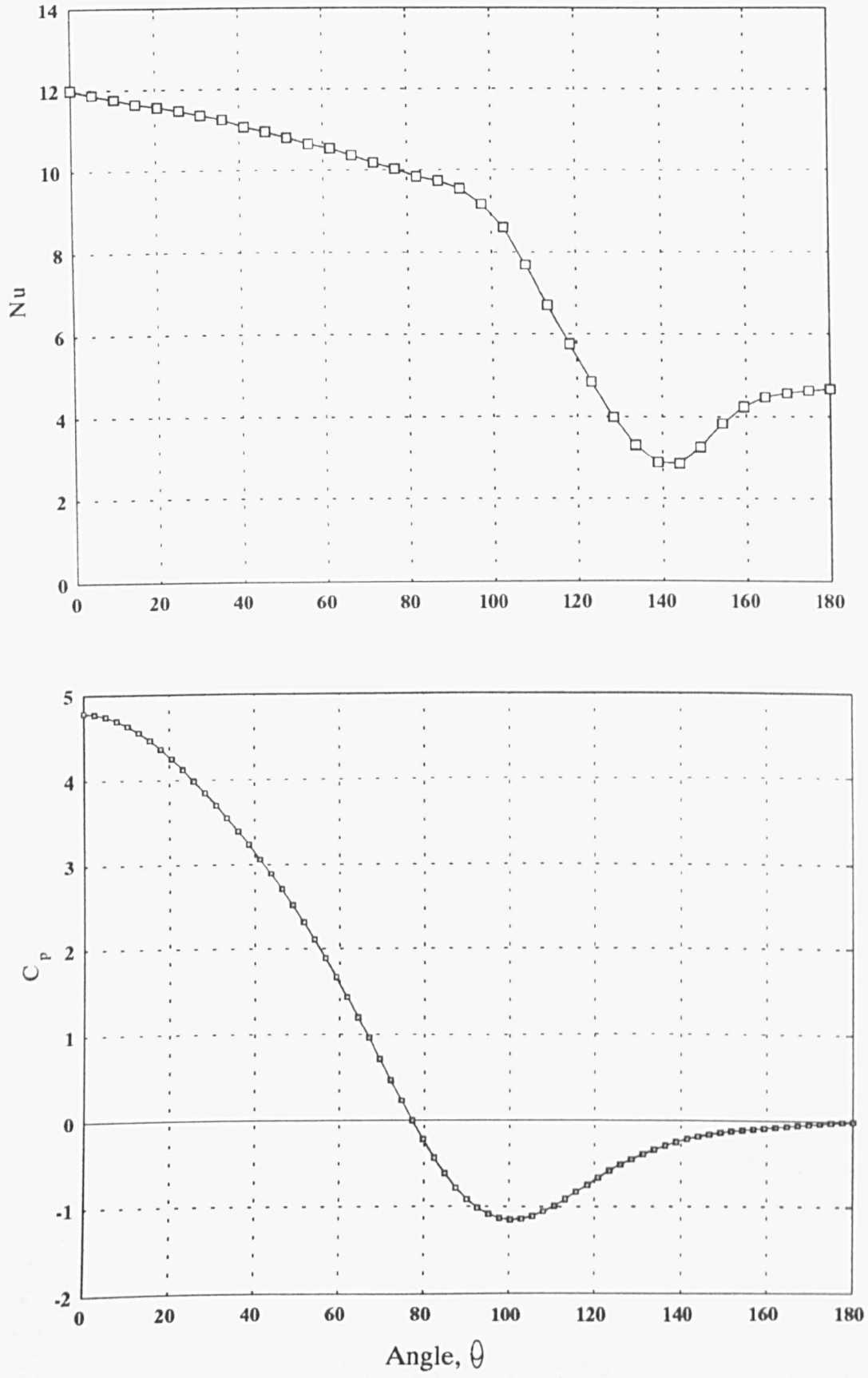

Figure 4.7 Calculated Local Nusselt Number and Pressure Coefficient for B=0.47 and Re=120

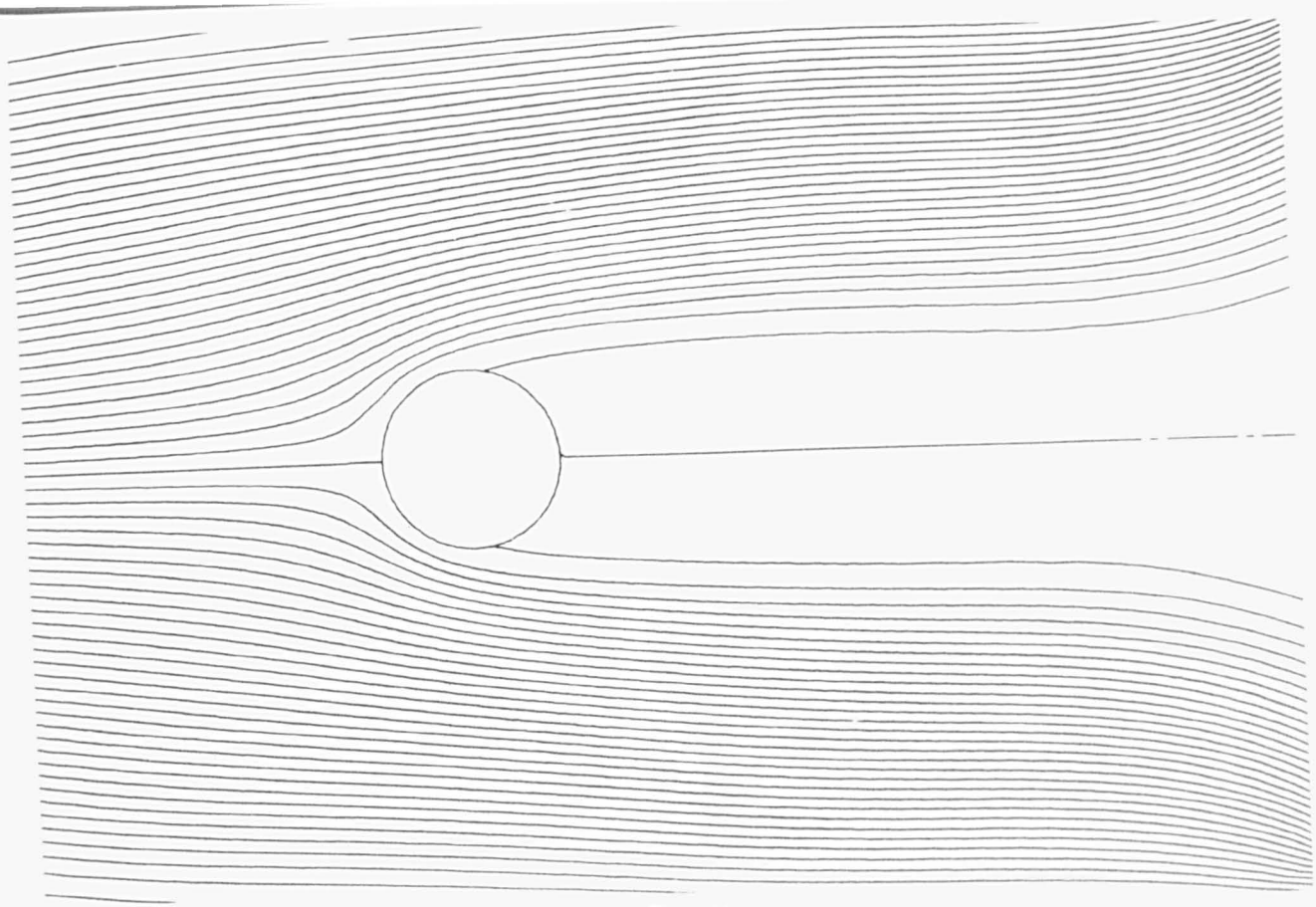

(a) B=0.18

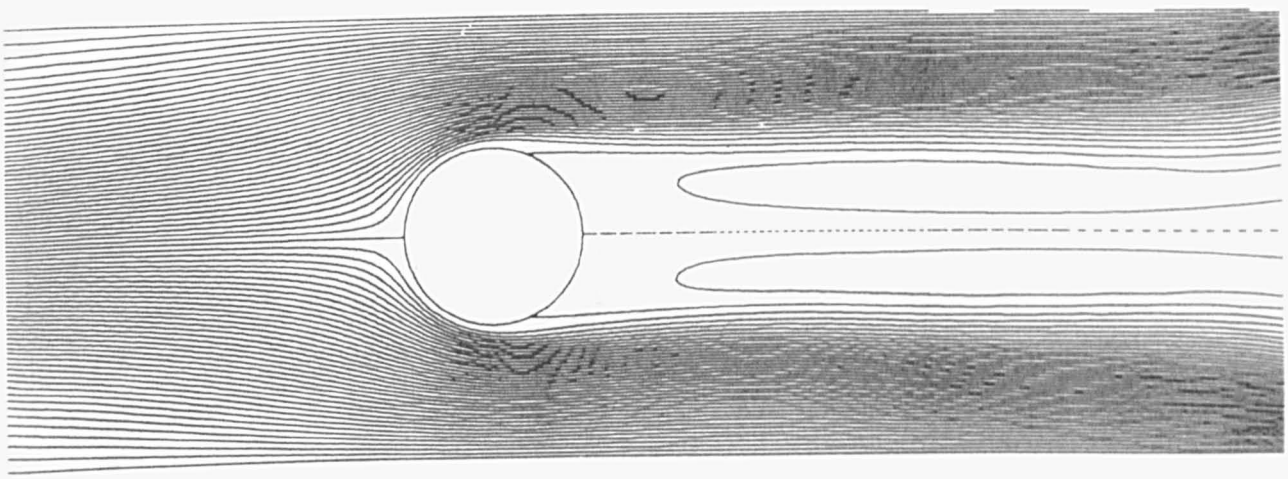

(b) B=0.4

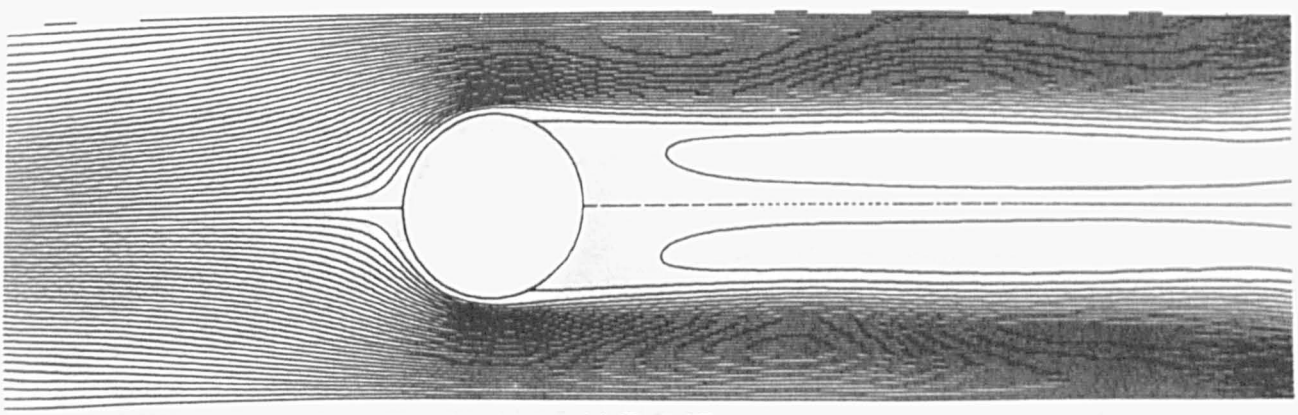

(c) B=0.47

Figure 4.8 Streamlines for Different Blockage Ratios with Re=390

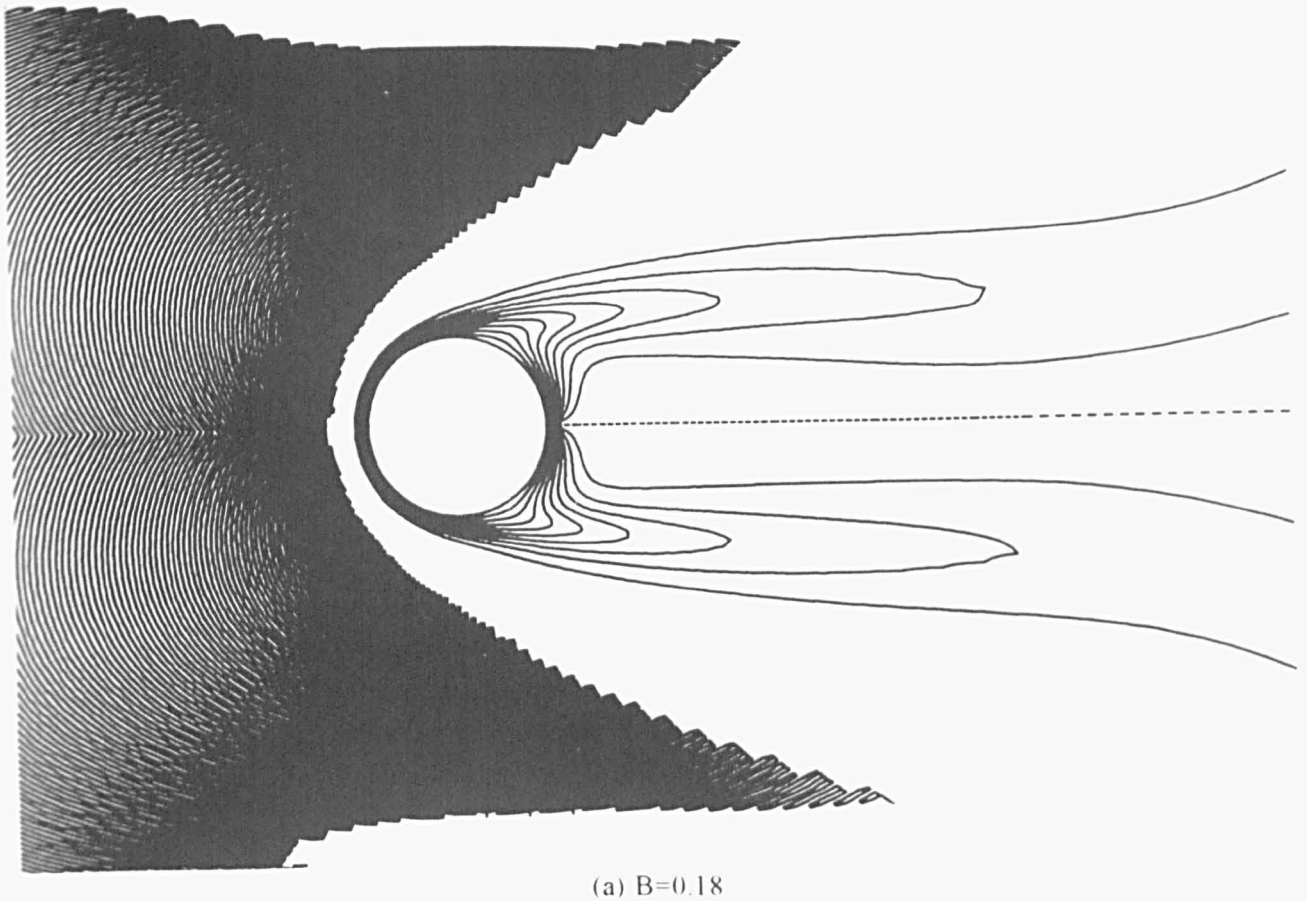

(a) B=0.18

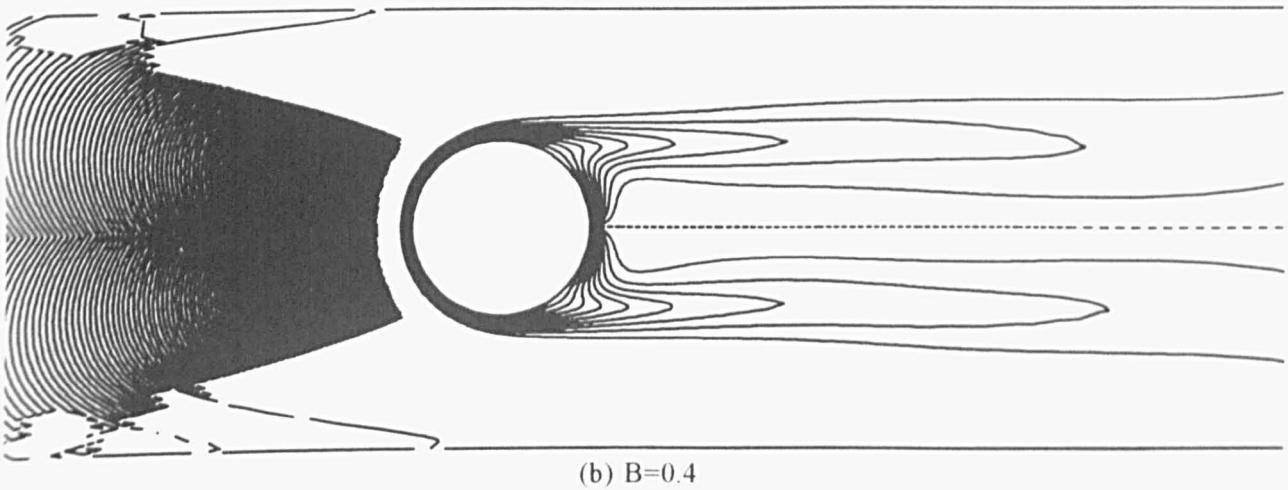

(b) B=0.4

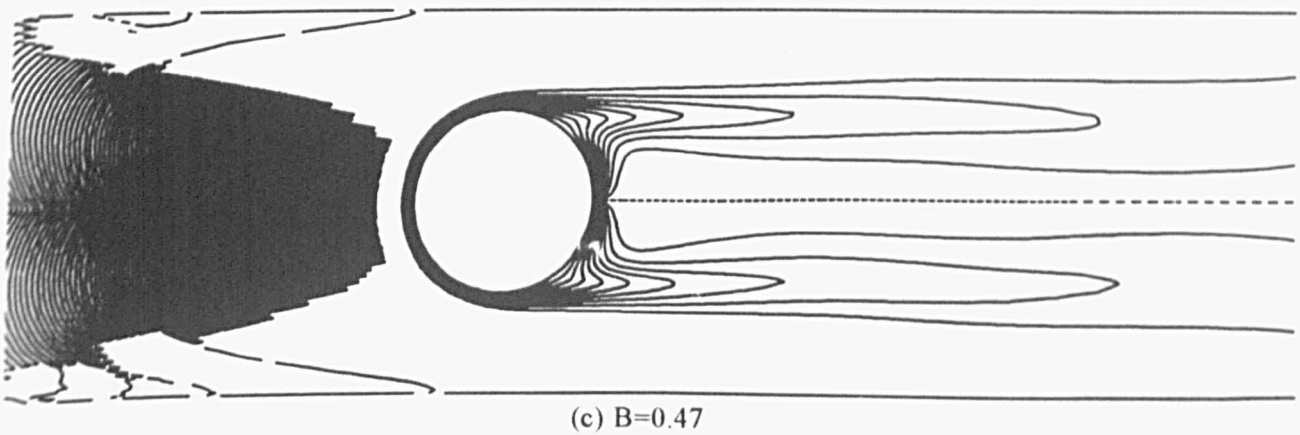

(c) B=0.47

Figure 4.9 Isotherms for Different Blockage Ratios with Re=390

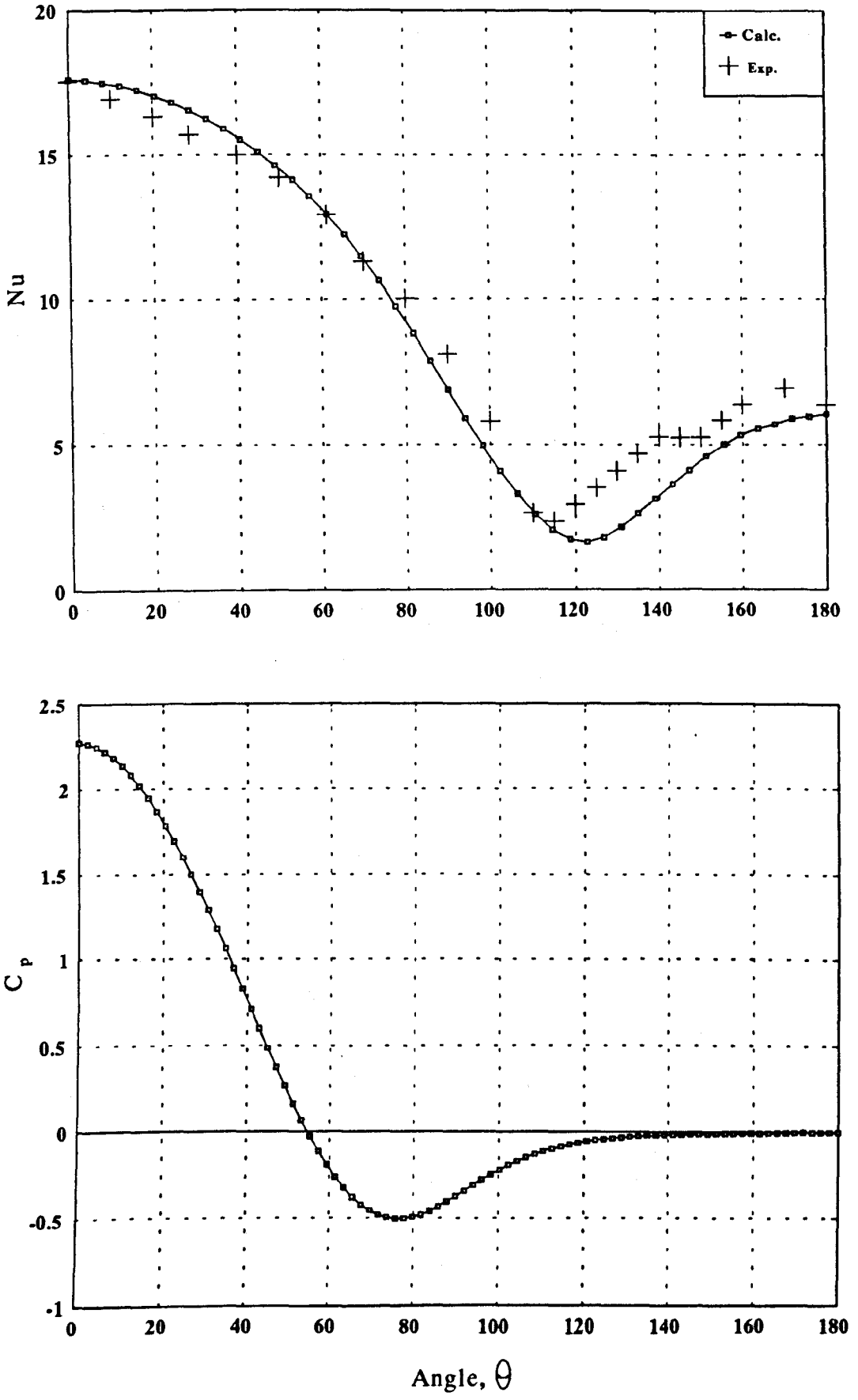

Figure 4.10 Calculated and Measured Local Nusselt Number and Calculated Pressure Coefficient for B=0.18 and Re=390

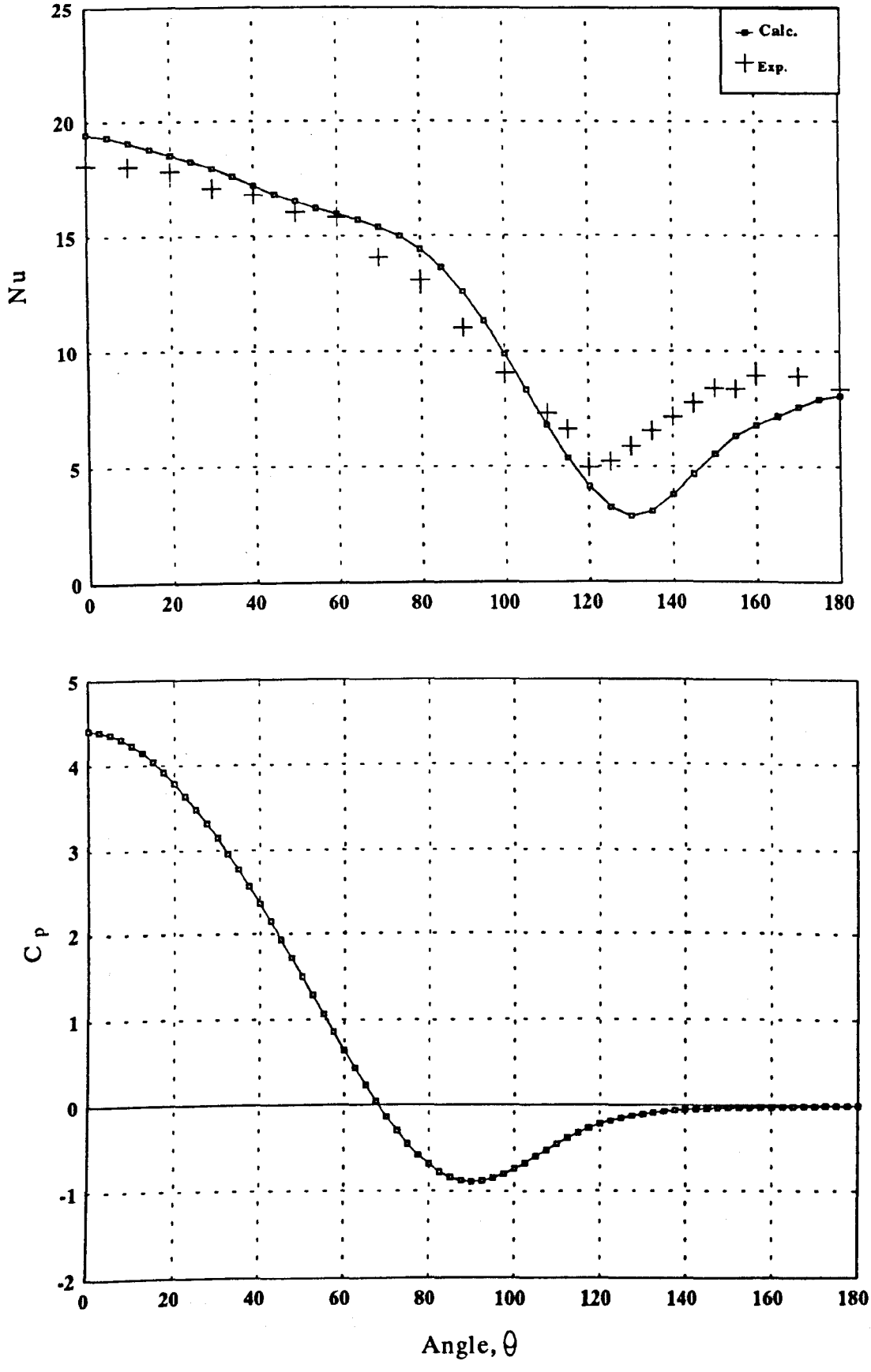

Figure 4.11 Calculated and Measured Local Nusselt Number and Calculated Pressure Coefficient for B=0.4 and Re=390

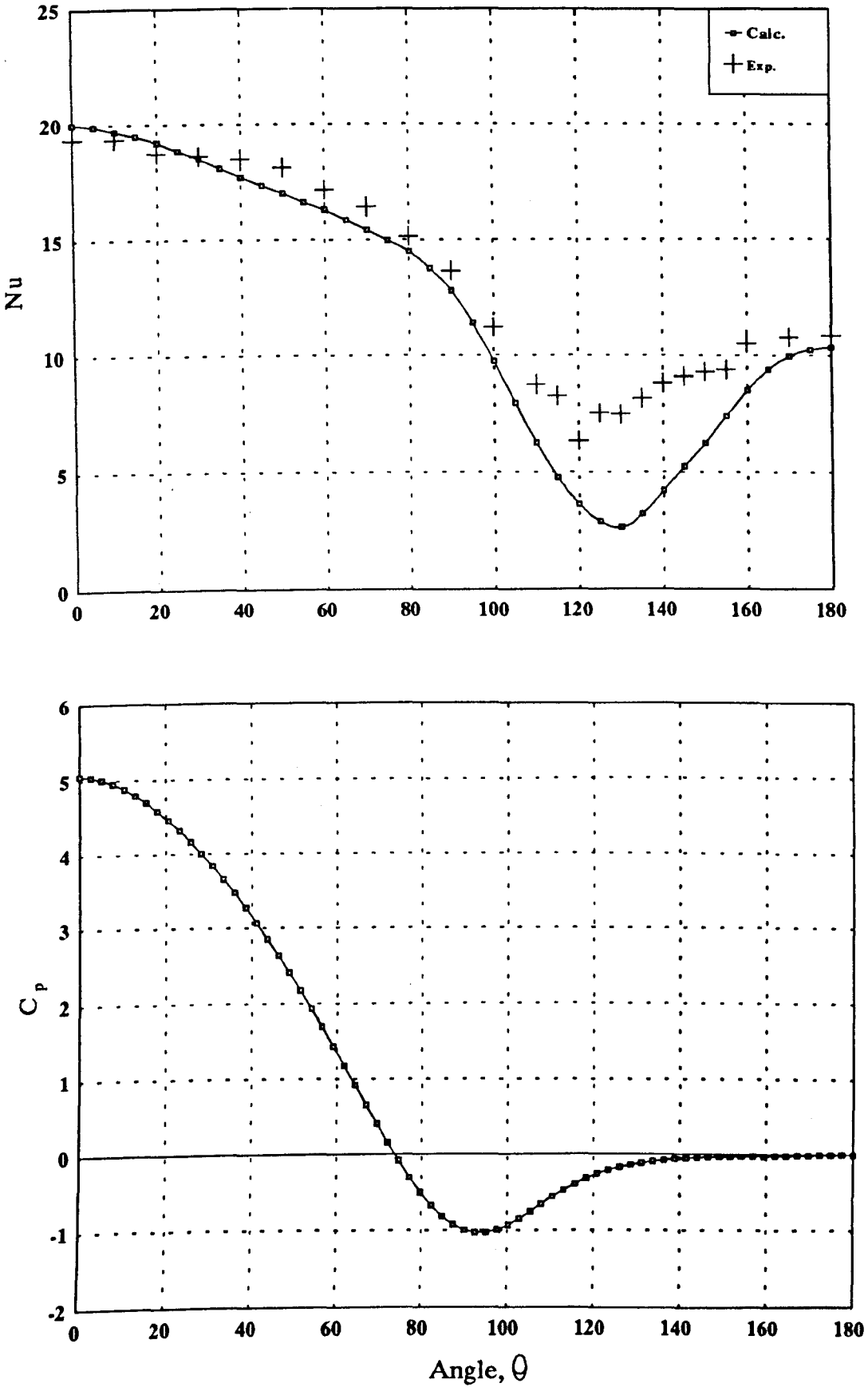

Figure 4.12 Calculated and Measured Local Nusselt Number and Calculated Pressure Coefficient for B=0.47 and Re=390

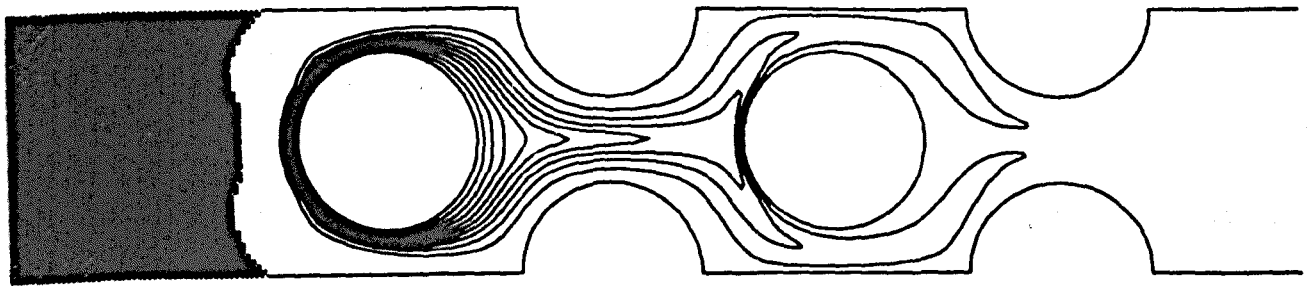

(a) First Tube

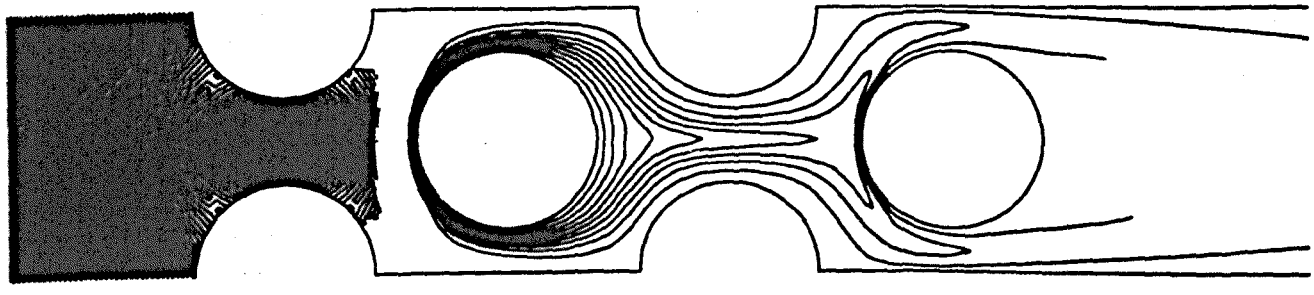

(b) Second Tube

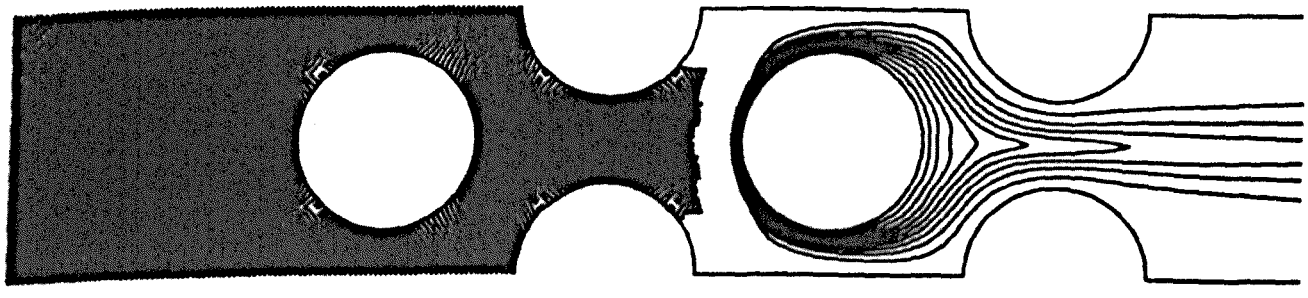

(c) Third Tube

Figure 4.13 Isotherm Patterns for 1.5x1.25 Staggered Tube Bank with Re=360

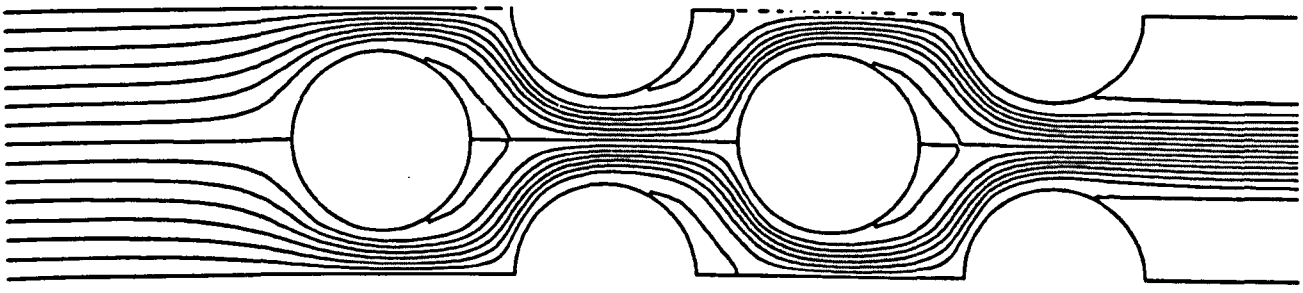

(a) First Tube

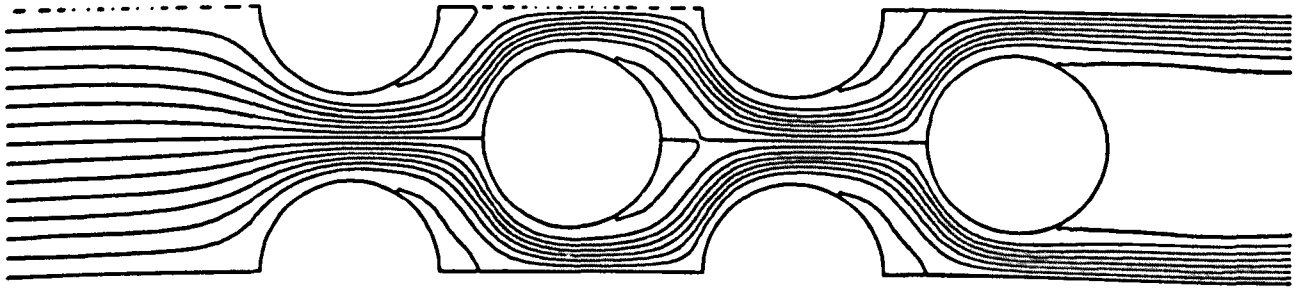

(b) Second Tube

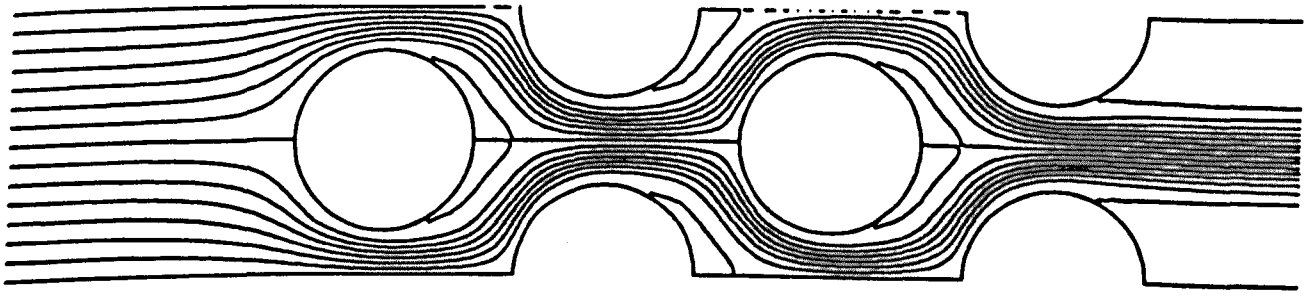

(c) Third Tube

Figure 4.14 Streamline Patterns for 1.5x1.25 Staggered Tube Bank with Re=360

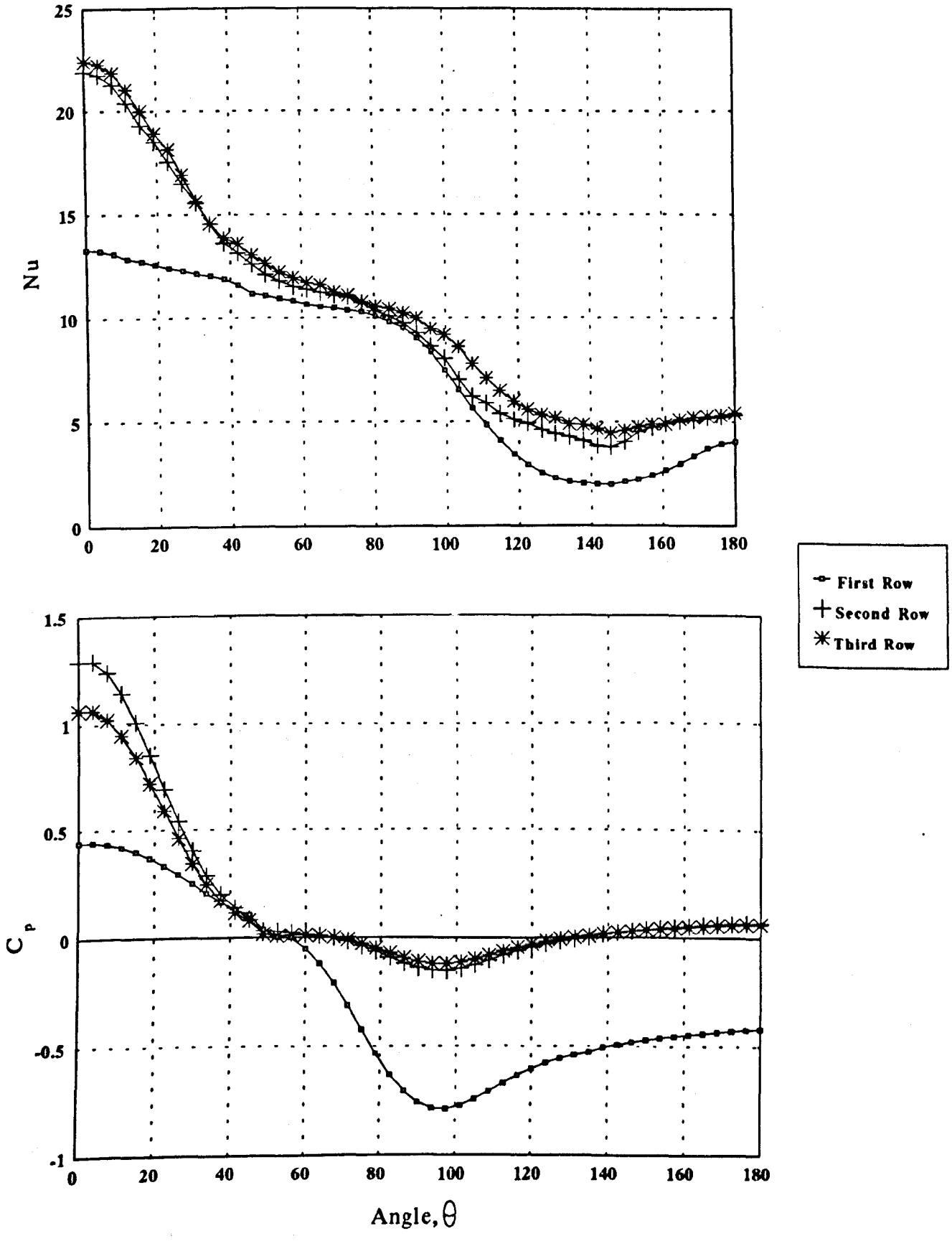

Figure 4.15 Calculated Local Nusselt Number and Pressure Coefficient for 1.5x1.25 Staggered Tube Bank and Re=360

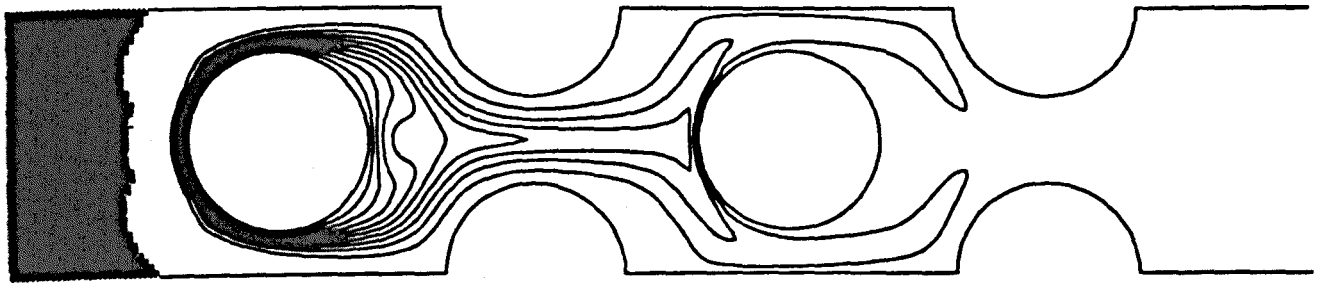

(a) First Tube

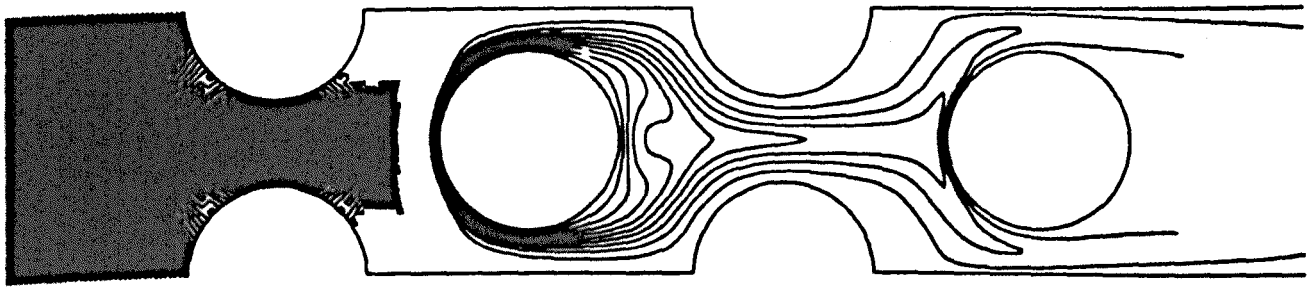

(b) Second Tube

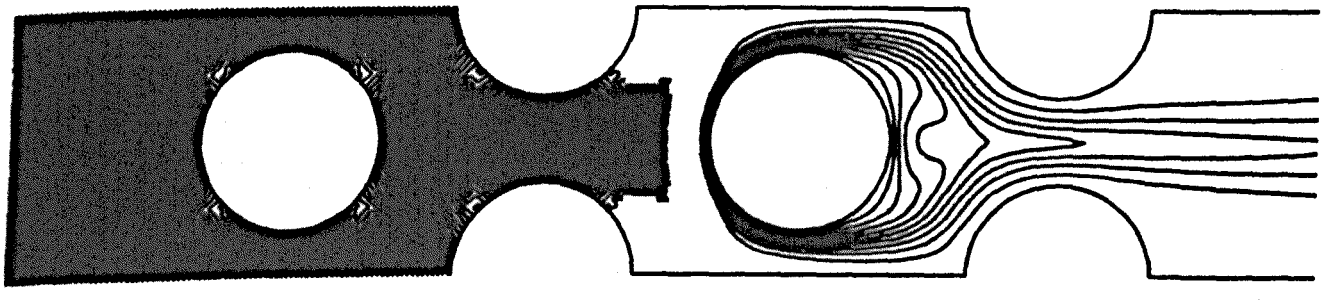

(c) Third Tube

Figure 4.16 Isotherm Patterns for 1.5x1.5 Staggered Tube Bank with Re=360

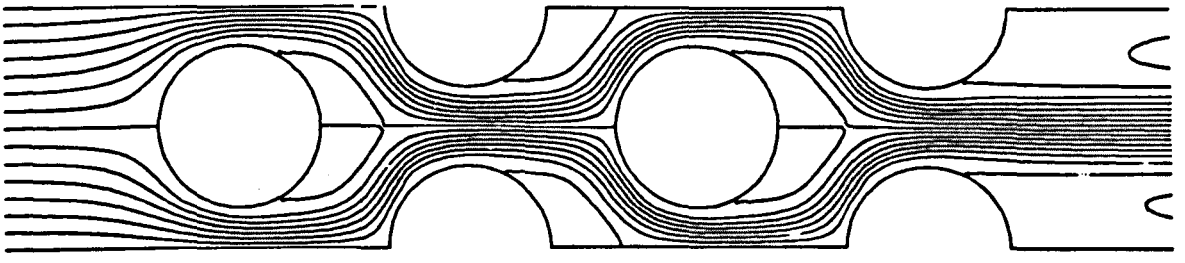

(a) First Tube

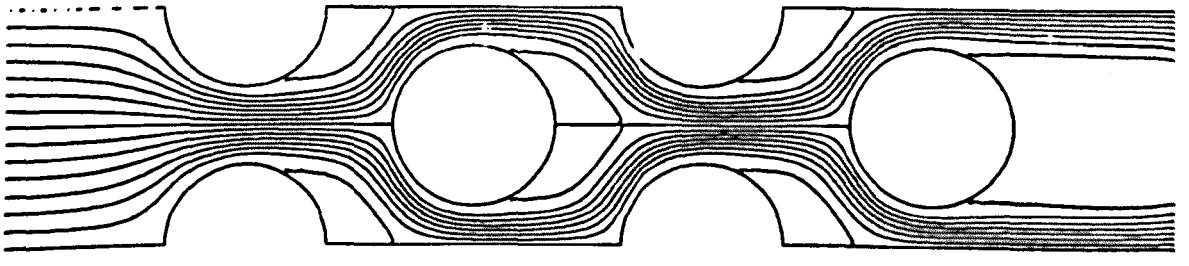

(b) Second Tube

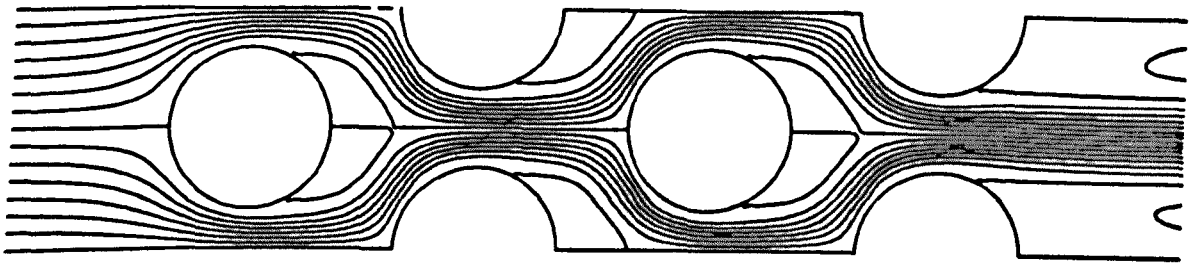

(c) Third Tube

Figure 4.17 Streamline Patterns for 1.5x1.5 Staggered Tube Bank with Re=360

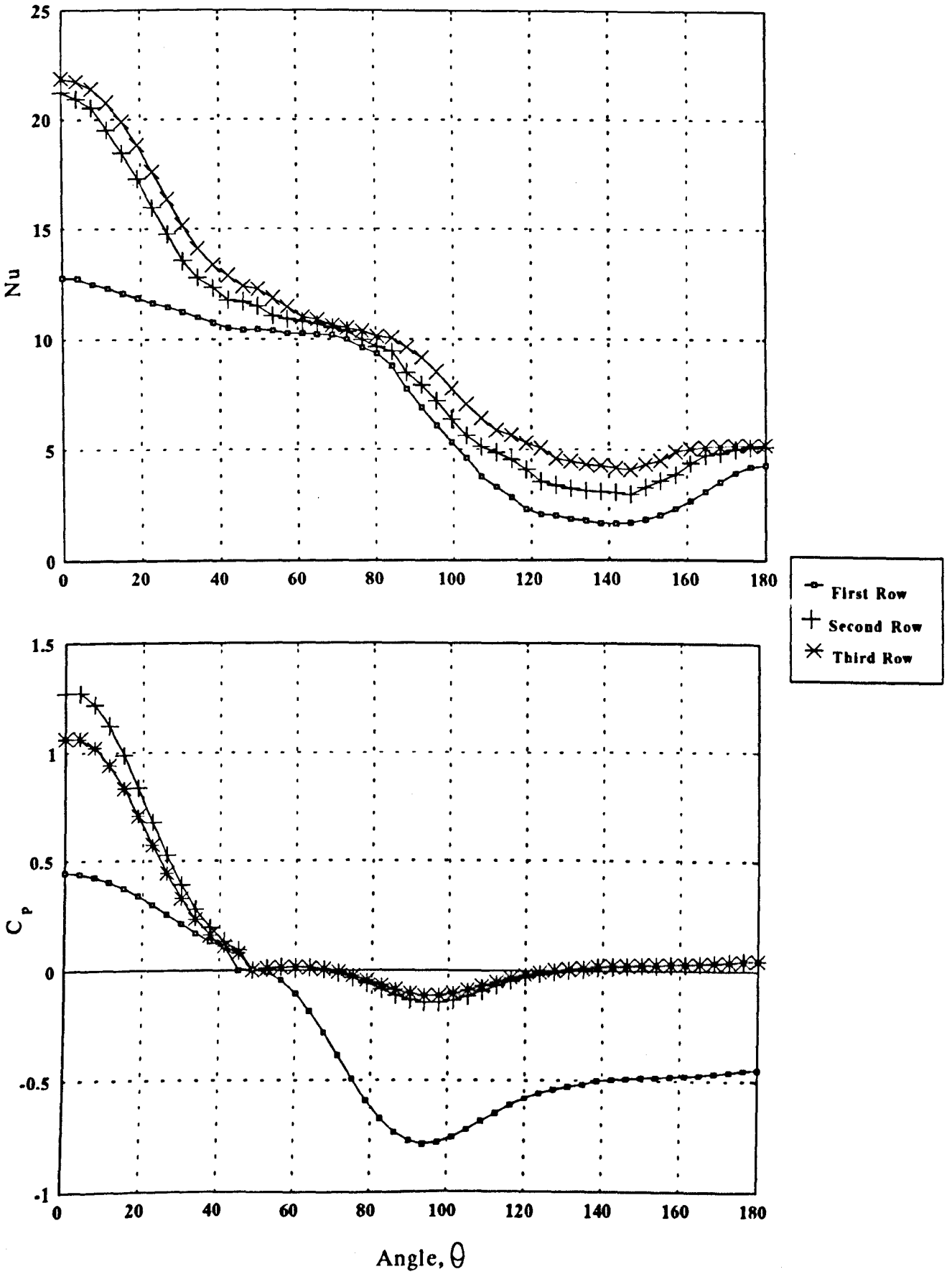

Figure 4.18 Calculated Local Nusselt Number and Pressure Coefficient for 1.5x1.5 Staggered Tube Bank and Re=360

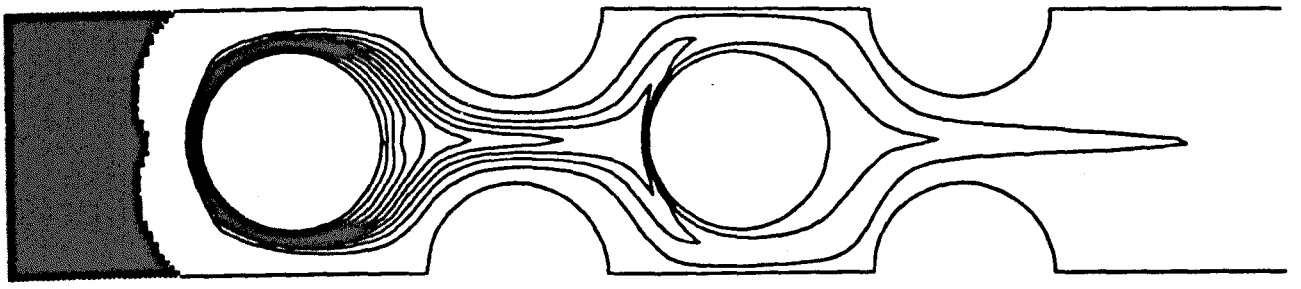

(a) First Tube

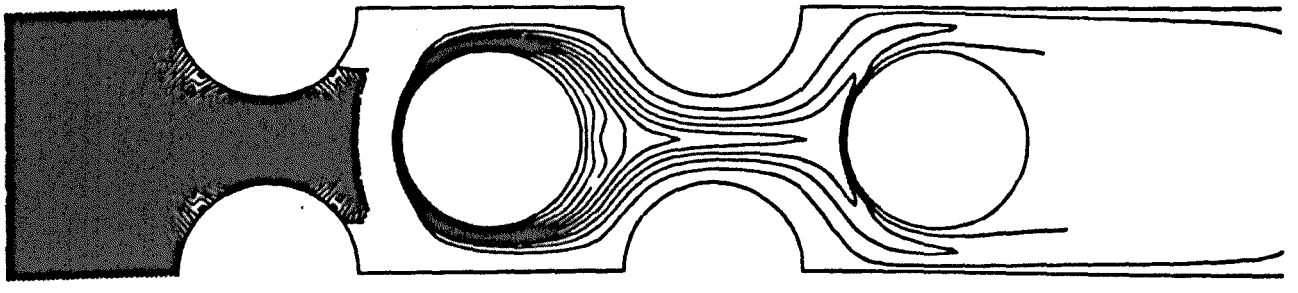

(b) Second Tube

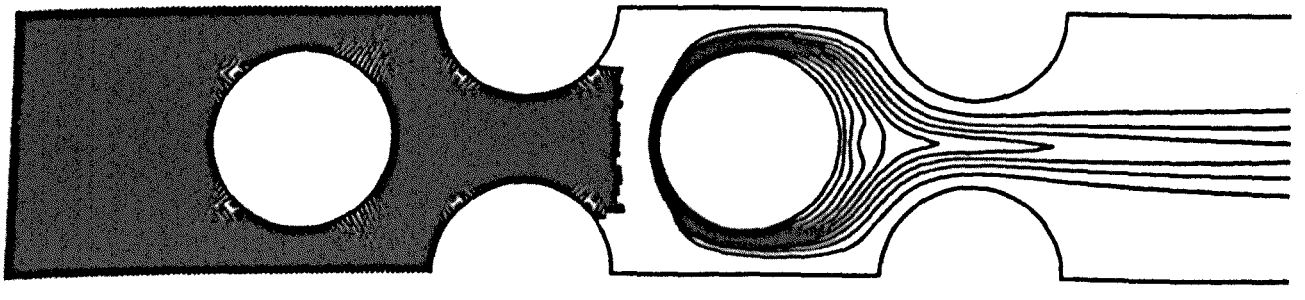

(c) Third Tube

Figure 4.19 Isotherm Patterns for 1.5x1.25 Staggered Tube Bank with Re=500

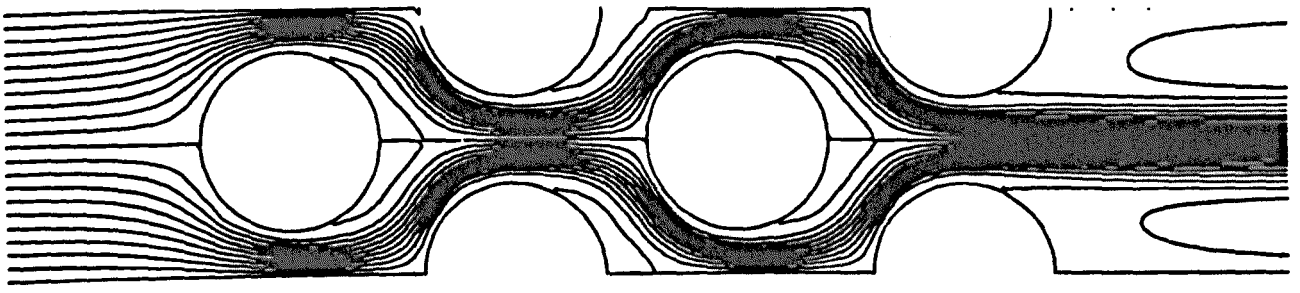

(a) First Tube

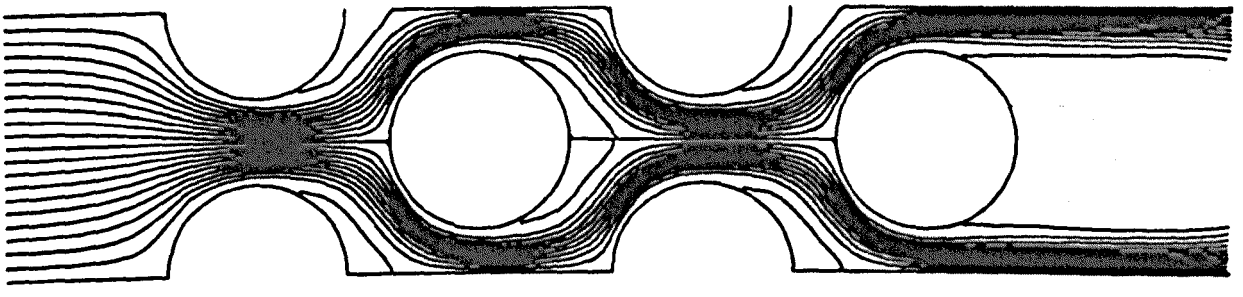

(b) Second Tube

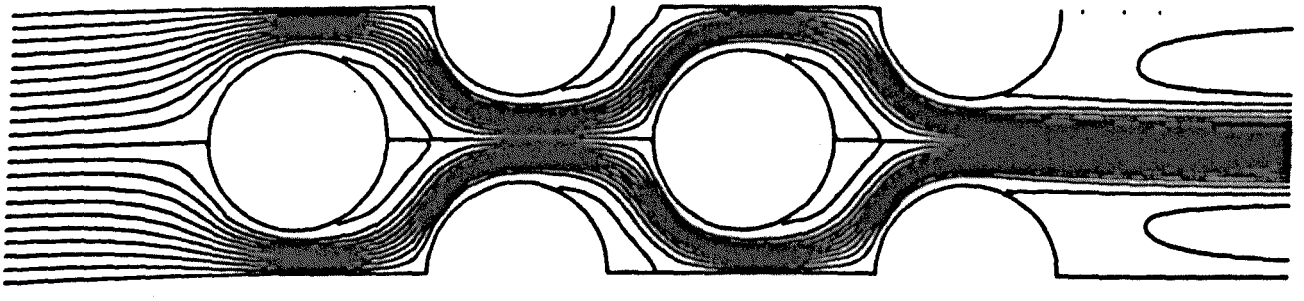

(c) Third Tube

Figure 4.20 Streamline Patterns for 1.5x1.25 Staggered Tube Bank with Re=500

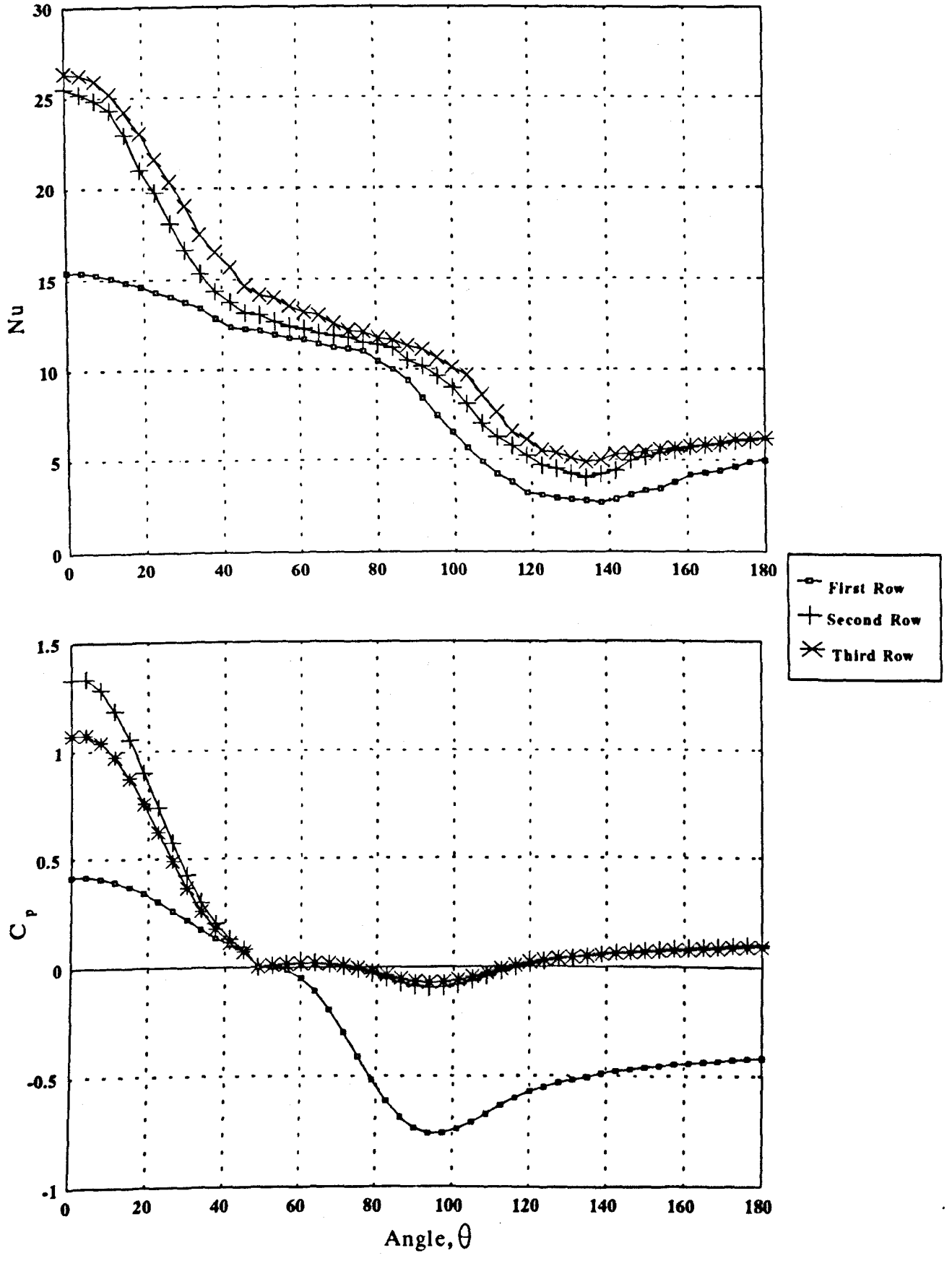

Figure 4.21 Calculated Local Nusselt Number and Pressure Coefficient for 1.5x1.25 Staggered Tube Bank with Re=500

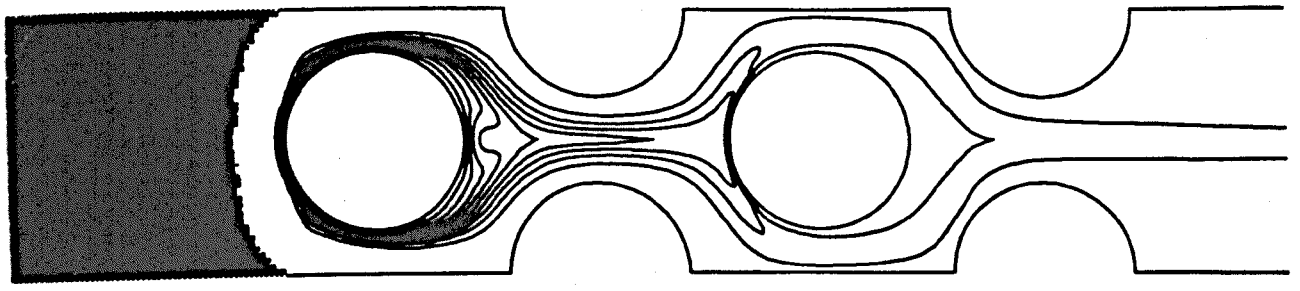

(a) First Tube

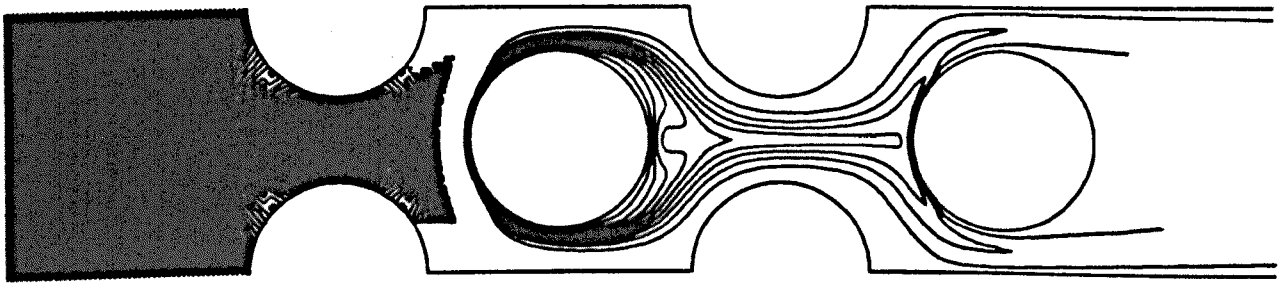

(b) Second Tube

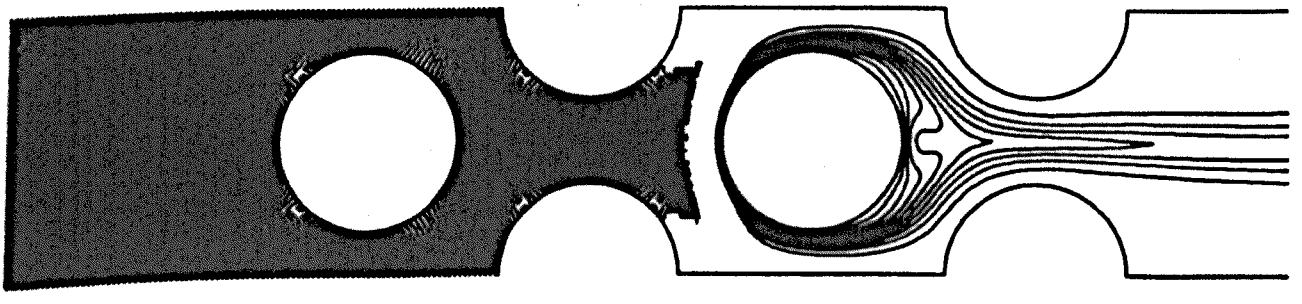

(c) Third Tube

Figure 4.22 Isotherm Patterns for 1.5x1.25 Staggered Tube Bank with Re=1180

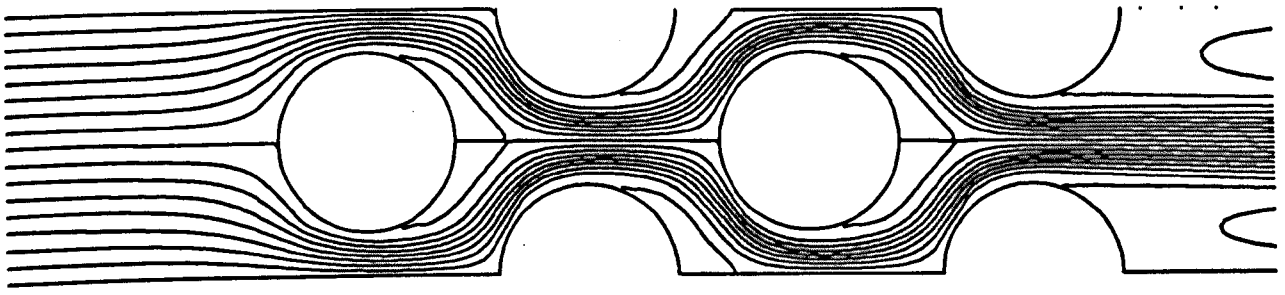

(a) First Tube

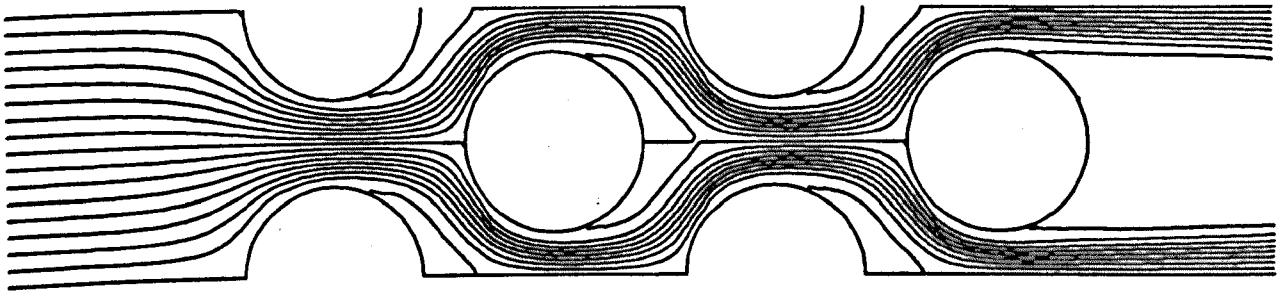

(b) Second Tube

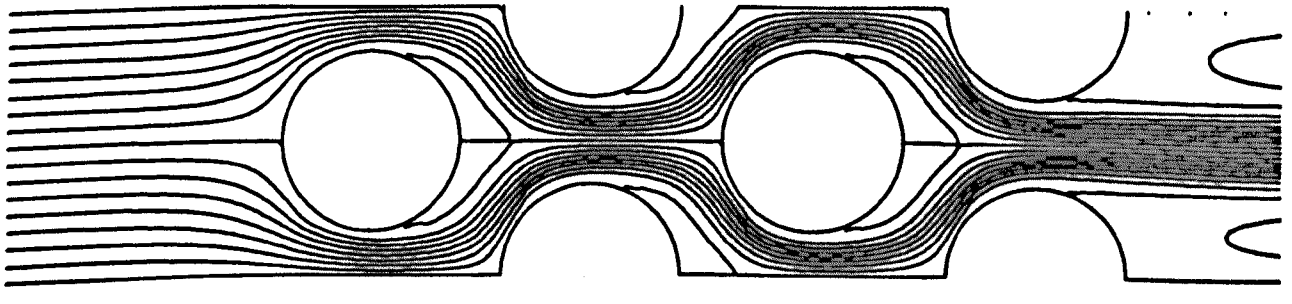

(c) Third Tube

Figure 4.23 Streamline Patterns for 1.5x1.25 Staggered Tube Bank with Re=1180

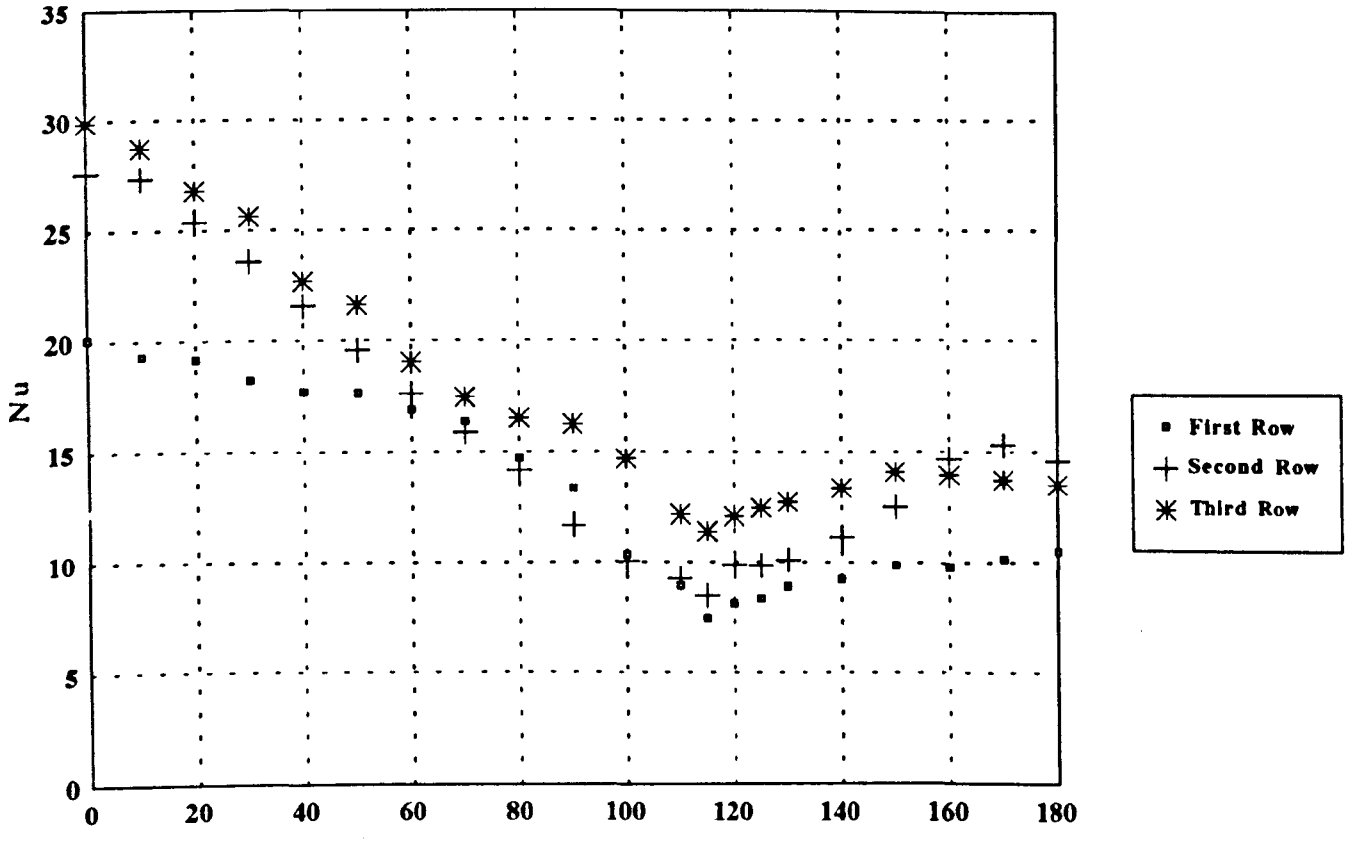

Figure 4.24 Experimental Local Nusselt Number Distribution for 1.5x1.25 Staggered Tube Bank and Re=1180

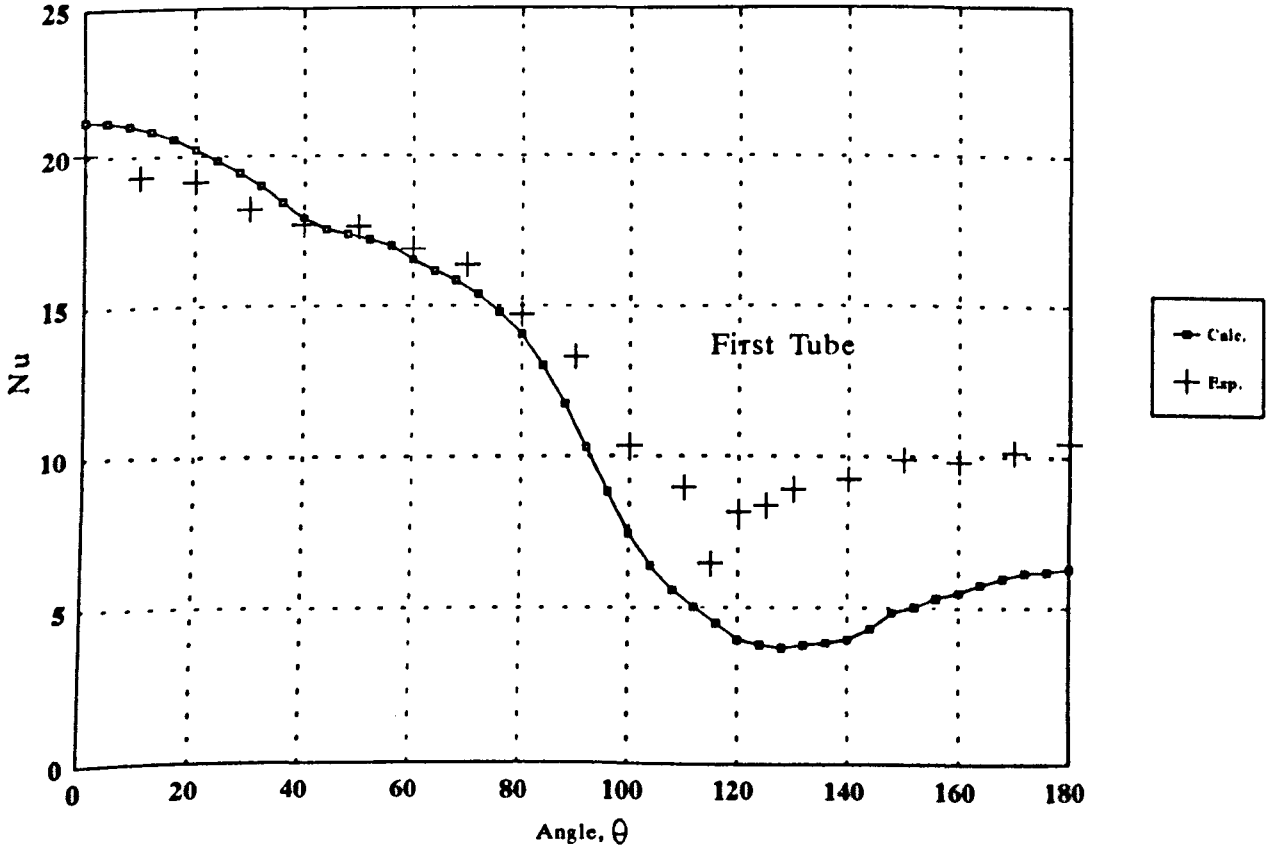

Figure 4.25 Calculated and Measured Local Nusselt Number for 1.5x1.25 Staggered Tube Bank and Re=1180

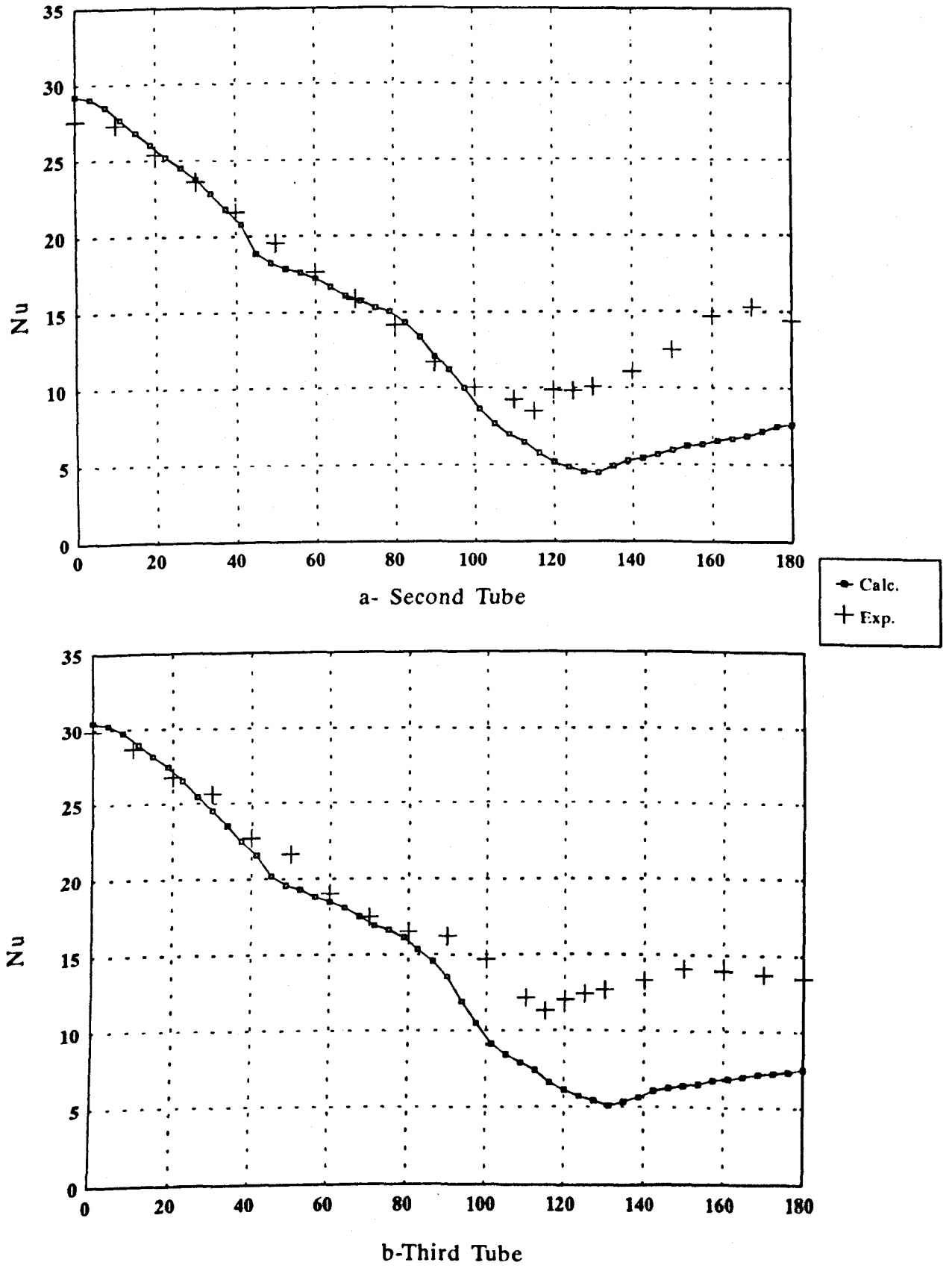

Figure 4.26 Calculated and Measured Local Nusselt Number Distribution of Second and Third Tubes, 1.5x1.25 Staggered Tube Bank and Re=1180

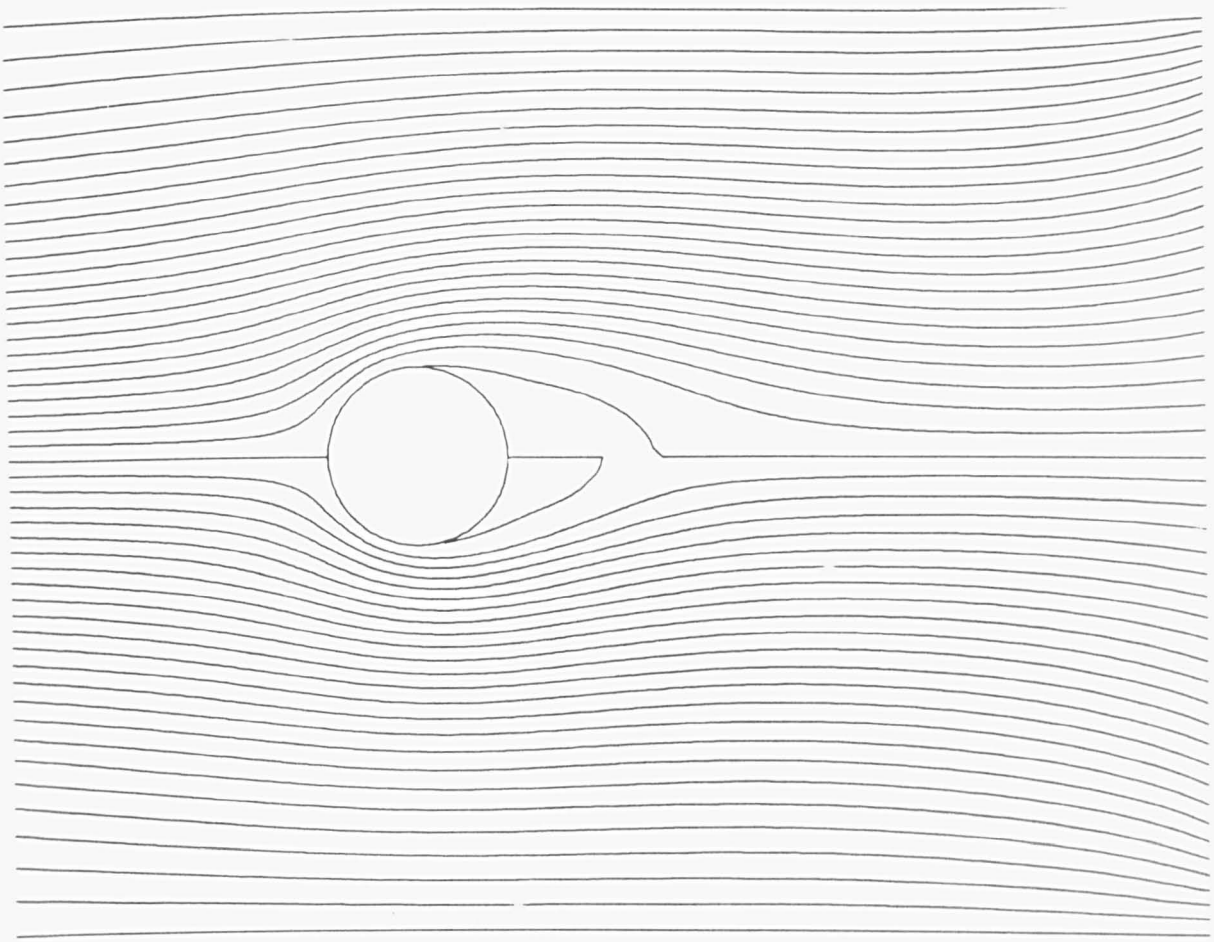

(a) Streamline

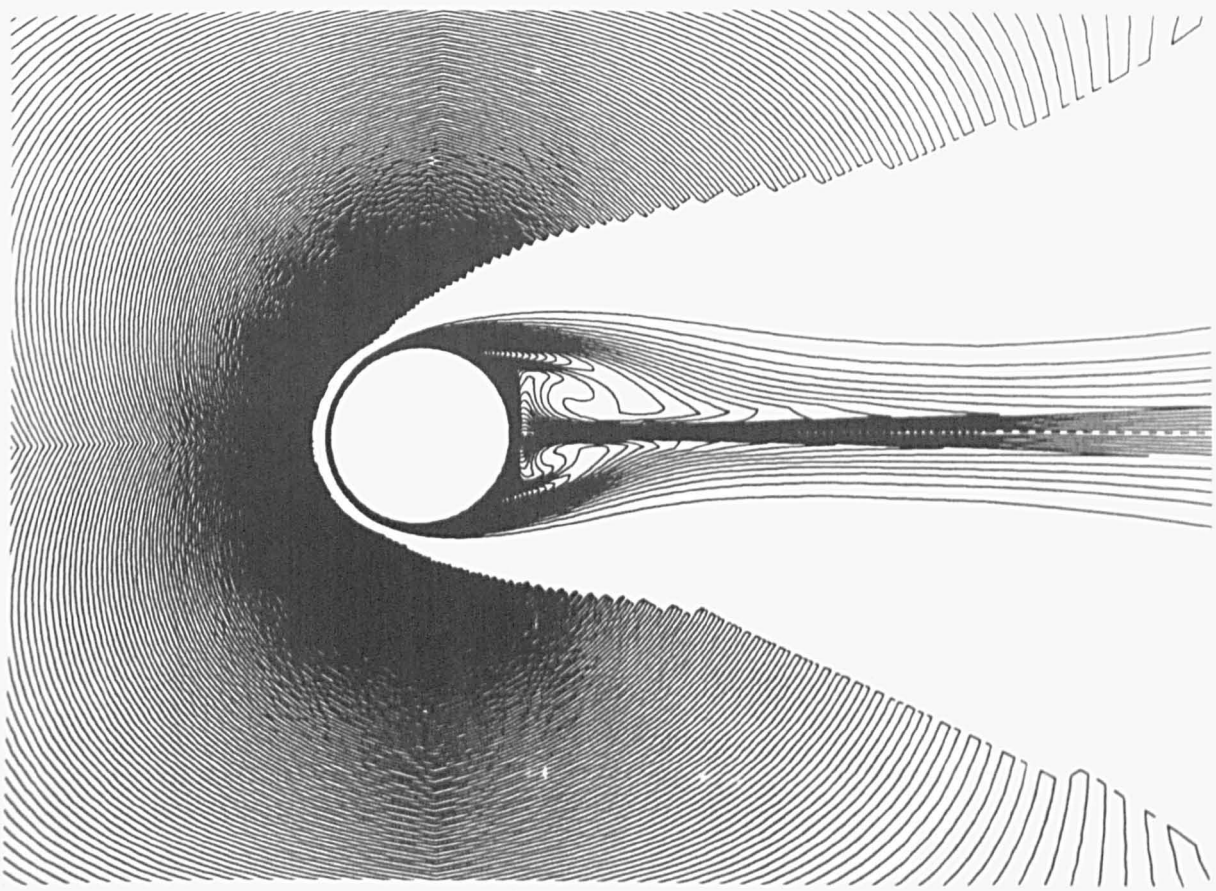

(b) Isotherm

Figure 4.27 Streamline and Isotherm Patterns for Turbulent Flow with B=0.18 and Re=7900

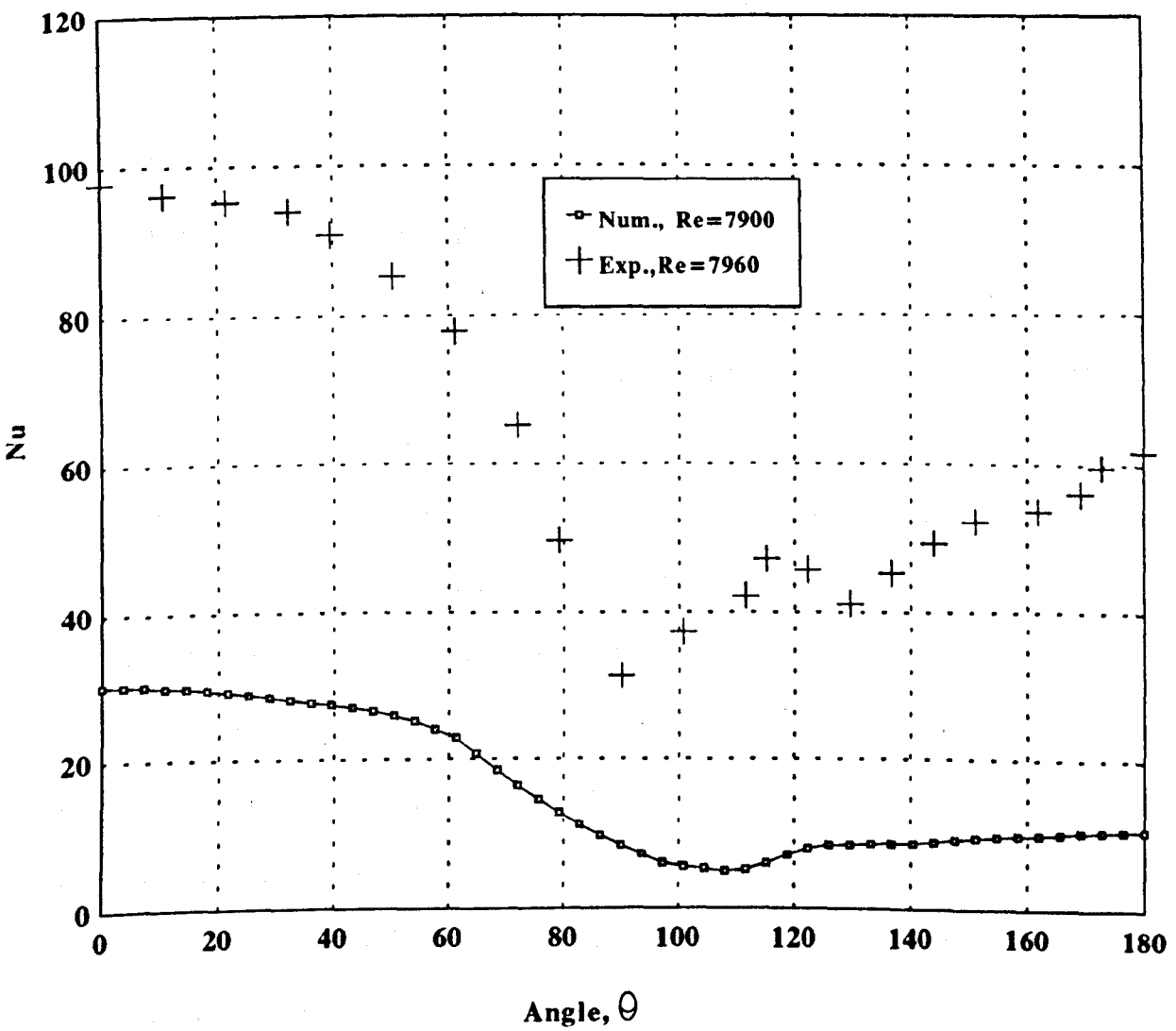

Figure 4.28 Comparison of Experimental and Numerical Local Nusselt Number for Turbulent Flow

CHAPTER 5

EXPERIMENTAL INVESTIGATION OF PARTICULATE FOULING ON THE GAS SIDE OF A HEAT EXCHANGER TUBE SURFACE

5.1 Introduction

Large coal-fired power plant use pulverized coal-fired furnaces. In the combustion zone of the pulverized coal-fired furnaces, the temperature will reach very high values, typically 2000 K. The organic matter of the coal reacts completely at this temperature, with the mineral matter oxidizing to form inorganic mixed oxide compounds. Part of these oxides vapourize under the high temperature conditions in the flame zone. The unvapourized parts form the residual particles, which may be liquid or solid. The residual particles may either fall to the bottom of the furnace or be carried up with the combustion gases. The combustion gases, in rising through the furnace chamber are cooled, causing the condensation of inorganic vapours. The condensation of these mixed oxide compounds may occur on particles in the flow or on the surfaces of the boiler tubes, which are usually several hundred degrees cooler than the surrounding gas. Particles that rise in the furnace thus grow by the condensation of the vapours. These particles, under the turbulent flow of gases, approach the walls and deposit on the boiler tubes. Depending on the composition of the particles and condensing vapours and the temperature of the wall, the deposit may be in liquid or solid form, thus resulting in slagging or fouling, respectively, Seapon and Lo, (1990)

The deposition of ash on the heat exchanger tubes generally reduces the heat transfer rate and changes the gas flow patterns around the tubes. The deposited ash may contribute to the corrosion and erosion of the boiler tubes. Accumulation of the deposit on the tube surfaces has been the major cause of significant operational problems and loss of efficiency in coal fired power plant.

The efficiencies of fossil-fuel boiler systems often rely on heat exchangers which extract energy from the flue gas before it is expelled to the atmosphere. The more energy that is extracted from the flue gas, the cooler the gas becomes. To avoid problems with condensation the gas temperatures are not normally reduced below about 175 °C. To obtain greater efficiencies, it will be necessary to reduce the gas temperature even lower than this. However by reducing the tube surface temperature too far the dew point is reached, water and sulphuric acid may condense and this leads to problems of aggravated fouling. Brown (1966) investigated the deposition of sodium sulphate from combustion gases and found no deposition above the dew point and maximum deposition just below the dew point.

A large number of investigations have been carried out to assess the effect of fouling on heat exchanger performance. Researchers have investigated different experimental conditions to obtain data to predict particulate fouling on heat exchanger tubes. Particle concentration, size of particle, velocity (Chomra and Webb (1993), Muller-Steinhagen et al.(1988), Blochl and Muller-Steinhagen(1990)), thermal conductivity of ash (Anderson et al.(1983), Wall et al.(1979) and Abraham and Rajaram (1983)) and different tube geometries of tube bank (Bembrose et al.(1984), Portyonko et al.(1980)) have been chosen as typical

process conditions for predictions. Bott (1990), Ots et al. (1986), Melo et al. (1984) and Petrov(1968) investigated deposit patterns around heat exchanger tubes. Figures showing some typical fouling have been given earlier in the thesis in Chapter 1. Deposition of particles around the boiler tubes depends on parameters such as gas inlet temperature, velocity, water content of the gas and also the heat exchanger surface temperature and condensation rates.

In the previous chapters, experimental and numerical investigations were concerned with the effect of blockage, of different tube geometries and of flow rate on the heat exchanger's performance. Also a theoretical study was carried out to predict the effect of deposit thermal conductivity, thickness of the deposit and eccentricity of deposit on the heat exchanger tubes. This chapter is concerned with the actual formation around heat exchanger tubes using a fouling heat exchanger rig that was manufactured with a compact gas fired burner with an output of up to 120 kW. The air flow rates, fuel gas and water into the system were measured to control the system conditions. Total gas flow rates through the system were recorded together with the gas and water temperatures across the heat exchanger. The intention was to show how heat exchanger characteristics change with deposit build up and also to monitor the conditions in the rig during the experiment. To maintain the feed rates of the fly ash, a vibrator/feeder system was used. To encourage of the ash deposition around the tubes, low inlet gas temperatures were set with the tube surface temperature below the dew point whilst other process conditions were fixed. Observations were carried out for different amount of ash and also for higher gas inlet temperatures. The original purpose of this experimental work was a detailed study into a heat exchanger that was being fouled. Unfortunately due to practical difficulties and limited time, observations were carried out for

only a small number of experiments.

5.2 Description of the Experimental Rig

A schematic diagram and photograph of the experimental rig are shown in Figure 5.1 and Figure 5.2 respectively. The fouling heat exchanger rig was built to investigate the characteristics of the deposit and of the heat exchanger during fouling. The gas flow range was up to 3 m/s with temperatures up to 350 °C. The general layout of the rig can be seen in Figure 5.2(a). Staggered and unfinned tubes were assembled in two separate banks with the water-side being in cross-flow. Air was drawn into the rig via the main fan. The air was heated using a compact gas-fired burner. After the furnace, a secondary air and a particle feed section were set up as seen in Figure 5.2(b). The secondary air was introduced via a fan to reduce gas temperatures and to obtain required gas flow rates. Between the furnace and tube bundle section adjustable vanes were installed to obtain a uniform flow distribution before entering the tube bundle. Two cyclone dust separators were located downstream of the outlet section to collect particles prior to exhausting the gases to the atmosphere; the cyclones can be seen in Figure 5.2(c). The air flow rate was measured using an orifice plate (Figure 5.2(d)) in accordance with British Standard BS1042 (1964). Temperatures and pressures through the rig were measured using thermocouples and water manometers. To maintain the feed rates of the fly ash, a vibrator/feeder system was placed after the furnace. The top panel of the tube bundle section was constructed to be removable to allow access for viewing the deposit.

5.2.1 Tube Bundle and Temperature Measurement

A schematic diagram of the tube arrangement is shown in Figure 5.3(a). Pitch

dimensions used were 1.5 x 2.9 (S_t x S_l). The tubes were 26.7 mm in diameter and 515 mm long; a total of 133 mild steel tubes were used. Two separate tube bundles of dimension 400x400x550 were installed between the entry and the cyclones. Water was passed through the tubes via a manifold from the bottom side of the tube bundles and it was collected by the manifold from the top side of the bundles. This gave a cross-flow configuration. Water flow rate was measured via a bank of flowmeters. All the temperatures were measured using copper-constantan thermocouples connected to digital Comark multichannel thermometer. Water outlet temperature was recorded and averaged using a sensitive digital thermometer. In the gas side section, three thermocouples were used; one before the tube bundle (for gas inlet temperature readings), one after the tube bundle (for gas outlet temperature readings) and one before the orifice plate. Before commencing experimentation the inlet temperature profile in the hot gas flow was measured across the inlet section using 10 thermocouples placed in thin, stainless steel tubes. The velocity distribution across the tube bundle inlet section was measured by a hotwire anemometer but without the burner in use (ie. cold air flow). These measurement were used to assess the flow uniformity entering the test section.

5.2.2 Air Flow Through Rig

Air flow was induced through the rig by the use of a fan. The air entered the rig and passed through the furnace and tube bundle. Secondary air was delivered by an additional fan to reduce the inlet temperature and to adjust the gas flow rate to the desired values. With the secondary air, particles were fed into the flow where they mixed before going through the adjustable vanes; a uniform distribution of flow and particles then entered tube bundles. After the test section the flow passed through the cyclone separator which removed the remaining

fly ash. A test was carried out to monitor the efficiency of the cyclones where it was found that about 90 percent of the ash was collected. The air/particle mixture then entered a long pipe and passed through the 100 mm diameter orifice plate. Figure 5.3(b) shows the orifice plate and pressure measurement tapping.

5.2.3 An Examination of the Orifice Plate Measurement

To examine the orifice plate measurement, the velocity profile of the unheated air upstream of the test section was measured using a hotwire. The flow rate thus obtained was compared with the orifice plate and a difference of nearly 40 % was found. The flow rate obtained from the orifice plate was the greater and very significant difference was found to be due to leakage through the gaps in the rig construction and also due to the porosity of the ceramic fibre board from which the rig was manufactured. Steps were taken to reduce this leakage but a difference of 10 % still remained. For this reason it was impractical to obtain a reliable energy balance for the heat exchanger and any associated experiments that had been planned had to be abandoned in view of the time limitations.

5.2.4 Fly Ash Particle Size and Vibrator/Feeder System

The fly ash used in the fouling tests was supplied by the Coal Research Establishment. The particle size distribution of the ash was obtained using a nest of sieves with the following results:

Percentage (%)	*Particle Size*
40	less than 38 μm
30	38-125 μm
25	125-180 μm
15	more than 180 μm

The ash was fed into the rig using a vibrator/feeder system. A stainless steel trough 25 mm wide and 300 mm long was vibrated and the feed rate could be adjusted via a controller.

5.3 Experimental Procedure and Initial Tests

To characterize the heat exchanger rig, initial tests were carried out in the clean condition. As explain earlier, the flow rate measured by the orifice plate was not consistent with the hotwire measurement in the unheated flow, nevertheless tests were carried out in which the water flow rate and gas temperature were varied. The enthalpy change for the gas-side and the water side were calculated and compared. The following table shows the gas and water duties in kW.

Water Flow Rate(kg/s)	m_w=0.1833	m_w=0.366	m_w=0.55	m_w=0.733	m_w=0.9166
T_i=311	Q_g=59.68 Q_w=32.02	Q_g= 61 Q_w= 41.91	Q_g=62.75 Q_w=42.76	Q_g=65.29 Q_w=47.49	Q_g= 66.27 Q_w=48.65
T_i=255	Q_g=48.37 Q_w=27.04	Q_g=50.19 Q_w=32.73	Q_g=52.47 Q_w=35.14	Q_g=53.39 Q_w=38.29	Q_g=53.61 Q_w=39.84
T_i=188	Q_g=33.20 Q_w=16.31	Q_g=35.09 Q_w=24.01	Q_g=36.88 Q_w=24.31	Q_g=38.89 Q_w=24.81	Q_g=39.36 Q_w=27.58

Table 5.1 Comparison of Water and Air Heat Transfer (kW)

As can be seen from results, there are significant differences in the energy balance and these are due to the leakage problem described earlier and also heat losses. All the remaining tests were carried out with internal pressure of rig being as close as possible to atmospheric to reduce leakage but as was said earlier, all thermal performance tests had to be abandoned since there was no time available to remedy the problem. Tests were therefore restricted to observations of fouling patterns.

To ensure reliable and uniform deposition across the heat exchanger it was important to ensure that the ash was well mixed in the flow and that this flow was uniformly distributed across the heat exchanger. To achieve this the rig had a set of adjustable vanes as shown in Figure 5.1. By adjusting these vanes the flow distribution was altered. Figures 5.4 and 5.5 show the velocity distribution and the temperature distribution upstream of the first row of

the tubes. As can be seen the profiles are relatively uniform.

After some initial tests, fly ash was used to perform fouling tests. The procedure for the fouling test was to first operate the burner with natural gas to provide the desired gas inlet temperature and flow rate. The gas inlet temperature was first set at value of 110 °C. This low temperature was applied to encourage condensation in the rig which will enhance the fouling rate. With the gas temperature entering the tube bundle set at 110 °C the dew point temperature value was calculated to be 66 °C. Also the tube surface temperature was calculated for known water and gas temperature conditions and surface heat transfer coefficient and found to be about 51 °C. These conditions ensured that the tube surface temperatures were below the dew point. The water flow rate was fixed during the experiment. With these conditions, the air flow rate was 0.28 kg/s calculated from the orifice plate pressure readings. According to this flow rate, the velocity at the inlet section was 1.96 m/s and the Reynolds number was calculated to be 6038, corresponding to the maximum velocity occurring at the minimum space of the transverse pitch. Once steady-state conditions were obtained fly ash was added to the flow by the vibrator/feeder system. Temperature readings were taken every 10 minutes during the test. For all measurements, the ash loading rate was fixed at 30 g/min and experiments were carried out for three different amounts of ash of 4, 6, and 10 kg. The feed rate was considered to be typical of the loading of gases from pulverised coal fired plant, Allmon et al. (1991). In a second experiment the gas inlet temperature was altered from 110 °C to 250 °C using 6 kg ash with a 30 g/min loading rate and fixed water flow rate.

5.4 Results and Observations

Following each deposition experiment, the top panel of the heat exchanger section was removed to expose the tube banks. The formation of the deposits that were observed are shown schematically in Figure 5.6. The Reynolds number for this case was calculated to be 6038. For different loads of ash added the deposition pattern did not alter significantly although there was a greater build up for the higher loading. The increased thickness of deposit was not in proportion to the increased load however, suggesting that the net deposition rate (i.e. deposition minus removal) had an upper limit. The first row had a unique deposition pattern as shown in figure 5.6 and 5.7(b) (first row on left). The deposition started at about 90° from the front stagnation point and continued over the whole rear surface. In the second, and subsequent rows of tubes the deposition is seen to start at about 100° to 110° and continue around to about 130° after which point there was only a light deposition. Bands of deposit were therefore formed at the upper and lower areas on the tube as shown in Figure 5.6 and 5.7(c).

The deposition patterns are clearly dictated by the gas flow over the tubes. In the first row the onset of deposition coincides with the flow separation and continues in the wake region. The pattern of deposition on the subsequent tubes is, however, not so readily reconciled with the flow pattern. The deposit is concentrated into bands between about 100° and 130°. There is only a limited amount of data available for the flow and heat transfer patterns around the inner tubes and these are for Reynolds numbers higher than 6000. At a Reynolds number of 14,000 Murray and Fitzpatrick (1988) identify two minima in the Nusselt number distribution around the tube (similar to those shown earlier in Chapter 3). These are

at 90° and 120° and at the lower Reynolds number of 6038 they might be expected to move further round the tube towards 100° and 130°. As discussed earlier in Chapter 3 there are two schools of thought as to what the two minima correspond to. One explanation is that the first minimum corresponds to laminar/turbulent transition and the second to separation. The second explanation is that the first minimum is due to flow separation and the second to a flow re-attachment. The more recent paper by Baughn et al. (1986) favours the second explanation. If the flow does separate and re-attach due to the confinement of the surrounding tubes then there will be a recirculating region (separation bubble) between these points and this would appear to correspond to the band of deposition. With this argument, however, it is not clear where the flow finally separates from the tube (this may not be indicated by the heat transfer distribution, but would be indicated by the pressure distribution) and does not explain why there is no deposition in the wake region as there is on the first row. At this stage therefore, a definitive explanation of the deposition pattern cannot be given.

During the fouling tests one of the rows of tubes in the first bank was isolated from the water supply. The purpose of this was to allow the tube surface temperature to be the same as the gas flow. Since the fouling is known to be affected by the dew point in the gas flow (Brown (1966)) one might expect a difference in the deposition between the hot and cold tubes. Sure enough, the deposition on the hot tube was significantly less than on the cold tube with a clean upstream face and just a light dusting on the downstream face. A second variation in the tests was to increase the incoming gas temperature to about 250°C. The deposition patterns were seen to be very similar to the previous tests which is not surprising since the tube surface temperatures are mostly dictated by the water temperatures, and these

were the same in both experiments.

The experiments using the fouling rig were therefore limited in scope. During the several hours it took to conduct the experiment readings of temperature and pressure were taken every 10 minutes. The changes in the conditions in the rig were, however, too small to make any significant changes in the measured parameters.

5.5 Significance of the Research for Heat Exchanger Design and Operation

After carrying out the experiments using the heat exchanger rig and gaining experience of the practical aspects of heat exchanger design and operation it was considered pertinent to relate this to the research reported in earlier chapters.

The research reported in this chapter, and in the rest of this thesis has implications for the design and operation of heat exchangers. When designing a tubular heat exchanger, for example to extract heat from combustion gases to raise hot water, there are a number of considerations to be made. Known conditions will probably be the flow rate and temperature of the gases and possibly the inlet temperature and flow rate of the water. The thermal design of the heat exchanger will yield a surface area but this has to be done in conjunction with a consideration of the pressure drop experienced by both the gas and water flows. Figure 3.13 showed how increasing the blockage gives a higher average Nusselt for each tube, at the same time the tubes will be occupying a smaller volume of space due to their reduced spacing. On the face of it therefore, it appears beneficial to increase the blockage. The consequence of this, however, will be to increase the pressure losses as indicated by the pressure coefficients

shown in Figures 3.6 to 3.11. There is little purpose in having the blockage so high that the additional heat transfer is outweighed by the additional pumping power required to maintain the flow rates.

An underlying theme of the research was to consider the effects of fouling on the heat transfer. If the gas flow is laden with particles, and particularly if the temperatures on the tube surface and in the gas fall below the gas dew point, fouling will be a problem and as the blockage is increased in the heat exchanger so the likelihood of fouling will increase. Furthermore, the cleaning of fouled heat exchanger tubes is normally carried out by high speed jets of air which are directed into the heat exchanger matrix. These jets will be unable to penetrate the heat exchanger if the blockage is too great. After taking into account the practical constraints of having the tubes too closely packed, the heat exchanger designer can select a suitable blockage and can get an indication of how this will affect the heat transfer by using the data in Fig 3.13.

Process conditions may be such that fouling is an unavoidable problem. If this is the case then the data and analytical techniques described in Chapter 2 can be used to assess the effect on the heat transfer. If the disposition of the deposit is non-uniform but generally circular then the thermal resistance can be estimated. If the deposit is more dense in some regions than others, for example it may be more dense close to the tube surface due to the effects of condensation or ageing, or it may be more dense in an impact zone, then again the effects of these conditions on heat transfer can be calculated. As the effective diameter of the fouled tube increases this will change the outside heat transfer coefficient as described

above. The modified values of outside heat transfer coefficient, together with the calculated thermal resistance of the deposit can be use to obtain a value of overall heat transfer coefficient.

The experimental technique of changing the heat exchanger configuration and measuring the resultant effect on heat transfer is time-consuming and can be costly. Chapter 4 has addressed the possibility of determining the effects of geometric changes on heat transfer by numerical modelling. The work has been reasonably successful in the laminar region but has shown that the turbulent case is more demanding. The turbulent case will need further investigation before it will be of use to the heat exchanger designer.

5.6 Concluding Remarks

A study was carried out to measure the effects of fouling on the heat transfer characteristics of a tubular heat exchanger. Due to limitations of the rig and of time the study had to confine itself to observations of the patterns formed by the deposit. The main conclusions of this chapter can be summarised as follows:

- The rig was capable of providing a uniform heated flow at entry to the tube banks but due to air leaking into the rig it was not possible to obtain a satisfactory energy balance between the air flow an the water flow. This prevented any sensible measurements on how the rig characteristics changed with time as the fouling proceeded.

- On the first row the front face of the tubes did not suffer from fouling but the rear section, from 90°, showed a relatively uniform build up of deposit. The onset of deposition was readily identified with the flow separation and wake region.

- On the second tube onwards the fouling was confined to narrow bands between about 100° and 130°. These were tentatively related to the existence of a separation/reattachment region but could not be reconciled with the pattern observed on the first tube.

- Fouling on a hot tube was less than that on cold tubes thereby confirming the effect of condensation on the fouling process.

- Increasing the total amount of fly ash passed through the rig did not produce a corresponding increase in the level of deposition, suggesting that the deposition process is self limiting.

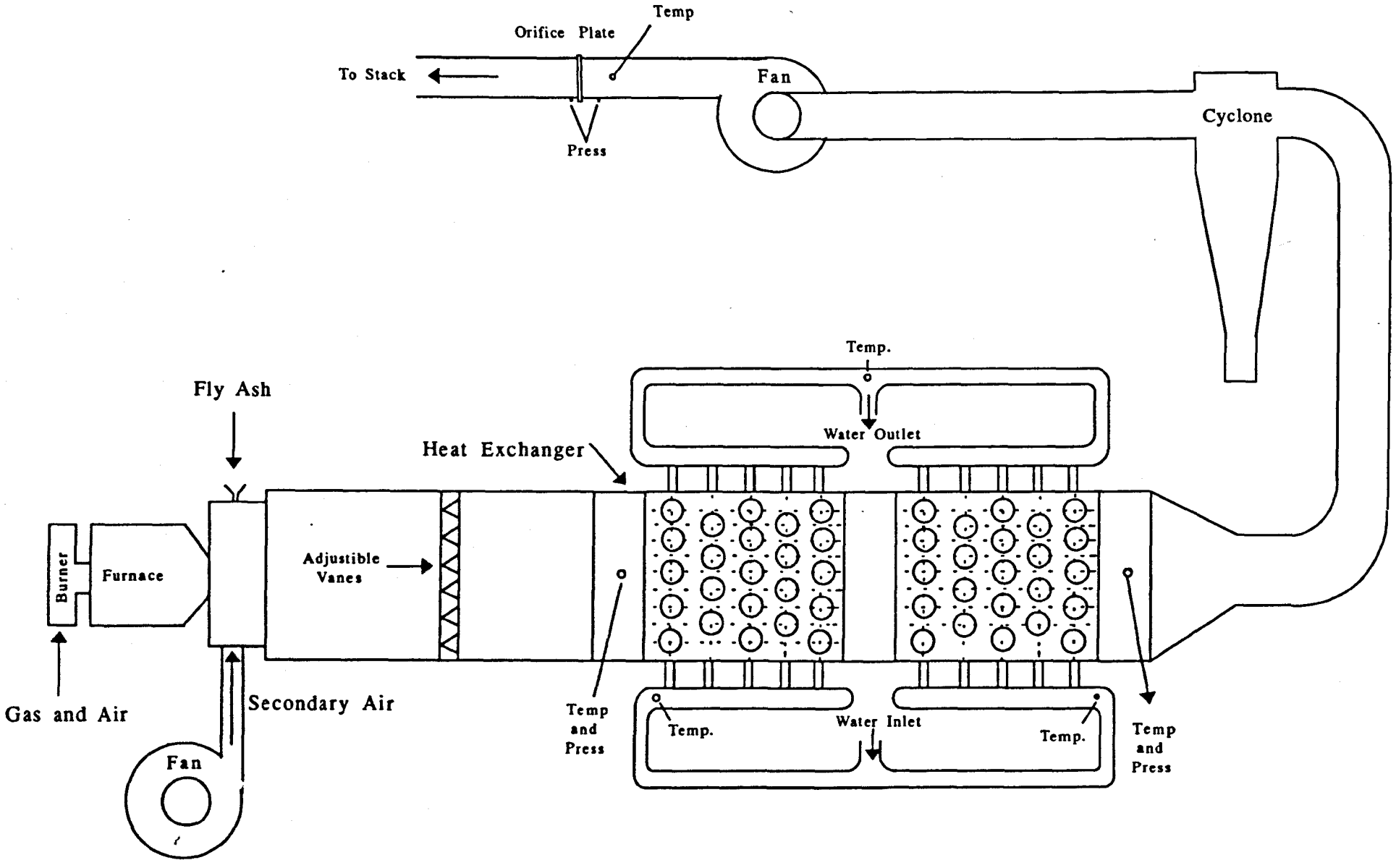

Figure 5.1 Schematic Diagram of the Heat Exchanger Rig

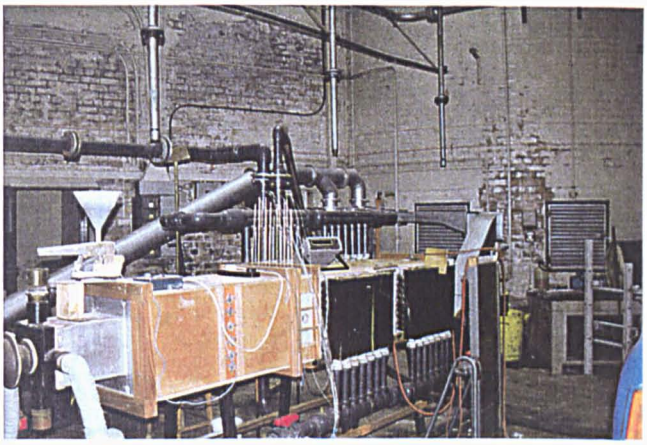

(a)

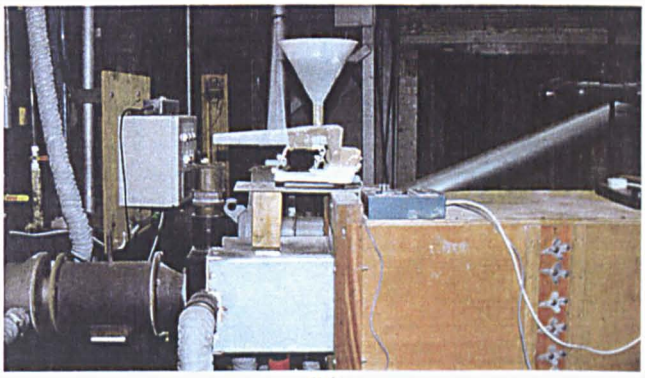

(b)

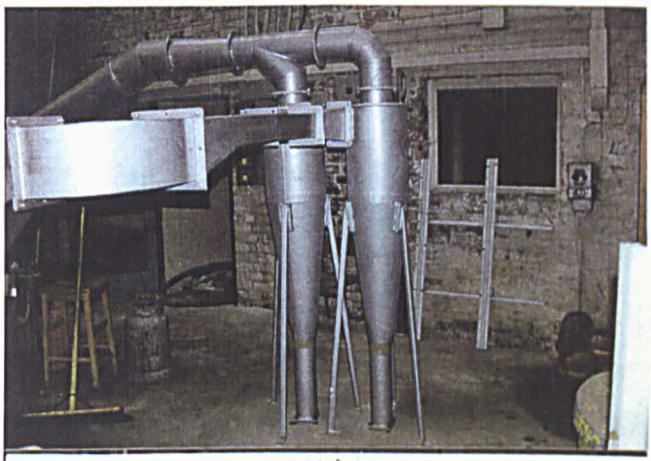

(c)

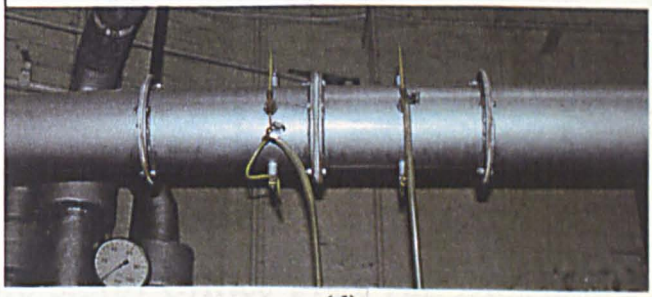

(d)

Figure 5.2 Photographs of Experimental Rig

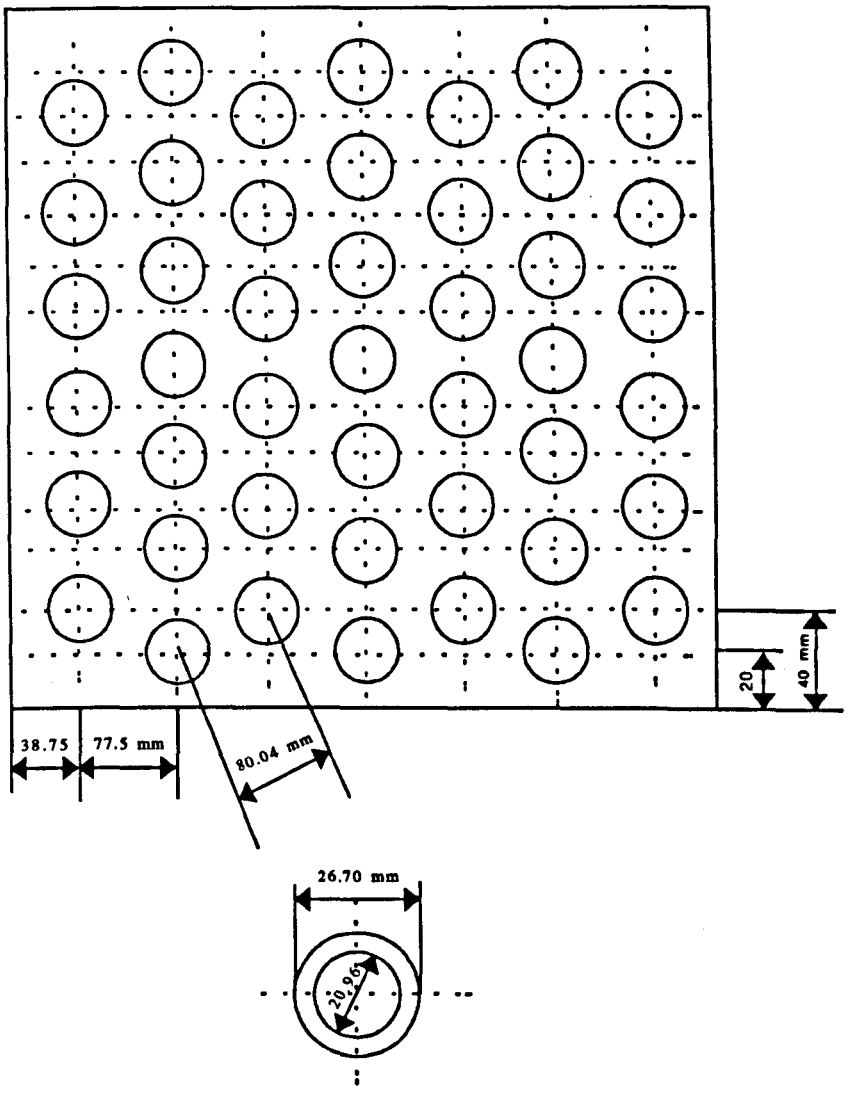

Figure 5.3(a) Staggered Tube Bundle and Tube Dimensions

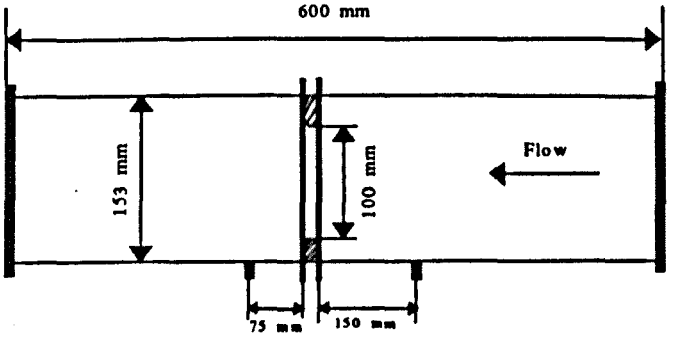

Figure 5.3(b) Orifice Plate and Dimensions

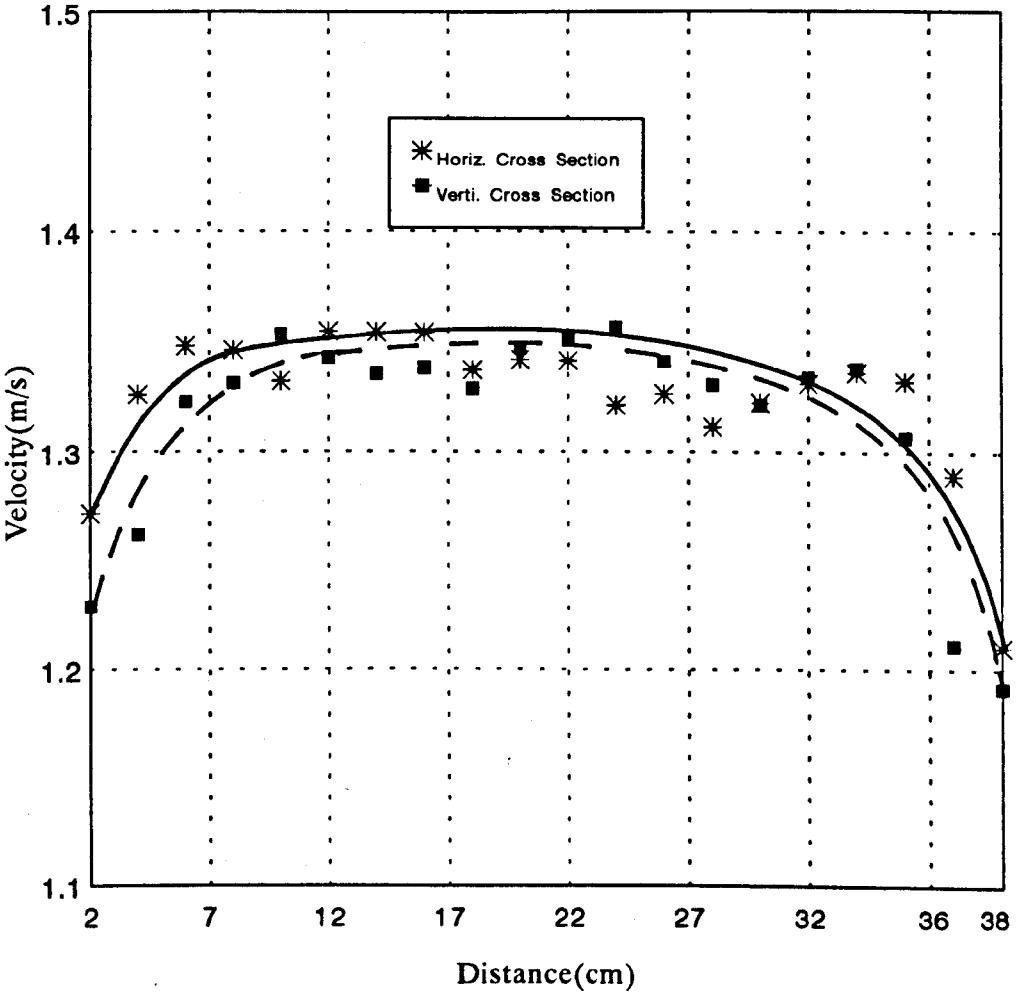

Figure 5.4 Velocity Profile Across the Inlet Section

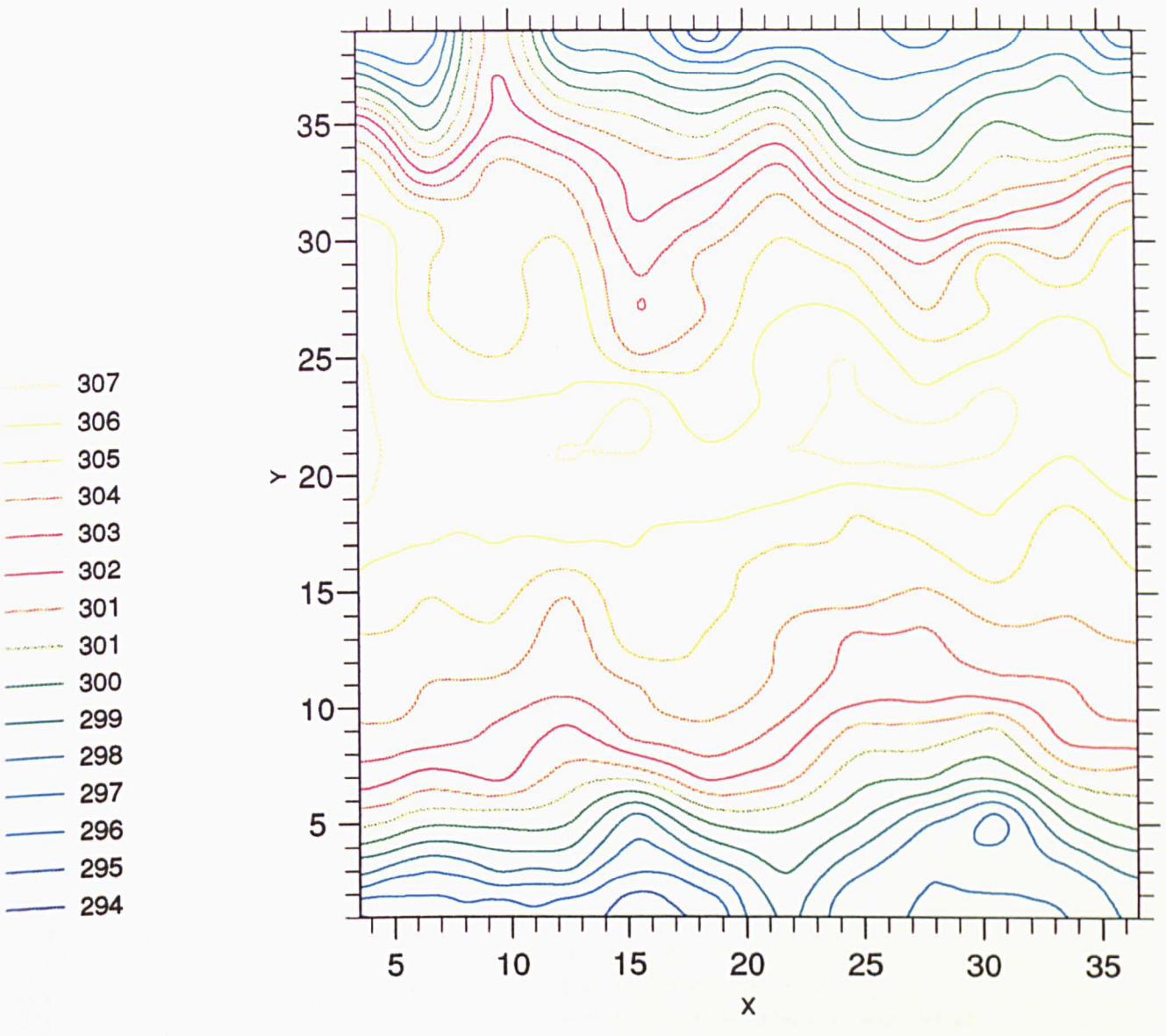

Figure 5.5 Temperature Distribution of the Inlet Section

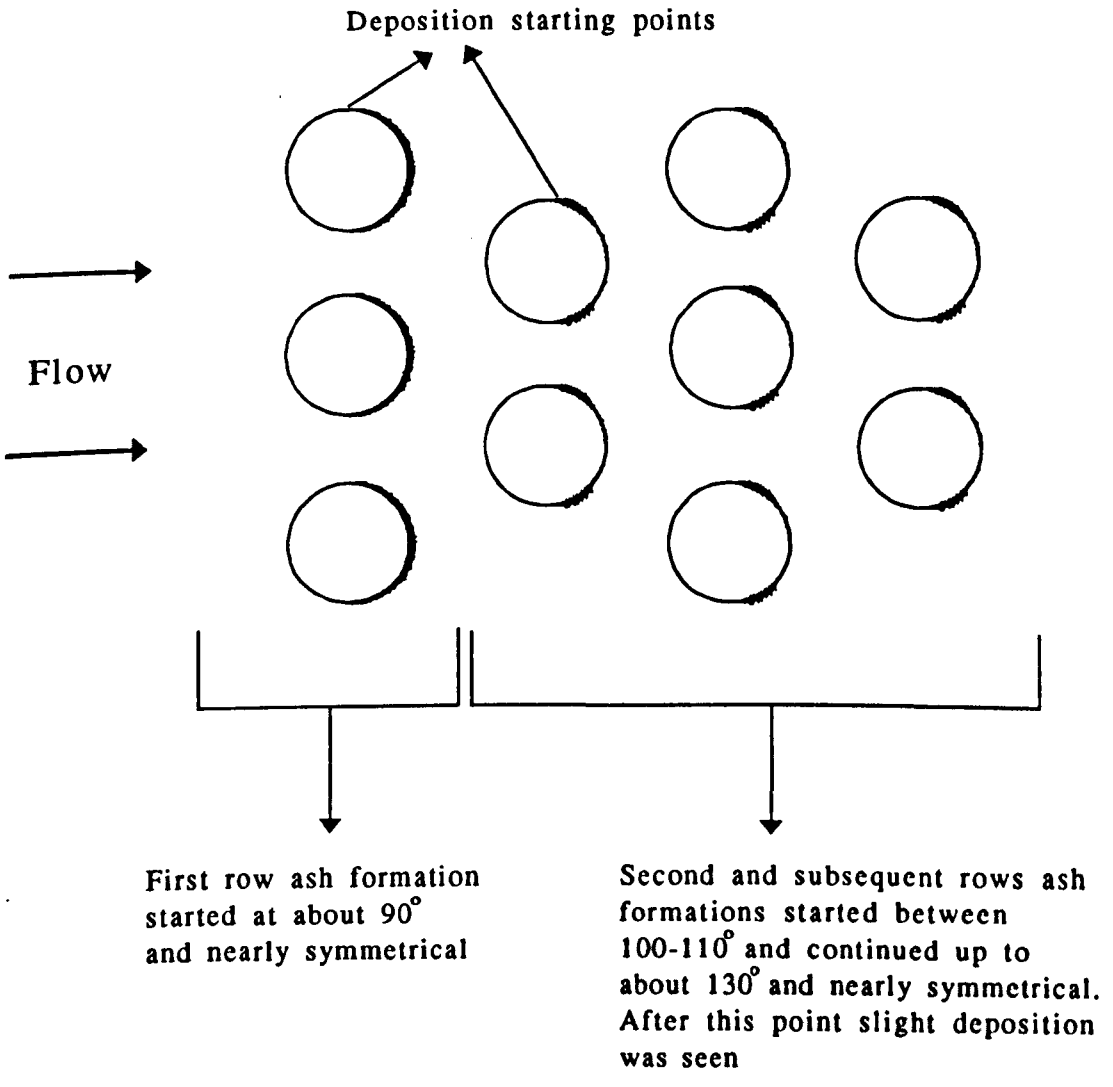

Figure 5.6 Schematic View of the Deposit Formation Around the Heat Exchanger Tubes

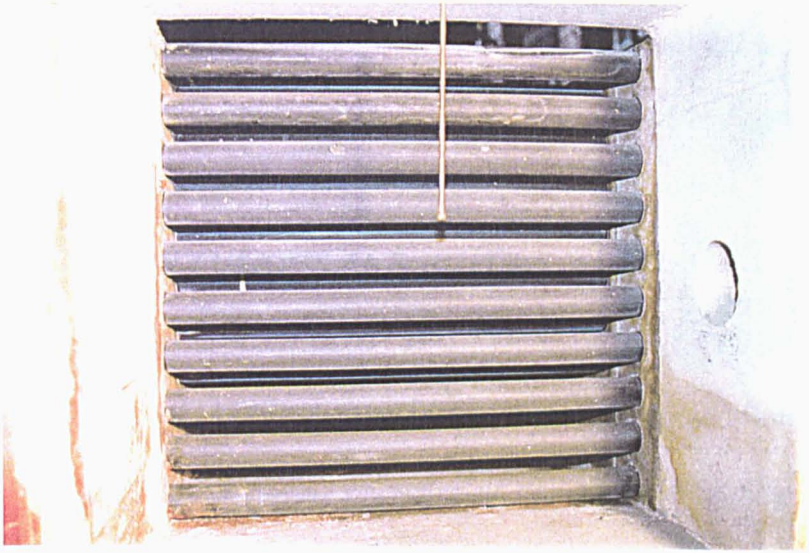

(a)

(b)

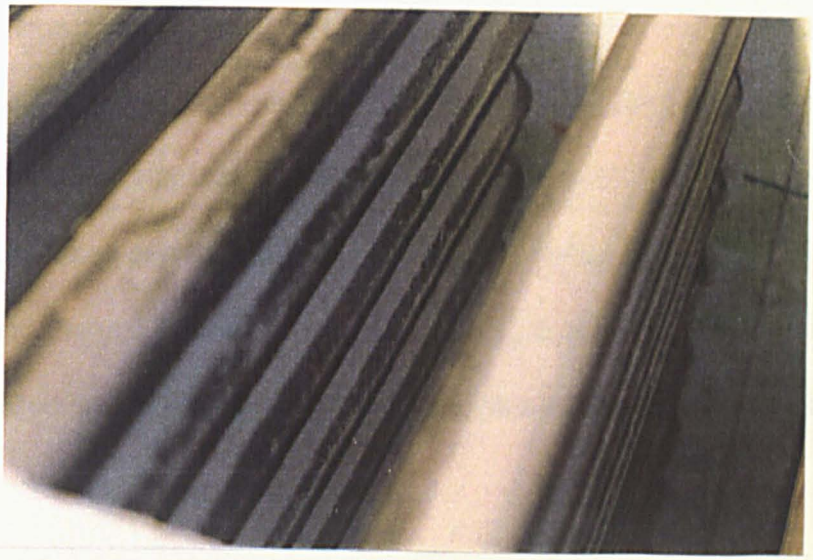

(c)

Figure 5.7 Photographs of Deposit Formation
Around Various Tubes

CHAPTER 6

CONCLUSIONS AND FUTURE WORK

This thesis has described an investigation into the heat transfer and flow characteristics around tubes in cross-flow with particular reference to the effect of fouling in tubular heat exchangers. The investigations have been both experimental and theoretical in nature. The following general conclusions can be drawn:

6.1 Conclusions

The theoretical study has approached some of the problems on the effect of fouling on heat exchangers tubes. The parameters that were investigated were homogenous and non-homogenous thermal conductivity of deposit, thickness and eccentricity of the deposits. Modelling the fouling geometry as an eccentric annulus, a finite difference procedure in bipolar coordinates has been developed to predict the effect of some process parameters on thermal performance. With this approach, increasing the asymmetry of the fouling changes the heat transfer for a given mass of fouling. It was found that the heat transfer rate is increased when the fouling concentrated towards to rear of the tube, and not surprisingly, increase in thermal conductivity leads to rising in heat transfer. As for the axi-symmetric case, the heat transfer rate for an asymmetrical by fouled tube may increase or decrease depending on the geometry and thermal conductivity of the fouling. A second theoretical approach was applied to the conduction domain to give a general solution for the temperature using the

point-matching method. The point-matching method was found to be a simple way of obtaining a numerical solution for the temperature. Both theoretical investigations were found to give comparable results.

An experimental study of the heat transfer and flow characteristics over the tubes in cross-flow with a range of subcritical Reynolds number has been carried out. For a single tube row, blockage has a significant influence on the local heat transfer and pressure distribution around the tubes. Increasing blockage causes the separation point to move to the downstream side of the tube and the overall heat transfer to increase. Due to the great acceleration of the flow there is a significant change in the flow compared with the low blockage case. A calculation of the heat transfer at the front stagnation point and in the laminar boundary layer region agreed well with experimental results and also with previous by published data for blockage ratios up to 0.5. For tube bank measurements, altering the longitudinal pitch ratio from 1.25 to 1.5 did not give noticeable changes for the local heat transfer and pressure distributions.

A numerical calculation of the heat transfer and flow characteristics for laminar flow in a low Reynolds number range was carried out to predict the effect of blockage, Reynolds number and longitudinal pitch ratio in a tube bank. The computational technique used was a stream function-vorticity formulation with second order accuracy differencing and a Gauss-Seidel over-relaxation technique. Single tube results show that increasing blockage causes the angle of the separation point's location to increase. Increasing Reynolds number causes the angle of separation point to decrease and overall heat transfer to increase. A comparison of

experimental and numerical predictions agree well up to the separation point, however in the rear circulation region, the results deviate probably due to the time dependency of the flow (vortex shedding) not being accounted for. For the tube bank, altering longitudinal pitch ratio from 1.25 to 1.5 did not have a significant effect on the heat transfer predictions. Experimental data agrees up to nearly 80° on the tube surface, and numerical flow separation predictions show good agreement with experiment. Non-uniformity of the grid at the junction point of the grid lines gives a distortion of the local Nusselt number and pressure distribution. Further consideration of the grid would improve the accuracy of the predictions. Generally predictions of local Nusselt number, pressure, streamline and isotherm contours are successfully compared with the present experimental data and previously published data.

The formation of ash deposits on the tubes of an experimental heat exchanger was examined for two different gas inlet temperatures of 110 °C and 250 °C with different amounts of ash. Increasing the total amount of ash passed through the rig did not produce a corresponding increase in the level of deposition. Observations show that for the first row of the bundle and with low gas temperature, no frontal deposit occurred, beyond about 90° a relatively uniform and symmetrical deposit was built up. For second and subsequent rows the deposition patterns was relatively constant. Deposit forms between 100°-110° and 130° which possibly corresponds with a recirculation region on the tube surface. Fouling on a hot tube was less than that on cold tubes thereby confirming the effect of condensation on the fouling process. Changing the gas inlet temperature from 110 °C to 250 °C did not cause the patterns of the deposits to change.

6.2 Future Work

The present investigation has provided useful information on the heat transfer and flow structures for tubes in cross-flow and on the effect of fouling on these. The study has also raised further questions and these could be answered with future studies.

1- Can the surface roughness of the fouling be adopted into the theoretical study of fouling predictions?

2- The copper foil technique gave unsatisfactory results. Can it be improved to measure heat transfer coefficient around the cylinder?

3- Will time dependent calculations improve the prediction of heat transfer coefficient beyond the separation point for a tube or a tube in a bank?

4- For the turbulent flow calculations, can the grid refinement be effective on the predictions and what effect does the wall functions have on the predictions of the local values?

5- Due to limitations of the heat exchanger rig and of time, the study was limited observations of the patterns formed by the deposit. Do the other process conditions (such as altering ash loading rate, condensation rate, and other parameters) change the deposit patterns around the heat exchanger tubes and cause a reduction in the heat transfer? Will more sensitive measurements be able to improve the explanation of deposit formation around the tubes?

REFERENCES

- ABRAHAM, K.U. and RAJARAM, S. (1983) "Measurement of Furnace Heat Transfer Performance in a Corner-Fired, Pulverized Coal Boiler." Journal Inst. of Energy, 551, 429, 217-225

- ACHENBACH, E. (1968) "Distribution of Local Pressure and Skin Friction Around a Circular Cylinder in Cross-Flow up to $Re=5x10^5$. " J.Fluid Mech., 34, 4, 625-636

- ACHENBACH, E. (1981) "Total and Local Heat Transfer and Pressure Drop of Staggered and In-line Tube Banks" In Heat Exchangers-Thermal Hydraulic Fundamentalist and Design Eds. Kakac, S., Bergles. A.E., Mayinser,F., McGrow Hill, NewYork, 85-96

- AIBA, S., YAMAZAKI,Y. (1976) "An Experimental Investigation of Heat Transfer Around a Tube in a Bank. " Journal of Heat Transfer, Paper 76, 503-508

- AIBA, S., OTA, T., and TSUCHIDA, H. (1980) "Heat Transfer of Tubes Closely Spaced in a Inline Bank. " Int. J. Heat and Mass Transfer, 23, 311-319

- AKILBAYEV, Z.S., ISOTA'YEV, P.A. (1966) "Prob. Teplo. Prikl. (Zukauskas, 1972, 93-160)

- ALLMON, B.A., WATSON, G.B. and CARPENDER, N.N. (1991) " Fouling and Cleaning of a Staggered, Finned Tube Bundle Under Coal-Fired Conditions." Fouling and Enhancement Interations, ASME HTD 164, 61-69

- ANDERSON, D.W., VISKONTA, R and INCROPERA, F.P. (1987) "Effective Thermal Conductivity of Coal Ash Deposits at Moderate to High Temperatures." Journal of Eng. for Gas Turbines and Power, 109, 215-221

- ANTONOPOULOS, K.A. (1985) "Heat Transfer in Tube Assemblies Under Conditions of Laminar Axial, Transverse and Inclined Flow. " Int. J. Heat&Fluid Flow, 6, 3, 193-204

- BARROW, H. (1986) "On Average Heat Transfer Coefficient. " Int. J. Heat &Fluid Flow, 7, 162-163

- BARROW,H. and SHERWIN, K. (1994)" Theoretical Investigation of the Effect of Fouling on the Performance of a Tube and Plate Fin Heat Exchanger. " Heat Recovery System&CHP, 14, 1, 1-5

- BAUGHN, J.W., ELDERKIN, M.J. and McKILLOP, A.A. (1986) " Heat Transfer from a Single Cylinder, Cylinders in Tandem and Cylinders in the Entrance Region of a Tube Bank with a Uniform Heat Flux." Trans. ASME, J. Heat Transfer, 108, 386-391

- BEMBROSE, C.R. and BOTT, T.R. (1984) "Correlation for Gas Side Fouling of Finned Tubes." Inst. of Chemical Eng. Symposium Series, 1, 86, 357-367

- BERGELIN, O.P., BROWN, G.A. and DOBERSTEIN, S.C. (1952) "Heat Transfer and Fluid Friction During Flow Across Banks of Tubes." Trans. ASME 74, 953-959

- BERGELIN, O.P., DAVIS, E.S., HULL, H.L. (1949) "A Study of Three Tube Arrangements in Unbaffled Tubular Heat Exchangers." Trans. ASME, 71, 369-374

- BLOCHL, R. and MULLER-STEINHAGER, H.(1990) "Influence of Particle Size and Particle/Fluid Combination on Particle Fouling in Heat Exchangers." The Canadian J. Chemical Engineering, 68, 585-591

- BIYIKLI, S., TUZLA, K., CHEN, J.C. (1983) "Heat Transfer around a Horizontal Tube in Freeboard Region of Fluidised. " AIChE Journal, 29, 5, 712-716

- BOTT, T.R. (1990) "Fouling Notebook, Inst. of Chemical Engineers"

- BOTT, T.R. and BEMBROSE, C.R.(1983) "Particulate Fouling on the Gas Side of Finned Tube Heat Exchangers." Trans. ASME, J. HeatTransfer 105, 178-183

- BOULAS, M.J. and PEI, D.C.T. (1974) "Dynamics of Heat Transfer from Cylinders in a Turbulent Airstream. " Int. J. Heat and Mass Transfer, 17, 767-783

- BROWN, T.D. (1966) " The Deposition of Sodium Suphate form the Combustion Gases." J. Inst. Fuel, 39, 378-385

- CHAMBRA, L.M. and WEBB, R.L. (1993) "Effect of Particle Size and Size Distribution on Paniculate Fouling in Enhanced Tubes." Enhanced Heat Transfer, 1, 1, 65-75

- CHAPMAN, A.J. (1987) "Fundamentals of Heat Transfer, MacMillan, NewYork"

- CHEN, C.K., WONG, K.L., CLEAVER, J.W. (1986) "Finite Element Solutions of Laminar Flow and Heat Transfer of Air in a Staggered and an In-line Tube Bank. " Int. J. Heat&Fluid Flow, 7, 4, 291-300.

- CHEN, Y.N. (1972) "Properties of the Karman Vortex Sheet." Sulzer Research, 68-80

-CHENG, K.C, INABA,H., GILPIN, R.R. (1981) "An Experimental Investigation of Ice Formation Around an Isothermally Cooled Cylinder in Crossflow." Journal of Heat Transfer, 103, 733-738

- DENNIS, S.C.R., HUDSON, J.D., SMITH, N. (1968) "Steady Laminar Forced Convection from a Circular Cylinder at Low Reynolds Number. " The Physics of Fluids, 11, 5, 933-940

- ECKERT, E.R.G. and DRAKE, R.M. (1959) "Heat and Mass Transfer 2nd Edition, McGrow Hill Book Co. Inc."

- ECKERT,E.R.G., SOEHNGEN,E. (1953) "Distribution of Heat Transfer Coefficients Around Circular Cylinders in Cross-Flow at Reynolds Number from 20 to 500." Trans. ASME, Paper 51-F9, 343-347

- EL-WAHED, A.K., JOHNSON, M.W., SPROSTON, L.J. (1993) "Numerical Study of Vortex Shedding form Different Shaped Bluff Bodies." Flow Meas. Instrum., 4, 4, 233-240

- FAGE, A and FALKNER, V.M. (1931) "Further Experiments on the Flow Around a Circular Cylinder. " Aero. Res.Counc. Reports and Memoranda No. 1369, London

- FAGHRI, M. and RAO, N. (1987) "Numerical Computation of Flow and Heat Transfer in Finned and Unfinned Tube Banks. " Int. J. Heat and Mass Transfer, 30, 2, 363-372

- FUJII ,M. FUJII ,T. SATO ,R. (1986) "A Theoretical Consideration for Predicting Heat Transfer Characteristics of a Tube Bank From Measurements with a Single Test Tube. " International Heat Transfer Conference ASME.,6,2751-2756

- GARDON, R. (1953) "An Instrument for Direct Measurement of Intense Thermal Radiation." Review of Scientific Instrument, 24, 366-370

- GIEDT,W.H.(1949) "Investigation of Variation of Point Unit Heat Transfer Coefficient Around a Cylinder Normal to an Air Stream" Transactions of ASME. 71, 375-381

- GRIMISON, E.D. (1937) "Correlation and Utilisation of New Data on Flow Resistance and Heat Transfer for Cross-flow of Gases over Tube Banks." Trans. ASME 59,583-594

- HIDEBRAND, F. B. (1976) "Advanced Calculus for Application, 2nd Edition Prentice Hall Inc., New Jersey"

- HIWADA, M. and MABUCHI, U. (1980) " Flow Behavior and Heat Transfer around a Circular Cylinder at High Blockage Ratios." Trans. JSME, 46, 409, 52-61

- HOLWORTH, B.R. and GERO, L.R. (1985) "Entraintment Effects of Impingement Heat Transfer Part II Local Heat Transfer Measurement" Trans. ASME J. Heat Transfer, 107, 910-915

- ISHIGASHI, T. (1986) "Characteristics of the Flow Around Four Circular Cylinders Arranged In-Line." Bulletin of JSME, 29, 249, 751-757

- JAIN, P.C. and GOEL, B.S. (1976) "A Numerical Study of Unsteady Laminar Forced Convection from a Circular Cylinder. " Trans. ASME, J. Heat Transfer, 1976,303-307

- JEAGER, J.C. (1951) "An Introduction to Applied Mathematics, Oxford Univ. Press, Oxford"

- JOHNSON,M.W. (1990) "Computation of Flow in a Vortex - Shedding Flowmeter." Flow Meas.Instrum., 1, 201-208

- KAYS, W.M. and CRAWFORD, M.E. (1994) "Convective Heat and Mass Transfer". Tata McGraw Hill, New Delhi, 139-155

- KRAABEL, J.S., BAUGHN,J.W., MCKILLOP,A.A. (1980) "An Instrument for the Measurement of Heat Flux from a Surface with Uniform Temperature." Journal of Heat Transfer, 102, 576-578

- KRAABEL, J.S., McKILLOP, A.A. and BAUGHN, J.W. (1982) "Heat Transfer to Air form a Yawed Cylinder." Int. J. Heat and Mass Transfer, 25, 409-418

- KRALL, K.M. and ECKERT, E.R.G. (1973) "Local Heat Transfer around a Cylinder at Low Reynolds Number. " Trans. ASME J. Heat Transfer, 273-275

- KREITH, F. (1965) "Principles of Heat Transfer," 2nd Edition, Int. Textbook Company, London

- KUZNETSOV, V.A. (1969) "Selecting Gas Velocities and Optimum Profiles for Convective Surfaces in Steam Boilers Taking Fouling into Account." Thermal Engineering, 16, 8, 68-72

- LAUNDER, B.E. and MASSEY, T.H.(1978) "The Numerical Prediction of Viscous Flow and Heat Transfer in Tube Bank. " Trans. ASME, J. Heat Transfer, 100, 565-571.

- MELO, L.F. and PONHEIRO, D.R.S. (1984) "Hydrodynamic Effect on Particulate Fouling" First U.K. National Conf. on Heat Transfer, Leeds 381-391

- MULLER-STEINHAGER, H., *REIF, F., EPSTEIN, N.*, and WATKINSON, A.P. (1988) "Influence of Operating Conditions on Particulate Fouling. " The Canadian J. Chemical Engineering, 66, 42-50

- MURRAY, D.B., FITZPATRICK, J.A. (1988) "Local Heat Transfer Coefficients for a Tube Array Using a Micro-Foil Heat Flow Sensor." Proc. 2nd U.K. Nat. Conf. on Heat Transfer, 2, 1635-1649

- OMOHUNDRO, C.A., BERGELIN, O.P. and COLBURN, A.P. (1949) " Heat Transfer and Fluid Friction During Viscous Flow Across Banks of Tubes." Trans. ASME 71, 27-34

- OTS, A.A., MIKK, I.R. and KAAR, H.A. (1986) "Heat Surface Fouling by Graphite Particles Depositing from Turbulent Gas Flow. " 8th Int. Heat Transfer Conf., San Francisco, USA, 2561-2565

- PAOLINO ,M.A. KINNEY ,R.B. CERUTTI ,E.A. (1986) "Numerical Analysis of the Unsteady Flow and Heat Transfer to a Cylinder in Crossflow." Trans. ASME, J. Heat Transfer, 108, 742-748.

- PERKINS, H.C. and LEPPERT, G. (1964) "Local Heat Transfer Coefficients on a uniformly Heated Cylinder. " Int. J. Heat and Mass Transfer, 7, 143-158

- PETROV, V.A. (1968) "Fouling of Air Heater Tubes on the Air Side." Thermal Engineering, 15, 3, 21-23

-PORTYANKO, A.A., LOKSHIN, V.A., FAMINA, V.V. (1980) "The Fouling of Transversely Swept Bundles of Tubes with Welded Spiral Finning." Thermal Engineering, 27, 12, 711-713

- POSKAS, P.S. and SURVILA, V.J. (1983) "Fluctuations of Velocity Cross-flow of Air in the Space Between Tubes in Bundle." Heat Transfer Soviet Research, 15, 1, 75-86

- PROFOS, P. and SAHARAN, H.N. (1960) "Effect of Tube Spacing and Arrangement Upon the Fouling Characteristics of Banks of Tubes." Sulzer Technical Review, 4, 31-43

- SEAPAN, M. and LO, J. Y. (1990) " A Simulation Model to Predict Slag Composition in a Coal-Fired Boiler. " High Temperature Science, 26, 295-311

- SCHMIDT, E., WENNER, K. (1943) "Heat Transfer Over The Circumference of a Heated Cylinder In Transverse Flow." NACA Technical Memorandum,1050

- SHOLLCROSS, D.C. and WOOD, D.G. (1986) "The Accurate Measurement of Heat Flux Using a Film Heat Flux Sensor with Application to Axisymmetric Bodies. " Proceedings of the Eighth Int. Heat Transfer Conference, San Francisco, 2, 477-482

- THOM, A. (1933) "The Flow Past Circular Cylinders at Low Speeds." Proc. Roy. Soc., A141, 651-669

- THOMPSON, J.F., THOMES, F.C. and MASTIN, C.W. (1974) "Automatic Numerical Generation of Body Fitted Curvilinear Coordinate System for Field Containing Any Number of Arbitrary Two Dimensional Bodies." J. of Computational Physics, 15, 299-319

- WALL,T.F., LOWE, A., WIBBERLEY, L.J. and STEWART. I.M. (1979) "Mineral Matter in Coal and the Thermal Performance of Large Boilers." Progress in Energy and Combustion

Science, 5, 1-29

- WATTS, J., WILLIAMS, F. (1980) "A Technique for the Measurement of Local Heat Coefficients Using Copper Foil." Report XD 183, Berkeley Nuclear Lab. U.K.

- WEST, G.S. and APELT, C.J. (1982) " The Effect of Tunnel Blockage and Aspect Ratio on the Mean Flow Past a Circular Cylinder with Reynolds Number between 10^4 and 10^5." J. Fluid Mech., 114, 361-377

- ZDROVISTCH, F., FLETCHER, A.C., BEHNIA, M. (1995) "Numerical Laminar and Turbulent Fluid Flow and Heat Transfer Predictions in Tube Banks." Int J. Num. Meth. Heat and Fluid Flow, 5, 717-733

- ZUKAUSKAS, A (1972) "Heat Transfer from tubes in Cross-flow." Advances in Heat Transfer, 8, 93-160

APPENDIX A

List of Temperature Calculation Programs

APPENDIX A

Temperature Calculation Program for Eccenteric Conduction Domain

```
5 REM WRITTEN BY E.BUYRUK
10 REM "BIPOLAR COORDINATE; CALCULATION OF THE HEAT TRANSFER RATE"
20 DIM ET(1000), X(1000), T(120, 120), H(1000), TH(1000), M(1000), L(1000), NU(1000)
30 R1 = 8.000001E-03: R2 = .011: D = .002: PI = 3.1415: TG = 373: KAIR = .0317
40 REM "D: ECCENTRICITY "
50 REM "XMAX: VALUE OF THE MAXIMUM MESH LINES IN RADIAL DIRECTION"
60 REM "EMAX: VALUE OF THE MAXIMUM MESH LINES IN CIRCUMFERENTIAL DIRECTION ""
80 INPUT "TYPE XMAX VALUE=", XMAX
100 INPUT "TYPE EMAX VALUE=", EMAX
120 X(1) = (D ^ 2 - (R1) ^ 2 + (R2) ^ 2) / (2 * D * R2)
130 X(1) = LOG(X(1) + SQR((X(1)) ^ 2 - 1))
140 X(XMAX) = (R2 / R1) * (EXP(X(1)) - EXP(-X(1))) / 2
150 X(XMAX) = LOG(X(XMAX) + SQR((X(XMAX)) ^ 2 + 1))
160 C = R2 * (EXP(X(1)) - EXP(-X(1))) / 2
170 ET(1) = -PI / (EMAX - 2)
175 DET = PI / (EMAX - 2): DX = (X(XMAX) - X(1)) / (XMAX - 1)
180 INPUT "TYPE OUTPUT FILE NAME      =", A$
190 OPEN "O", #1, A$
200 REM "CALCULA. SURF."
210 FOR I = 2 TO EMAX
240 ET(I) = ET(1) + DET * (I - 1)
250 Y = C * SIN(ET(I)) / ((EXP(X(1)) + EXP(-X(1))) / 2 - COS(ET(I)))
260 Z = C * (EXP(X(1)) - EXP(-X(1))) / 2
270 Z = Z / ((EXP(X(1)) + EXP(-X(1))) / 2 - COS(ET(I)))
280 GOSUB 1070
290 TH(I) = ATN(Y / (Z - ZO))
300 TH(I) = TH(I) * 180 / PI
310 IF TH(I) < 0 GOTO 330
320 GOTO 340
330 TH(I) = 180 + TH(I)
340 PRINT Z, Y
350 PRINT #1, Z, Y
362 NU(I) = 36.181 - .2312 * TH(I) + .0137504 * TH(I) ^ 2 - 3.7657E-04 * TH(I) ^ 3 + 3.27664E-06 * TH(I)
^ 4 - 7.114398E-09 * TH(I) ^ 5 - 2.62708E-11 * TH(I) ^ 6 + 9.47087E-14 * TH(I) ^ 7
363 H(I) = (KAIR * NU(I) / (2 * R1)) * (R2 / R1) ^ (.618 - 1)
370 NEXT I
380 REM " M: METRIC COEFFICIENT "
390 FOR I = 2 TO EMAX
400 M(I) = C / ((EXP(X(1)) + EXP(-X(1))) / 2 - COS(ET(I)))
410 NEXT I
470 FOR J = 1 TO XMAX
480 X(J) = X(1) + DX * (J - 1)
490 PRINT X(J)
500 NEXT J
510 FOR I = 1 TO (EMAX + 1)
520 FOR J = 1 TO XMAX
```

```
530 T(I, J) = 283
540 NEXT J
550 NEXT I
560 PRINT "ITERATION NUMBER = ", N
570 FOR I = 3 TO (EMAX - 1)
600 T(I, 1) = ((M(I) + M(I - 1)) / 2) * H(I) * DET * TG + K * DX * T(I - 1, 1) * .5 / DET
610 T(I, 1) = T(I, 1) + K * DX * T(I + 1, 1) * .5 / DET + K * DET * (M(I - 1) + M(I)) * T(I, 2) * .5 / (M(I) *
DX)
611 T(I, 1) = T(I, 1) / (K * DX / DET + K * (M(I - 1) + M(I)) * DET * .5 / (M(I) * DX) + H(I) * DET * .5 *
(M(I - 1) + M(I)))
630 NEXT I
631 T(2, 1) = (H(2) * M(2) * DET * TG + K * DET * T(2, 2) / DX + K * T(3, 1) * DX / DET)
632 T(2, 1) = T(2, 1) / (K * DET / DX + H(2) * M(2) * DET + K * DX / DET)
633 T(22, 1) = (H(22) * M(22) * DET * TG + K * DET * T(22, 2) / DX + K * T(21, 1) * DX / DET)
634 T(22, 1) = T(22, 1) / (K * DET / DX + H(22) * M(22) * DET + K * DX / DET)
640 FOR I = 2 TO EMAX
650 FOR J = 2 TO (XMAX - 1)
660 REM "INTERNAL NODES TEMPERATURE CALCULATION"
670 T(I, J) = (T(I, J + 1) + T(I, J - 1)) / (DX ^ 2) + (T(I + 1, J) + T(I - 1, J)) / (DET ^ 2)
680 T(I, J) = T(I, J) / (2 / (DX ^ 2) + 2 / (DET ^ 2))
690 NEXT J
700 NEXT I
710 FOR J = 1 TO (XMAX - 1)
720 T(1, J) = T(3, J)
730 NEXT J
740 FOR J = 1 TO (XMAX - 1)
750 T(EMAX + 1, J) = T(EMAX - 1, J)
760 NEXT J
770 N = N + 1
780 IF N < 500 THEN GOTO 560
790 FOR J = 1 TO XMAX
800 FOR I = 2 TO EMAX - 1
810 PRINT Z, Y, T(I, J)
820 PRINT #1, T(I, J)
830 NEXT I
840 NEXT J
850 END
860 FOR I = 2 TO EMAX
870 IF I < 3 OR I > (EMAX - 1) THEN P = .5 ELSE P = 1
880 REM "HK: CONVECTIVE HEAT TRANSFER RATE"
920 HK = H(I) * (TG - T(I, 1)) * M(I) * P * 2 * DET
930 HT = HK + HT
1040 'PRINT I, HT, H(I), TH(I)
1050 'PRINT #1, I, HT, H(I), TH(I)
1060 NEXT I
1070 REM "CALCULATION Zo"
1080 Z1 = C * ((EXP(X(1)) - EXP(-X(1))) / 2)
1090 Z1 = Z1 / ((EXP(X(1)) + EXP(-X(1))) / 2 - 1)
1100 ZO = Z1 - R2
1110 RETURN
```

Temperature Calculation Program for Concentric Conduction Domain

```
1 REM WRITTEN BY E.BUYRUK
5 REM POLAR COORDINATE; CONCENTRIC TUBE
10 CLS
20 DIM T(100, 100), R(100), H(100), THETA(100, 100), NU(100, 100), QW(100)
30 INPUT "PLEASE TYPE MAX. N VALUE          =          ", NAX
40 INPUT "PLEASE TYPE MAX. M VALUE          =          ", MAX
50 PRINT "*****************************************************************"
60 R1 = .008: I = 0: K = 1: KAIR = .0317: TG = 373: RNAX = .011: PI = 3.1415
70 INPUT "TYPE OUTPUT FILE NAME             =          ", D$
80 OPEN "O", #1, D$
90 FOR N = 1 TO NAX
100 FOR M = 2 TO MAX - 1
110 R(N) = R1 + (N - 1) * DR
120 DR = (RNAX - R1) / (NAX - 1)
130 DT = PI / (MAX - 3)
136 THETA(M, NAX) = (M - 2) * 180 / (MAX - 3)
139 NU(M, NAX) = 36.181 - .2312 * THETA(M, NAX) + .0137504 * THETA(M, NAX) ^ 2 - 3.7657E-04 *
THETA(M, NAX) ^ 3 + 3.27664E-06 * THETA(M, NAX) ^ 4 - 7.114398E-09 * THETA(M, NAX) ^ 5 -
2.62708E-11 * THETA(M, NAX) ^ 6 + 9.47087E-14 * THETA(M, NAX) ^ 7
140 H(M) = (KAIR * NU(M, NAX) / (2 * R1)) * (RNAX / R1) ^ (.618 - 1)
141 PRINT DR, DT, THETA(M, NAX), R(N)
142 NEXT M
150 NEXT N
160 FOR N = 1 TO NAX
170 FOR M = 1 TO MAX
180 T(M, N) = 283
190 NEXT M
200 NEXT N
210 FOR N = 2 TO NAX - 1
220 FOR M = 2 TO MAX - 1
230 T(M, N) = T(M, N + 1) * (1 / DR ^ 2 + 1 / (R(N) * 2 * DR))
240 T(M, N) = T(M, N) + T(M, N - 1) * (1 / DR ^ 2 - 1 / (R(N) * 2 * DR))
250 T(M, N) = T(M, N) + (T(M + 1, N) + T(M - 1, N)) * (1 / (DT ^ 2 * R(N) ^ 2))
260 T(M, N) = T(M, N) / (2 / DR ^ 2 + 2 / (DT ^ 2 * R(N) ^ 2))
280 NEXT M
290 NEXT N
300 FOR N = 2 TO NAX
310 FOR M = 2 TO MAX - 1
320 IF M = 2 THEN T(1, N) = T(3, N)
330 IF M = MAX - 1 THEN T(MAX, N) = T(MAX - 2, N)
340 NEXT M
350 NEXT N
360 FOR N = 2 TO NAX
370 FOR M = 2 TO MAX - 1
380 T(M, NAX) = H(M) * DT * TG + ((K * DR / 2) / (DT)) * (T(M + 1, NAX) + T(M - 1, NAX)) + (K * DT
/ DR) * T(M, NAX - 1)
390 T(M, NAX) = T(M, NAX) / (K * DT / DR + H(M) * DT + (K * DR / (DT)))
428 'T(M, NAX) = 373
430 NEXT M
440 NEXT N
460 I = I + 1
```

```
470 IF I < 500 GOTO 210
480 PRINT #1, "*****ITERATION NUMBER=", I
481 FOR M = 2 TO MAX - 1
482 FOR N = 1 TO NAX
483 IF M = 2 OR M = MAX - 1 THEN P = .5 ELSE P = 1
485 HC = 2 * P * H(M) * DT * R(N) * (TG - T(M, NAX))
487 KC = 2 * P * K * DT * (R(N) - DR / 2) * (T(M, NAX - 1) - T(M, NAX)) / DR + K * DR / 2 * (T(M - 1,
NAX) + T(M + 1, NAX) - 2 * T(M, NAX)) / (R(N) * DT)
490 NEXT N
491 HT = HT + HC
492 KT = KT + KC
493 PRINT KT, KC, HT
494 PRINT #1, KC, KT
498 NEXT M
499 FOR N = 1 TO NAX
500 FOR M = 2 TO (MAX - 1)
510 'PRINT M, N, T(M, N)
520 PRINT #1, M, T(M, N)
530 NEXT M
540 NEXT N
550 END
```

PAGE/PAGES EXCLUDED UNDER INSTRUCTION FROM THE UNIVERSITY